

# The application of novel mass spectrometric techniques for the analysis of volatile organic compounds in different environments

W. Joe. F. Acton  
MChem. (Hons)

December 2015

Lancaster Environment Centre  
Faculty of Science and Technology  
Lancaster University

This thesis is submitted in fulfilment of the requirements for the degree of  
Doctor of Philosophy.

## **Declaration:**

I confirm that this work is my own, except where otherwise stated and that this work has not been submitted for the award of a higher degree elsewhere. Some sections of this thesis have been published in journals as indicated within.

Joe Acton

December 2015

# Acknowledgements

I would like first and foremost to thank by supervisors Nick Hewitt and Jane Taylor, without whose guidance and advice none of this would have been possible. I would also like to thank Ben Langford and Eiko Nemitiz for always being willing to make time to offer me advice and answer what were often obscure and technical questions.

Special thanks go to Amy, Matt, Brian, Hannah, Marvin, Anna, Annette, Antonio, Shane and many others in the LEC and particularly the atmospheric sciences group for their advice and good company throughout my time here in Lancaster.

I extremely grateful to Philipp Sulzer and all the staff at Ionicon for welcoming me into their company and for all the help and assistance they gave during my time in Innsbruck. I would also like to thank Armin Hansel and his entire research group for inviting me to work with them at the University of Innsbruck and for sharing their enthusiasm and wisdom with me. Special thanks also must go to Matteo and Werner for all their friendship and support during my time in Innsbruck and to Philipp and Markus for many welcome coffee (pepsi) breaks and distractions.

I am indebted to the Biotechnology and Biological Sciences Research Council (BBSRC) and Ionicon Analytik GmbH for the funding of my studentship and to the

William Ritchie Travel Fund for the opportunity to participate in the European Geosciences Union General Assembly 2015.

I would like to thank my family and friends for their support and encouragement over the last 4 years. And last but by no means least, this wouldn't have been possible without the unfailing support, encouragement and patience of my partner Felicity.

Thank you!

# The application of novel mass spectrometric techniques for the analysis of volatile organic compounds in different environments

W. Joe. F. Acton MChem. (Hons)

December 2015

## Abstract

Volatile organic compounds (VOCs) are released into the atmosphere from numerous anthropogenic and biogenic sources. Traditionally VOCs have been measured using offline techniques such as Gas Chromatography-Mass Spectrometry (GC-MS). The development of the proton transfer reaction mass spectrometer (PTR-MS) has enabled the online analysis of VOC's from both biogenic and anthropogenic sources. This instrument, however, provides little structural information making it impossible to distinguish between isomeric compounds. Here a range of New-Psychoactive-Substances (NPS) are analysed using the recently developed Selective Reagent Ion-Time of Flight-Mass Spectrometer (SRI-ToF-MS) demonstrating its ability to distinguish between isomeric compounds. This instrument is then applied to the analysis of biogenic VOCs (bVOCs).

Plants emit a wide variety of VOCs into that atmosphere. These compounds play an important role in plant communication and defence, with predatory insects making use of VOC emissions from plants following biotic stress to identify and locate their prey.

This process is termed tritrophic signalling. Ozone will readily react with any bVOCs containing an alkene functional group, and as many alkenes (primarily monoterpenes and sesquiterpenes) have been shown to play a significant role in tritrophic signalling it was hypothesised that ozone may disrupt this signalling.

This thesis investigates the effect of ozone on tritrophic signalling using a *Brassica napus* – *Myzus persicae* – *Adalia bipunctata* larvae (rapeseed – green peach aphid – two-spotted ladybird larvae) model system. Plant volatile emission was monitored using a PTR-MS and SRI-ToF-MS which enabled the better detection and identification of bVOCs than is possible using a traditional PTR-MS. Following ozone fumigation of *B. napus* it was shown that a large number of oxygenated compounds are emitted by the plant and that the emission of monoterpenes and sesquiterpenes from a plant chamber is reduced. However, ozone fumigation of the plant leaves was shown to have no impact on the emission of bVOCs below ground.

Using a Y-tube olfactometer it was shown that ozone at environmentally-realistic mixing ratios (ca. 100 ppbv) disrupts the ability of *M. persicae* to locate a host plant. Ozone was also shown to disrupt tritrophic signalling by inhibiting the location of prey by *A. bipunctata* larvae. This disruption in tritrophic signalling was shown to be caused by degradation of bVOCs via ozonolysis and not changes to bVOC emission from the plant.

Finally fluxes of VOCs above a temperate forest canopy were recorded using PTR-MS and a Proton Transfer Reaction-Time of Flight-Mass Spectrometer (PTR-ToF-MS) enabling a direct comparison to be made between these instruments during field scale measurements.

# Contents

## Chapter I

Introduction.....	1
-------------------	---

## Chapter II

Volatile emission from plants and their role in the earth's atmosphere.....	6
2.1 Emission of volatiles from vegetation.....	6
2.2 Role of bVOCs in tropospheric chemistry.....	9
2.2.1 Secondary organic aerosol (SOA) formation.....	10
2.2.2 Tropospheric ozone formation.....	10
2.2.3 The reaction of ozone with bVOCs.....	12
2.3 bVOC emissions from plants in response to stress.....	13
2.3.1 bVOC emissions from plants in response to abiotic stress.....	13
2.3.2 The effect of biotic stress on bVOC emissions and tritrophic signalling.....	16
2.3.3 The effect of multiple stresses.....	18
2.3.4 The effect of ozone on tritrophic signalling.....	20
2.4 Measurement of bVOCs.....	22
2.4.1 Instrumentation.....	22
2.5 Measurement of bVOC fluxes.....	30
2.5.1 Eddy covariance.....	30
2.5.2 Disjunct and virtual disjunct eddy covariance.....	31

## Chapter III

The analysis of complex organic compounds using SRI-ToF-MS.....	33
3.1 Headspace analysis of new psychoactive substances using a Selective Reagent Ionisation-Time of Flight-Mass Spectrometer.....	36
3.1.1 Introduction.....	38
3.1.2 Experimental.....	41
3.1.3 Results and discussion.....	45
3.1.3.1 4-fluoroamphetamine (4-FA).....	48
3.1.3.2 Methiopropamine (MPA).....	53
3.1.3.3 5-(2-aminopropyl)benzofuran (5-APB).....	54
3.1.3.4 Ethcathinone.....	58
3.1.3.5 4-Methylethcathinone (4-MEC) and N- Ethylbuphedrone (NEB).....	59
3.1.3.6 Ethylphenidate (EP).....	61
3.1.3.7 5-MeO-Dalt.....	62
3.1.3.8 Dimethocaine.....	63
3.1.3.9 Nitracaine.....	65
3.1.4 Conclusions.....	67
3.2 Distinguishing two isomeric mephedrone substitutes with selective-reagent-ionization mass spectrometry (SRI-MS).....	69
3.2.1 Introduction.....	70
3.2.2 Experimental.....	73
3.2.3 Results.....	74

3.2.4 Conclusions.....	79
Chapter IV	
The effect of ozone fumigation on the emission of biogenic volatile organic compounds (bVOCs) from <i>Brassica napus</i> .....	81
4.1 Introduction.....	84
4.2 Methodology.....	87
4.2.1 Plant material.....	88
4.2.2 Experimental setup.....	88
4.2.3 SRI-ToF-MS measurements.....	92
4.2.4 SRI-ToF-MS calibration and data analysis.....	94
4.2.5 GC-MS measurements.....	94
4.2.6 Emission rate calculation.....	96
4.3 Results and discussion.....	97
4.3.1 Root chamber measurements.....	97
4.3.2 bVOC emission from healthy leaves.....	99
4.3.3 Volatile emission from leaf chamber following ozone fumigation.....	101
4.4 Conclusions.....	112
Chapter V	
Ambient ozone degrades plant volatiles and disrupts tritrophic signalling.....	114
5.1 Introduction.....	117
5.2 Methodology.....	120
5.2.1 Plant material and insects.....	120

5.2.2 Experimental setup.....	120
5.2.3 Preliminary experiments.....	123
5.2.3 Statistical analysis.....	124
5.2.4 GC-MS measurements.....	124
5.2.6 Emission rate calculation.....	126
5.2.7 PTR-MS measurements.....	126
5.3 Results.....	130
5.3.1 Insect behavioural tests.....	130
5.3.2 Effect of <i>M. persicae</i> infestation on bVOC emission.....	132
5.3.3 Effect of ozone on bVOC emission.....	133
5.4 Discussion.....	136
5.5 Conclusions.....	141

## Chapter VI

Canopy-scale flux measurements and bottom-up emission estimates of volatile organic compounds from a mixed oak and hornbeam forest in northern Italy.....	142
6.1 Introduction.....	147
6.2 Methods.....	149
6.2.1 Site description.....	149
6.2.2 PTR-MS and PTR-ToF-MS setup and measurement procedure.....	150
6.2.2.1 PTR-MS calibration.....	154
6.2.2.2 PTR-ToF-MS calibration.....	156

6.2.3 Calculation of volume mixing ratios.....	156
6.2.4 Flux calculations from PTR-MS.....	157
6.2.4.1 Flux quality assessment and potential losses.....	159
6.2.5 Flux calculations from PTR-ToF-MS.....	162
6.2.6 Leaf level GC-MS measurements.....	163
6.2.7 Mapping tree species distribution.....	164
6.3 Results and discussion.....	165
6.3.1 Meteorological conditions.....	165
6.3.2 bVOC mixing ratios and fluxes.....	168
6.3.2.1 bVOC correlations.....	178
6.3.2.2 Short-chain oxygenated bVOCs.....	179
6.3.2.3 MVK + MACR and MEK.....	180
6.3.2.4 Isoprene and monoterpenes.....	182
6.3.3 Impacts on air quality.....	186
6.3.4 Calculation of isoprene and monoterpene canopy level emission factors.....	187
6.3.5 Speciated bottom-up isoprene and monoterpene flux estimates derived from leaf-level measurements.....	191
6.4 Conclusions.....	197
6.5 Supplementary material for “Canopy-scale flux measurements and bottom-up emission estimates of volatile organic compounds from a mixed oak and hornbeam forest in northern Italy”.....	199
6.5.1 Virtual disjunct eddy covariance lag time determination..	199

6.5.2 Assessment of the underestimation of total flux through the loss of low frequency fluxes.....	200
6.5.3 The uncertainty caused by disjunct eddy covariance.....	201
6.5.4 Flux quality assessment.....	201
6.5.5 The effect of the tower on atmospheric flow.....	202
6.5.5 Leaf surface temperature.....	205
6.5.6 Discussion of flux measurements.....	205
Chapter VII	
Conclusions.....	220
7.1 General conclusions.....	222
Bibliography.....	227
Appendix.....	259

# Figures

2.1 Representative structures of some of the major classes of stress-induced bVOCs.....	8
2.2 A schematic overview of the chemistry of VOCs in the troposphere.....	9
2.3 Schematic representations of the PTR-MS and the PTR-ToF-MS.....	26
3.1 Chemical structures of new psychoactive substances.....	40
3.2 The variation of the percentage product ion branching ratios following the reactions of the various drug compounds with $\text{H}_3\text{O}^+$ .....	50
3.3 The variation of the percentage product ion branching ratios following the reactions of the drug species with $\text{NO}^+$ .....	52
3.4 The variation of the percentage product ion branching ratios following the reactions of the drug species with $\text{O}_2^+$ .....	56
3.5 The variation of the percentage product ion branching ratios following the reactions of the drug species with $\text{Kr}^+$ .....	57
3.6 Chemical structures of 4-MEC and NEB.....	72
3.7 Mass spectrum sections for 4-MEC and NEB with $\text{H}_3\text{O}^+$ being used as reagent ions.....	75
3.8 Mass spectra for 4-MEC and NEB obtained with $\text{NO}^+$ chemistry.....	76
3.9 Mass spectra for 4-MEC and NEB obtained with $\text{O}_2^+$ chemistry.....	77
3.10 Mass spectra for 4-MEC and NEB obtained with $\text{Kr}^+$ chemistry.....	79
4.1 Ozonolysis of alkenes leading to the formation of a carbonyl and a Criegee intermediate.....	86
4.2 Plant chamber and schematic diagram of experimental setup.....	90

4.3 Drop in sesquiterpenes and increase in ozonolysis products following ozone fumigation.....	111
5.1 <i>Myzus persicae</i> and <i>Adalia bipunctata</i> larvae.....	121
5.2 Experimental setup used for behavioural tests.....	122
5.3 Proportion of <i>M. persicae</i> choosing host plant instead of blank chamber when exposed to clear air and ozone and proportion of <i>A. bipunctata</i> larvae choosing <i>M. persicae</i> infested plant instead of a healthy plant in experiment 1	131
5.4 Proportion of <i>M. persicae</i> choosing host plant instead of blank chamber when exposed to clear air and ozone and proportion of <i>A. bipunctata</i> larvae choosing <i>M. persicae</i> infested plant instead of a healthy plant in experiment 2	132
5.5 bVOC emission from healthy and <i>M. persicae</i> infested <i>B. napus</i> .....	133
5.6 The change in bVOC volume mixing ratios following ozone fumigation of <i>B. napus</i> .....	135
6.1 Time series of meteorological conditions recorded over the campaign period.....	166
6.2 Measurement site and flux footprint.....	167
6.3 Mean 4 m above-canopy diurnal volume mixing ratios of volatile organic compounds.....	171
6.4 Time series of isoprene (top) and monoterpene (bottom) fluxes.....	174
6.5 Mean diurnal fluxes of volatile organic compounds.....	175
6.6 Comparison of PTR-MS and PTR-ToF-MS mass scans.....	177
6.7 Scatter plots displaying the relationship between the volume mixing ratios of methanol, acetone and MEK.....	178
6.8 The relationship between temperature and isoprene fluxes and volume mixing ratios.....	184

6.9 Measured isoprene fluxes against the product of $\gamma$ and $\rho$ .....	188
6.10 Residual values from the temperature only monoterpene emission model plotted against PAR.....	189
6.11 The contribution of individual tree species to the speciated isoprene and monoterpene flux.....	195
6.12 Histogram of isoprene lag times calculated using the MAX method.....	199
6.13 Impact of loss of low frequency flux on total flux.....	200
6.14 Sensible heat flux calculated calculated using eddy covariance and disjunct eddy covariance.....	201
6.15 Wind rose plots showing the effect of wind direction on the rotation angle required to set $w$ to zero and the % difference between the measured and modelled turbulence statistic .....	204
6.16 The diurnal pattern of average ambient temperature and leaf surface temperature.....	205
6.17 Time series of bVOC volume mixing ratios during the Bosco fontana campaign.....	219
7.1. The effect of anthropogenic pollution by the oxides of nitrogen on signalling in the <i>B. napus</i> – <i>M. persicae</i> – <i>A. bipunctata</i> tritrophic system.....	225

# Tables

3.1 Product ions and their associated percentage ion branching ratios for reactions of NPS with $\text{H}_3\text{O}^+$ , $\text{NO}^+$ , $\text{O}_2^+$ and $\text{Kr}^+$ , recorded at $E/N$ of 130 Td.....	46
4.1 bVOC species detected from <i>Brassica napus</i> root zone measurements.....	98
4.2 The principle leaf emitted bVOCs from <i>Brassica napus</i> .....	102
4.3. Gas phase rate coefficients (k) for the reaction of selected terpenes with ozone and their expected half-lives.....	112
5.1 The mixing ratios of the major bVOCs present in the plant chamber prior to and during ozone fumigation.....	129
6.1 Unit masses measured using the PTR-MS during the Bosco Fontana campaign.....	155
6.2 Summary of the bVOC mixing ratios during the Bosco Fontana campaign..	169
6.3 Summary of the BVOC fluxes .recorded during the Bosco Fontana campaign.....	170
6.4 Non-exhaustive summary of isoprene fluxes recorded in the Mediterranean region.....	185
6.5 Leaf level isoprene and monoterpene emission from single leaves.....	190
6.6 Species specific isoprene and monoterpene emission factors.....	196
6.7 Summary of flux quality assessment test results.....	202

# Chapter I

## Introduction

Plants are sessile, so cannot flee in order to avoid attack by harmful organisms. They have therefore evolved numerous mechanisms by which to defend themselves, the most obvious of these being the direct, physical, defences offered by the cuticle and periderm which provide a barrier against ingress by bacteria and fungi. Additional defences such as thorns and spines can provide protection against herbivorous vertebrates. As well as physical defences, plants have also developed a plethora of chemical mechanisms by which to defend themselves. These mechanisms include the production of a wide range of secondary metabolites such as alkaloids, terpenoids and glucosinolates which can directly deter or intoxicate herbivores (Fürstenberg-Hägg et al., 2013; Mithöfer and Boland, 2012). The emission of volatile organic compounds (VOCs) can also provide the plant with an indirect defence, by attracting a predator or a parasite of the organism attacking the plant (De Moraes et al., 1998; Heil, 2008; Kessler and Baldwin, 2001).

The attraction of the predators and parasites of herbivores by biogenically emitted volatile organic compounds (bVOCs) is termed tritrophic signalling. Following attack by herbivorous insects bVOCs emissions can occur as a result of constitutive or induced processes (Maffei et al., 2010). Constitutive bVOCs are stored within the plant in structures such as glandular trichomes and resin ducts and upon insect feeding these structures are broken, releasing an immediate burst of compounds into the

atmosphere. Induced bVOCs are, however, synthesised *de novo* within the plant in response to herbivore attack (Paré and Tumlinson, 1997). The distinct feeding behaviours of different herbivorous species leads to different contributions of constitutive and *de novo* emissions to the total bVOC emission, resulting in the emission of a unique blend of bVOCs (McCormick et al., 2012) thus enabling predators to locate their prey. It has been shown that tritrophic signalling can occur both above and below ground (Kessler and Baldwin, 2001; Rasmann et al., 2005). Numerous compounds have been shown to mediate this plant-insect signalling, including monoterpenes, sesquiterpenes, green leaf volatiles such as hexenol and aromatic compounds such as benzyl cyanide and methyl salicylate (Kessler and Baldwin, 2001; Rasmann et al., 2005; Pinto et al., 2007).

The emission of bVOCs is widely measured using Gas Chromatography-Mass Spectrometry (GC-MS) providing high sensitivity and selectivity (Jansen et al., 2011; Tholl et al., 2006), however, the requirement for sampling prior to lengthy laboratory analysis introduces a significant time delay. The need to achieve analysis at high time resolution has led to the development of a range of novel instruments such as E-noses and biosensors as well as rapid mass spectrometers, for example the proton transfer reaction - mass spectrometer (PTR-MS). Recent developments in PTR-MS technology have improved both the mass resolution and sensitivity of the instrument (Jordan et al., 2009a) and the use of alternative reagent ions has offered an enhanced ability to identify analyte compounds (Jordan et al. 2009b).

Non-methane bVOCs represent a large source of reactive carbon into the atmosphere with  $10^{15}$  g emitted globally (Guenther et al., 2012). As well as their ecological role, these compounds also play an important role in atmospheric chemistry. They contribute to the formation of secondary organic aerosol and, in the presence of  $\text{NO}_x$  ( $\text{NO}$ ,  $\text{NO}_2$  and  $\text{NO}_3$ ), can lead to ozone formation in the troposphere, thus impacting upon both climate and local air quality (Atkinson and Arey, 2003a). While the concentration of ground-level ozone has stabilised in some industrial countries (Oltmans et al., 2013) concentrations are still increasing in parts of Asia (Fu and Tai, 2015). Given the high reactivity of many bVOCs with ozone, it has been hypothesised that ozone may disrupt plant-insect tritrophic signalling. This hypothesis is investigated in detail in some of the following chapters.

In Chapter II the emissions of bVOCs from plants in response to stress and their impact on tritrophic signalling are reviewed, together with a brief discussion of the chemistry of bVOCs in the atmosphere. The instrumentation and techniques currently applied to the measurement and monitoring of bVOC emissions together with their respective advantages and disadvantages are also discussed.

Chapter III, entitled “The analysis of complex organic compounds using SRI-ToF-MS” reports on the application of the recently developed selective reagent ionisation – time of flight – mass spectrometer (SRI-ToF-MS) to the analysis of a series of complex organic compounds. This instrument combines the high time resolution and mass sensitivity of the earlier proton transfer reaction – time of flight – mass spectrometer (PTR-ToF-MS) with the ability to change the ionisation chemistry

within the instrument, thus providing additional structural information on analyte compounds. This instrument is then applied to the analysis of bVOCs in Chapter IV.

In Chapter IV, entitled “The effect of ozone fumigation on the emission of biogenic volatile organic compounds (bVOCs) from *Brassica napus*” the SRI-ToF-MS instrument detailed in Chapter III is used to study the impact of ozone on bVOC emissions from oilseed rape (*B. napus*) plants. Above-ground and below-ground emissions from *B. napus* are reported, prior to and during ozone fumigation, with particular focus on the impact of ozone on both monoterpenes and sesquiterpenes emissions. The mixing ratios of ozone used in these experiments (~100 ppbv) are typical of those that occur during summertime photochemical smog episodes in North America, Europe and Asia.

The effect of ozone on tritrophic signalling is investigated in Chapter V entitled “Ambient ozone degrades plant volatiles and disrupts tritrophic signalling”. This chapter builds on Chapter IV to investigate the impact of ozone on herbivore host location and tritrophic signalling using a *B. napus* – *Myzus persicae* – *Adalia bipunctata* larvae plant-herbivore-predator model system. Insect decision making is monitored using a Y-tube olfactometer and bVOC emissions are recorded using PTR-MS. This experiment is designed to determine a. whether ozone fumigation disrupts insect decision making and b. whether disruption is a result of changes in bVOC emission from the plant or the degradation of bVOCs between the plant and insect.

Chapter VI: “Canopy-scale flux measurements and bottom-up emission estimates of volatile organic compounds from a mixed oak and hornbeam forest in northern Italy” reports bVOC emission at a field scale in a high ambient ozone environment. This chapter compares three methods by which bVOC emission can be determined at the canopy scale: disjunct eddy covariance measurements using PTR-MS, eddy covariance measurements using PTR-ToF-MS and the up-scaling of leaf level GC-MS measurements to the canopy scale.

In Chapter VII the general conclusions of this work are discussed bringing together the research presented in chapters III to VI. The strengths and weaknesses of the findings are highlighted and potential future avenues of research are discussed.

## Chapter II

# Volatile emission from plants and their role in the earth's atmosphere

### 2.1 Emission of volatiles from vegetation

Vegetation covering the Earth's surface releases a diverse range of biogenic volatile organic compounds (bVOCs), the emissions of which are primarily influenced by sunlight and leaf temperature. However abiotic stresses, for example water availability and ozone and biotic stresses such as herbivores and pathogens also influence emissions. These secondary metabolites synthesised by plants have been shown to have many functions including plant-plant communication (Terry et al., 1995; Baldwin et al., 2006), attraction of beneficial organisms such as seed dispersers and pollinators (Pichersky and Gershenzon, 2002; Knudsen et al., 2006), direct defence (i.e. deterring or harming an attacker) (Pichersky and Gershenzon, 2002; Arroyo et al., 2007), indirect defence (i.e. attracting a predator of an attacker) (Dicke et al., 1990; Turlings et al., 1990; Kessler and Baldwin, 2001; Pichersky and Gershenzon, 2002) and mediating the effects of abiotic stresses (Tingey et al., 1980; Sharkey and Singsaas, 1995; Loreto et al., 2006; Sharkey et al., 2008; Holopainen and Gershenzon, 2010). The physiochemical properties of these compounds suggest that bVOC emissions are likely to increase in the future in response to climate change because of their volatile nature and as a result of increased rates of synthesis (Laothawornkitkul et al., 2009; Peñuelas and Staudt, 2010).

Isoprene is the predominant bVOC emitted by plants into the atmosphere with 500-600 × 10<sup>12</sup> g C emitted each year (Arneth et al. 2008; Guenther et al. 2012). In addition to isoprene a wide variety of other bVOCs are released into the atmosphere, with major chemical groups including terpenoids, aromatics, alcohols, aldehydes, ketones, esters, alkanes and alkenes (Kesselmeier and Staudt, 1999; Knudsen et al., 2006; Pichersky et al., 2006; Maffei, 2010). Representative structures of the major classes of bVOCs emitted by plants in response to stress are displayed in Fig. 2.1.

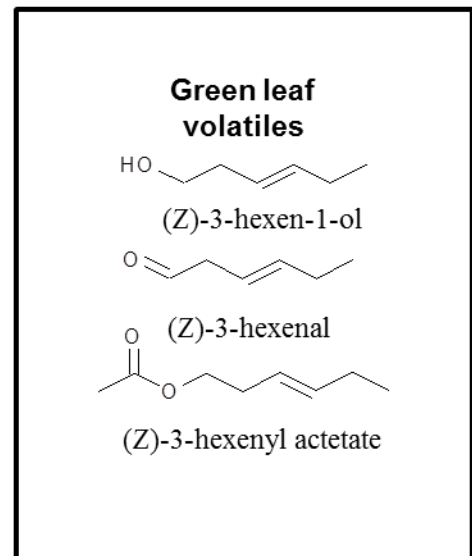
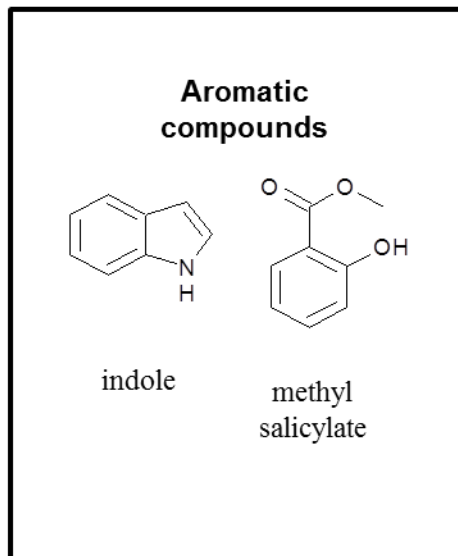
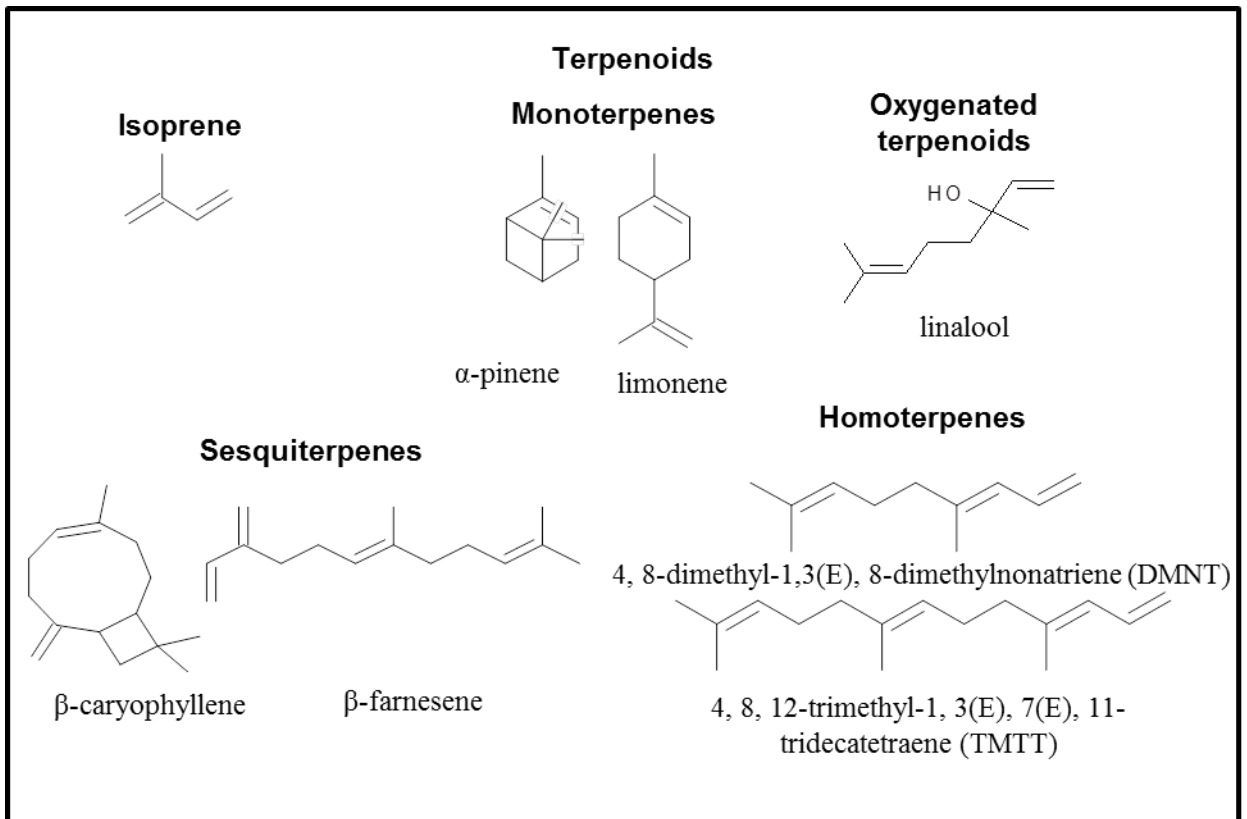


Figure 2.1 Representative structures of some of the major classes of stress-induced bVOCs

## 2.2 Role of bVOCs in tropospheric chemistry

Due to the high levels of bVOC emission into the atmosphere (ca.  $10^{15}$  g year<sup>-1</sup> (Guenther et al., 2012)) and their high reactivity bVOCs play a significant role in the chemistry of the troposphere. bVOCs have lifetimes in the troposphere ranging from minutes to days (Atkinson and Arey, 2003a) depending on their reactivity with respect to NO<sub>3</sub>, O<sub>3</sub> and the OH radical. The fate of VOCs in the troposphere is summarised in Fig. 2.2. The formation of two products of bVOC reactions in the troposphere known to have important impacts on the climate and local air quality, secondary organic aerosol (SOA) and tropospheric ozone, are discussed in sections 2.2.1 and 2.2.3 respectively.

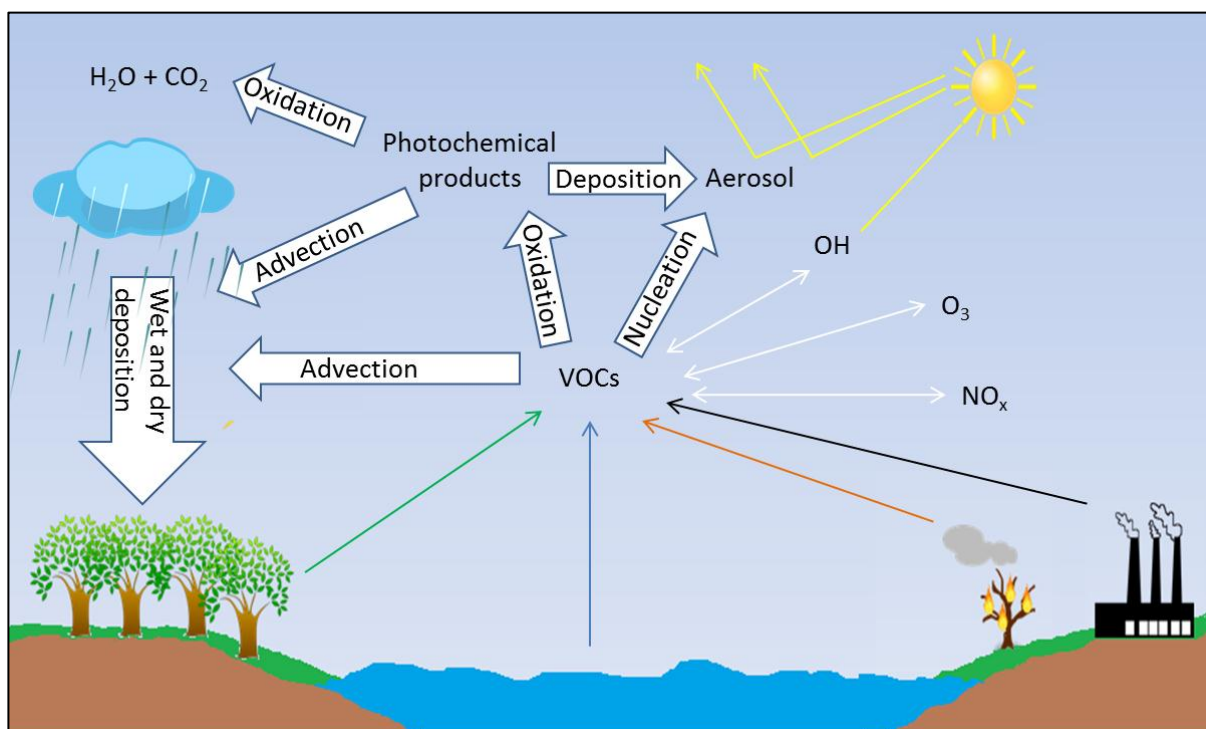


Figure 2.2. A schematic overview of the chemistry of VOCs in the troposphere.

### 2.2.1 Secondary organic aerosol (SOA) formation

The oxidation of bVOCs in the atmosphere by  $\text{NO}_3$ ,  $\text{O}_3$  or OH leads to the formation of a wide range of low volatility oxygenated species. Recent chamber experiments by Ehn et al. (2014) demonstrated that the oxidation of the monoterpene  $\alpha$ -pinene causes the formation of large quantities of extremely low volatility organic compounds (ELVOCs). These compounds can then play an important role in aerosol formation (Kulmala et al., 2013) and growth through condensation onto aerosol surfaces (Kulmala et al., 2013; Ehn et al., 2014). Lee et al. (2006) investigated the yield of SOA from the ozonolysis of ten different terpenes observing yields of SOA in the range 1 to 54 %.

Aerosol plays a key role in many atmospheric processes; providing a site for heterogeneous reactions, acting as cloud condensation nuclei and absorbing and scattering radiation (Hallquist et al., 2009; Monks et al., 2009). Aerosols, therefore, have a significant impact upon both atmospheric chemistry as well as climate through their contribution to radiative forcing (IPCC, 2007).

### 2.2.2 Tropospheric ozone formation

Ozone is formed in the troposphere by the photolysis of  $\text{NO}_2$ :



where M represents another molecule, normally N<sub>2</sub> because of its overwhelming abundance in the atmosphere. In the presence of VOCs, NO<sub>2</sub> can be reformed by the reaction of NO with RO<sub>2</sub><sup>•</sup> and HO<sub>2</sub><sup>•</sup> radicals formed by the oxidation of VOCs:



therefore resulting in the net production of ozone (Atkinson and Arey, 2003a). Tropospheric ozone concentrations in industrialised countries have stabilised recently due to enhanced control of ozone precursor (NO<sub>x</sub> (NO and NO<sub>2</sub>) and VOCs) emissions (Parrish et al., 2012; Oltmans et al., 2013), however in high pollution episodes such as the 2003 European heat wave ozone mixing ratios can reach ca. 200 ppb (Royal Society, 2008). In some parts of the world, for example East Asia, ozone concentrations in the troposphere may still be increasing (Fu and Tai, 2015). Tropospheric ozone is an important atmospheric pollutant with substantial impacts on human health, for example contributing to ca. 21000 premature deaths in the European Union each year (Royal Society, 2008). Ozone may also impact upon crop yields (Ashmore, 2005) with an estimated \$14 – 26 billion in global yield losses in the year 2000 (Royal Society, 2008).

### 2.2.3 The reaction of ozone with bVOCs

In the troposphere ozone reacts with bVOCs leading to the rapid loss of many compounds directly emitted by plants. The lifetime of bVOCs with respect to ozone in the atmosphere ranges from years for simple oxygenated compounds such as methanol and acetone to minutes for large hydrocarbons such as the sesquiterpene  $\beta$ -caryophyllene (Atkinson and Arey, 2003a). bVOCs are also oxidised through reaction with OH radicals, the lifetime of bVOCs with respect to OH radicals ranges from days for small oxygenated compounds to tens of minutes for large hydrocarbons like sesquiterpenes (Atkinson and Arey, 2003a). Ozone reacts rapidly with molecules containing an alkene functional group via the mechanism proposed by Criegee (1975). In this reaction ozone reacts with the carbon-carbon double bond leading to the formation of a primary ozonide. This primary ozonide then rapidly decays to form an energy rich Criegee intermediate and a carbonyl compound. The Criegee intermediate may be then be collisionally stabilised, or, in the case of dialkyl and syn-monosubstituted substituted Criegee intermediates, decay to OH and a substituted alkyl compound and in case of unsubstituted and anti-monosubstituted Criegee intermediates decompose to  $\text{CO}_2$  and RH (Kroll et al., 2001; Atkinson and Arey, 2003a). As many bVOC species contain alkene functional groups (Fig. 2.1) the reaction of ozone with these compounds leads to the rapid oxidation of many bVOCs in the atmosphere.

## **2.3 bVOC emissions from plants in response to stress**

### **2.3.1 bVOC emissions from plants in response to abiotic stress**

bVOC emissions from plants have been shown to change in response to abiotic stresses such as drought, flooding, ozone, transient high temperature and changes in light level. The emission rates of many bVOCs have been shown to increase exponentially with temperature as enzyme activities rise and bVOC vapour pressures are increased (Tingey et al., 1980; Peñuelas and Llusà, 2001). High light intensity increases the rate of photosynthesis which in turn increases the rate of bVOC emission as many non-stored bVOCs require photosynthetic products for their synthesis (Peñuelas and Llusà, 2001). Whilst the effect of light and temperature on bVOC emission has been investigated, there is limited data available on their influence on many major agricultural crop species. Schuh et al. (1997) investigated the effect of temperature and light on bVOC emission from sunflowers, demonstrating an increase in bVOC emissions (isoprene and monoterpenes) in response to increasing light and temperature. Maes and Dedergh (2003) established that continuous light induced the continuous emission of the sesquiterpene  $\alpha$ -copaene from tomatoes.

Ozone stress has been particularly widely studied because of its ubiquitous presence as a ground level air pollutant (Laothawornkitkul et al., 2009). Ozone pollution causes oxidative stress and is known to have an adverse effect on crop yields (Ashmore, 2005). Much of this work has focussed on tree species (Heiden et al., 1999; Llusà et al., 2002; Vuorinen et al., 2005; Fares et al., 2010) because of their large contribution to total bVOC emissions, but the effects of ozone on bVOC emissions from a range of crop plants has also been investigated. bVOC emissions and ozone effects have been

reported from lima beans (Vuorinen et al., 2004), maize (Heiden et al., 2003; Wildt et al., 2003), canola (Wildt et al., 2003) tomato (Heiden et al., 2003) and sunflower (Heiden et al., 2003; Wildt et al., 2003).

Investigations into the effect of ozone on the emission of isoprene have shown conflicting results with Fares et al. (2006) reporting an increase in isoprene emission following ozone exposure, whilst Ryan et al. (2009) and Fares et al. (2010) observed a decrease or no significant effect. The effect of ozone on the emission of monoterpenes has been shown to vary between species and time of year (Llusià et al., 2002; Vuorinen et al., 2005). However, ozone has been shown to enhance the emissions of a wide variety of compounds include methyl salicylate, sesquiterpenes (Heiden et al., 1999), homoterpenes (Vuorinen et al., 2004) and a range of C<sub>6</sub> to C<sub>10</sub> aldehydes (Wildt et al., 2003).

Lack or excess of water is known to affect bVOC emissions from plants with changes in emissions having been reported in tree species in response to both flooding (Copolovici and Niinemets, 2010) and drought (Fang et al., 1996; Brüggemann and Schnitzler, 2002; Pegoraro et al., 2004; Plaza et al., 2005; Rennenberg et al., 2006; Ormeño et al., 2007). In response to water logging Copolovici and Niinemets (2010) reported increased emissions of ethanol and products of the lipoxygenase pathway initially, followed by a full or partial recovery. The effect of drought on bVOC emissions has been more widely studied than flooding with a decrease in isoprene emission following drought observed in a number of studies (Fang et al., 1996; Brüggemann and Schnitzler, 2002; Pegoraro et al., 2004). The effect of drought on monoterpene emissions varies between species with both increases and decreases

observed following drought (Rennenberg et al., 2006; Ormeño et al., 2007). The threat of climate change has led to increased research into agricultural plants' responses to drought (Chaves and Davies, 2010) but there has been little research published on the effect of flooding or drought on bVOC emissions from significant crop species. Use of the term bVOC here excludes ethylene (for reasons described below) which is known to be intimately involved in such responses and for which there is wealth of supporting literature.

Other abiotic factors which have been shown to affect the bVOC emissions from plants include soil nutrient availability and the application of agrochemicals. Herbicides such as paraquat have been shown to induce the emissions of isothiocyanates from model plant species (Vercammen et al., 2001) but there is no literature detailing the effect of pesticides on bVOC emissions. Soil nutrient availability has been shown to have some effect on emissions from wheat plants (Szpeiner et al., 2009). This investigation used an e-nose to distinguish between different soil and herbivore treatments but volatile identification was not possible.

### **2.3.2 The effect of biotic stress on bVOC emissions and tritrophic signalling**

After attack by a herbivore or pathogen there is an immediate release of a range of bVOCs into the atmosphere (Dudareva et al., 2006), from a variety of plant structures. In many species bVOCs, particularly terpenoids, are synthesised and stored in resin ducts or glandular trichomes (Maffei, 2010). These stored bVOCs are released into the atmosphere when the structure is damaged, providing direct and indirect defence against feeding herbivores (Kessler and Baldwin, 2001; Unsicker et al., 2009). As with stored terpenoids, green leaf volatiles (GLV), a family of compounds predominantly consisting of isomers of hexenol, hexenal and hexenyl acetate, are released rapidly following plant damage (Dicke, 2009). These compounds are produced by lipoxygenase activity and make up the smell of freshly cut grass (Maffei, 2010). A study into the effect of these compounds on *Colletotrichum acutatum* demonstrated an inhibition of mycelial growth upon exposure to hexanal and (E)-hex-2-enal and that some effect may also be shown by hexanol, (Z)-hex-3-enol and (E)-hex-2-enol (Arroyo et al., 2007).

As well as emissions from pools of stored compounds, it has been shown that synthesis of bVOCs can be induced by exposure to biotic stresses (Paré and Tumlinson, 1997) and even herbivore egg deposition (Hilker and Meiners, 2006). bVOCs such as indole and some acyclic terpenes and homoterpenes have been shown to be synthesised *de novo* with emissions occurring after a lag time of up to a day after insect feeding (Paré and Tumlinson, 1997). Unlike the release of stored compounds, emissions of induced compounds require the recognition of an attacking insect and

often occur systematically throughout the whole plant rather than just at the wounding site (Maffei, 2010).

Most research reporting bVOC emissions from plants focuses primarily on terpenoids, green leaf volatiles, polar molecules such as methanol and other relatively large or polar species. This is a result of a greater interest in the role of these species in atmospheric science and the development of analytical technologies optimised for isoprene and monoterpenes. For example proton transfer reaction-mass spectrometry would not usually detect ethylene as it has a lower proton affinity than water (although it has been shown by Soukoulis et al. (2012) that ethylene can be detected via a charge transfer reaction in the presence of  $O_2^+$ ). As a result several stress-induced compounds which should fall under the definition bVOC, notably ethylene, are seldom reported in literature focusing on bVOC emission. Ethylene is a plant hormone responsible for the regulation of many plant metabolic processes and is emitted in response to both biotic and abiotic stress (Bari and Jones, 2009; Bleeker and Kende, 2000).

Variations in the emissions of bVOCs in response to biotic stresses have been shown to be dependent on the plant structures damaged by pest/disease attack. For example Jansen et al. (2009) demonstrated that stroking the stems of tomatoes resulted in the emission of a range of terpenes from trichomes whereas side shoot removal lead to an increase in the emission of green leaf volatile species caused by damage to cell membranes. As different species of insect and pathogen have different modes of attack, different plant structures will be damaged in different ways, potentially inducing the emission of a unique bouquet of bVOCs.

There is now a significant body of evidence which demonstrates that insects are able to make use of bVOC patterns emitted by healthy and biotically stressed plants to locate suitable hosts and prey from a complex background bVOC emission caused by abiotic stresses and neighbouring plant species (Quiroz et al., 1997; Krieger and Breer, 1999; Dicke and van Loon, 2000; Dicke, 2009; McCormick et al., 2012). In addition, such volatile blends ensure that herbivorous insects can actively avoid non-host species or nutritionally inferior plants, e.g. plants already harbouring significant numbers of insects, and avoid consequential inappropriate behaviour such as egg laying (Bruce and Pickett, 2011). Exposure to blends of bVOCs induces stronger insect behavioural responses than individual compounds, and if the ratio between the compounds is altered, an attractive blend of bVOCs can become less attractive or even repellent (Visser and Avé, 1978; Bruce et al., 2005; Bruce and Pickett, 2011). Despite the specificity of bVOC blends it has been shown that there is a degree of flexibility in the signal, some compounds are essential for the signal and others can be omitted or substituted with little effect on signalling (Cha et al., 2008; Bruce and Pickett, 2011). The essential component of the volatile signal is not necessarily the most abundant in a blend - indeed the volatile that conveys most information to the insect detector can be quite a minor component.

### **2.3.3 The effect of multiple stresses**

Plants are rarely exposed to one stress in isolation, and in the real world they are likely to be exposed to multiple stresses simultaneously. For predatory insects reliant upon identifying the specific cause of plant stress in order to locate their prey this presents a challenge, as many plant species emit the same bVOC species in response to both biotic and abiotic stress (Heiden et al., 2003). The research that has been carried out

into the effect of multiple stresses on plant volatile emissions has been reviewed by Holopainen and Gershenzon (2010). The effect of a range of abiotic stresses on plants exposed to both true biotic (Ibrahim et al., 2008; Himanen et al., 2009; Winter et al., 2012) and ‘artificial’ biotic stress mimicked by wounding and exposure to one of caterpillar regurgitant (Gouinguene and Turlings, 2002), volicitin, jasmonic acid or ethylene (Schmelz et al., 2003), have been investigated. It has been shown that nutrient level (Schmelz et al., 2003; Ibrahim et al., 2008), high copper concentrations (Winter et al., 2012) and elevated carbon dioxide and ozone (Himanen et al., 2009) all affect emissions in response to biotic stress. Gouinguéné and Turlings (2002) found that soil humidity, temperature, light and fertilization rate influenced both the quantity and, significantly, the relative ratios of the compounds emitted from maize plants exposed to artificially replicated caterpillar feeding. Such a change in the ratio of compounds emitted introduces additional complexity into plant – insect signalling.

Research into the effect of multiple biotic stresses has focused on maize (Rostás et al., 2006; Rasmann and Turlings, 2007; Erb et al., 2010). Rostás and co-workers (2006) demonstrated that when challenged by fungal infection (*Setosphaeria turcica*) the volatile emissions from maize plants subject to herbivory (*Spodoptera littoralis*) were reduced by 47 % but that the parasitoids *Cotesia marginiventris* and *Microplitis rufiventris* responded equally well to herbivore-damaged and fungus-herbivore-damaged plants. With respect to combined attack from multiple herbivores to either the root and leaves (Rasmann and Turlings, 2007) or different leaves on the same plant (Erb et al., 2010) it was shown that despite multiple biotic stresses altering the bVOC emission from maize, tritrophic signalling continued to function. Other studies indicate that the effect on volatile emission of infestation by two differing pest species

may be a reduction (Rodriguez-Saona et al., 2003) or an increase (Moayeri et al., 2007) in emission using cotton or pepper plants respectively.

#### **2.3.4 The effect of ozone on tritrophic signalling**

In response to ozone, some tritrophic systems have been shown to be robust and to continue to function despite the effects of multiple stresses. Vuorinen et al. (2004) demonstrated that both ozone and two-spotted spider mites (*Tetranychus urticae*) induced the emission of the homoterpenes (E)-4,8-dimethyl-1,3,7-nonatriene (DMNT) and (E,E)-4,8,12-trimethyl-1,3,7,11-tridecatetraene (TMTT) from lima beans but that predatory mites (*Phytoseiulus persimilis*) could distinguish between infested and uninfested plants when both were exposed to ozone.

As well as affecting bVOC emissions from plants, abiotic factors such as ozone concentration also influence the lifetime of primary bVOCs in the atmosphere. It has been shown for both lima bean and cabbage that while enhanced ozone levels degrade terpenes and green leaf volatiles in the head space above herbivore infested plants, other bVOCs such as methyl salicylate were not significantly reduced and tritrophic signalling was not disrupted (Pinto et al., 2007a; Pinto et al., 2007b). Owing to the stability of these compounds in the presence of ozone, host location by the parasitic wasp *Cotesia plutellae* has been shown to be unaffected by ozone both at the laboratory and field scales (Pinto et al., 2007a; Pinto et al., 2007b; Pinto et al., 2008). However, both plant–plant and plant–pollinator communications have been shown to be disrupted by ozone exposure (Blande et al., 2010; Farre-Armengol et al., 2015). These data underpin the notion that key volatiles in a mixture mediate the plant–insect or tritrophic interaction and those systems dependent on bVOCs which are more

sensitive to ozone may be at greater risk of disruption under elevated ozone concentrations.

The disruption of plant-insect signalling could also impact upon a number of integrated pest management (IPM) strategies. IPM strategies are agricultural techniques developed in order to minimise agricultural pesticide requirements through the complementary adoption of alternative methods to control pests, diseases and weeds. While many IPM strategies are unaffected by changes in plant volatile emissions the use of push – pull and VOC monitoring systems could be significantly inhibited. Push – pull strategies are crop protection strategies which aim to manipulate the behaviour of insect pests and their natural enemies by the integration of stimuli with the protected crop which deter pests (push) while luring them towards an attractive source (pull). While some systems make use of visual stimuli, many are dependent on olfactory stimuli such as the aphid alarm pheromone (E)- $\beta$ -farnesene (Cook et al., 2007; Khan et al., 2010) making them sensitive to ozone-induced disruption to plant–insect communication. VOC monitoring strategies in the context of IPM work by eavesdropping upon tritrophic communication to enable targeted, and therefore reduced, pesticide application (Laothawornkitkul et al., 2008; Jansen et al., 2011). The loss of key bVOCs by ozonolysis or changes in the emission of bVOCs in response to oxidative stress could significantly hamper the application of this developing technology.

## **2.4 Measurement of bVOCs**

The instrumentation and experimental techniques commonly used to detect bVOCs in the atmosphere has already been comprehensively reviewed (e.g. Tholl et al., 2006; Ortega and Helmig, 2008; Zhang and Li, 2010). This section is not therefore designed to discuss every aspect of the detection of VOCs but is instead focussed on the application of these instruments to the detection of biotic and abiotic stresses in plants and the relative advantages and disadvantages of different analytical methods.

### **2.4.1 Instrumentation**

Gas liquid chromatography (GC) coupled with either mass spectrometry (GC-MS) or flame ionisation detection (GC-FID) is the most widely applied method for the detection of VOCs released from plants in response to both biotic and abiotic stresses (Sankaran et al., 2010; Jansen et al., 2011). Sample collection methods vary but the general principle is as follows. A VOC sample is trapped onto an adsorbent allowing the VOC to be concentrated prior to analysis; the trapped VOCs are then released by solvent extraction or by thermal desorption. The gas chromatograph then separates compounds based on their affinity for a stationary phase, a polymer on an inert support, and a mobile phase, usually an inert gas such as helium, thus allowing the compounds to enter the detector individually. Once separated, the compounds are identified using one of a range of detectors, the two most commonly used for plant volatile analysis being FID and MS. FID has traditionally been used because of its wide linear dynamic range, stable response, and high sensitivity with limits of detection in the  $10^{-15} - 10^{-12}$  g range (Tholl et al. 2006). Increasingly, MS is becoming the preferred method of detection because of its high sensitivity with limits of detection now also possible in the  $10^{-15} - 10^{-12}$  g range and because the observed

molecular fragmentation patterns provide the structural information needed to aid compound identification.

The principle disadvantages of GC-MS when compared to the other analytical tools discussed below is that conventional GC-MS instruments are delicate and expensive, and the analysis of results requires skilled operatives. The time delay inevitable between the collection of a sample and full data analysis makes the GC-MS less suitable for monitoring bVOC emissions and reactions at high time resolution in the laboratory and field. Despite these hurdles, advances in the portability and automation of instruments are beginning to make the use of GC-based methods in the field a possibility (Kunert et al., 2002; Smith et al., 2005; Su et al., 2008). The widespread use of GC-MS for the detection of bVOCs emitted from plants has led to the use of GC-MS as a standard method to which other instruments are compared (Laothawornkitkul et al., 2008; Kajos et al., 2015). Due to the structural information provided by GC-MS this technique is often used to support analysis by high time resolution instruments (Schaub et al., 2010; Kreuzwieser et al., 2014). Notwithstanding this, GC-FID is also often used to complement GC-MS methods.

Differential mobility spectrometry (DMS) and field asymmetric waveform ion mobility spectrometry (FAIMS) separate ions on the basis of their differing mobilities in high and low electric fields. These technologies has been applied either alone, or with gas chromatography or mass spectrometry, to the analysis of chemical weapons, explosives, pharmaceuticals, pollutants and biologically active molecules (Guevremont, 2004; Kolakowski and Mester, 2007; Kanu, et al., 2008). A miniature spectrometer based around this technology has been described by Wilks et al. (2012);

coupled with gas chromatography (GC-FAIMS) this instrument has been shown to detect volatiles emitted from wooden panels at ppb concentrations showing the potential of this technology to detect blends of biogenic molecules (Schumann et al., 2012). Zhang and co-workers (Zhang et al., 2011) used a Lonestar FAIMS device in a short study to observe the gradual development of powdery mildew in tomatoes but it has yet to be shown that a DMS or FAIMS device can successfully distinguish between stresses in plants.

Electronic noses (e-noses) make use of an array of sensors in an attempt to mimic a mammalian nose. A basic e-nose consists of an array of chemical sensors which undergo a reversible chemical interaction when exposed to gaseous chemicals (VOCs) altering the physical properties of the sensor (e.g. electrical properties, mass, colour or temperature) indicating the presence of the VOC (Wilson and Baietto, 2009). This gives a signal which corresponds to one particular VOC finger print e.g. a healthy plant, and using statistical methods (Ghaffari et al., 2010; Sankaran et al., 2010) this can be distinguished from the signal produced as a result of exposure to VOCs emitted by a plant under biotic stress. Therefore whilst plant stress can be identified, the individual compounds emitted by the plant cannot be identified. For a detailed description of the operating principles and alternative applications of e-noses see Arshak et al., (2004) and Wilson and Baietto (2009).

E-noses have limits of detection in the range of ca.  $10^{-6}$  as a volume mixing ratio (i.e. ppmv, rather than ppbv; Zhou & Wang 2011) making them less sensitive than chromatographic and mass spectrometric methods. Despite this, they are used in a wide variety of industries because they are comparatively cheap and portable. These

attributes have increasingly led to them being applied to the detection of plant stress. For example Laothawornkitkul et al. (2008) and Ghaffari et al. (2010) have both shown the potential of e-noses to distinguish between healthy and infected tomato plants, and Zhou and Wang (2011) were able to distinguish between rice plants with different types of damage. To improve the limits of detection they have also been used in combination with pre-concentration followed by chromatography (Kunert et al., 2002; Miresmailli et al., 2010).

Biosensors are chemical sensors which make use of the high sensitivity of biological components. A generic biosensor is made up of a biological component (e.g. enzymes, antibodies, nucleic acid, microorganism and cells) responsible for chemical detection, connected to an electronic component which transforms the chemical signal produced by the biological component into an electrical signal (Sevonkaev and Katz, 2008). It has been proposed that small, low cost biosensors could play a significant role in the detection of plant diseases due to their ability to provide on-line measurements (Velasco-Garcia and Mottram, 2003). Whilst biosensors have been used to detect VOC emissions associated with plant stress, for example Schütz et al., 1999 used a biosensor to detect potato tubers infected with *Phytophthora infestans*, with the possible exception of DMS and FAIMS they have received far less attention than the other instruments discussed here.

The analytical method most widely used for the detection of bVOCs is now proton transfer reaction-mass spectrometry (PTR-MS). Increasingly proton transfer reaction-time of flight-mass spectrometry (PTR-ToF-MS) is also becoming applied as well (Fig. 2.3). PTR-MS and PTR-ToF-MS are widely used in the atmospheric chemistry

community to measure concentrations of VOCs in the atmosphere due to their ability to provide real time measurements of concentrations in the  $10^{-9}$  -  $10^{-12}$  volume mixing ratio range (Lindinger et al., 1998a; Lindinger et al., 1998b; Hayward et al., 2002; Hewitt et al., 2003; Blake et al., 2009).

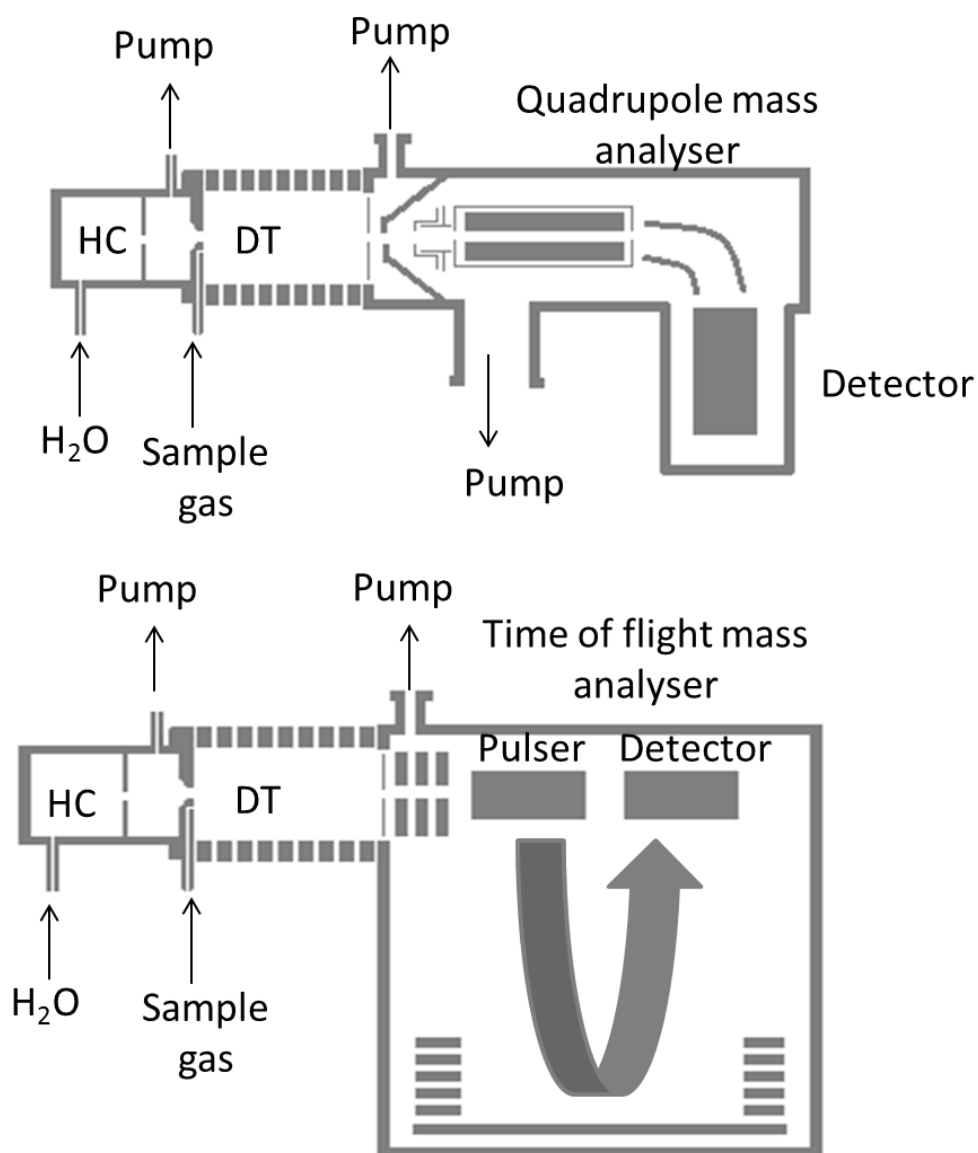


Figure 2.3 Schematic representations of the PTR-MS (top) and the PTR-ToF-MS (bottom). HC represents hollow cathode and DT represents drift tube.

PTR-MS has been thoroughly reviewed (Blake et al. 2009) so the operating principle will only be briefly described here.  $H_3O^+$  ions are formed from water in the hollow

cathode ion source, these ions then enter the drift tube where they undergo a proton transfer reaction with any molecule with a proton affinity greater than water (166.5 kcal mol<sup>-1</sup> (Lindinger et al., 1998b)). Most organic molecules (represented by *R* in equation 1), with the exception of most alkanes, have a proton affinity greater than this so they react as shown in equation 5, the principle components of air have a lower proton affinity than water so act as a buffer gas.



Fragmentation within the drift tube is controlled by the ratio of the electric field applied across the drift tube and the buffer gas number density (*E/N*). The *E/N* is usually controlled so that both fragmentation and cluster formation within the drift tube is minimised. This generally corresponds to an *E/N* value within the range 120 – 130 Td (1 Td = 10<sup>-21</sup> V m<sup>-2</sup>). Increasing or decreasing the *E/N*, leading respectively to an increase in fragmentation or an increase in cluster formation can, however, provide valuable structural information.

Upon leaving the drift tube the ionised molecules then enter a quadrupole mass filter which selects molecules on the basis of their mass to charge ratio prior to detection. The proton transfer reaction is a form of chemical ionisation, this can be thought of as a soft method of ionising molecules so that fragmentation is reduced, simplifying the observed mass spectrum. Unlike GC-MS, in PTR-MS the sample does not require pre-concentration or separation prior to detection, enabling it to provide real time measurements of VOC emission from plants. As a result of this PTR-MS has become widely used for high time resolution bVOC measurements such as recording fluxes of

VOCs (Davison et al., 2008; Müller et al., 2010) and wounding events (Peñuelas et al., 2005; van Dam et al., 2012).

At field scale PTR-MS and PTR-ToF-MS have been used to monitor bVOC emissions during high stress events such as grazing by large herbivores (Bartolome et al., 2007) and harvesting (Ruuskanen et al., 2011). Research at plant and branch scale has shown the potential of PTR-MS to detect smaller stress events. Both PTR-MS and PTR-ToF-MS have been shown to be effective in the detection of plant wounding (Fall et al., 1999; Brilli et al., 2011) and it has been used to detect plant response to insect feeding (Peñuelas et al., 2005; von Dahl et al., 2006; Danner et al., 2012). Schaub and co-workers (2010) used PTR-MS to monitor real time VOC emissions from *Populus tremula* L. × *P. tremuloides* showing that the VOC emissions released in response to insect feeding were quantitatively and qualitatively different to emissions in response to wounding.

The principal disadvantage of PTR-MS when compared with GC-based methods is that the identification of an analyte is solely reliant upon the protonated parent ion or, in some cases, a principal fragment ion at unit mass resolution. It is therefore impossible to separate isobaric compounds. Maleknia and co-workers (2007) evaluated the PTR-MS analysis of the major classes of plant-emitted VOCs and concluded that the ions formed were not simply  $MH^+$  but that proton-bound clusters and fragmentation ions were formed, highlighting the difficulty of using this technique alone for VOC identification. For this reason, the complementary use of GC-FID or GC-MS to provide unambiguous compound identification is essential. The development of the time-of-flight variant of PTR-MS (PTR-ToF-MS) overcame this

issue, operating at a mass spectral resolution  $> 5000 \text{ m}/\Delta\text{m}$ , thereby enabling the separation of isobaric compounds and the identification of the analytes molecular formula. Additional advantages of the time of flight mass spectrometer as opposed to the quadrupole mass spectrometer used in the PTR-MS are the ability to analyse the entire mass range with a very short response time (ca. 100 ms) and with a much higher degree of sensitivity at high masses ( $> \sim 150$  mass units; Jordan et al., 2009a; Müller et al., 2010) allowing a much wider spectrum of compounds to be monitored. However, in order to determine the structural formula of a molecule a chromatographic method is still required.

An additional disadvantage of PTR-MS is that only compounds with a hydrogen ion affinity greater than that of water will be protonated in the instrument. Hence some potentially important compounds, including for example ethylene, do not undergo proton transfer reactions so cannot be detected. This problem has been at least partially overcome by the recently developed selective reagent ion – time of flight – mass spectrometer (SRI-ToF-MS) which allows ionisation with  $\text{O}_2^+$ ,  $\text{NO}^+$  or  $\text{Kr}^+$  in addition to  $\text{H}_3\text{O}^+$ , hence enabling the analysis of a greater variety of analyte compounds and the identification of functional groups (Jordan et al., 2009b; Sulzer et al., 2012a). For example Soukoulis et al. (2012) demonstrated that the use of  $\text{O}_2^+$  as a reagent ion enabled the detection of ethylene. In the field this instrument operated using  $\text{NO}^+$  as the reagent ion has enabled the separation of isoprene and 2-methyl-3-buten-2-ol (MBO) (Karl et al., 2012). The principle mass spectral fragment formed following the ionisation of MBO with  $\text{H}_3\text{O}^+$  is  $\text{C}_5\text{H}_9^+$  making it indistinguishable from isoprene. When both species are ionised using  $\text{NO}^+$  isoprene undergoes charge transfer giving a mass spectral peak at  $\text{C}_5\text{H}_8^+$  and MBO undertakes hydroxide ion

transfer leading to the formation of a mass spectral peak at  $C_5H_9^+$  thus enabling the two compounds to be separated. As with chromatographic techniques both PTR-MS and SRI-MS instruments are costly and the analysis and interpretation of results requires highly skilled operatives.

## **2.5 Measurement of bVOC fluxes**

Chemistry in the lower atmosphere is largely driven by the emission and deposition of trace gases from the earth's surface (Monks et al., 2009). In order to understand chemistry in the lower atmosphere it is important that fluxes of trace gases can be quantified. Fluxes of bVOCs can be recorded at a canopy or regional scale through “top down” and “bottom up” measurements. The “bottom up” approach is carried out by up scaling branch or plant scale measurements to a regional or canopy scale using models such as the Model of Emissions of Gases and Aerosols from Nature (MEGAN) developed by Guenther et al. (2006). “Top down” measurements are performed using remote sensing or micrometeorological techniques. In Chapter VI “bottom up” measurements are compared with “top down” micrometeorological measurements made using virtual disjunct eddy covariance (vDEC) measurements recorded using a PTR-MS.

### **2.5.1 Eddy covariance**

Eddy covariance is the most direct and one of the most widely applied techniques for the measurement of atmospheric fluxes (Burba, 2013) and is based upon the recording of turbulent transport. Atmospheric turbulence is the principle transport mechanism in the planetary boundary layer (PBL). Eddies are formed within the PBL by wind shear and these eddies can vary greatly in size from greater than 1 h to less than 0.1 s.

Molecules, aerosol particles and heat momentum are all transported in the PBL by the random motion of these eddies. By recording, at a high frequency, both the mixing ratio of the species of interest ( $\chi$ ) and the vertical wind speed ( $w$ ) over time ( $t$ ) the vertical flux of the species of interest can be determined (Aubinet et al., 2012). Due to the random nature of eddies measurements are typically averaged over a period of ca. 30 min to ensure that the flux contribution from low frequency eddies are captured within the averaging period.

The principle disadvantage of direct eddy covariance is the requirement for a very high (ca. 10 Hz) measurement response time. Vertical wind speed and concentration measurements must be made at a frequency sufficient to resolve all the turbulent eddies contributing to the flux (McMillen, 1988). In order to capture high frequency eddies sensors must, therefore, be able to record at ca. 10 Hz. The PTR-ToF-MS is capable of operating at these frequencies so may be used for direct eddy covariance measurements. Prior to the development of the PTR-ToF-MS disjunct and virtual disjunct eddy covariance systems were developed to enable eddy covariance VOC flux measurements to be made using PTR-MS. Another disadvantage of direct eddy covariance measurements is the large volumes of data generated over short measurement periods making data storage and processing challenging.

### **2.5.2 Disjunct and virtual disjunct eddy covariance**

During eddy covariance measurements air is sampled continuously, however, fluxes can be calculated using a subset of this time series. It is therefore possible to rapidly trap air samples for analysis at comparatively large time intervals (Rinne et al., 2001). This leads to the formation of a discontinuous time series but each point still represent

a fast response measurement. Instruments operating at a lower time resolution, such as the PTR-MS can then be used to record VOC concentrations within the trapped samples. By combining this, disjunct, concentration data set with high resolution vertical wind velocities the VOC flux can be calculated in the same manner as in direct eddy covariance measurements. This method is termed disjunct eddy covariance (Rinne et al., 2001). Grabmer et al. (2004) compared this technique to relaxed eddy accumulation and enclosure measurements at field scale concluding that the disjunct eddy covariance flux measurements compared well with fluxes calculated using established techniques.

Virtual disjunct eddy covariance is a variation of the disjunct eddy covariance method described by Rinne et al. (2001). This method was first applied to VOC flux measurement by Karl et al. (2002) above a subalpine forest. The virtual disjunct eddy covariance system removes the need for a grab sampling system. Instead air is purged continuously through the PTR-MS and the time interval between measurements is controlled by the dwell time of the PTR-MS's quadruple mass analyser. This leads to a virtually disjunct concentration data set which may be treated in the same manner as the disjunct eddy covariance data set. As the virtual disjunct eddy covariance system does not require air samples to be trapped prior to analysis this leads to a much simpler inlet system.

## Chapter III

# The analysis of complex organic compounds using SRI-ToF-MS

This chapter aims to investigate the impact of changing the drift tube energy and ionisation chemistry on the ionisation and fragmentation of a range of complex organic molecules using the recently developed selective reagent ionisation - time of flight - mass spectrometer (SRI-ToF-MS). Ten new psychoactive substances (NPS) were used to study ionisation within the SRI-ToF-MS as the detection of these compounds is highly topical and they provide a structurally diverse group of compounds to study. The effect of the chemical ionisation of a range of NPS using the reagent ions  $\text{H}_3\text{O}^+$ ,  $\text{NO}^+$ ,  $\text{O}_2^+$  and  $\text{Kr}^+$  on the formation of mass spectral fragments and clusters in the  $E/N$  (the ratio of the electric field,  $E$ , to the buffer gas number density,  $N$ ) range 85-225 Td (45-115 Td when using  $\text{Kr}^+$ ) was investigated. It was also demonstrated that by changing the ionisation chemistry two isomeric species could be separated. The findings presented here, while focused on NPS, can equally be applied to biogenically emitted compounds.

This work is presented as two papers. The first was submitted to the International Journal of Mass Spectrometry on the 23<sup>th</sup> October 2013, accepted for publication on the 13<sup>th</sup> December and published online on the 22<sup>th</sup> December. The second was submitted to Journal of Mass Spectrometry on 6<sup>th</sup> June 2013, accepted for publication

on the 11<sup>th</sup> July and published in September 2013. The authors and their contributions are listed below:

**Headspace analysis of new psychoactive substances using a Selective Reagent Ionisation-Time of Flight-Mass Spectrometer**

Acton W. J., Lanza M., Agarwal B., Jürschik S., Sulzer P., Breiev K., Jordan A., Hartungen E., Hanel G., Märk L., Mayhew C. A. and Märk T. D.: Headspace analysis of new psychoactive substances using a Selective Reagent Ionisation-Time of Flight-Mass Spectrometer, International Journal of Mass Spectrometry, 360, 28-38, 2014.

**Acton W. J. (Lancaster University):** Designed experiment, carried out data processing and analysis and wrote manuscript.

**Lanza M. (Iconicon Analytik):** Designed experiment, carried out data processing and analysis and wrote manuscript.

**Agarwal B. (Iconicon Analytik):** Carried out preliminary experiments and helped with manuscript preparation.

**Jürschik S. (Iconicon Analytik):** Provided guidance on data analysis and helped with manuscript preparation.

**Sulzer P. (Iconicon Analytik):** Provided guidance on experimental design and data analysis and helped with manuscript preparation.

**Breiev K., Jordan A., Hartungen E., Hanel G., Märk L. and Märk T. D. (Iconicon Analytik):** Offered advice on experimental design and manuscript preparation.

**Mayhew C. A. (University of Birmingham):** Helped with interpretation of results and manuscript preparation.

**Distinguishing two isomeric mephedrone substitutes with selective-reagent-ionization mass spectrometry (SRI-MS)**

Lanza M., Acton W. J., Jürschik S., Sulzer P., Breiev K., Jordan A., Hartungen E., Hanel G., Märk L., Mayhew C. A. and Märk T. D.: Distinguishing two isomeric mephedrone substitutes with selective-reagent-ionization mass spectrometry (SRI-MS), *Journal of Mass Spectrometry*, 48, 1015-1018, 2013.

**Lanza M. (Iconicon Analytik):** Designed experiment, carried out data processing and analysis and contributed to manuscript preparation.

**Acton W. J. (Lancaster University):** Designed experiment, carried out data processing and analysis and contributed to manuscript preparation.

**Jürschik S. (Iconicon Analytik):** Provided guidance on data analysis and helped with manuscript preparation.

**Sulzer P. (Iconicon Analytik):** Provided guidance on experimental design and data analysis and led manuscript preparation.

**Breiev K., Jordan A., Hartungen E., Hanel G., Märk L. and Märk T. D. (Iconicon Analytik):** Offered advice on experimental design and manuscript preparation.

**Mayhew C. A. (University of Birmingham):** Helped with interpretation of results and manuscript preparation.

### **3.1 Headspace analysis of new psychoactive substances using a Selective Reagent Ionisation-Time of Flight-Mass Spectrometer**

W. Joe Acton <sup>1,2</sup>, Matteo Lanza <sup>1,3</sup>, Bishu Agarwal <sup>1,#</sup>, Simone Jürschik <sup>1</sup>, Philipp Sulzer <sup>1,\*</sup>, Kostiantyn Breiev <sup>1,3</sup>, Alfons Jordan <sup>1</sup>, Eugen Hartungen <sup>1</sup>, Gernot Hanel <sup>1</sup>, Lukas Märk <sup>1</sup>, Chris A. Mayhew <sup>4</sup>, and Tilmann D.Märk <sup>1,3</sup>

[1] {Ionicon Analytik GmbH., Eduard-Bodem-Gasse 3, 6020 Innsbruck, Austria}

[2] {Lancaster Environment Centre, Lancaster University, LA1 4YQ, Lancaster, UK}

[3] {Institut für Ionenphysik und Angewandte Physik, Leopold-Franzens Universität Innsbruck, Technikerstr. 25, 6020 Innsbruck, Austria}

[4] {School of Physics and Astronomy, University of Birmingham, Edgbaston, Birmingham, B15 2TT, UK}

# current address: Helmholtz Zentrum München Research Unit Environmental Simulation (EUS), Ingolstädter Landstraße 1, 85764 Neuherberg, Germany

\*corresponding author: philipp.sulzer@ionicon.com, Tel: +43 512 214 800 050, Fax: +43 512 214 800 099

## Abstract

The rapid expansion in the number and use of new psychoactive substances presents a significant analytical challenge because highly-sensitive instrumentation capable of detecting a broad range of chemical compounds in real-time with a low rate of false positives is required. A Selective Reagent Ionisation – Time of Flight – Mass Spectrometer (SRI-ToF-MS) is capable of meeting all of these requirements. With its high mass resolution (up to  $m/\Delta m$  of 8000), the application of variations in reduced electric field strength ( $E/N$ ) and use of different reagent ions, the ambiguity of a nominal (monoisotopic)  $m/z$  is reduced and hence the identification of chemicals in a complex chemical environment with a high level of confidence is enabled. In this study we report the use of a SRI-ToF-MS to investigate the reactions of  $\text{H}_3\text{O}^+$ ,  $\text{O}_2^+$ ,  $\text{NO}^+$  and  $\text{Kr}^+$  with 10 readily available (at the time of purchase) new psychoactive substances, namely 4-fluoroamphetamine, methiopropamine, ethcathinone, 4-methylethcathinone, N-ethylbuphedrone, ethylphenidate, 5-MeO-Dalt, dimethocaine, 5-(2-aminopropyl)benzofuran and nitracaine. In particular, the dependence of product ion branching ratios on the reduced electric field strength for all reagent ions was investigated and is reported here. The results reported represent a significant amount of new data which will be of use for the development of drug detection techniques suitable for real world scenarios.

### 3.1.1 Introduction

The abuse of drugs is an important issue affecting today's society. Although many drug species are controlled by law, a market for new psychoactive substances (*i.e.* legal highs, research chemicals, and designer drugs) which are not controlled by drug legislation, has recently emerged. These readily available drugs are increasingly being used as substitutes for prohibited drugs, especially by those who are looking for a high, but who do not wish to commit a criminal act (Werse and Morgenstern, 2012).

A review of the current literature shows that most new psychoactive substances have received little scientific interest, especially substances new to the market. For many of these compounds the only up-to-date source of information (e.g. synthesis, purity, side-effects etc.) is to be found online in user forums (drugsforum; drugsyn) and no data on properties like proton affinity, ionisation energy, etc. are available. As new psychoactive substances regularly enter the market, it is important that broad-based analytical methods exist which have the ability to rapidly detect them, without the need for major changes in operational procedures. This rapid identification is especially important if a user has taken an unidentified drug and requires urgent medical treatment. Gas chromatography-mass spectrometry (GC-MS) has traditionally been used for the identification of drugs (Westwell et al., 2013), providing both high selectivity and sensitivity. This comes at the expenses of fast analysis, making a real-time and therefore on-the-spot analysis impossible. Chemical test strips and ion mobility spectrometry (IMS) are much faster methods of analysis, but these have a limited selectivity (Biermann et al., 2004).

Proton-Transfer-Reaction – Time of Flight - Mass-Spectrometry (PTR-ToF-MS), which relies on the use of  $\text{H}_3\text{O}^+$  as the reagent ion, provides both a rapid detection capability and a high sensitivity (pptv within seconds). In addition, the soft ionisation capabilities of PTR-ToF-MS generally avoid significant fragmentation of the analytes which enables drug identification with a high level of confidence (low rate of false positives). However, relying on a nominal  $m/z$  makes unambiguous identification impossible. High mass resolution instruments provide higher confidence in assignment, but still isomeric compounds cannot be ruled out. In addition to changing operational parameters, *e.g.* the voltage applied to the drift tube, the recently developed Selective Reagent Ionisation (SRI) technology, (Jordan et al., 2009b; Sulzer et al., 2012a) to change the reagent ion and hence alter the ion-molecule chemistry in the drift tube of a PTR-ToF-MS, has significantly increased the instrument's selectivity, making it a multidimensional technique (Lanza et al., 2013). Given that we have used SRI in this study, we will not refer to the instrument as PTR-ToF-MS, but as a Selective Reagent Ionisation – Time of Flight- Mass Spectrometry (SRI-ToF-MS) instrument to reflect this multidimensional use.

Previous studies have illustrated the applicability of SRI-ToF-MS to the detection of several illicit and controlled prescription drugs (Agarwal et al., 2011) and numerous other threat substances, such as explosives (Jürschik et al., 2010; Mayhew et al., 2010; Sulzer et al., 2012b), chemical warfare agent simulants and toxic industrial compounds (Agarwal et al., 2012; Kassebacher et al., 2013; Petersson et al., 2009). In addition, it has been shown that in case of some explosives, selectivity can be enhanced by changing the voltage applied to the drift tube (*e.g.* with the use of  $\text{H}_3\text{O}^+$  as the reagent ion, by increasing reduced electric field strengths  $E/N$  – the ratio of the

electric field,  $E$ , to the buffer gas number density,  $N$ , in the drift tube – the protonated parent molecule signals of TNT and TNB are increased) (Sulzer et al., 2012b).

In this paper a detailed study of the principle product ions observed following reactions of  $\text{H}_3\text{O}^+$ ,  $\text{NO}^+$ ,  $\text{O}_2^+$  and  $\text{Kr}^+$  with a number of new psychoactive substances, namely 4-fluoroamphetamine, methiopropamine, ethcathinone, 4-methylethcathinone, N-ethylbuphedrone, ethylphenidate, 5-MeO-DALT, dimethocaine, 5-(2-aminopropyl)benzofuran and nitracaine (for structural information see Fig. 3.1) is reported. In particular, the effects of  $E/N$  on the fragmentation pathways are also discussed in detail. These datasets, i.e. the information on the exact masses and  $E/N$  dependence for all abundant fragments and with all four reagent ions, respectively, should help for the development of a nearly unambiguous drug detection technique based on SRI-ToF-MS suitable for real world scenarios.

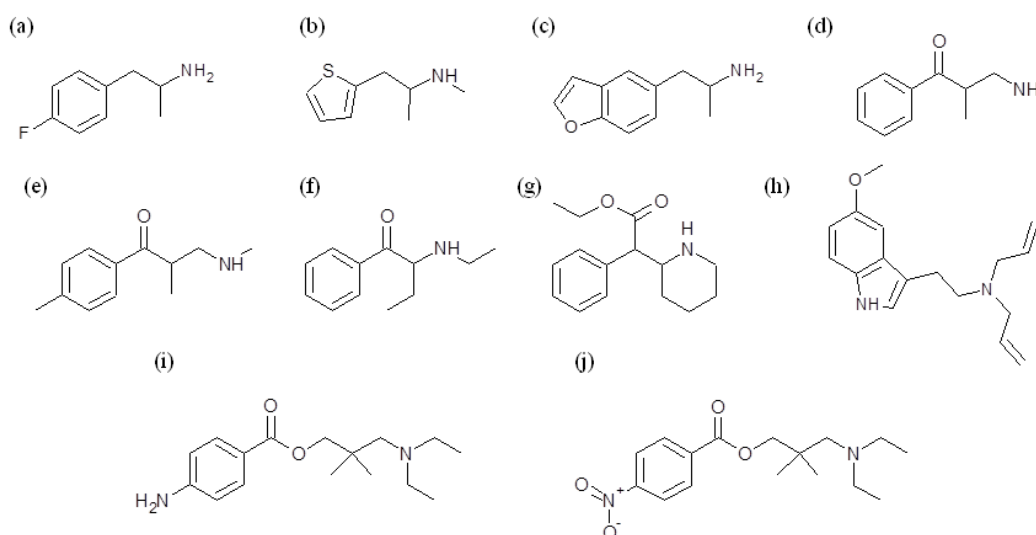
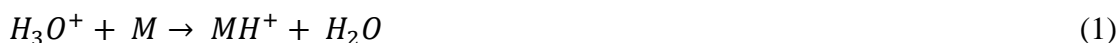


Figure 3.1: Chemical structures of (a) 4-fluoroamphetamine, (b) methiopropamine, (c) 5-(2-aminopropyl)benzofuran, (d) ethcathinone, (e) 4-methylethcathinone, (f) N-ethylbuphedrone, (g) ethylphenidate, (h) 5-MeO-DALT, (i) dimethocaine and (j) nitracaine

### 3.1.2 Experimental

All new psychoactive substance samples were analysed using a PTR-TOF 8000 (Ionicon Analytik GmbH, Austria) equipped with a SRI capability, thus allowing a change in the reagent ion used for chemical ionisation from  $H_3O^+$  to  $O_2^+$ ,  $NO^+$  or  $Kr^+$ . For all reagent ions, the reagent ions and the resulting product ions are separated and detected using a ToF mass analyser. PTR-ToF-MS and SRI have both been described in detail in previous publications (Jordan et al., 2009b; Jordan et al., 2009a; Karl et al., 2012; Sulzer et al., 2012a) and therefore they will only be briefly discussed here.

For the production of  $H_3O^+$  ions water vapour from a reservoir of pure water enters a hollow cathode discharge source. Following ionisation and a series of ion-molecule reactions the resulting  $H_3O^+$  ions are directed into the drift tube by an applied voltage gradient. Within the drift tube proton transfer reactions will take place only with those chemical species (M) that have a proton affinity (PA) greater than that of water ( $PA(H_2O) = 691 \text{ kJ mol}^{-1}$ ) (Lindinger et al. 1998a). This could either be via non-dissociative proton transfer:

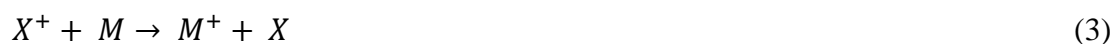


and/or via dissociative proton transfer:



where *A* represents an elimination of a molecule from the transient protonated parent molecule.

For the production of  $O_2^+$ ,  $NO^+$  and  $Kr^+$ , water vapour is replaced by oxygen, oxygen/nitrogen mixture and krypton, respectively. If exothermic, the reactions with  $NO^+$ ,  $O_2^+$  and  $Kr^+$  may proceed via charge transfer, which may also be either non-dissociative:



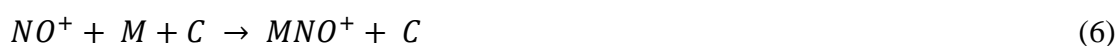
where  $X^+$  represents the reagent ion, and/or dissociative:



resulting in the elimination of  $B$  from the parent ion.  $NO^+$  has the lowest recombination energy (RE) of these three reagent ions (9.6 eV) and therefore may only charge transfer to neutral species whose ionisation energies (IE) are less than 9.6 eV. However, reaction of  $NO^+$  and a molecule may also take place via a chemical reaction, for example hydride abstraction:



Reaction with  $NO^+$  may result in an adduct ion being formed:



where  $C$  represents a third body (the buffer gas) that is required to remove some of the energy resulting from the association, otherwise the adduct would dissociate rapidly.

The  $E/N$  value used can be rapidly adjusted by changing the voltage applied across the drift tube; this enables the investigation of fragmentation pathways offering a more selective method for compound identification. In the reported experiments the  $E/N$  value was varied between 85 and 225 Td ( $1 \text{ Td} = 10^{-21} \text{ V m}^2$ ) when  $\text{H}_3\text{O}^+$ ,  $\text{NO}^+$  and  $\text{O}_2^+$  were used as reagent ions and between 45 and 115 Td for the investigations using  $\text{Kr}^+$ . The 10 new psychoactive substances studied, legal in most European countries at the time of purchase, were obtained from various online vendors. These new psychoactive substances studied were 4-fluoroamphetamine, methiopropamine, ethcathinone, 4-methylethcathinone, N-ethylbuphedrone, ethylphenidate, 5-MeO-DALT, dimethocaine, 5-(2-aminopropyl)benzofuran and nitracaine. Most can be classified as cathinones or piperazines, which include a large list of analogues of amphetamines, with psychoactive and stimulant effects (Henderson, 1988; Rösner et al., 2005). Most of the chemicals were supplied in powder (or crystal) form. However, two were supplied in tablet form (4-fluoroamphetamine and ethcathinone). Therefore, before any measurements were taken these two compounds were first crushed into a fine powder. This ensured that all samples were of comparable surface area. All of the supplied chemicals were used with no purification. In addition to the detection of the advertised new psychoactive substance analysis with SRI-ToF-MS enables the detection of most solvents, synthetic reagents and intermediates, but not "extenders" (usually low cost inorganics such as sodium bicarbonate), however due to low costs of production and tough competition, with rankings in online forums, the use of these "extenders" is less likely in new psychoactive substances than in illegal drugs.

The following procedure was adopted for the dynamic headspace sampling of all 10 chemicals with  $\text{H}_3\text{O}^+$ ,  $\text{NO}^+$  and  $\text{O}_2^+$  as the reagent ions. A few mg of the drug were

added to a glass vial, the vial was then sealed with a septum. An inlet and an outlet line (1/16th inch PEEK, internal diameter 1 mm, VICI AG International) were inserted through the septum to allow for dynamic headspace sampling. The inlet line was connected to a charcoal filter so that purified laboratory air entered the vials. The outlet line was directly connected to the heated sampling line of the SRI- ToF-MS instrument. Samples were heated to a temperature between 60°C and 100°C and the sampling line and drift tube were maintained at a temperature of 110 °C in order to minimise adsorption of the analytes onto the surface and memory effects.

Once the dynamic headspace concentration had equilibrated, an investigation of the reaction processes as a function of  $E/N$  began. For  $\text{H}_3\text{O}^+$  the  $E/N$  value was increased from 85 to 225 Td in steps of 5 Td. A similar range in the reduced electric field was used for  $\text{NO}^+$  and  $\text{O}_2^+$ , but  $E/N$  was increased in  $\sim 25$  Td steps, as no significant changes in the product ion branching ratios were observed for small variations in  $E/N$ . For  $\text{Kr}^+$  the method was similar to the above with the only exception being that helium was used as buffer gas, instead of charcoal filtered air. This was required to prevent loss of  $\text{Kr}^+$  via charge transfer to the main components of air (Sulzer et al., 2012a). The use of helium as the buffer gas necessitated restricting the range of the  $\text{Kr}^+$   $E/N$  study to a maximum value of 115 Td, to prevent plasma formation in the drift tube. Rapid switching between  $\text{H}_3\text{O}^+$ ,  $\text{NO}^+$  and  $\text{O}_2^+$  is possible (tens of seconds). However switching from  $\text{H}_3\text{O}^+$  to  $\text{Kr}^+$  requires several (if not tens) of minutes, because of the need of a dry system (Sulzer et al., 2012a).

Prior to the analysis of each chemical with a new reagent ion an empty vial was connected to the instrument. The  $E/N$  was varied over the same range used for the

drugs, as described above, in order to provide background mass spectra which could be subtracted from those obtained when using the drug sample. For all measurements an integration time of 40 seconds was used.

### 3.1.3 Results and discussion

Product ion branching ratios for each drug species are summarised in Figs 3.2-3.5 for reactions with  $\text{H}_3\text{O}^+$ ,  $\text{NO}^+$ ,  $\text{O}_2^+$  and  $\text{Kr}^+$ , respectively. Only product ions which have branching ratios of greater than or equal to 3 % within the  $E/N$  range studied have been included in the figures, because below this value there is greater uncertainty as to whether they belong to the drug or to an impurity.

Table 3.1 summarises the product ions and their branching ratios at a standard operating condition of 130 Td.

Table 3.1 (Overleaf). List of the investigated drugs (in order of increasing mass) and the product ions and their associated percentage ion branching ratios (in brackets) for reactions with  $\text{H}_3\text{O}^+$ ,  $\text{NO}^+$ ,  $\text{O}_2^+$  and  $\text{Kr}^+$ , recorded at  $E/N$  of 130 Td (45 Td in case of  $\text{Kr}^+$ ). NR is used to represent no reaction and NOP means no observable product ions that can be identified to the drug as a result of substantial fragmentation.

Compound name	H <sub>3</sub> O <sup>+</sup>	NO <sup>+</sup>	O <sub>2</sub> <sup>+</sup>	Kr <sup>+</sup>
4-Fluoroamphetamine (C <sub>9</sub> H <sub>12</sub> FN; <i>m/z</i> 153.10)	<i>m/z</i> 154.10 – C <sub>9</sub> H <sub>13</sub> FN <sup>+</sup> (19) <i>m/z</i> 137.07 – C <sub>9</sub> H <sub>10</sub> F <sup>+</sup> (44) <i>m/z</i> 109.04 – C <sub>7</sub> H <sub>6</sub> F <sup>+</sup> (37)	<i>m/z</i> 153.09 – C <sub>9</sub> H <sub>12</sub> FN <sup>+</sup> (7)	<i>m/z</i> 152.09 – C <sub>9</sub> H <sub>11</sub> FN <sup>+</sup> (24) <i>m/z</i> 151.08 – C <sub>9</sub> H <sub>10</sub> FN <sup>+</sup> (27) <i>m/z</i> 138.07 – C <sub>8</sub> H <sub>9</sub> FN <sup>+</sup> (17) <i>m/z</i> 136.07 – C <sub>9</sub> H <sub>9</sub> F <sup>+</sup> (11) <i>m/z</i> 109.04 – C <sub>7</sub> H <sub>6</sub> F <sup>+</sup> (21)	<i>m/z</i> 152.09 – C <sub>9</sub> H <sub>11</sub> FN <sup>+</sup> (26) <i>m/z</i> 138.07 – C <sub>8</sub> H <sub>9</sub> FN <sup>+</sup> (34) <i>m/z</i> 109.04 – C <sub>7</sub> H <sub>6</sub> F <sup>+</sup> (40)
		<i>m/z</i> 152.09 – C <sub>9</sub> H <sub>11</sub> FN <sup>+</sup> (64)	<i>m/z</i> 151.08 – C <sub>9</sub> H <sub>10</sub> FN <sup>+</sup> (23)	<i>m/z</i> 136.07 – C <sub>9</sub> H <sub>9</sub> F <sup>+</sup> (11)
		<i>m/z</i> 151.08 – C <sub>9</sub> H <sub>10</sub> FN <sup>+</sup> (23)	<i>m/z</i> 109.04 – C <sub>7</sub> H <sub>6</sub> F <sup>+</sup> (6)	<i>m/z</i> 109.04 – C <sub>7</sub> H <sub>6</sub> F <sup>+</sup> (21)
		<i>m/z</i> 152.09 – C <sub>9</sub> H <sub>11</sub> FN <sup>+</sup> (64)	<i>m/z</i> 151.08 – C <sub>9</sub> H <sub>10</sub> FN <sup>+</sup> (23)	<i>m/z</i> 136.07 – C <sub>9</sub> H <sub>9</sub> F <sup>+</sup> (11)
		<i>m/z</i> 151.08 – C <sub>9</sub> H <sub>10</sub> FN <sup>+</sup> (23)	<i>m/z</i> 109.04 – C <sub>7</sub> H <sub>6</sub> F <sup>+</sup> (6)	<i>m/z</i> 109.04 – C <sub>7</sub> H <sub>6</sub> F <sup>+</sup> (21)
Methiopropamine (C <sub>8</sub> H <sub>13</sub> NS; <i>m/z</i> 155.08)	<i>m/z</i> 156.08 – C <sub>8</sub> H <sub>14</sub> SN <sup>+</sup> (36) <i>m/z</i> 125.04 – C <sub>7</sub> H <sub>9</sub> S <sup>+</sup> (19) <i>m/z</i> 58.06 – C <sub>3</sub> H <sub>8</sub> N <sup>+</sup> (45)	<i>m/z</i> 97.01 – C <sub>5</sub> H <sub>5</sub> S <sup>+</sup> (1) <i>m/z</i> 58.06 – C <sub>3</sub> H <sub>8</sub> N <sup>+</sup> (99)	<i>m/z</i> 97.01 – C <sub>5</sub> H <sub>5</sub> S <sup>+</sup> (2) <i>m/z</i> 58.06 – C <sub>3</sub> H <sub>8</sub> N <sup>+</sup> (98)	<i>m/z</i> 97.01 – C <sub>5</sub> H <sub>5</sub> S <sup>+</sup> (6) <i>m/z</i> 73.05 – C <sub>4</sub> H <sub>11</sub> N <sup>+</sup> (7) <i>m/z</i> 58.06 – C <sub>3</sub> H <sub>8</sub> N <sup>+</sup> (87)
		<i>m/z</i> 97.01 – C <sub>5</sub> H <sub>5</sub> S <sup>+</sup> (1)	<i>m/z</i> 58.06 – C <sub>3</sub> H <sub>8</sub> N <sup>+</sup> (99)	<i>m/z</i> 58.06 – C <sub>3</sub> H <sub>8</sub> N <sup>+</sup> (98)
5-(2-aminopropyl)benzofuran (C <sub>11</sub> H <sub>13</sub> NO; <i>m/z</i> 175.10)	<i>m/z</i> 176.11 – C <sub>11</sub> H <sub>14</sub> NO <sup>+</sup> (14) <i>m/z</i> 159.08 – C <sub>11</sub> H <sub>11</sub> O <sup>+</sup> (27) <i>m/z</i> 131.05 – C <sub>9</sub> H <sub>7</sub> O <sup>+</sup> (59)	<i>m/z</i> 175.12 – C <sub>11</sub> H <sub>13</sub> NO <sup>+</sup> (32)	<i>m/z</i> 175.12 – C <sub>11</sub> H <sub>13</sub> NO <sup>+</sup> (48)	NOP
		<i>m/z</i> 131.05 – C <sub>9</sub> H <sub>7</sub> O <sup>+</sup> (68)	<i>m/z</i> 131.05 – C <sub>9</sub> H <sub>7</sub> O <sup>+</sup> (52)	
		<i>m/z</i> 176.12 – C <sub>11</sub> H <sub>14</sub> NO <sup>+</sup> (4)	<i>m/z</i> 176.12 – C <sub>11</sub> H <sub>14</sub> NO <sup>+</sup> (2)	
Ethcathinone (C <sub>11</sub> H <sub>15</sub> NO; <i>m/z</i> 177.12)	<i>m/z</i> 178.12 – C <sub>11</sub> H <sub>16</sub> NO <sup>+</sup> (90) <i>m/z</i> 160.11 – C <sub>11</sub> H <sub>14</sub> N <sup>+</sup> (10)	<i>m/z</i> 175.10 – C <sub>11</sub> H <sub>13</sub> NO <sup>+</sup> (3)	<i>m/z</i> 146.10 – C <sub>10</sub> H <sub>12</sub> N <sup>+</sup> (2)	<i>m/z</i> 105.04 – C <sub>7</sub> H <sub>5</sub> O <sup>+</sup> (4) <i>m/z</i> 72.08 – C <sub>4</sub> H <sub>10</sub> N <sup>+</sup> (96)
		<i>m/z</i> 146.10 – C <sub>10</sub> H <sub>12</sub> N <sup>+</sup> (3)	<i>m/z</i> 107.05 – C <sub>7</sub> H <sub>7</sub> O <sup>+</sup> (4) <i>m/z</i> 105.04 – C <sub>7</sub> H <sub>5</sub> O <sup>+</sup> (9)	
		<i>m/z</i> 105.04 – C <sub>7</sub> H <sub>5</sub> O <sup>+</sup> (10)	<i>m/z</i> 77.04 – C <sub>6</sub> H <sub>5</sub> <sup>+</sup> (2) <i>m/z</i> 72.08 – C <sub>4</sub> H <sub>10</sub> N <sup>+</sup> (73)	
		<i>m/z</i> 72.08 – C <sub>4</sub> H <sub>10</sub> N <sup>+</sup> (80)	<i>m/z</i> 70.07 – C <sub>4</sub> H <sub>8</sub> N <sup>+</sup> (8)	
4-Methylethcathinone (C <sub>12</sub> H <sub>17</sub> NO; <i>m/z</i> 191.13)	<i>m/z</i> 192.14 – C <sub>12</sub> H <sub>18</sub> NO <sup>+</sup> (80) <i>m/z</i> 190.13 – C <sub>12</sub> H <sub>16</sub> NO <sup>+</sup> (18) <i>m/z</i> 174.14 – C <sub>12</sub> H <sub>16</sub> N <sup>+</sup> (2)	<i>m/z</i> 190.12 – C <sub>12</sub> H <sub>16</sub> NO <sup>+</sup> (3)	<i>m/z</i> 119.05 – C <sub>8</sub> H <sub>7</sub> O <sup>+</sup> (4) <i>m/z</i> 91.05 – C <sub>7</sub> H <sub>7</sub> <sup>+</sup> (5)	<i>m/z</i> 72.08 – C <sub>4</sub> H <sub>10</sub> N <sup>+</sup> (100)
		<i>m/z</i> 119.05 – C <sub>8</sub> H <sub>7</sub> O <sup>+</sup> (1)	<i>m/z</i> 72.08 – C <sub>4</sub> H <sub>10</sub> N <sup>+</sup> (91)	
		<i>m/z</i> 72.08 – C <sub>4</sub> H <sub>10</sub> N <sup>+</sup> (96)		

Table 3.1 (continued)

Compound name	H <sub>3</sub> O <sup>+</sup>	NO <sup>+</sup>	O <sub>2</sub> <sup>+</sup>	Kr <sup>+</sup>
N-Ethylbuphedrone (C <sub>12</sub> H <sub>17</sub> NO; <i>m/z</i> 191.13)	<i>m/z</i> 192.14 – C <sub>12</sub> H <sub>18</sub> NO <sup>+</sup> (84) <i>m/z</i> 190.13 – C <sub>12</sub> H <sub>16</sub> NO <sup>+</sup> (13) <i>m/z</i> 174.14 – C <sub>12</sub> H <sub>16</sub> N <sup>+</sup> (3)	<i>m/z</i> 190.12 – C <sub>12</sub> H <sub>16</sub> NO <sup>+</sup> (3) <i>m/z</i> 105.03 – C <sub>7</sub> H <sub>5</sub> O <sup>+</sup> (4) <i>m/z</i> 86.10 – C <sub>5</sub> H <sub>12</sub> N <sup>+</sup> (93)	<i>m/z</i> 105.03 – C <sub>7</sub> H <sub>5</sub> O <sup>+</sup> (9) <i>m/z</i> 86.10 – C <sub>5</sub> H <sub>12</sub> N <sup>+</sup> (91)	<i>m/z</i> 162.10 – C <sub>10</sub> H <sub>12</sub> NO <sup>+</sup> (40) <i>m/z</i> 105.03 – C <sub>7</sub> H <sub>5</sub> O <sup>+</sup> (60)
Ethylphenidate (C <sub>15</sub> H <sub>21</sub> NO <sub>2</sub> ; <i>m/z</i> 247.16)	<i>m/z</i> 248.16 – C <sub>15</sub> H <sub>22</sub> NO <sub>2</sub> <sup>+</sup> (81) <i>m/z</i> 165.09 – C <sub>10</sub> H <sub>13</sub> O <sub>2</sub> <sup>+</sup> (1) <i>m/z</i> 84.08 – C <sub>5</sub> H <sub>10</sub> N <sup>+</sup> (18)	NR	NOP	NOP
5-MeO-DALT (C <sub>17</sub> H <sub>22</sub> N <sub>2</sub> O; <i>m/z</i> 270.13)	<i>m/z</i> 271.18 – C <sub>17</sub> H <sub>23</sub> N <sub>2</sub> O <sup>+</sup> (91) <i>m/z</i> 174.09 – C <sub>11</sub> H <sub>12</sub> NO <sup>+</sup> (6) <i>m/z</i> 160.08 – C <sub>10</sub> H <sub>10</sub> NO <sup>+</sup> (3)	<i>m/z</i> 270.19 – C <sub>17</sub> H <sub>22</sub> N <sub>2</sub> O <sup>+</sup> (14) <i>m/z</i> 175.08 – C <sub>11</sub> H <sub>13</sub> NO <sup>+</sup> (15) <i>m/z</i> 159.06 – C <sub>10</sub> H <sub>9</sub> NO <sup>+</sup> (26) <i>m/z</i> 110.09 – C <sub>7</sub> H <sub>12</sub> N <sup>+</sup> (45)	<i>m/z</i> 175.08 – C <sub>11</sub> H <sub>13</sub> NO <sup>+</sup> (52) <i>m/z</i> 110.09 – C <sub>7</sub> H <sub>12</sub> N <sup>+</sup> (48)	NOP
Dimethocaine (C <sub>16</sub> H <sub>26</sub> N <sub>2</sub> O <sub>2</sub> ; <i>m/z</i> 278.20)	<i>m/z</i> 279.20 – C <sub>16</sub> H <sub>27</sub> N <sub>2</sub> O <sub>2</sub> <sup>+</sup> (91) <i>m/z</i> 142.16 – C <sub>9</sub> H <sub>20</sub> N <sup>+</sup> (2) <i>m/z</i> 120.04 – C <sub>7</sub> H <sub>6</sub> NO <sup>+</sup> (4) <i>m/z</i> 86.10 – C <sub>5</sub> H <sub>12</sub> N <sup>+</sup> (3)	<i>m/z</i> 278.19 – C <sub>16</sub> H <sub>26</sub> N <sub>2</sub> O <sub>2</sub> <sup>+</sup> (1) <i>m/z</i> 165.07 – C <sub>9</sub> H <sub>11</sub> NO <sub>2</sub> <sup>+</sup> (3) <i>m/z</i> 86.10 – C <sub>5</sub> H <sub>12</sub> N <sup>+</sup> (96)	<i>m/z</i> 149.03 – C <sub>8</sub> H <sub>7</sub> NO <sub>2</sub> <sup>+</sup> (4) <i>m/z</i> 120.05 – C <sub>7</sub> H <sub>6</sub> NO <sup>+</sup> (5) <i>m/z</i> 86.10 – C <sub>5</sub> H <sub>12</sub> N <sup>+</sup> (91)	<i>m/z</i> 120.05 – C <sub>7</sub> H <sub>6</sub> NO <sup>+</sup> (100)
Nitracaine (C <sub>16</sub> H <sub>24</sub> N <sub>2</sub> O <sub>4</sub> ; <i>m/z</i> 308.17)	Crystal: <i>m/z</i> 309.17 – C <sub>16</sub> H <sub>25</sub> N <sub>2</sub> O <sub>4</sub> <sup>+</sup> (100)	NR	NR	NOP

### 3.1.3.1 4-fluoroamphetamine (4-FA)

#### *Reaction with $H_3O^+$*

Fig. 3.2 (a) shows the effect of changing  $E/N$  on product ion abundance when  $H_3O^+$  is used as the reagent ion. It can be seen from the figure that the protonated parent molecule ( $m/z$  154.10,  $[MH]^+$ ,  $C_9H_{13}FN^+$ ) dominates at  $E/N < 105$  Td, whilst  $m/z$  137.07 ( $[MH-NH_3]^+$ ,  $C_9H_{10}F^+$ ) becomes the most abundant species between 105 and 135 Td. Above 135 Td the ion branching ratio of  $m/z$  109.04 ( $[MH-C_2NH_7]^+$ ,  $C_7H_6F^+$ ) increases rapidly and becomes the dominant fragment ion. These ionic species have also been observed in a previous study using chemical ionisation-mass spectrometry (Westphal et al., 2010). However in that study the reagent gas used was methane, resulting in higher reaction energies than associated with the reagent ion  $H_3O^+$  and hence increased fragmentation. Additional fragment ions were also detected in that earlier study, which we did not observe, the most notable at  $m/z$  134 corresponding to  $[MH-HF]^+$ .

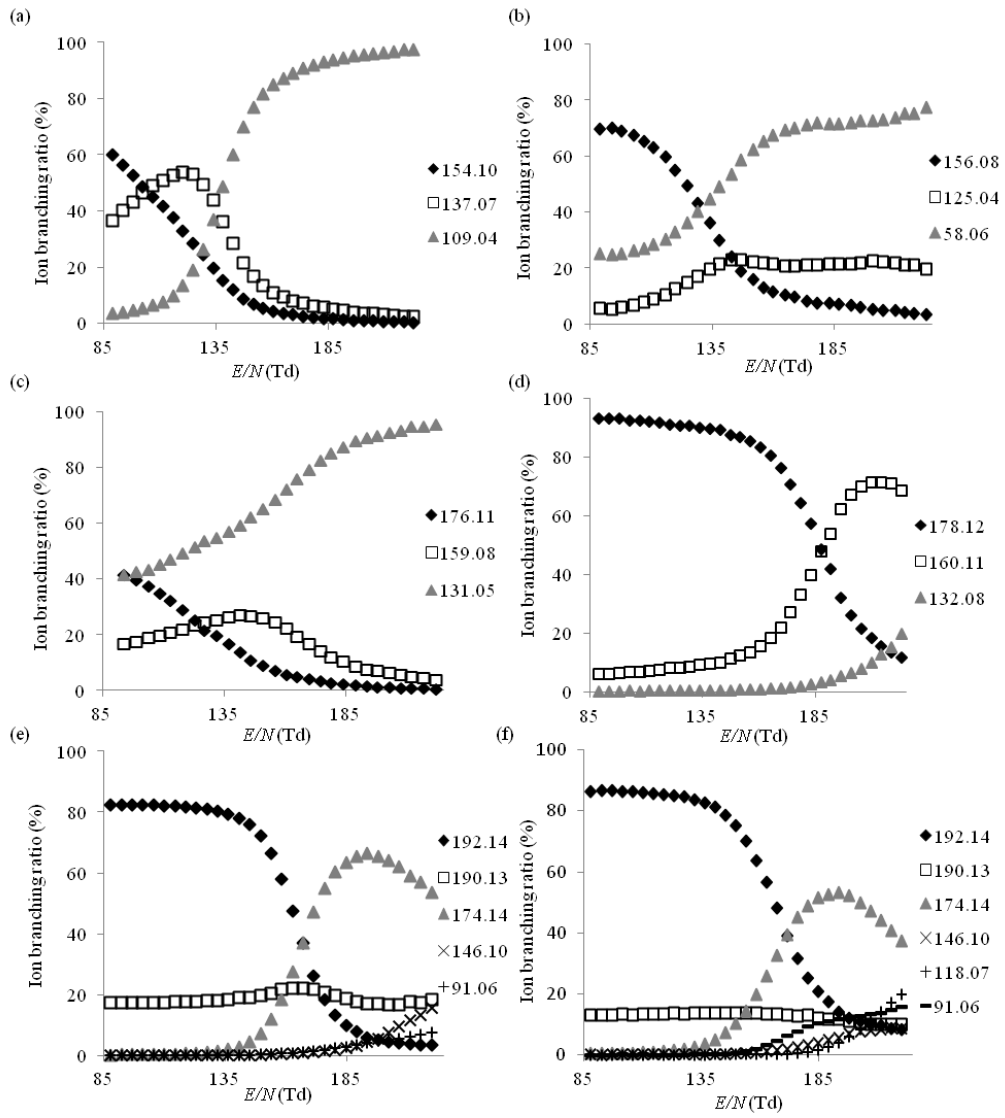
#### *Reaction with $NO^+$ , $O_2^+$ and $Kr^+$*

When  $NO^+$  was used as the reagent ion, see Fig 3.3(a), the dominant product ion observed across the whole  $E/N$  range was at  $m/z$  152.09, assigned to  $[M-H]^+$  ( $C_9H_{11}FN^+$ ). The parent ion,  $m/z$  153.09, was observed with an ion branching ratio which decreased from 9 % to 4% as  $E/N$  was increased from 85 to 225 Td. An additional product ion was observed at  $m/z$  109.04 corresponding to  $[M-C_2H_6N]^+$  ( $C_7H_6F^+$ ), which became the dominant product ion above 225 Td. A significant mass spectral peak assigned to an impurity was seen at  $m/z$  124.03, which we assume resulted from non-dissociative charge transfer to 4-fluorobenzaldehyde ( $C_7H_5OF^+$ ),

one of the reagents reported in the synthesis of the drug by the online community (erowid).

When  $O_2^+$  was used as the reagent ion, Fig 3.4(a), the parent ion peak was not observed. Instead we observed a product ion at  $m/z$  152.09 which we attribute to the  $[M-H]^+$  ion, a fragmentation pathway which has been observed previously following the reaction of  $O_2^+$  with chemical compounds (Anicich, 2003), as well as product ions at  $m/z$  138.07 ( $[M-CH_3]^+$ ,  $C_8H_9FN^+$ ) and  $m/z$  109.04 ( $[M-C_2H_6N]^+$ ,  $C_7H_6F^+$ ). As found with the  $NO^+$  study, we also observed a mass spectral peak at  $m/z$  124.03 which we attribute to a reaction with an impurity.

Results similar to those found for  $O_2^+$  and  $NO^+$  were observed for the reactions with  $Kr^+$ , Fig. 3.5(a), *i.e.* the same principle product ions observed across the whole  $E/N$  range, namely ions at  $m/z$  152.09 ( $[M-H]^+$ ,  $C_9H_{11}FN^+$ ),  $m/z$  138.07 ( $[M-CH_3]^+$ ,  $C_8H_9FN^+$ ) and  $m/z$  109.04 ( $[M-C_2H_6N]^+$ ,  $C_7H_6F^+$ ). Again a mass spectral peak at  $m/z$  124.03 ( $C_7H_5OF^+$ ) resulting from an impurity was observed.



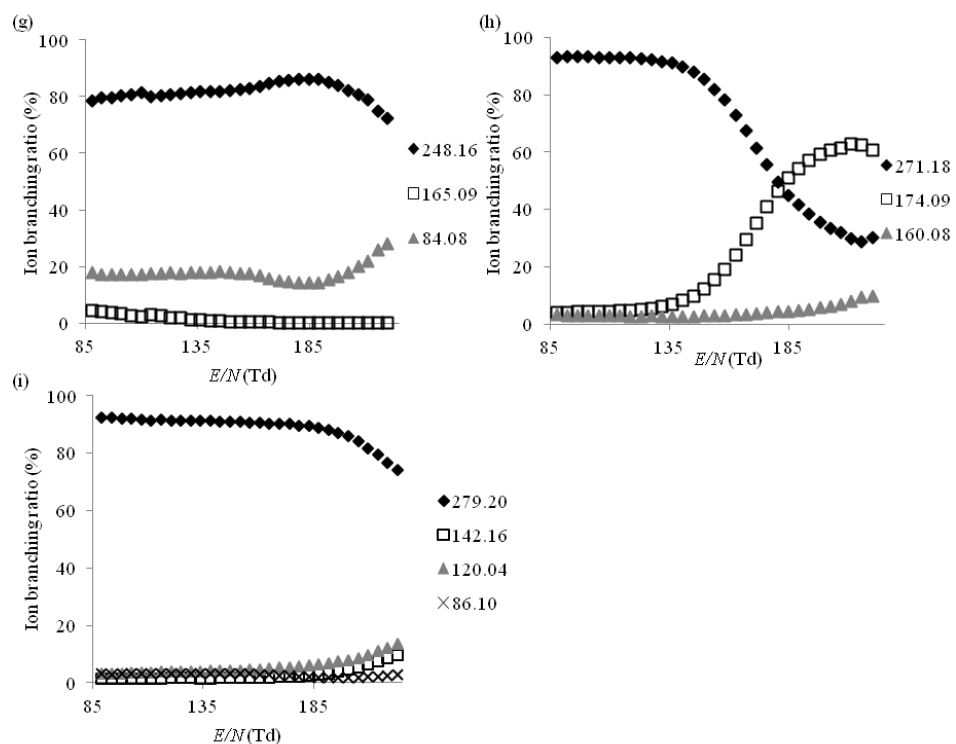


Figure 3.2: The variation of the percentage product ion branching ratios following the reactions of the various drug compounds with  $\text{H}_3\text{O}^+$  as a function of  $E/N$  for (a) 4-fluoroamphetamine, (b) methiopropamine, (c) 5-(2-aminopropyl)benzofuran, (d) ethcathinone, (e) 4-methylethcathinone, (f) N-ethylbuphedrone, (g) ethylphenidate, (h) 5-MeO-DALT and (i) dimethocaine.

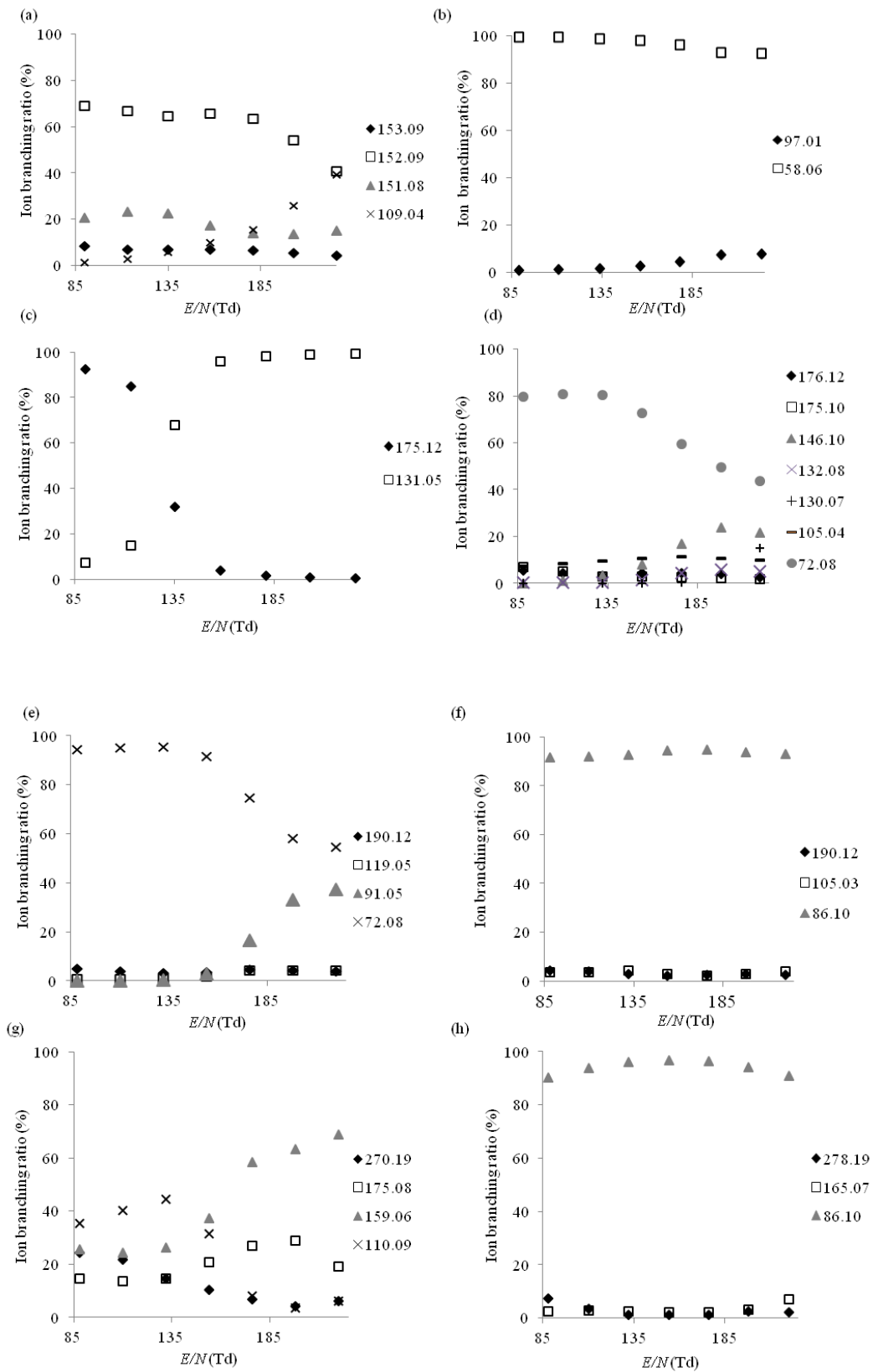


Figure 3.3 (overleaf): The variation of the percentage product ion branching ratios following the reactions of the drug species with  $\text{NO}^+$  as a function of  $E/N$  for (a) 4-fluoroamphetamine, (b) methiopropamine, (c) 5-(2-aminopropyl)benzofuran, (d) ethcathinone, (e) 4-methylethcathinone, (f) N-ethylbuphedrone, (g) 5-MeO-DALT and (h) dimethocaine.

### 3.1.3.2 Methiopropamine (MPA)

#### *Reaction with $\text{H}_3\text{O}^+$*

The reaction of MPA with  $\text{H}_3\text{O}^+$ , Fig 3.2(b), results in three main product ions, namely the protonated parent at  $m/z$  156.08 ( $[\text{MH}]^+$ ,  $\text{C}_8\text{H}_{14}\text{SN}^+$ ),  $m/z$  125.04 ( $[\text{MH}-\text{CH}_5\text{N}]^+$ ,  $\text{C}_7\text{H}_9\text{S}^+$ ) and  $m/z$  58.06 ( $[\text{MH}-\text{C}_5\text{H}_6\text{S}]^+$ ,  $\text{C}_3\text{H}_8\text{N}^+$ ). Significant spectral peaks were also observed at  $m/z$  151.06 and  $m/z$  63.03; the latter is attributed to  $\text{NaBH}_3\text{CN}$ , which has been reported as a reagent in the synthesis of MPA (Angelov et al., 2011), and this is supported by a distinctive isotopic pattern. The mass spectral peak at  $m/z$  151.06 is unidentified.

At  $E/N$  values below 135 Td the protonated parent molecule was the dominant species, whilst both  $m/z$  125.04 and  $m/z$  58.06 increased with increasing  $E/N$  and  $m/z$  58.06 (*i.e.*  $[\text{MH}-\text{C}_5\text{H}_6\text{S}]^+$ ,  $\text{C}_3\text{H}_8\text{N}^+$ ) became the most abundant product ion at values greater than 135 Td.

#### *Reactions with $\text{NO}^+$ , $\text{O}_2^+$ and $\text{Kr}^+$*

For both,  $\text{NO}^+$  and  $\text{O}_2^+$ , Figs. 3.3(b) and 3.4(b), respectively,  $m/z$  58.06 ( $[\text{M}-\text{C}_5\text{H}_5\text{S}]^+$ ,  $\text{C}_3\text{H}_8\text{N}^+$ ) was the dominant product ion observed across the whole  $E/N$  range investigated. Above 155 Td the ion branching ratio of  $m/z$  58.06 decreased slightly

because a new ion channel opens resulting in a product ion at  $m/z$  97.01, which we identify as  $[M-C_3H_8N]^+$  ( $C_5H_5S^+$ ). Two additional ions were observed for reactions with  $NO^+$  and  $O_2^+$  at  $m/z$  111.99 and 169.02, tentitatively assigned to  $C_5H_4SO^+$  and  $C_7H_7SNO_2^+$ , respectively. The corresponding neutral species are known intermediates used in the synthesis of MPA (Angelov et al., 2011). Other, but unknown impurities resulted in ion signals observed at  $m/z$  149.98 and  $m/z$  137.09.

Product ions at  $m/z$  58.06 and  $m/z$  97.01 were also observed to result from reactions with  $Kr^+$  (Fig 3.5(b)), with  $m/z$  58.06 being again the dominant one. However, an additional fragment ion was observed at  $m/z$  73.05 which is tentatively assigned to  $C_4H_{11}N^+$ , an ion that could be formed either via cleavage at the thiophene ring (i.e.  $[M-C_4H_2S]^+$ ), or this ion could result from charge transfer to n-BuNH<sub>2</sub>, a compound which has been reported as a reagent in the synthesis of MPA (Angelov et al., 2011) but we consider this to be unlikely as it was not observed with reactions of  $NO^+$  and  $O_2^+$ .

### 3.1.3.3 5-(2-aminopropyl)benzofuran (5-APB)

#### *Reaction with $H_3O^+$*

In the case of reactions with  $H_3O^+$  (Fig 3.2(c)), the dominant product ion over the whole  $E/N$  range was at  $m/z$  131.05 ( $[MH-C_2H_7N]^+$ ,  $C_9H_7O^+$ ). The protonated parent molecule ( $[MH]^+$ ,  $C_{11}H_{14}NO^+$ ) was observed at  $m/z$  176.11. Another peak observed in the mass spectra was found at  $m/z$  159.08. We assign this to  $[MH-NH_3]^+$  ( $C_{11}H_{11}O^+$ ). The supplied sample of 5-APB showed major contributions from a series of impurities, mass spectral peaks observed which cannot be assigned to the drug, included  $m/z$  119.03,  $m/z$  101.02, and  $m/z$  59.05 tentatively assigned to protonated

benzofuran ( $C_8H_7O^+$ ), isopropenyl acetate ( $C_5H_8O_2^+$ ), a solvent used in the synthesis of both 4-(2-aminopropyl)benzofuran (4-APB) and 6-(2-aminopropyl)benzofuran (6-APB), which are structural isomers of 5-APB (Casale and Hays, 2012), and acetone ( $C_3H_7O^+$ ), respectively.

*Reactions with  $NO^+$ ,  $O_2^+$  and  $Kr^+$*

Two product ions attributed to 5-APB, which resulted from the reaction with  $O_2^+$  (Fig 3.4(c)), *i.e.*  $m/z$  175.12 ( $[M]^+$ ,  $C_{11}H_{13}NO^+$ ) and  $m/z$  131.05 ( $[M-C_2H_6N]^+$ ,  $C_9H_7O^+$ ) were observed. In agreement with the study involving  $H_3O^+$ , the reaction of  $O_2^+$  with the supplied sample of 5-APB also indicates that it is impure, *i.e.* mass spectral peaks observed at  $m/z$  100.04 (ionised isopropenyl acetate,  $C_5H_7O_2^+$ ) and at  $m/z$  74.05 (an unknown compound). In the case of  $NO^+$  (Fig 3.3(c)), the same two products ions were observed, but with different branching ratios. A significant impurity resulted in an ion being observed at  $m/z$  147.96. As a result of considerable fragmentation no product ions could be confidently attributed to 5-APB following its reaction with  $Kr^+$ .

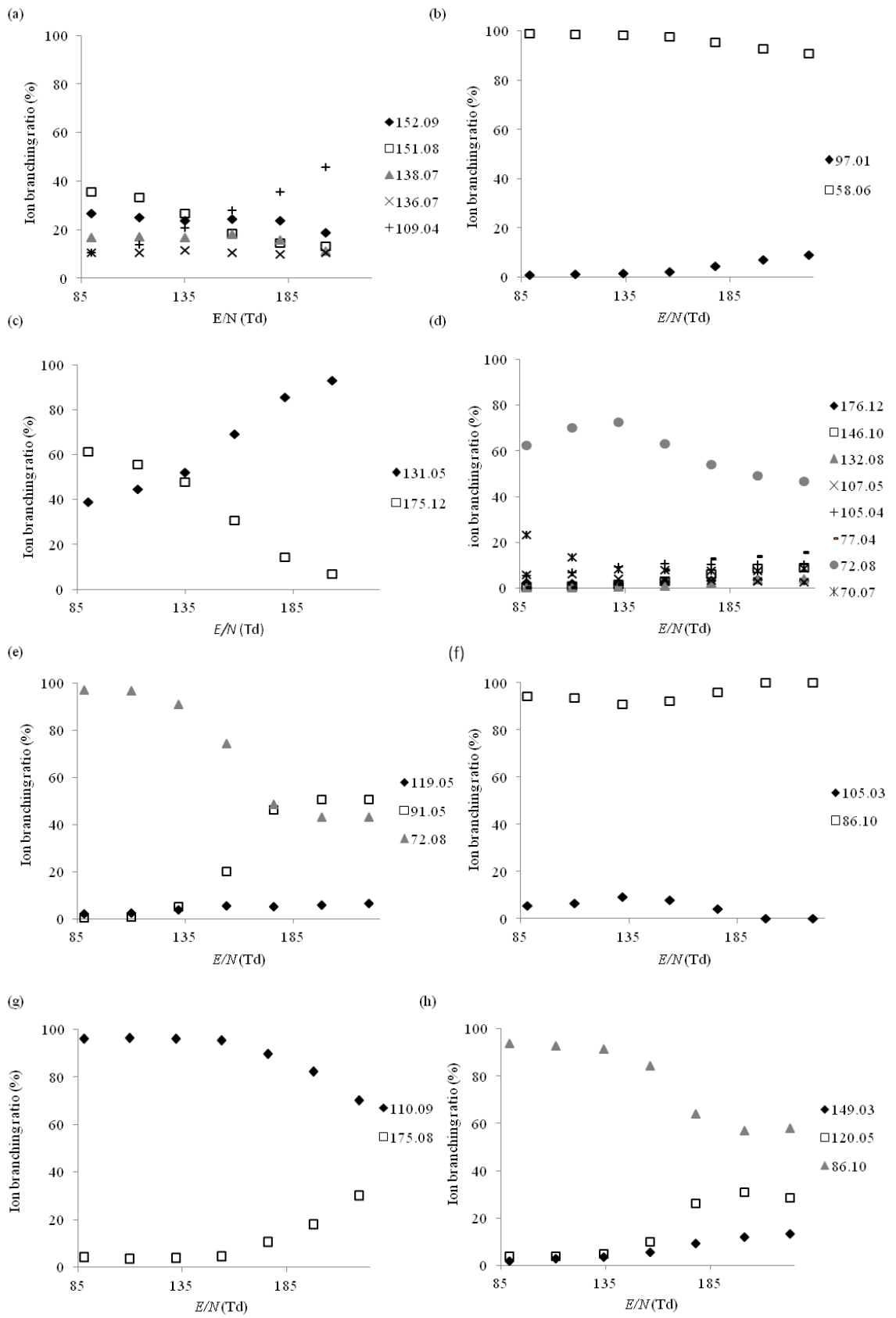


Figure 3.4 (overleaf): The variation of the percentage product ion branching ratios following the reactions of the drug species with  $O_2^+$  as a function of  $E/N$  for (a) 4-fluoroamphetamine, (b) methiopropamine, (c) 5-(2-aminopropyl)benzofuran, (d) ethcathinone, (e) 4-methylethcathinone, (f) N-ethylbuphedrone, (g) 5-MeO-DALT and (h) dimethocaine.

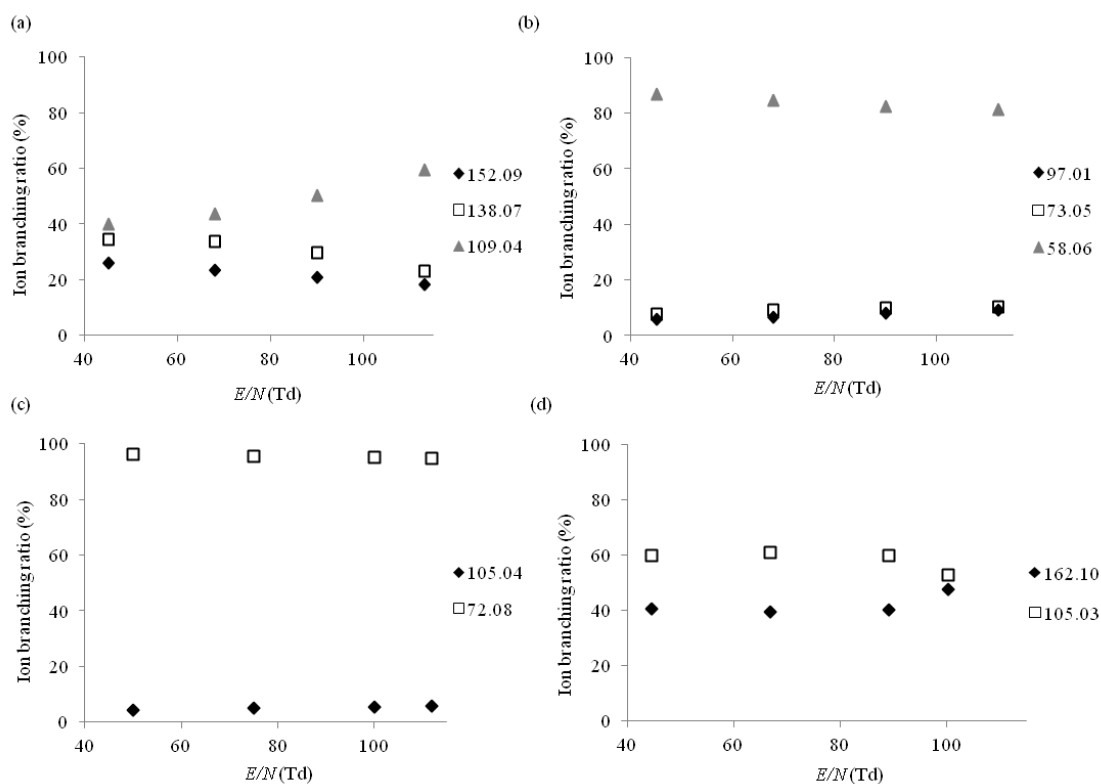


Figure 3.5: The variation of the percentage product ion branching ratios following the reactions of the drug species with  $Kr^+$  as a function of  $E/N$  for (a) 4-fluoroamphetamine, (b) methiopropamine, (c) ethcathinone and (d) N-ethylbuphedrone.

### 3.1.3.4 Ethcathinone

#### *Reactions with $H_3O^+$*

Following reaction with  $H_3O^+$  (Fig 3.2(d)), the dominant product ion observed at  $E/N$  values below 185 Td is the protonated parent molecule at  $m/z$  178.12 ( $[MH]^+$ ,  $C_{11}H_{16}NO^+$ ). Both  $m/z$  160.11 ( $[MH-H_2O]^+$ ,  $C_{11}H_{14}N^+$ ) and  $m/z$  132.08 ( $[MH-C_2H_6O]^+$ ,  $C_9H_{10}N^+$ ), were also observed and their associated branching ratios are found to increase with increasing  $E/N$ . Once  $E/N$  became greater than 185 Td,  $m/z$  160.11 became the dominant product ion.

#### *Reactions with $NO^+$ , $O_2^+$ and $Kr^+$*

The dominant product ion observed from the dissociative charge transfer reaction with  $NO^+$  (Fig. 3.3(d)) was  $m/z$  72.08, assigned to  $[M-C_7H_5O]^+$  ( $C_4H_{10}N^+$ ) which most probably is formed by  $\alpha$ -cleavage at the ketone functional group. Other ions were observed at  $m/z$  105.04 ( $[M-C_4H_{10}N]^+$ ,  $C_7H_5O^+$ ),  $m/z$  146.10, ( $[M-CH_3O]^+$ ,  $C_{10}H_{12}N^+$ ),  $m/z$  175.10 ( $[M-H_2]^+$ ,  $C_{11}H_{13}NO^+$ ) and  $m/z$  176.12 ( $[M-H]^+$ ,  $C_{11}H_{14}NO^+$ ). At  $E/N > 175$  Td the fragments  $m/z$  132.08 ( $[M-C_2H_5O]^+$ ,  $C_9H_{10}N^+$ ) and  $m/z$  130.07 ( $[M-C_2H_7O]^+$ ,  $C_9H_8N^+$ ) were also observed. The use of  $O_2^+$  as the reagent ion (Fig. 3.4(d)) led to the formation of many of the same product ions as were identified with  $NO^+$ , i.e.  $m/z$  72.08 ( $[M-C_7H_5O]^+$ ,  $C_4H_{10}N^+$ ),  $m/z$  105.04 ( $[M-C_4H_{10}N]^+$ ,  $C_7H_5O^+$ ),  $m/z$  132.08 ( $[M-C_2H_5O]^+$ ,  $C_9H_{10}N^+$ ),  $m/z$  146.10 ( $[M-CH_3O]^+$ ,  $C_{10}H_{12}N^+$ ) and  $m/z$  176.12 ( $[M-H]^+$ ,  $C_{11}H_{14}NO^+$ ), with the ion at  $m/z$  72.08 again being the dominant fragment ion. Additional ions were seen at  $m/z$  107.05 ( $[M-C_4H_8N]^+$ ,  $C_7H_7O^+$ ),  $m/z$  77.04 ( $[M-C_5H_{10}NO]^+$ ,  $C_6H_5^+$ ) and  $m/z$  70.07 ( $[M-C_7H_7O]^+$ ,  $C_4H_8N^+$ ).

When  $\text{Kr}^+$  was used as the reagent ion (Fig. 3.5(c)) only two significant product ions were observed in the mass spectra at  $m/z$  72.08 which, as in case of  $\text{NO}^+$  and  $\text{O}_2^+$ , is the dominant fragment ion  $[\text{M}-\text{C}_7\text{H}_5\text{O}]^+$  and  $m/z$  105.04 ( $[\text{M}-\text{C}_4\text{H}_{10}\text{N}]^+$ ,  $\text{C}_7\text{H}_5\text{O}^+$ ) which is observed at comparatively low relative abundances.

No significant contaminants were observed for reactions with any of the reagent ions, indicating that the supplied ethcathinone was reasonably pure.

There is little data available in the literature on the mass spectral analysis of ethcathinone, but the GC-MS analysis of dimethylcathinone, a close structural isomer of ethcathinone, is reported (Dal Cason, 2007). This shows a fragmentation pattern comparable to the observed results obtained when the analyte was ionised via charge transfer ( $\text{NO}^+$ ,  $\text{O}_2^+$  and  $\text{Kr}^+$ ) with the most abundant ion observed at  $m/z$  72. However, GC-MS also observed a significant peak at  $m/z$  44 assigned to the loss of ethane from the fragment at  $m/z$  72 which was not observed in the present study.

### **3.1.3.5 4-Methylethcathinone (4-MEC) and N-Ethylbuphedrone (NEB)**

The principle product ions observed when the structural isomers 4-MEC and NEB react with  $\text{H}_3\text{O}^+$ ,  $\text{NO}^+$ ,  $\text{O}_2^+$  and  $\text{Kr}^+$  have been discussed previously (Lanza et al., 2013) but only at an  $E/N$  of 130 Td for  $\text{H}_3\text{O}^+$ ,  $\text{NO}^+$  and  $\text{O}_2^+$  and 95 Td for  $\text{Kr}^+$ . Therefore we present here a much more extensive study with results covering a wide range in  $E/N$ .

### *Reaction with H<sub>3</sub>O<sup>+</sup>*

When H<sub>3</sub>O<sup>+</sup> was used as the reagent ion at low  $E/N$  values (less than approximately 160 Td), the protonated molecular ion at  $m/z$  192.14 ([MH]<sup>+</sup>, C<sub>12</sub>H<sub>18</sub>NO<sup>+</sup>) was the dominant product ion for both 4-MEC and NEB (Figs 3.2(e) and (f)). Above 170 Td,  $m/z$  174.14 ([MH-H<sub>2</sub>O]<sup>+</sup>, C<sub>12</sub>H<sub>16</sub>N<sup>+</sup>) became the dominant product ion. An ion with a constant branching ratio was observed at  $m/z$  190.13 in both 4-MEC and NEB, this is assigned to [MH-H<sub>2</sub>]<sup>+</sup> (C<sub>12</sub>H<sub>16</sub>NO<sup>+</sup>). The loss of H<sub>2</sub> from the protonated parent molecule is a reaction channel that has been observed in previous studies dealing with illicit drugs with a similar structure (Agarwal et al., 2011). At  $E/N > 135$  Td, additional peaks were observed at  $m/z$  146.10 and  $m/z$  91.06 in both isomers; these masses are tentatively assigned to [MH-C<sub>2</sub>H<sub>8</sub>N]<sup>+</sup> (C<sub>10</sub>H<sub>10</sub>O<sup>+</sup>) and [MH-C<sub>5</sub>H<sub>11</sub>NO]<sup>+</sup> (C<sub>7</sub>H<sub>7</sub><sup>+</sup>) respectively. In the investigation of NEB, an additional peak at  $m/z$  118.07 was observed at  $E/N > 150$  Td, which is assigned to [MH-C<sub>4</sub>H<sub>12</sub>N]<sup>+</sup> (C<sub>8</sub>H<sub>6</sub>O<sup>+</sup>). A mass spectral peak observed at  $m/z$  130.07 is assigned to result from a reaction with an impurity.

### *Reactions with NO<sup>+</sup>, O<sub>2</sub><sup>+</sup> and Kr<sup>+</sup>*

The most significant fragmentation pathway observed following the reaction of NEB with NO<sup>+</sup> and O<sub>2</sub><sup>+</sup> is  $\alpha$  cleavage at the ketone functional group leading to the formation of [M-C<sub>7</sub>H<sub>5</sub>O]<sup>+</sup> at  $m/z$  86.10 (C<sub>5</sub>H<sub>12</sub>N<sup>+</sup>) (Figs. 3.3(f) and 3.4(f)). This product ion could not be observed in the Kr<sup>+</sup> system as it falls within the same  $m/z$  value as the very abundant <sup>86</sup>Kr<sup>+</sup> reagent ion. A second fragment ion was observed with ion branching ratios below 10 %, at  $m/z$  105.03 ([M-C<sub>5</sub>H<sub>12</sub>N]<sup>+</sup>, C<sub>7</sub>H<sub>5</sub>O<sup>+</sup>) when NEB was ionised by NO<sup>+</sup> and O<sub>2</sub><sup>+</sup> via dissociative charge transfer and higher ion branching ratios for the reaction with Kr<sup>+</sup> (Fig. 3.5(d)). Another product ion was

observed at  $m/z$  162.10 ( $[M-C_2H_5]^+$ ,  $C_{10}H_{12}NO^+$ ) for the reaction with  $Kr^+$ . It should be noted that its branching ratio is artificially raised for the  $Kr^+$  data because we cannot determine the product ion signal strength at  $m/z$  86.10. In the case of  $O_2^+$  and  $NO^+$  the associated branching ratio for this product ion was less than 3% throughout the complete  $E/N$  range and hence is not included in that data.

The dominant product ion formed from the reaction of 4-MEC with  $NO^+$ ,  $O_2^+$  (Figs 3.3(e) and 3.4(e)) and the only observed product ion for  $Kr^+$  was  $m/z$  72.08 ( $[M-C_8H_7O]^+$ ,  $C_4H_{10}N^+$ ), formed via  $\alpha$  cleavage at the ketone functional group, the same mechanism that leads to the formation of the product ion  $[M-C_7H_5O]^+$  at  $m/z$  86.10 in NEB. The product ion  $[M-C_4H_{10}N]^+$  at  $m/z$  119.05, equivalent to  $m/z$  105.03 in NEB, was observed at ion branching ratios below 10 % in the  $NO^+$  system. In both the  $NO^+$  and  $O_2^+$  systems the tropylium cation  $[M-C_5H_{10}NO]^+$  was observed at  $m/z$  91.05 with its ion branching ratio increasing significantly with increasing  $E/N$ .

### 3.1.3.6 Ethylphenidate (EP)

#### *Reaction with $H_3O^+$*

For  $H_3O^+$  (Fig. 3.2(g)), the protonated parent molecule ( $[MH]^+$ ,  $C_{15}H_{22}NO_2^+$ ,  $m/z$  248.16) was the dominant product ion throughout the  $E/N$  range; its branching ratio began to decrease only at  $E/N > 200$  Td, thus demonstrating a relatively high stability of the protonated species. Two principle fragment ions were detected, one at  $m/z$  84.08 ( $[MH-C_{10}H_{12}O_2]^+$ ,  $C_5H_{10}N^+$ ) and the other at  $m/z$  165.09 ( $[MH-C_5H_9N]^+$ ,  $C_{10}H_{13}O_2^+$ ); the latter was only observed for  $E/N < 135$  Td. No significant organic impurities were detected. A similar fragmentation pattern was observed in previous studies, where Gas Chromatography-Electron Ionisation-Mass Spectrometry (GC-EI-MS) was used,

although it is not possible to make a comparison of the branching ratios, due to the different nature of the ionisation methods (Casale and Hays, 2011).

#### *Reaction with NO<sup>+</sup>, O<sub>2</sub><sup>+</sup> and Kr<sup>+</sup>*

No reaction with NO<sup>+</sup> was observed, not even adduct formation. For O<sub>2</sub><sup>+</sup> and Kr<sup>+</sup> dissociative charge transfer dominated and very high levels of fragmentation were observed, thus preventing identification of any characteristic peaks.

### **3.1.3.7 5-MeO-Dalt**

#### *Reaction with H<sub>3</sub>O<sup>+</sup>*

Reaction with H<sub>3</sub>O<sup>+</sup> (Fig. 3.2(h)) showed that the protonated parent molecule ([MH]<sup>+</sup>, C<sub>17</sub>H<sub>23</sub>N<sub>2</sub>O<sup>+</sup>, *m/z* 271.18) dominated for *E/N* < 185 Td; at higher *E/N* values *m/z* 174.09 ([MH-C<sub>6</sub>H<sub>11</sub>N]<sup>+</sup>, C<sub>11</sub>H<sub>12</sub>NO<sup>+</sup>, α-cleavage at the amino group) became the most abundant species. A third fragment ion, which was present at low branching ratios (<3%) at *E/N* < 155 Td but which increased to 10% by *E/N* 225 Td, was detected at *m/z* 160.08 ([MH-C<sub>7</sub>H<sub>13</sub>N]<sup>+</sup>, C<sub>10</sub>H<sub>10</sub>NO<sup>+</sup>). This fragment ion is most likely formed via β-cleavage at the amino group.

#### *Reaction with NO<sup>+</sup>, O<sub>2</sub><sup>+</sup> and Kr<sup>+</sup>*

When NO<sup>+</sup> was used as the reagent ion (Fig. 3.3(g)), at *E/N* values below 150 Td the dominant peak was observed at *m/z* 110.09 which is considered to be [M-C<sub>10</sub>H<sub>10</sub>NO]<sup>+</sup> (C<sub>7</sub>H<sub>12</sub>N<sup>+</sup>), corresponding to a tertiary amine fragment. The branching ratio of the parent ion, *m/z* 270.19 ([M]<sup>+</sup>, C<sub>17</sub>H<sub>22</sub>N<sub>2</sub>O<sup>+</sup>), decreases from 25 % to 6 % as *E/N* is increased from 85 Td to 225 Td. Two additional ions were observed *i.e.* *m/z* 175.08 and *m/z* 159.06, tentatively identified as [M-C<sub>6</sub>H<sub>9</sub>N]<sup>+</sup> (C<sub>11</sub>H<sub>13</sub>NO<sup>+</sup>) and [M-C<sub>7</sub>H<sub>13</sub>N]<sup>+</sup>

( $C_{10}H_9NO^+$ ), respectively. When  $O_2^+$  was used as the reagent ion (Fig. 3.4(g)), the parent ion peak was not observed, whilst  $m/z$  175.08 and  $m/z$  110.09 were, again, detected. Finally, when  $Kr^+$  was used as the reagent ion, dissociative charge transfer dominates. However, the very high levels of fragmentation observed prevent the identification of any characteristic peaks.

### 3.1.3.8 Dimethocaine

#### *Reaction with $H_3O^+$*

Reaction of dimethocaine with  $H_3O^+$  led to the production of 4 significant ions (Fig. 3.2(i)). Non dissociative proton transfer at  $m/z$  279.20, ( $[MH]^+$ ,  $C_{16}H_{27}N_2O_2^+$ ), dominates across the whole  $E/N$  range investigated. At  $E/N$  greater than 185 Td fragment ions were observed at  $m/z$  120.04 ( $[MH-C_9H_{21}NO]^+$ ,  $C_7H_6NO^+$ ) and 142.16 ( $[MH-C_7H_7NO_2]^+$ ,  $C_9H_{20}N^+$ ) assigned to  $\alpha$  and  $\beta$  cleavage at the ester functional group respectively. The product ion observed at  $m/z$  86.10 remains at a constant low branching ratio for the whole  $E/N$  range investigated and is assigned to  $[MH-C_{11}H_{15}NO_2]^+$  ( $C_5H_{12}N^+$ ).

Unidentified peaks observed in the mass spectra at  $m/z$  307.24,  $m/z$  265.19,  $m/z$  251.18 and  $m/z$  124.04, are attributed to reactions with unknown impurities in the sample. It has been suggested (Kelleher et al., 2011; drugsyn) that the synthesis of dimethocaine could proceed via the condensation of diethylamino-t-butanol and 4-aminobenzoic acid ethyl ester. The latter has a protonated parent molecule at  $m/z$  166.09; this  $m/z$  was observed and therefore attributed to a reactant (or possibly an intermediate product) in the synthesis of dimethocaine.

Two additional ions at  $m/z$  160.17 and  $m/z$  138.06 are tentatively assigned to be  $C_9H_{22}NO^+$  and  $C_7H_8NO_2^+$  respectively. These two ions may both be formed from proton transfer reactions with a neutral species formed by hydrolysis of dimethocaine producing 3-(diethylamino)-2,2-dimethylpropanol and 4-amino benzoic acid.

#### *Reactions with $NO^+$ , $O_2^+$ and $Kr^+$*

Following reaction with  $NO^+$  (Fig. 3.3(h)) the fragment ion  $[M-C_{11}H_{24}NO_2]^+$  at  $m/z$  86.10 becomes the dominant product ion across the  $E/N$  range investigated although the parent ion at  $m/z$  278.19 ( $[M]^+$ ,  $C_{16}H_{26}N_2O_2^+$ ) is still detected at ion branching ratios below 10 %. At  $E/N$  greater than 185 Td a mass spectral peak is seen at  $m/z$  165.07 which is tentatively assigned to  $[M-C_7H_{15}N]^+$  ( $C_9H_{11}NO_2^+$ ). The fragment ion at  $m/z$  86.10 dominates throughout the  $E/N$  range investigated when  $O_2^+$  is used as the reagent ion (Fig. 3.4(h)), with additional ions at  $m/z$  149.03 and  $m/z$  120.05 assigned to  $[M-C_8H_{19}N]^+$  ( $C_8H_7NO_2^+$ ) and  $[M-C_9H_{20}NO]^+$  ( $C_7H_6NO^+$ ), respectively. Only one significant product ion is observed when  $Kr^+$  is used as the reagent ion at  $m/z$  120.05, attributed to  $[M-C_9H_{20}NO]^+$  ( $C_7H_6NO^+$ ). No previous determination of the fragmentation pathways via chemical ionisation have come to our attention but a study of a related compound (procaine using positive-ion ESI) revealed similar fragmentation pathways (Dhananjeyan et al., 2007) with  $\alpha$  and  $\beta$  cleavage at the ester functional group also observed.

Following reactions with  $NO^+$ ,  $O_2^+$  and  $Kr^+$ , the most significant contaminant observed was at  $m/z$  137.12 ( $C_7H_7NO_2^+$ ) which agrees with the amino benzoic acid impurity found at  $m/z$  138.06 from the  $H_3O^+$  reaction. Additional ions resulting from

reactions with impurities were observed at  $m/z$  223.27 and 230.33 for  $\text{NO}^+$  and at  $m/z$  53.01 in the  $\text{O}_2^+$  system.

### 3.1.3.9 Nitracaine

Two batches with a different appearance, *i.e.* one in powder and one in fine crystal form, were analysed. The powder form of nitracaine did not show any mass spectral peak which could be attributed with any degree of certainty to nitracaine using any of the reagent ions, suggesting that it contained no active ingredient.

#### *Reaction of powder form with $\text{H}_3\text{O}^+$*

In the case of  $\text{H}_3\text{O}^+$ , the principle mass spectral peak over the whole the  $E/N$  range was observed at  $m/z$  160.17 ( $\text{C}_9\text{H}_{22}\text{NO}^+$ ). This is tentatively attributed to protonated 3-(diethylamino)-2,2-dimethylpropanol, a reagent which may be used in nitracaine synthesis (Kelleher et al., 2011; drugsyn). Support for this assignment comes from the fact that this compound is a known irritant (sigmaaldrich), and several online user forums mentioned that nasal irritation occurs following the use of nitracaine (drugsforum; drugsyn). Additional ions were observed at  $m/z$  86.10 ( $\text{C}_5\text{H}_{12}\text{N}^+$ ),  $m/z$  142.10 ( $\text{C}_9\text{H}_{20}\text{N}^+$ , loss of water from the amino alcohol) and  $m/z$  158.15 ( $\text{C}_9\text{H}_{20}\text{NO}^+$ , loss of  $\text{H}_2$  from the amino alcohol) and  $m/z$  63.02, tentatively assigned to  $\text{HNO}_3^+$ .

#### *Reaction of powder form with $\text{NO}^+$ , $\text{O}_2^+$ and $\text{Kr}^+$*

When  $\text{O}_2^+$  was used as a reagent ion,  $m/z$  86.10 was again observed, this was the dominant ion. An additional ion was observed at  $m/z$  128.14, tentatively attributed to  $\text{C}_8\text{H}_{18}\text{N}^+$ , formed by the dissociative charge transfer reaction of  $\text{O}_2^+$  with 3-(diethylamino)-2,2-dimethylpropanol, whilst two unidentified peaks, were detected at

$m/z$  93.99 and 99.96. In the case of  $\text{NO}^+$ ,  $m/z$  86.10 was again the dominant ion. Additional peaks with lower branching ratios were observed at  $m/z$  142.10 (tentatively assigned to  $\text{C}_9\text{H}_{20}\text{N}^+$ ),  $m/z$  158.15 ( $\text{C}_9\text{H}_{20}\text{NO}^+$ ) and again an unknown peak at  $m/z$  93.99. Reaction with  $\text{Kr}^+$  shows no significant peaks in the mass spectra.

#### *Reaction of crystal form with $\text{H}_3\text{O}^+$*

Many of the ions observed in the nitracaine powder form are also observed following reaction of the crystal form with  $\text{H}_3\text{O}^+$  but in this case a mass spectral peak corresponding to the protonated molecule was observed at  $m/z$  309.17 ( $[\text{MH}]^+$ ,  $\text{C}_{16}\text{H}_{25}\text{N}_2\text{O}_4^+$ ). This indicates that unlike the powder, the crystalline form contains nitracaine. Other ions were detected at  $m/z$  160.17 ( $\text{C}_9\text{H}_{22}\text{NO}^+$ , again the dominant mass spectral peak over the whole  $E/N$  range),  $m/z$  86.10 ( $\text{C}_5\text{H}_{12}\text{N}^+$ ) and two unknown mass spectral peaks at  $m/z$  107.05 and 101.02. Furthermore, a peak at  $m/z$  63.02, corresponding to  $\text{HNO}_3^+$ , was observed.

#### *Reaction of crystal form with $\text{NO}^+$ , $\text{O}_2^+$ and $\text{Kr}^+$*

The only ions detected formed from the reaction of the reagent ion with impurities in the sample, as mentioned above for the powder form, but identical  $m/z$  values were not necessarily observed. Two ions, corresponding to  $\text{C}_5\text{H}_{12}\text{N}^+$  and  $\text{C}_7\text{H}_4\text{NO}_3^+$ , at  $m/z$  86.10 and  $m/z$  149.95, were detected for reactions with  $\text{O}_2^+$  and  $\text{NO}^+$ , with  $m/z$  86.10 always being the most abundant. When  $\text{O}_2^+$  was used as the reagent ion, an impurity at  $m/z$  63.02, assigned to  $\text{HNO}_3^+$  was detected; while after switching to  $\text{NO}^+$ , an ion at  $m/z$  142.10 ( $\text{C}_9\text{H}_{20}\text{N}^+$ ) became significant. When  $\text{Kr}^+$  was used as the reagent ion a large number of low intensity mass spectral peaks were observed preventing identification of any characteristic peaks.

The fact that the molecular parent ion was observed in the crystal but not in the powder form indicates that the supplied nitracaine in powder form contained nitracaine at insufficient levels to be detected (probably because of improper synthesis), thus explaining contradictory reports on the effect of nitracaine seen on online user forums (drugsforum; drugsyn).

### **3.1.4 Conclusions**

Although some impurities were found in the drugs, all of the supplied compounds with the exception of nitracaine powder were found to contain the advertised active ingredient. This is surprising considering drugs counselling reports (eve-rave) on designer drugs (e.g. ecstasy = MDMA) purchased from the black market, which can contain virtually everything, from various mixtures of legal and illegal ingredients to common caffeine.

The fast pace of legislation designed to control new psychoactive substances leads to extremely short "invention to market" times and thus to increasing risks for the consumers; e.g. in the unfortunate case of the very recent UK ban on 5-APB, which was replaced by the presumably highly toxic 5-EAPB that has already caused fatalities among its first users (the Guardian ). However, the rapid spread of new psychoactive substances (United Nations, 2013) means that the ability to rapidly detect and identify these species is gaining increasing importance for both policing and medical applications.

The reported product ion branching ratios formed from the analysis of a number of common new psychoactive substances (some, while legal at the time of purchase, are now controlled in some states) by SRI-ToF-MS is designed to provide a reference for the development of techniques, capable of identifying these drug species in more complex ‘real world’ environments. These results add to the already large list of threat compounds detectable by SRI-ToF-MS. The potential role of this technology for the detection of threat agents has been established including research focusing on the detection of rape drugs in beverages (Jürschik et al., 2012). This paves the way for the application of this technology to real-world situations, such as the detection of compounds adhered to surfaces (e.g. skin or fabrics) and the rapid identification of the constituents of blended drugs.

### **Acknowledgements**

ML and KB have received funding through the PIMMS ITN which is supported by the European Commission’s 7<sup>th</sup> Framework Programme under Grant Agreement Number 287382. WJA is in receipt of a BBSRC-Industrial CASE studentship in association with IONICON Analytik GmbH.

### 3.2 Distinguishing two isomeric mephedrone substitutes with selective-reagent-ionization mass spectrometry (SRI-MS)

Lanza M.<sup>1</sup>, Acton W. J.<sup>2</sup>, Jürschik S.<sup>1</sup>, Sulzer P.<sup>1,\*</sup>, Breiev K.<sup>1</sup>, Jordan A.<sup>1</sup>, Hartungen E.<sup>1</sup>, Hanel G.<sup>1</sup>, Märk L.<sup>1</sup>, Mayhew C. A.<sup>3</sup> and Märk T. D.<sup>1,4</sup>

[1] {Ionicon Analytik GmbH., Eduard-Bodem-Gasse 3, 6020 Innsbruck, Austria}

[2] {Lancaster Environment Centre, Lancaster University, Lancaster, LA1 4YQ, UK}

[3] {School of Physics and Astronomy, University of Birmingham, Edgbaston, Birmingham, B15 2TT, UK}

[4] {Institut für Ionenphysik und Angewandte Physik, Leopold-Franzens Universität Innsbruck, Technikerstr. 25, 6020 Innsbruck, Austria}

\* corresponding author: philipp.sulzer@ionicon.com, Tel: +43 512 214 800 050, Fax: +43 512 214 800 099

#### Abstract

The isomers 4-methylethcathinone (4-MEC) and N-ethylbuphedrone (NEB) are substitutes for the recently banned drug mephedrone (4-MMC). We find that with conventional Proton-Transfer-Reaction Mass Spectrometry (PTR-MS) it is not possible to distinguish between these two isomers, because essentially for both substances only the protonated molecules are observed at  $m/z$  192 ( $C_{12}H_{18}NO^+$ ). However, when utilizing an advanced Proton-Transfer-Reaction Mass Spectrometry (PTR-MS) instrument, which allows us to switch the reagent ions (Selective-Reagent-Ionization / SRI-MS) from  $H_3O^+$  (which is commonly used in PTR-MS) to  $NO^+$ ,  $O_2^+$  and  $Kr^+$ , characteristic product (fragment) ions are detected:  $C_4H_{10}N^+$  (72 Da) for 4-

MEC and  $C_5H_{12}N^+$  (86 Da) for NEB; thus, SRI-MS proves to be a powerful tool for fast detection and identification of these compounds.

### **3.2.1 Introduction**

New psychoactive substances (NPS), research chemicals (RC), legal highs and designer drugs are just some names for psychoactive chemicals which are not controlled by drug legislation. Importantly, these are increasingly being used as substitutes for "classic" prohibited drugs by persons who are looking for intoxicating effects but do not wish to commit a criminal act (Werse, 2012). Probably the most popular representative of these NPS was 4-methylmethcathinone (4-MMC;  $C_{11}H_{15}NO$ ), better known as mephedrone, a cathinone derivative (Kelly, 2011). However, after several lurid articles in the boulevard press all over Europe, mephedrone became a controlled substance in virtually all European countries in 2010.

During our literature research it turned out that user forums on the internet provide the most up-to-date source of information on NPS (e.g. bluelight; drugs-forum). According to these forums, as long as mephedrone was legal, there was only mediocre interest in it and positive and negative experience reports were more or less in balance. Immediately after the ban, mephedrone became a "martyr", i.e. a process of glorification started and hardly any comments on drawbacks and negative side effects were posted after that. A majority of users in the legal high community rather started considering mephedrone as the "gold standard" for NPS and typical reviews about new NPS nowadays usually contain sentences like e.g. "if mephedrone is rated 10, I would give this substance a 5". Thus it is not surprising that immediately after the ban numerous (legal) mephedrone substitutes flooded the market. These substances are

either isomers or other cathinone derivatives or completely new RCs (especially in countries with analogue laws in force) with supposedly similar psychoactive effects (European Union, 2013). Examples of these mephedrone substitutes include: 3-methylmethcathinone (3-MMC), 4-methylethcathinone (4-MEC), N-ethylbuphedrone (NEB), 3,4-dimethylmethcathinone (3,4-DMMC), and 3-Fluoromethcathinone (3-FMC). For these substances even less information about toxicity and long term effects are available than for 4-MMC. Wersé and Morgenstern state in their publication “that many NPS show side effects that are at least as serious as those associated with illicit drugs, and that long-time risks are unpredictable” and they conclude that “repressive drug policy enforcement may lead to increased public health risks regarding drug users.” (Wersé, 2012) This is a serious issue that needs to be thought through by our legislative bodies.

Regardless of the future development of drug policies there is an obvious current need for fast and reliable detection of NPS, either for law enforcement agencies or for forensic and medical laboratories. The most commonly used analytical procedures for drug detection are based on gas chromatographic (GC) methods e.g. in toxicological analysis (Westwell et al., 2013). GC, especially in combination with mass spectrometry (GC/MS), is a very selective and sensitive method. However, this comes at the expense of fast analysis. GC-MS is time consuming, so that a real-time and therefore on-the-spot analysis becomes impossible. Ion mobility spectrometry (IMS) and chemical test strips are much faster methods, but these only have very limited selectivity (Biermann et al., 2004). Furthermore, in the case of IMS only those compounds that are included in the instrument's library can be identified (Keller et al., 1999). This limitation on selectivity results from the lack of information on the molecular masses of the compounds being detected. In comparison to GC techniques,

PTR-MS is a faster detection system (response times of about 100 ms). In addition, PTR-MS is far more selective than IMS and chemical test strips. The only limitation is that it is a one dimensional analytical technique with only the  $m/z$  of an ion being identified, making unambiguous compound identification difficult. However, recent advances in PTR-MS technology (e.g. switchable reagent ion source and changing operational parameters) are beginning to address this drawback.

In earlier studies we have illustrated the applicability of proton-transfer-reaction mass spectrometry (PTR-MS) for the detection of several illicit and controlled prescription drugs (Agarwal et al., 2011) and numerous other threat substances that can harm people, such as explosives (Jürschik et al., 2010; Mayhew et al., 2010; Sulzer et al., 2012b), chemical warfare agents and toxic industrial compounds (Agarwal et al., 2012; Kassebacher et al., 2013; Petersson et al., 2009). For explosives we additionally presented a method of increasing selectivity by changing operational parameters (reduced electric field in the drift tube) (Sulzer et al., 2012b). In this paper we present data obtained with an advanced PTR-MS instrument that shows a new level of selectivity for this technology, i.e. the separation and hence the unambiguous identification of the two isomeric mephedrone substitutes 4-MEC and NEB ( $C_{12}H_{17}NO$ ; see Fig. 3.6 for their chemical structures).

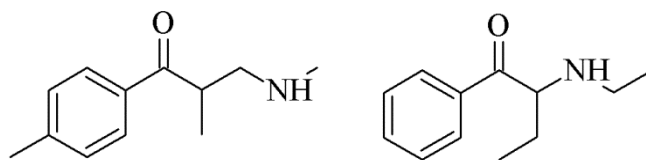


Figure 3.6: Chemical structures of 4-MEC (left) and NEB (right)

### 3.2.2 Experimental

For the present studies we used a PTR-MS instrument equipped with switchable reagent ion capability (PTR-TOF 8000, Ionicon Analytik (Jordan et al., 2009a)). Switchable reagent ion in this context means that the reagent ions used for chemical ionization of the sample molecules can be switched from  $\text{H}_3\text{O}^+$  (Lindinger et al., 1998a) to either  $\text{O}_2^+$ ,  $\text{NO}^+$  (Jordan et al., 2009b) or  $\text{Kr}^+$  (Sulzer et al., 2012a), by changing the source gas used in the hollow cathode discharge source. Such an instrument has recently been called a selective-reagent-ionization mass spectrometry (SRI-MS) device by Karl et al. (2012), which we adopt here. Details about the instrument and ionization processes can be found in (Jordan et al., 2009b; Jordan et al., 2009a; Sulzer et al., 2012a).

The two cationones investigated in this study, which are not controlled in many European countries, were purchased from a popular (according to user forums) internet vendor and used without further purification. A few mg of the samples were put into glass vials, which were then sealed with septa through which inlet and outlet PEEK (polyether ether ketone) tubing was inserted. Purified air was then drawn through the vials for subsequent analysis of the air (dynamic headspace) with the SRI-MS instrument. The vials were heated respectively to  $65^\circ$  (NEB) and  $90^\circ\text{C}$  (4-MEC) to ensure high signal intensity and to prevent variations in the dynamic headspace concentration due to changes in the room temperature. The lines connecting the respective vial to the instrument were heated to  $110^\circ\text{C}$  to limit surface adsorption. The data obtained are presented without any post-processing, i.e. without reagent ion signal intensity normalization or other corrections (e.g. transmission factors), as we only wish to demonstrate in this paper the advantages in selectivity when using a SRI-MS compared to classical PTR-MS instrument.

### 3.2.3 Results

We first investigated the reactions of 4-MEC and NEB with  $\text{H}_3\text{O}^+$ . Surprisingly the mass spectra of both substances showed no major impurities, i.e. the samples from the RC vendor were exceptionally pure. The majority of the impurities would be expected to originate from residual solvents from the synthesis process. Given that these solvents will possess much higher vapour pressures than 4-MEC or NEB, then in combination with the observed intensities of the impurities being far less than 1% of the protonated molecule ion intensity, we estimate that the sample purities are better than 99.9%, i.e. they are at a purity level that would be expected from a certified chemical supplier. Fig. 3.7 shows the sections of the mass spectra in the region around the protonated molecules.

The dominant product ion observed is the protonated parent ion for both NPS at  $m/z$  192.14. The peak to the right of this originates from the  $^{13}\text{C}$  isotopes. The product ion observed at  $m/z$  190.12 is a result of  $\text{H}_2$  elimination from the protonated molecule, a reaction channel we have already observed in our previous studies on illicit drugs (e.g. for the chemically related MDMA (ecstasy) (Agarwal et al., 2011)). Further high mass fragments were identified as  $\text{C}_{12}\text{H}_{16}\text{N}^+$  ( $\text{H}_2\text{O}$  loss) and  $\text{C}_{10}\text{H}_{10}\text{O}^+$  ( $\text{C}_2\text{H}_8\text{N}$  loss) for both isomers, both of which have intensities well below 10% of the protonated molecule signal intensity. The investigation of branching ratios and the identification of some low intensity fragment ions is work in progress and beyond the scope of this Application Note.

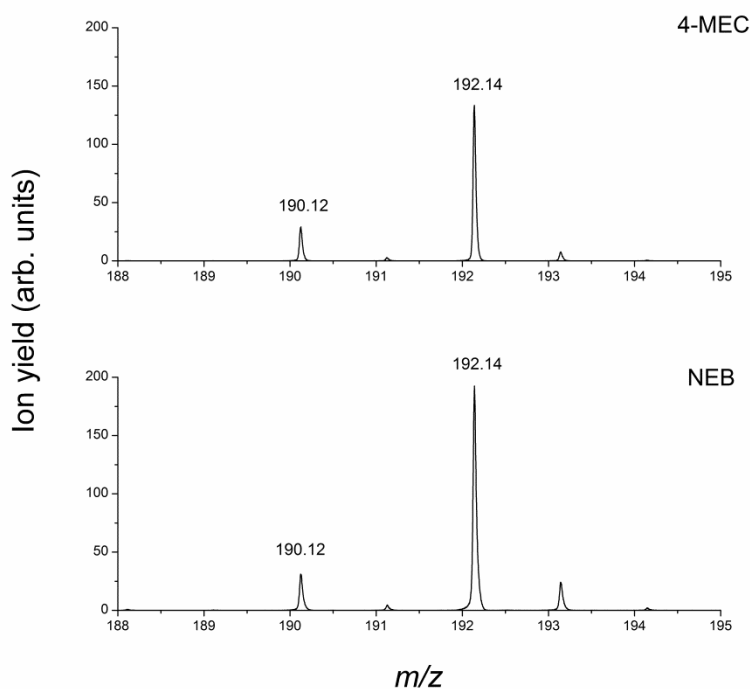


Figure 3.7: Mass spectrum sections for 4-MEC (upper) and NEB (lower) with  $\text{H}_3\text{O}^+$  being used as reagent ions

Utilizing  $\text{H}_3\text{O}^+$  chemistry makes it impossible to separate the two isomers 4-MEC and NEB, i.e. the most abundant product ions are identical. However, switching to  $\text{NO}^+$  as reagent ions solves this problem immediately (Fig. 3.8). We comment that this switching from water to NO chemistry is rapid being approximately 10 seconds (Jordan et al., 2009b). The most abundant product ions now observed are different for the two compounds. We find that 4-MEC fragments upon reaction with  $\text{NO}^+$  mainly to  $\text{C}_4\text{H}_{10}\text{N}^+$  ( $m/z$  72.08), which corresponds to the loss of  $\text{C}_8\text{H}_7\text{O}$  from the singly charged parent (compare Fig. 3.6). On the other hand, the reaction of  $\text{NO}^+$  with NEB results in  $\text{C}_5\text{H}_{12}\text{N}^+$  ( $m/z$  86.10), which corresponds to the loss of  $\text{C}_7\text{H}_5\text{O}$ , via  $\alpha$ -cleavage at the ketone functional group.

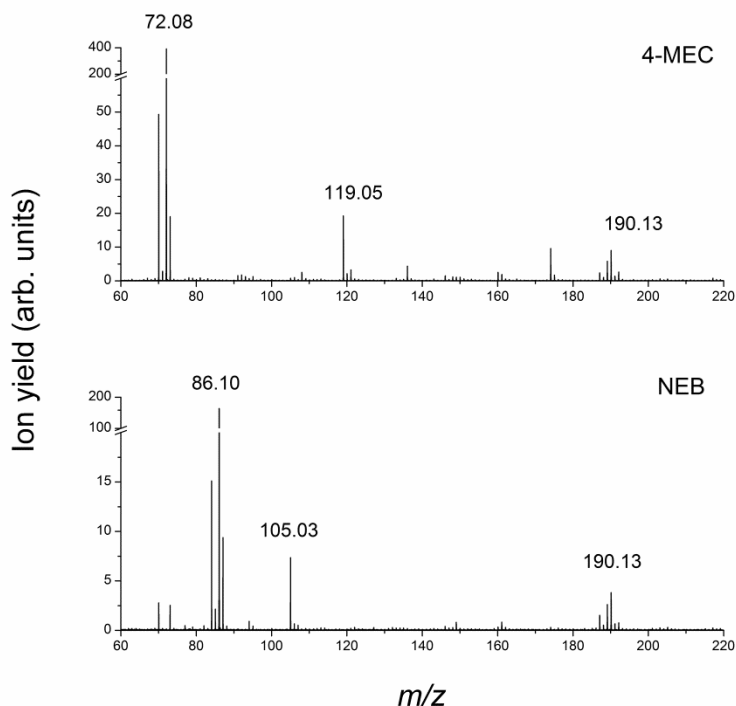


Figure 3.8: Mass spectra for 4-MEC (upper) and NEB (lower) obtained with  $\text{NO}^+$  chemistry

After switching to  $\text{O}_2^+$  the situation does not change dramatically. As can be seen in Fig. 3.9, the most abundant product ions are again  $\text{C}_4\text{H}_{10}\text{N}^+$  ( $m/z$  72.08) for 4-MEC and  $\text{C}_5\text{H}_{12}\text{N}^+$  ( $m/z$  86.10) for NEB. Other product ions formed both when  $\text{NO}^+$  and  $\text{O}_2^+$  were used as reagent ions were far less abundant and therefore less suitable for substance identification; these ions include:  $m/z$  190.12 ( $\text{C}_{12}\text{H}_{16}\text{NO}^+$ , hydride abstraction),  $m/z$  119.05 ( $\text{C}_8\text{H}_7\text{O}^+$ ) for 4-MEC;  $m/z$  190.13 ( $\text{C}_{12}\text{H}_{16}\text{NO}^+$ , hydride abstraction),  $m/z$  105.03 ( $\text{C}_7\text{H}_5\text{O}^+$ ) for NEB. Therefore, again the two most abundant product ions can be used for the identification of the two isomers. It has to be noted that although switching between  $\text{H}_3\text{O}^+$ ,  $\text{NO}^+$  and  $\text{O}_2^+$ , respectively, can be done within 10 s, i.e. there is no disadvantage in terms of the rapidity of measurements, a pure  $\text{O}_2$

supply gas cylinder is required for the generation of  $O_2^+$  reagent ions. In contrast, for the  $NO^+$  mode no external gas supply is necessary, instead charcoal filtered air can be used as source gas. This means, that for field measurements  $NO^+$  would be the preferred reagent ion.

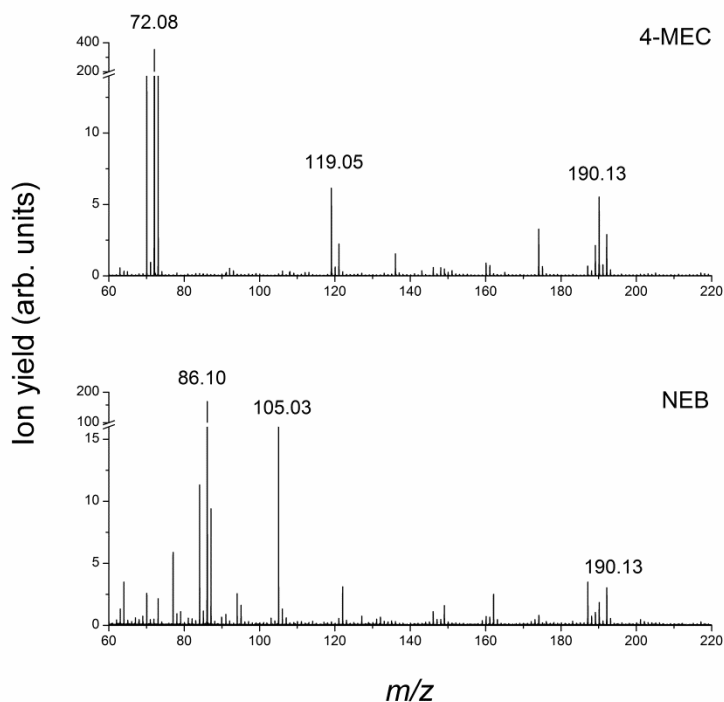


Figure 3.9: Mass spectra for 4-MEC (upper) and NEB (lower) obtained with  $O_2^+$  chemistry

By utilizing  $Kr^+$  chemistry we discovered some issues that lead us to the conclusion that  $Kr^+$  is somehow less suitable for the present application.  $Kr^+$  reacts with the two common air constituents  $H_2O$  and  $O_2$ , resulting in the production of  $H_3O^+$  (produced through secondary reactions of  $H_2O^+$  and  $H_2O$ ) and  $O_2^+$ . This means that the  $Kr^+$  reagent ions will be rapidly converted to these ions and hence will not be available to react with the trace compounds. Sulzer et al. (2012a) recently suggested the use of a

buffer gas in the drift tube, such as He or N<sub>2</sub>, which effectively helps to overcome this problem. However, after the instrument has been operated in H<sub>3</sub>O<sup>+</sup> mode a considerable amount of water will cover the surfaces inside the SRI-MS instrument and will only slowly evaporate.

Thus, in contrast to NO<sup>+</sup> and O<sub>2</sub><sup>+</sup>, switching to Kr<sup>+</sup> from H<sub>3</sub>O<sup>+</sup> cannot be done within seconds but needs several minutes. Regardless of this disadvantage we have also investigated the reactions of the two mephedrone substitutes with Kr<sup>+</sup>. For 4-MEC the situation is quite clear. Owing to the high ionization potential of Kr (14 eV) the chemical ionization process is highly exothermic and therefore extensive fragmentation of the sample molecule is expected. Indeed, we do not see any high mass fragments (which were observed in small quantities for NO<sup>+</sup> and O<sub>2</sub><sup>+</sup>, respectively, see Fig. 3.8 and Fig. 3.9) and again the most abundant product is C<sub>4</sub>H<sub>10</sub>N<sup>+</sup> (*m/z* 72.08), i.e. 4-MEC can be identified via this fragment (Fig. 3.10 upper panel). For NEB there is a major problem. From the NO<sup>+</sup> and O<sub>2</sub><sup>+</sup> results we can expect Kr<sup>+</sup> to react with NEB via dissociative charge transfer to produce C<sub>5</sub>H<sub>12</sub>N<sup>+</sup> (*m/z* 86.10). However, Kr has an isotope at *m/z* 85.91 (30% abundance) which will overwhelm any signal associated with *m/z* 86, and therefore (if produced) this ion is not detectable (Fig. 3.10 lower panel). This means that by utilizing Kr<sup>+</sup> chemistry we can indeed still separate the two isomeric compounds, but with somehow limited certainty, as one of the two respective characteristic fragment ions is not available for identification.

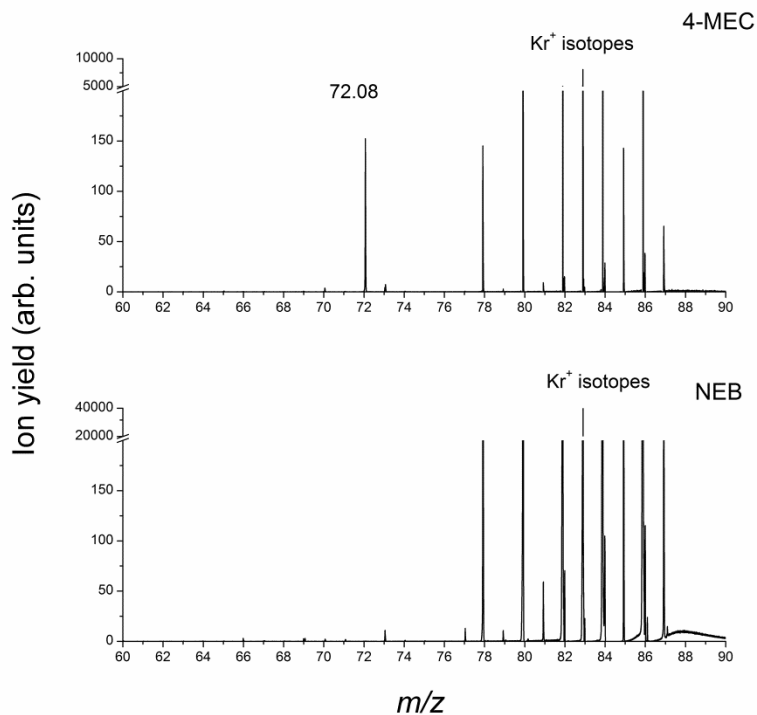


Figure 3.10: Mass spectra for 4-MEC (upper) and NEB (lower) obtained with  $\text{Kr}^+$  chemistry

### 3.2.4 Conclusions

In summary, after a series of studies on various threat agents (e.g. explosives, chemical warfare agents, toxic industrial compounds) and illicit and controlled prescription drugs, which have demonstrated the high sensitivity capabilities of the PTR-MS technology, in the present paper we have additionally shown the applicability of the latest generation of PTR-MS technology (SRI-MS) for highly selective separation of isomers by switching the reagent ions with the help of the two mephedrone substitutes 4-MEC and NEB and switching between  $\text{H}_3\text{O}^+$  and  $\text{NO}^+$  chemistry. NPS are a hot-topic in our society (European Union, 2013) and will have to

be widely discussed in the near future, given the number of users and the potentially harmful side effects of these chemicals.

Independent of the way the European policies on NPS will develop - either banning a constantly increasing amount of substances or easing prohibition to prevent even more dangerous and toxic NPS from being introduced onto the market - there is a need for fast and reliable detection and identification of these compounds. We have shown that SRI-MS is a technology that has the potential to fulfill these needs.

### **Acknowledgements**

The research leading to these results has received funding through the PIMMS ITN which is supported by the European Commission's 7th Framework Programme under Grant Agreement Number 287382. WJA is in receipt of a BBSRC-Industrial CASE studentship in association with Ionicon Analytik.

## Chapter IV

# **The effect of ozone fumigation on the emission of biogenic volatile organic compounds (bVOCs) from *Brassica napus***

This chapter demonstrates the effect of ozone fumigation on the emissions of bVOCs from oilseed rape (*Brassica napus*) both above and below ground. The emissions of bVOCs are recorded using an SRI-ToF-MS operated in  $\text{H}_3\text{O}^+$  mode and  $\text{NO}^+$  mode as described in Chapter III. The use of  $\text{NO}^+$  mode provides additional structural information enabling the identification of analyte functional groups. Ozone fumigation of the plant leaves is shown not to effect bVOC emissions below ground. Following ozone fumigation the emissions of monoterpenes and sesquiterpenes from the leaf chamber are shown to drop dramatically. The reduction in monoterpene emission was attributed to a reaction with OH radicals and the reduction in sesquiterpene emission to ozonolysis. A large increase in the emission of oxygenated species was observed following ozone fumigation with an increase in the concentration of ca. 20 compounds.

This work is being prepared for submission to the journal Environmental Science and Technology. The authors and their contributions are listed below:

**Acton W. J. F. (Lancaster University):** Planned and carried out experiments, analysed data and prepared manuscript.

**Jud W. (University of Innsbruck):** Helped with the experimental design, data processing, the interpretation of results and manuscript preparation.

**Ghirardo A. (Helmholtz Zentrum Munich):** Analysed GC-MS samples.

**Wohlfahrt G. (University of Innsbruck):** Provided growth space and offered advice on experimental design.

**Hewitt C. N. (Lancaster University):** Helped with manuscript preparation and with the interpretation of results.

**Taylor J. E. (Lancaster University):** Helped with manuscript preparation and with the interpretation of results.

**Hansel A. (University of Innsbruck):** Helped with the experimental design, data processing and with the interpretation of results.

# The effect of ozone fumigation on the emission of biogenic volatile organic compounds (bVOCs) from *Brassica napus*

Acton W. J. F.<sup>1</sup>, Jud W.<sup>2</sup>, Ghirardo A.<sup>3</sup>, Wohlfahrt G.<sup>4</sup>, Hewitt C. N.<sup>1</sup>, Taylor J. E.<sup>1</sup>, and Hansel A.<sup>2</sup>

[1] {Lancaster Environment Centre, Lancaster University, Lancaster, LA1 4YQ, United Kingdom}

[2] {Institute of Ion and Applied Physics, University of Innsbruck, 6020 Innsbruck, Austria}

[3] {Helmholtz Zentrum München, Institute of Biochemical Plant Pathology, Research Unit Environmental Simulation (EUS), 85764 Neuherberg, Germany}

[4] {Institute of Ecology, University of Innsbruck, 6020 Innsbruck, Austria}

## Abstract

Here we report the emissions of bVOCs from oilseed rape (*Brassica napus*) both when the plant is exposed to clear air and when it is fumigated with ozone at environmentally-relevant mixing ratios (~100 ppbv) under controlled laboratory conditions. Emissions of bVOCs were recorded from both leaves and roots using a recently developed selective reagent ionisation - time of flight - mass spectrometer (SRI-ToF-MS) enabling bVOC detection with high time and mass resolution, together with the ability to identify certain molecular functionality. Emissions of bVOCs from

the roots were found to be dominated by sulfur compounds including methanethiol, dimethyl disulfide and dimethyl sulphide, and these below-ground emissions did not change following fumigation of the plant with ozone.

Ozone fumigation of the plant caused a rapid decrease in monoterpene and sesquiterpene concentrations in the leaf chamber and increased concentrations of ca. 20 oxygenated species. The drop in sesquiterpenes concentrations was attributed to ozonolysis occurring to a major extent on the leaf surface. The drop in monoterpene concentrations was attributed to gas phase reactions with OH radicals deriving from ozonolysis reactions. As plant-emitted terpenoids have been shown to play a role in plant-plant and plant-insect signalling, the rapid loss of these species in the air surrounding the plants following ozone fumigation may have a significant impact on plant-plant and plant-insect communications.

#### **4.1 Introduction**

Biogenic volatile organic compounds (bVOCs) are a large and diverse group of molecules released from plants into the atmosphere (Dudareva et al., 2006). Plants have been shown to emit bVOC from both above- and below-ground organs and these emissions are known to change in response to both biotic and abiotic stress (Holopainen and Gershenzon, 2010). These molecules represent a major source of reactive carbon released into the atmosphere, with ca.  $10^{15}$  g emitted annually (Guenther et al., 2012), and hence play a significant role in tropospheric chemistry both by acting as a sink for atmospheric oxidants, such as OH radicals, and through their effects on the formation of secondary organic aerosol (SOA) and tropospheric

ozone (Atkinson and Arey, 2003a). bVOCs therefore impact significantly on both the climate system and local-to-regional air quality.

Ozone is formed photochemically in the troposphere by reactions involving volatile organic compounds (VOCs) and NO<sub>x</sub> (NO and NO<sub>2</sub>) (Logan, 1985; Atkinson and Arey, 2003a). In the northern hemisphere background ozone levels are generally in the range 35-40 ppbv, but locally can peak above 100 ppbv depending on concentrations of precursors and weather conditions (Royal Society, 2008). Recent studies indicate that tropospheric ozone concentrations have stabilised, or are decreasing, in some industrialised areas due to reductions in precursor emissions (Oltmans et al., 2013). However, ozone concentrations in the troposphere continue to rise in parts of Asia (Fu and Tai, 2015). Tropospheric ozone is an especially important pollutant due to the detrimental impact it has been shown to have on both human health and crop yields (WHO, 2003; Ashmore, 2005; Royal Society, 2008).

bVOC emissions from plants are affected by both biotic stress and the abiotic physical conditions to which they are exposed (Laothawornkitkul et al., 2009; Holopainen and Gershenson, 2010), including the ambient concentrations of ozone. These effects are not yet fully understood, with experimental evidence showing an increase (Heiden et al., 1999), decrease (Ryan et al., 2009) or no significant effect (Ryan et al., 2009) on bVOC emission from different plant species in response to ozone. However, an increase in bVOC emissions, together with a change in the chemical composition of the bVOC blend emitted, is commonly observed in response to biotic stresses. Both constitutive and induced bVOC emissions can act as a direct defence, repelling herbivores, or as an indirect defence through a “cry for help” (Dicke, 2009; Kessler

and Baldwin, 2001) to attract the predators of the herbivorous organisms attacking them.

Both monoterpenes and sesquiterpenes are commonly emitted in response to biotic stress (Gosset et al., 2009; Laothawornkitkul et al., 2008) and have been shown to play an important role in plant signalling (Degenhardt et al., 2009; Kappers et al., 2005; Kessler and Baldwin 2001). There have been limited studies on the effect of ozone on plant volatile signalling but the few available studies suggest that ozone may affect plant-insect signalling (Pinto et al., 2010). Upon exposure to ozone, bVOCs containing an alkene functional group, such as monoterpenes and sesquiterpenes, may undergo ozonolysis in the gas phase or liquid phase, inside or outside of the plant (Hewitt and Terry 1992). The gas phase ozonolysis of alkenes (Fig. 4.1) leads to the formation of an energy-rich ozonide, which rapidly decomposes to a carbonyl and a high energy Criegee intermediate (Criegee, 1975). The Criegee intermediate can then be collisionally-stabilised or, depending on the structure of the Criegee intermediate, can decay to either  $\text{CO}_2 + \text{RH}$  or to the OH radical and a substituted alkyl radical (Atkinson and Arey, 2003b). Thus the ozonolysis of terpenoids can act as a source of OH and a range of oxygenated VOCs.

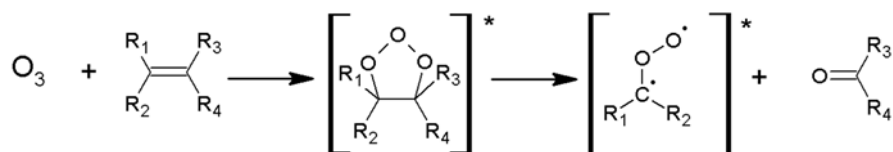


Figure 4.1, ozonolysis of alkenes leading to the formation of a carbonyl and a Criegee intermediate where [ ]\* represents a high energy species.

Here we report, for the first time, bVOC emissions from the whole plant measured simultaneously in the leaf and root zone, using the recently developed selective reagent ionisation-time of flight-mass spectrometer (SRI-ToF-MS). The effect of ozone fumigation on bVOC emissions both above- and below-ground is reported. Using the highly time-resolved and sensitive SRI-ToF-MS, we could follow the initial reaction of several biogenically emitted terpenoids with ozone and observed the formation of a number of atmospherically-abundant oxygenated compounds. *Brassica napus* (oilseed rape) was selected as the model plant species due to its wide geographic distribution, its importance as a crop and its known emission of both monoterpenes and sesquiterpenes (Himanen et al., 2009).

## **4.2 Methodology**

Experiments were carried out in two blocks, July-September 2013 and April-June 2014. In 2013, bVOC emissions from potted plants enclosed in chambers were recorded from both plant leaves and from the soil and roots using a SRI-ToF-MS. During the 2014 experiments, measurements were made from above ground alone using a SRI-ToF-MS in order to increase the time resolution of the leaf emission data. Additionally, leaf chamber samples were collected for chemical identification by GC-MS analysis.

#### **4.2.1 Plant material**

*Brassica napus* plants (DK Cabernet, Monsanto) were grown from seed under natural light with supplementary heating in glass houses at the University of Innsbruck Botanical Gardens from May-July 2013 and January-April 2014. The soil used was made up of steamed leaf mould (31%), steamed basic soil (15%), coconut fibre (15%), sand (15%), rock flour (15%) and lava (12%). Measurements were carried out when plants were at growth stages 1.4-1.6 (HGCA, 2012) meaning that plants had between 3 and 5 open adult leaves and had not yet undergone stem extension. Plants were transplanted prior to experiments into 2 L root chambers and given a week to acclimatise to lab conditions. In 2013 six replicates were carried out using unique plants and in 2014 a further seven replicates were carried out.

#### **4.2.2 Experimental setup**

The experimental setup was based on that described by Jud et al. (2016) and is shown in Fig. 4.2. Both the leaf and root chambers were designed with glass and PFA/PTFE surfaces in order to limit background VOC emissions, loss of low volatility compounds and to prevent artefact formation during ozone fumigation. Care was taken to avoid skin contact with both the leaf and root chamber in order to prevent artefact formation through the ozonolysis of lipids present on human skin (Fruekilde et al., 1998; Wisthaler and Weschler, 2010). All tubing was PFA or PEEK and air flow rates were controlled using mass flow controllers (Bronkhorst, Ruurlo, NL). Zero air was generated by passing ambient air through a catalyst (Zero Air Generator HPZA-7000, Parker Balston, Haverhill, USA) heated to 300 °C. This air flow was then split between root and leaf chambers with ca. 0.5 L min<sup>-1</sup> directed into the root

chamber and ca.  $3.0 \text{ L min}^{-1}$  to the leaf chamber. Ozone was produced by passing the leaf chamber air stream through an ozone generator (UVP, Upland, CA, USA).

The root chamber consisted of a 2 L glass vessel with  $\frac{1}{4}$  inch (6.35 mm) inlet ports 20 mm from the top and bottom of the vessel and a 32 mm port capped with a PTFE coated septum mid-way down the chamber. Zero air entered the root chamber through a ring of PFA tubing, pierced in many places, at the base of the chamber and exited the chamber through the top port situated above the soil level. Soil humidity was recorded via a soil water content sensor (SM300, Delta-T Devices Ltd., Cambridge, UK) inserted through the septum and temperature was recorded via a thermocouple attached to the exterior of the chamber.

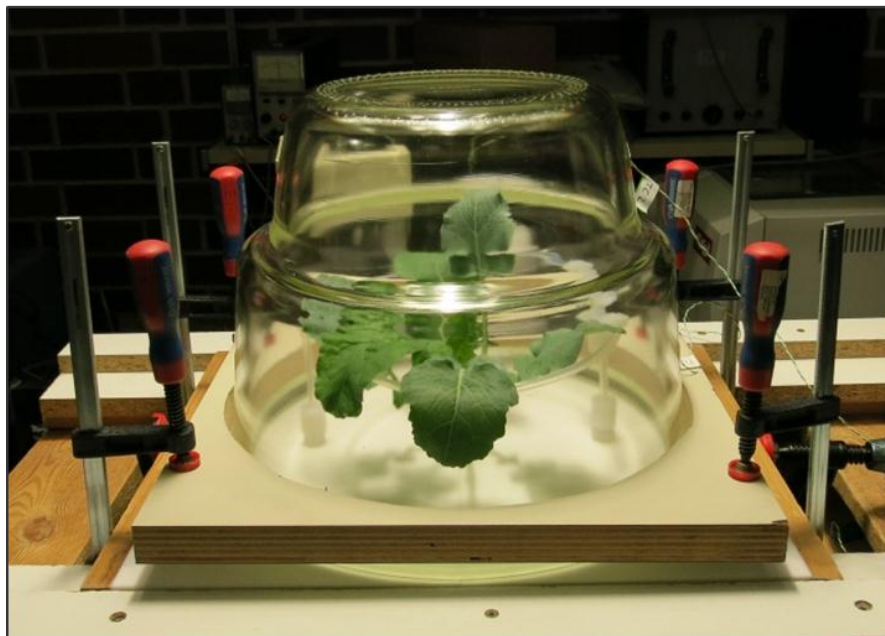
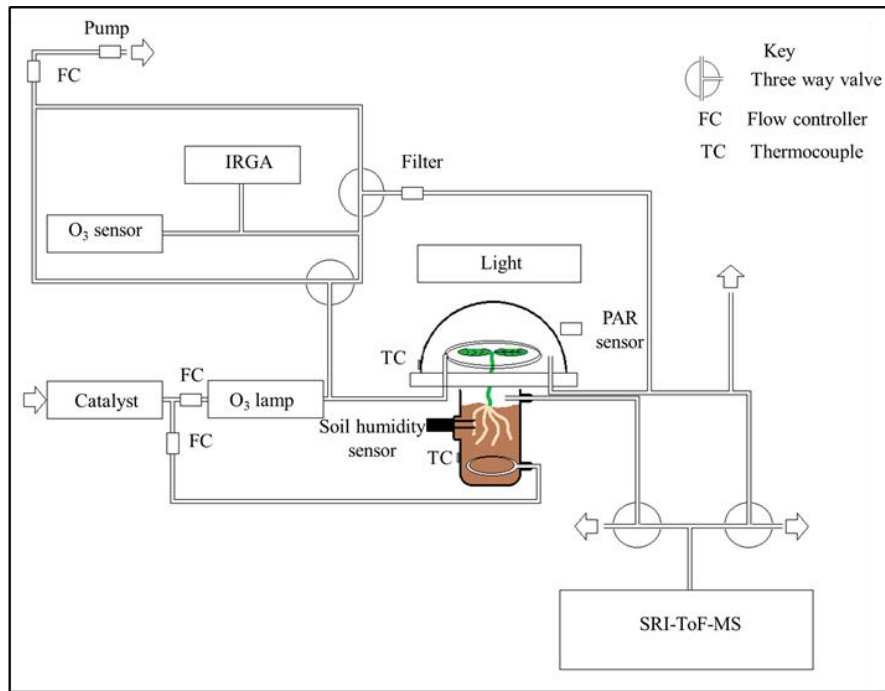


Figure 4.2, plant chamber (bottom) and schematic diagram of experimental setup (top)

The leaf chamber was made up of a 17.2 L glass chamber resting on two  $400 \times 200 \times 15$  mm PTFE plates with a semi-circle of radius 6.3 mm cut for the plant stem in each plate. As with the root chamber, zero air was introduced to the leaf chamber through a ring of PFA tubing pierced in many places in order to facilitate air mixing. The PTFE plates and the glass leaf and root chambers were held in place by external clamps (see

Fig. 4.2). PTFE tape was used between the PTFE plates, around the plant stem, and between both the glass leaf and root chambers and the PTFE plates in order to prevent leaks. Following installation of every new plant into the chamber tests were carried out to ensure that the air flow in the root chamber was independent of that in the leaf chamber and *vice versa*. An overflow PFA tube (ca. 3 m length, ¼ inch/6.35 mm diameter), was installed between the leaf chamber and the SRI-ToF-MS in order to prevent pressure changes when the SRI-ToF-MS was switched from leaf to root chamber measurements. Light was provided from a growth lamp (Dakar, MT / HQI-T/D, Lanzini Illuminazione, Brescia, Italy) positioned ca. 1 m above the chamber and a water bath was installed between the lamp and the growth chamber to filter infra-red radiation and so limit chamber heating. Light and temperature were monitored using a BF3 Sunshine Sensor (Delta-T Devices Ltd., Cambridge, UK) and a thermocouple beside and affixed to the exterior of the leaf chamber respectively. Light levels at the chamber were ca.  $400 \mu\text{mol m}^{-2} \text{s}^{-1}$  and the chamber temperature was  $25 \pm 3 \text{ }^\circ\text{C}$ .

Approximately  $1 \text{ L min}^{-1}$  of air was subsampled before and after passing through the leaf chamber for analysis of  $\text{O}_3$  (ozone analyser, Model 49i, Thermo Fisher Scientific Inc. Franklin (MA), USA),  $\text{CO}_2$  and  $\text{H}_2\text{O}$  (LI-840A  $\text{CO}_2/\text{H}_2\text{O}$  Analyzer, LI-COR Inc., Lincoln (NE), USA) concentrations. Measurements of these inorganic gases were switched between the inlet and outlet every two minutes. In order to maintain a constant rate of flow into the chamber and to the SRI-ToF-MS, the same volume of air was pumped from the inlet line while air was subsampled from the chamber outlet and *vice versa* (see Fig. 4.2). The carbon dioxide mixing ratio entering the chamber was found to be ca. 450 ppm.

Background measurements were made weekly with the leaf chamber background consisting of the empty leaf chamber with and without ozone. The soil chamber background consisted of a soil sample watered and cared for as if it contained a plant.

#### **4.2.3 SRI-ToF-MS measurements**

bVOC measurements were made using the University of Innsbruck SRI-ToF-MS. This instrument is based on the proton transfer reaction time-of-flight mass spectrometer (PTR-ToF-MS) developed at the University of Innsbruck (Graus et al., 2010), with the additional ability to ionise analyte species using alternative reagent ions (in this case  $\text{NO}^+$ ) as well as the more usual  $\text{H}_3\text{O}^+$ . This instrument is similar to the commercial SRI-ToF-MS instruments produced by Ionicon Analytik GmbH (Jordan et al., 2009a, 2009b). A detailed description of the theory behind PTR-MS has previously been described in detail (Hansel et al., 1995; Hewitt et al., 2003; Lindinger et al., 1998b). The University of Innsbruck SRI-ToF-MS differs from the commercial instruments in that it uses a much higher sampling flow (ca.  $500 - 1000 \text{ ml min}^{-1}$  compared to  $10-20 \text{ ml min}^{-1}$ ) increasing the instrument's ability to detect semi and low volatility compounds by reducing the residence time in the inlet system and has a modified ion source which enables rapid switching between the different reagent ions.

While analyte ionisation by  $\text{H}_3\text{O}^+$  takes place predominantly via proton transfer, chemical ionisation with  $\text{NO}^+$  can proceed via a number of chemical pathways. This enables SRI-ToF-MS to provide more structural information than traditional PTR-ToF-MS. For example an aldehyde and a ketone with the same sum formula (M) would be indistinguishable using PTR-ToF-MS as both would be detected at their protonated mass,  $\text{MH}^+$ . However when ionised using  $\text{NO}^+$  the aldehyde will typically

undergo hydride ion abstraction to give  $[M-H]^+$  and the ketone will cluster with  $NO^+$  to give  $MNO^+$ , thereby allowing aldehydes and ketones to be measured individually (Španěl et al., 1997).

The SRI-ToF-MS was operated in  $H_3O^+$  mode with a drift tube pressure of 2.3 mbar, a temperature of 60 °C and with an applied voltage of 540 V, giving an  $E/N$  (the ratio of electric field strength ( $E$ ) and the buffer gas number density ( $N$ )) of 120 Td (1 Td =  $10^{-21} \text{ V m}^{-2}$ ). When  $NO^+$  was used as the reagent ion the drift tube temperature and pressure remained the same but the applied voltage was reduced to 350 V, giving an  $E/N$  of 78 Td.  $E/N$  was reduced in the  $NO^+$  mode in order to facilitate cluster formation and therefore provide greater information with respect to the chemical structure of the analyte.

The SRI-ToF-MS was switched from  $H_3O^+$  to  $NO^+$  mode every 6 minutes. During the first measurement period, July-September 2013, the SRI-ToF-MS sampled for 24 minutes from the soil chamber followed by 36 minutes from the leaf chamber before switching back to the soil chamber. As is discussed above, from April-June 2014 measurements were made from the leaf chamber alone.

#### **4.2.4 SRI-ToF-MS calibration and data analysis**

Six point calibrations were carried out weekly using dynamic dilution of a gas standard (Apel-Riemer Environmental Inc.) comprising 20 VOC species with protonated masses ranging from  $m/z$  31 to 205. Mixing ratios within the gas standard were  $1000 \pm 150$  ppb for all compounds with the exception of formaldehyde (5280 ppb), acetonitrile (1186 ppb), decanal (770 ppb) and 1,3,5-triisopropylbenzene (666 ppb) with a  $\pm 5\%$  uncertainty. Monoterpenes were calibrated using  $\alpha$ -pinene and sesquiterpenes using 1,3,5-triisopropylbenzene. Compounds not present in the calibration gas standard were quantified using the sensitivity calculated for the closest calibrated mass with an equivalent dipole moment and oxidation state. Calibrations were carried out in  $\text{H}_3\text{O}^+$  and  $\text{NO}^+$  modes and using both ambient and humidified air, the latter generated by passing ambient air through a water bubbler before catalytic purification. Humidification of the air, however, had little effect on the sensitivities calculated. Mass scale calibration was enabled by the addition of either 1-chloro-2-iodobenzene or, in 2014, 1,2,4-trichlorobenzene to the sample air prior to the drift tube. SRI-ToF-MS data were analysed using the PTR-TOF Data Analyser described by Müller et al. (2013) and references therein.

#### **4.2.5 GC-MS measurements**

Sample collection for GC-MS analysis was performed throughout the 2014 measurement period to provide identification of isomeric terpene species. Samples for GC-MS analysis were taken from the leaf chamber outflow prior to plant ozone fumigation. Substantial losses of sesquiterpenes occur during sampling in the presence of ozone (Pollmann et al., 2005) therefore GC-MS data are not available for the ozone fumigation period. GC-MS analysis was performed following established procedures

(Ghirardo et al., 2012; Kreuzwieser et al., 2014; Ghirardo et al., 2016; Weikl et al., 2016). Air samples (30 L) were trapped at flow rate of 200 ml min<sup>-1</sup> onto glass tubes containing polydimethylsiloxane-foam-adsorbent material (Gerstel GmbH, Mülheim an der Ruhr, Germany). Samples were then analysed using a thermo-desorption unit (TDU, Gerstel GmbH) coupled to a GC-MS (GC type: 7890A; S type: 5975C Agilent Technologies, Palo Alto, USA). VOCs were separated using a 5% phenyl 95% methylpolysiloxane capillary column (60 m × 250 µm × 0.25 µm DB-5MS + 10 m DG, Agilent Technologies) with a helium flow rate of 1.2 mL min<sup>-1</sup> and a temperature programme of 40 °C for 2 min, followed by ramping at 6 °C min<sup>-1</sup> to 80 °C, holding for 3 min, ramping at 3.4 °C min<sup>-1</sup> to 170 °C and finally at 12 °C min<sup>-1</sup> to 300 °C before holding for 4 min. Calibration was achieved by injecting pure standard mixtures in hexane at seven different concentrations (20-800 pmol µl<sup>-1</sup>). Each concentration mixture was made independently in triplicate, and measured twice. The resulting MS signal responses were found to be linear with increasing standard concentrations ( $R^2$  0.978-0.999). Limits of detection (LOD) were set to twice  $\sigma$ , and the limit of quantification (LOQ) to 5-fold of LOD. Sensitivity changes during sample analysis were accounted for, by the use of a fix amount of  $\delta$ -2-carene used as internal standard.

Chemical identification was achieved by comparing the mass spectra obtained from samples and commercially available authentic standards (Sigma-Aldrich, Taufkirchen, Germany). When standards were not available, sample spectra were compared to those found in the 2011 National Institute of Standards and Technology Mass Spectral Library (NIST11) and Wiley library (v.275), and by comparing the non-isothermal

Kovats retention indices (RI) calculated following standard procedure (Gonzalez and Nardillo, 1999).

#### 4.2.6 Emission rate calculation

Volume mixing ratios ( $\chi$ , ppbv) were calculated from the raw SRI-ToF-MS data in  $\text{H}_3\text{O}^+$  mode (in counts per second) using the equation below.

$$\chi_{\text{bVOC}} = \frac{I(\text{RH}^+)_{\text{norm}}}{S_{\text{norm}}} \quad (1)$$

Where  $I(\text{RH}^+)_{\text{norm}}$  represents the count rate observed for each of the protonated bVOC species ( $I(\text{RH}^+)$ ), normalised to a primary ion ( $\text{H}_3\text{O}^+$ ) and primary ion-water cluster ( $\text{H}_3\text{O}^+\cdot\text{H}_2\text{O}$ ) count of  $10^6$  and background corrected.  $S_{\text{norm}}$  is the normalised sensitivity at that mass. This method is based on that described by Tani et al. (2004) and Taipale et al. (2008) as applied by Acton et al. (2016). Concentrations ( $\mu\text{g m}^{-3}$ ) were then calculated from the volume mixing ratios using the ideal gas law.

The emission rate from the leaf chamber ( $\mu\text{g min}^{-1}$ ) was then calculated from the concentration and the flow rate into the chamber, which was recorded daily. Following the chamber experiments leaf areas were calculated. Leaves were removed from plants and scanned, leaf areas were then calculated using a program written in MATLAB (MathWorks, USA). From the leaf area and chamber emission rate the bVOC per  $\text{m}^2$  of leaf area was then calculated.

## **4.3 Results and discussion**

### **4.3.1 Root chamber measurements**

The aim of this work was to identify the species emitted into the soil and to monitor changes following ozone fumigation of the above ground foliage. However, as zero air is introduced at the base of the chamber and passed up through the soil, thereby artificially increasing diffusion from the soil, realistic emission rates cannot be determined. It should also be noted that the term “root emitted bVOC” is used here to describe the emission of bVOCs from both the roots of the plant and their associated micro-organisms. A summary of the masses detected by the SRI-ToF-MS in H<sub>3</sub>O<sup>+</sup> mode when sampling from the root chamber and their likely identity are shown in Table 4.1. The mass spectral peaks, where observed, in NO<sup>+</sup> mode are also reported. Methanethiol, which has been shown to react slowly with NO<sup>+</sup> (Pysanenko et al., 2008) was not detected in NO<sup>+</sup> mode. Mass spectral peaks in NO<sup>+</sup> mode were assigned to compounds identified in H<sub>3</sub>O<sup>+</sup> mode on the basis of their exact mass and agreement between the times traces recorded in each mode.

Table 4.1, bVOC species detected from *Brassica napus* root zone measurements following background correction against a soil filled chamber. Emission is compared with previous studies made using *Brassica* species.

Mass detected in $\text{H}_3\text{O}^+$ ionisation mode	$\text{NO}^+$ ionisation expected	Mass detected in $\text{NO}^+$ ionisation mode	Molecular formula	Proposed compound	Previously reported emission
49.011	no	not detected	$\text{CH}_4\text{S}$	methanethiol	van Dam et al., 2012 ; Danner et al., 2012
63.026	yes	62.017	$\text{C}_2\text{H}_6\text{S}$	dimethyl sulfide	van Dam et al., 2012; Danner et al., 2012
74.005	no	not detected	$\text{C}_2\text{H}_3\text{NS}$	methyl thiocyanate	
80.962	no	not detected	$\text{CH}_4\text{S}_2$	methanedithiol	
94.991	yes	93.990	$\text{C}_2\text{H}_6\text{S}_2$	dimethyl disulfide	van Dam et al., 2012; Danner et al., 2012

The dominant bVOCs detected in the root chamber were the sulfur compounds,  $\text{CH}_4\text{S}$ ,  $\text{C}_2\text{H}_6\text{S}_2$  and  $\text{C}_2\text{H}_6\text{S}$  which were assigned to methanethiol, dimethyl disulfide (DMDS) and dimethyl sulfide (DMS), respectively, in agreement with the observations made by van Dam et al. (2012) using *Brassica* species. While the isothiocyanate marker reported by van Dam et al. (2012) at m/z 60 was not observed, a mass spectral peak at m/z 74.0052 in the SRI-ToF-MS's  $\text{H}_3\text{O}^+$  mode was assigned tentatively to methyl thiocyanate. Both monoterpene and sesquiterpene emissions have previously been reported from roots (for example by Lin et al., 2007), but in the study presented here significant emissions could only be detected following damage to the plant, these data are however not shown. Following ozone fumigation to the vegetation in the leaf

chamber, we did not observe any significant changes to the bVOC emissions from the roots.

#### 4.3.2 bVOC emission from healthy leaves

bVOC emissions from leaves of *B. napus* prior to ozone fumigation are summarised in Table 4.2. bVOCs were quantified from measurements taken using the SRI-ToF-MS operated in  $\text{H}_3\text{O}^+$  mode.  $\text{NO}^+$  ionisation was then used to provide additional structural information aiding the identification of bVOC species. The bVOC emissions from leaves prior to ozone fumigation were dominated by methanol and monoterpenes, with emission rates of 24 and  $3.4 \text{ nmol m}^{-2} \text{ min}^{-1}$  respectively. These species were detected at  $m/z$  33.034 and 137.134 in the  $\text{H}_3\text{O}^+$  spectrum, and at  $m/z$  62.018 and 136.130 in the  $\text{NO}^+$  spectrum, suggesting that ionisation of methanol proceeded via cluster formation (Španěl and Smith, 1997), and the ionisation of monoterpenes via charge transfer, as would be expected for an alkene (Diskin et al., 2002).

Significant mass spectral peaks were also observed at  $m/z$  49.011, 101.061, 139.114, 151.112, 153.053, 153.132 and 205.198 in the  $\text{H}_3\text{O}^+$  spectrum and were tentatively assigned to methanethiol ( $\text{CH}_3\text{S}$ ), oxopentanal ( $\text{C}_5\text{H}_8\text{O}_2$ ), an unknown aldehyde with the molecular formula  $\text{C}_9\text{H}_{14}\text{O}$  (as hydride ion abstraction is seen in the  $\text{NO}^+$  spectrum), an unsaturated oxygenated species with the molecular formula  $\text{C}_{10}\text{H}_{14}\text{O}$ , methyl salicylate ( $\text{C}_8\text{H}_8\text{O}$ ), an unsaturated aldehyde with the molecular formula  $\text{C}_{10}\text{H}_{14}\text{O}$  (as hydride ion abstraction is seen in the  $\text{NO}^+$  spectrum) and sesquiterpenes ( $\text{C}_{15}\text{H}_{25}$ ) respectively.

GC-MS analysis of trapped samples was used to identify the species contributing to the monoterpenes and sesquiterpene peaks identified using the SRI-ToF-MS. The monoterpene emission was predominantly made up of  $\alpha$ -pinene (36%),  $\alpha$ -thujene (29%),  $\beta$ -pinene (23%) and  $\gamma$ -terpinene (13%). The C<sub>15</sub>H<sub>25</sub> signal was made up of four sesquiterpenes:  $\beta$ -elemene (43%), isolongifolene (15%),  $\beta$ -caryophyllene (36%) and  $\alpha$ -farnesene (5%) together with the aromatic compound 1,3,5-tris(1-methylethyl)benzene (1%). The sesquiterpene emission rate calculated using the GC-MS agreed well with that calculated using the SRI-ToF-MS, but the GC-MS significantly underestimated the total monoterpene emission rate. This may, in part, be caused by a contribution from the fragmentation of higher masses to  $m/z$  137.134 (for example, sesquiterpenes are known to fragment to this mass) in the SRI-ToF-MS when operated in H<sub>3</sub>O<sup>+</sup> mode (Kim et al., 2009). The GC-MS analysis also detected significant emission of the oxygenated monoterpene cis- $\beta$ -terpineol. This compound is likely to fragment after ionisation in the SRI-ToF-MS operated in H<sub>3</sub>O<sup>+</sup> mode, eventually leading to interference at the monoterpene's mass 137.134. High levels of monoterpene contamination in GC-MS background samples, however, suggest that an overestimation of the GC-MS background may have resulted in an underestimation of total monoterpene emission rate.

Previous analysis of bVOC emissions from oilseed rape (Himanen et al., 2009; Ibrahim et al., 2008; McEwan and Macfarlane Smith, 1998) also reported significant emissions of monoterpenes and sesquiterpenes. However, the blend of individual monoterpenes and sesquiterpenes differs between these studies and ours. This is likely caused by changes in cultivar and growth stage. Ibrahim et al. (2008) and McEwan and Macfarlane Smith (1998) also reported a large emission of hexenyl-acetate, which

was not detected in this study. This compound is associated with leaf wounding (Fall et al., 1999; Maffei, 2010) so may have been caused by leaf damage as result of leaf bagging prior to sampling in both studies.

#### **4.3.3 Volatile emission from leaf chamber following ozone fumigation**

Following fumigation of the *B. napus* leaf tissue with ozone (ca. 70 ppbv at the chamber outlet) a burst of ca. 20 compounds was observed using SRI-ToF-MS operating in  $\text{H}_3\text{O}^+$  mode. The emission rates of these compounds averaged over 2 h are displayed in Table 4.2.

Table 4.2. The principle leaf emitted bVOCs from *Brassica napus* before and during the first 2 h of ozone fumigation detected using SRI-ToF-MS. bVOC species quantified from measurements carried out in H<sub>3</sub>O<sup>+</sup> mode. Standard deviations represent the standard deviation in emission across the 13 plants measured.

Mass detected in H <sub>3</sub> O <sup>+</sup> ionisation mode (sum formula)	NO <sup>+</sup> ionisation expected	Mass detected in NO <sup>+</sup> ionisation mode (sum formula)	Molecular formula	Proposed compound	Clean air		Ozone fumigation	
					Emission (nmol m <sup>-2</sup> min <sup>-1</sup> )	Standard deviation	Emission (nmol m <sup>-2</sup> min <sup>-1</sup> )	Standard deviation
33.03 (CH <sub>5</sub> O <sup>+</sup> )	yes	62.02 (NO.CH <sub>4</sub> O <sup>+</sup> )	CH <sub>4</sub> O	methanol	24.29	8.23	24.83	9.12
49.01 (CH <sub>5</sub> S <sup>+</sup> )	no	not detected	CH <sub>4</sub> S	methanethiol	1.79	0.99	1.97	0.79
57.04 (C <sub>3</sub> H <sub>5</sub> O <sup>+</sup> )	yes	55.04 (C <sub>3</sub> H <sub>3</sub> O <sup>+</sup> )	C <sub>3</sub> H <sub>4</sub> O	propenal	0.05	0.05	0.07	0.05
57.07 (C <sub>4</sub> H <sub>9</sub> <sup>+</sup> )	yes	57.07 (C <sub>4</sub> H <sub>9</sub> <sup>+</sup> )	C <sub>4</sub> H <sub>10</sub> O	butanol fragment	0.02	0.08	0.14	0.24
59.05 (C <sub>3</sub> H <sub>7</sub> O <sup>+</sup> )	yes	88.04 (NO.C <sub>3</sub> H <sub>6</sub> O <sup>+</sup> )	C <sub>3</sub> H <sub>6</sub> O	acetone	0.42	0.33	1.14	1.10
63.03 (C <sub>2</sub> H <sub>7</sub> S <sup>+</sup> )	yes	not detected	C <sub>2</sub> H <sub>6</sub> S	dimethyl sulfide	0.37	0.19	0.32	0.19

Table 4.2 (continued)

Mass detected in H <sub>3</sub> O <sup>+</sup> ionisation mode (sum formula)	NO <sup>+</sup> ionisation expected	Mass detected in NO <sup>+</sup> ionisation mode (sum formula)	Molecular formula	Proposed compound	Clean air		Ozone fumigation	
					Emission (nmol m <sup>-2</sup> min <sup>-1</sup> )	Standard deviation	Emission (nmol m <sup>-2</sup> min <sup>-1</sup> )	Standard deviation
69.07 (C <sub>5</sub> H <sub>9</sub> <sup>+</sup> )	yes	69.07 (C <sub>5</sub> H <sub>9</sub> <sup>+</sup> )	C <sub>5</sub> H <sub>10</sub> O	fragment of a secondary/tertiary unsaturated alcohol	0.42	0.28	0.83	1.19
71.05 (C <sub>4</sub> H <sub>7</sub> O <sup>+</sup> )	yes	100.04 (NO.C <sub>4</sub> H <sub>6</sub> O <sup>+</sup> )	C <sub>4</sub> H <sub>6</sub> O	methyl vinyl ketone	0.02	0.02	0.02	0.04
73.07 (C <sub>4</sub> H <sub>9</sub> O <sup>+</sup> )	yes	102.06 (NO.C <sub>4</sub> H <sub>8</sub> O <sup>+</sup> )	C <sub>4</sub> H <sub>8</sub> O	methyl ethyl ketone	0.11	0.80	0.12	0.07
74.01 (C <sub>2</sub> H <sub>4</sub> NS <sup>+</sup> )	no	not detected	C <sub>2</sub> H <sub>3</sub> NS	methyl thiocyanate	0.15	0.18	0.17	0.16
74.06 (C <sub>3</sub> H <sub>8</sub> NO <sup>+</sup> )	yes	73.06 (C <sub>3</sub> H <sub>7</sub> NO <sup>+</sup> )	C <sub>3</sub> H <sub>7</sub> NO	unknown	0.12	0.11	0.11	0.09

Table 4.2 (continued)

Mass detected in H <sub>3</sub> O <sup>+</sup> ionisation mode (sum formula)	NO <sup>+</sup> ionisation expected	Mass detected in NO <sup>+</sup> ionisation mode (sum formula)	Molecular formula	Proposed compound	Clean air		Ozone fumigation	
					Emission (nmol m <sup>-2</sup> min <sup>-1</sup> )	Standard deviation	Emission (nmol m <sup>-2</sup> min <sup>-1</sup> )	Standard deviation
83.09 (C <sub>6</sub> H <sub>11</sub> <sup>+</sup> )	yes	83.09 (C <sub>6</sub> H <sub>11</sub> <sup>+</sup> )	C <sub>5</sub> H <sub>12</sub> O	fragment of a secondary/ tertiary unsaturated alcohol, hexenol?	0.03	0.06	0.53	0.90
85.07 (C <sub>5</sub> H <sub>9</sub> O <sup>+</sup> )	yes	85.07 (C <sub>5</sub> H <sub>9</sub> O <sup>+</sup> )	C <sub>5</sub> H <sub>10</sub> O <sub>2</sub>	unknown	0.01	0.01	0.01	0.02
88.08 (C <sub>4</sub> H <sub>10</sub> NO <sup>+</sup> )	yes	87.06 (C <sub>4</sub> H <sub>9</sub> NO <sup>+</sup> )	C <sub>4</sub> H <sub>9</sub> NO	unknown	0.12	0.07	0.14	0.06
93.04 (C <sub>3</sub> H <sub>9</sub> OS <sup>+</sup> )	yes	122.04(NO.C <sub>3</sub> H <sub>8</sub> OS <sup>+</sup> )	C <sub>3</sub> H <sub>8</sub> OS	unknown	0.39	0.47	0.61	0.37
97.10 (C <sub>7</sub> H <sub>13</sub> <sup>+</sup> )	yes	97.10 (C <sub>7</sub> H <sub>13</sub> <sup>+</sup> )	C <sub>7</sub> H <sub>14</sub> O	fragment of a secondary/ tertiary unsaturated alcohol	0.00	0.00	0.09	0.17
100.08 (C <sub>5</sub> H <sub>10</sub> NO <sup>+</sup> )	yes	129.07 (NO. C <sub>5</sub> H <sub>9</sub> NO <sup>+</sup> )	C <sub>5</sub> H <sub>9</sub> NO	unknown	0.80	0.53	0.77	0.55

Table 4.2 (continued)

Mass detected in H <sub>3</sub> O <sup>+</sup> ionisation mode (sum formula)	NO <sup>+</sup> ionisation expected	Mass detected in NO <sup>+</sup> ionisation mode (sum formula)	Molecular formula	Proposed compound	Clean air		Ozone fumigation	
					Emission (nmol m <sup>-2</sup> min <sup>-1</sup> )	Standard deviation	Emission (nmol m <sup>-2</sup> min <sup>-1</sup> )	Standard deviation
101.06 (C <sub>5</sub> H <sub>9</sub> O <sub>2</sub> <sup>+</sup> )	yes	99.04 (C <sub>5</sub> H <sub>7</sub> O <sub>2</sub> <sup>+</sup> )	C <sub>5</sub> H <sub>8</sub> O <sub>2</sub>	(4)-oxopentanal	2.91	2.26	7.43	14.41
107.08 (C <sub>7</sub> H <sub>7</sub> O <sup>+</sup> )	yes	105.04 (C <sub>7</sub> H <sub>5</sub> O <sup>+</sup> )	C <sub>7</sub> H <sub>6</sub> O	benzaldehyde	0.01	0.01	0.02	0.02
109.10 (C <sub>8</sub> H <sub>13</sub> <sup>+</sup> )	yes	108.09 (C <sub>8</sub> H <sub>12</sub> <sup>+</sup> )	C <sub>7</sub> H <sub>8</sub> O	unknown alkene	0.04	0.05	0.16	0.25
123.12 (C <sub>9</sub> H <sub>15</sub> <sup>+</sup> )	yes	123.12 (C <sub>9</sub> H <sub>15</sub> <sup>+</sup> )	C <sub>9</sub> H <sub>16</sub> O	fragment of a secondary/ tertiary unsaturated alcohol	0.01	0.02	0.09	0.15
125.13 (C <sub>9</sub> H <sub>17</sub> <sup>+</sup> )	yes	125.13 (C <sub>9</sub> H <sub>17</sub> <sup>+</sup> )	C <sub>9</sub> H <sub>18</sub> O	fragment of a secondary/tertiary unsaturated alcohol	0.00	0.00	0.03	0.05
127.11 (C <sub>8</sub> H <sub>15</sub> O <sup>+</sup> )	yes	126.10 (C <sub>8</sub> H <sub>15</sub> O <sup>+</sup> )	C <sub>8</sub> H <sub>14</sub> O	6-methyl-5- hepten-2-one	0.65	0.43	2.57	3.27

Table 4.2 (continued)

Mass detected in H <sub>3</sub> O <sup>+</sup> ionisation mode (sum formula)	NO <sup>+</sup> ionisation expected	Mass detected in NO <sup>+</sup> ionisation mode (sum formula)	Molecular formula	Proposed compound	Clean air		Ozone fumigation	
					Emission (nmol m <sup>-2</sup> min <sup>-1</sup> )	Standard deviation	Emission (nmol m <sup>-2</sup> min <sup>-1</sup> )	Standard deviation
135.12 (C <sub>10</sub> H <sub>15</sub> <sup>+</sup> )	yes	134.10 (C <sub>10</sub> H <sub>14</sub> <sup>+</sup> )	C <sub>10</sub> H <sub>14</sub>	p-cymene	0.13	0.05	0.11	0.07
137.13 (C <sub>10</sub> H <sub>17</sub> <sup>+</sup> )	yes	136.13 (C <sub>10</sub> H <sub>16</sub> <sup>+</sup> )	C <sub>10</sub> H <sub>16</sub>	monoterpenes	3.44	1.84	2.86	1.72
139.11 (C <sub>9</sub> H <sub>15</sub> O <sup>+</sup> )	yes	137.13 (C <sub>9</sub> H <sub>13</sub> O <sup>+</sup> )	C <sub>9</sub> H <sub>14</sub> O	unsaturated aldehyde	1.56	1.29	2.95	2.14
143.14 (C <sub>9</sub> H <sub>19</sub> O <sup>+</sup> )	yes	141.12 (C <sub>9</sub> H <sub>17</sub> O <sup>+</sup> )	C <sub>9</sub> H <sub>18</sub> O	nonanal	0.43	0.50	3.52	3.21
151.11 (C <sub>10</sub> H <sub>15</sub> O <sup>+</sup> )	yes	150.11 (C <sub>10</sub> H <sub>14</sub> O <sup>+</sup> )	C <sub>10</sub> H <sub>14</sub> O	unknown	1.29	0.83	3.13	1.85
153.05 (C <sub>8</sub> H <sub>9</sub> O <sub>3</sub> <sup>+</sup> )	yes	152.05 (C <sub>8</sub> H <sub>8</sub> O <sub>3</sub> <sup>+</sup> )	C <sub>8</sub> H <sub>8</sub> O <sub>3</sub>	methyl salicylate	1.53	1.15	0.72	0.76
153.13 (C <sub>10</sub> H <sub>17</sub> O <sup>+</sup> )	yes	151.12 (C <sub>10</sub> H <sub>15</sub> O <sup>+</sup> )	C <sub>10</sub> H <sub>16</sub> O	unsaturated aldehyde	1.43	0.71	1.78	1.33
157.16 (C <sub>10</sub> H <sub>21</sub> O <sup>+</sup> )	yes	155.15 (C <sub>10</sub> H <sub>19</sub> O <sup>+</sup> )	C <sub>10</sub> H <sub>20</sub> O	decanal	0.33	0.30	5.47	5.10

Table 4.2 (continued)

Mass detected in $\text{H}_3\text{O}^+$ ionisation mode (sum formula)	$\text{NO}^+$ ionisation expected	Mass detected in $\text{NO}^+$ ionisation mode (sum formula)	Molecular formula	Proposed compound	Clean air		Ozone fumigation	
					Emission (nmol $\text{m}^{-2} \text{min}^{-1}$ )	Standard deviation	Emission (nmol $\text{m}^{-2} \text{min}^{-1}$ )	Standard deviation
171.16 ( $\text{C}_{11}\text{H}_{23}\text{O}^+$ )	yes	169.15 ( $\text{C}_{11}\text{H}_{21}\text{O}^+$ )	$\text{C}_{11}\text{H}_{22}\text{O}$	undeacanal	0.11	0.24	0.62	0.92
205.20 ( $\text{C}_{15}\text{H}_{25}^+$ )	yes	204.20 ( $\text{C}_{15}\text{H}_{24}^+$ )	$\text{C}_{15}\text{H}_{25}$	sesquiterpenes	0.33	0.27	0.06	0.03

Previous investigations into the effect of ozone on plants have shown that ozone can cause a change in constitutive bVOC emissions from plants. Ryan et al. (2009) observed a decrease in isoprene emissions following ozone fumigation of an ozone-sensitive poplar genotype, but observed no change in emission following fumigation of an ozone-tolerant genotype. Both Heiden et al. (1999) and Vuorinen et al. (2004) reported an increase in terpene emissions following ozone fumigation of pine, tobacco and lima bean, whereas Himanen et al. (2009) observed a decrease in monoterpene emissions following ozone fumigation of oilseed rape. In this present study no significant increase in monoterpenes or sesquiterpene emission was observed directly after ozone fumigation or during the following 24 hours. As was observed by Wildt et al. (2003), ozone fumigation caused significant emissions of the saturated aldehydes nonanal and decanal.

In contrast, during ozone fumigation, monoterpene and sesquiterpene emissions from the above-ground leaf tissue were observed to decrease immediately, by 17 % and 82 % respectively. Both monoterpenes and sesquiterpenes contain alkene functional groups and so would be expected to undergo ozonolysis via the mechanism proposed by Criegee (1975) (Fig. 4.1). Rate constants ( $k$ ) for the gas phase ozonolysis (at room temperature) of the detected terpenes, where known, are shown in Table 4.3, together with expected half-lives ( $\tau$ ) at an ozone mixing ratio of 100 ppbv. Gas phase rate constants for the reaction of ozone with  $\alpha$ -thujene and  $\beta$ -elemene have yet to be reported. The calculated half-lives for ozonolysis range from 11.4 min to 7.5 h (Table 4.3). However, given the short residence time of air in the leaf chamber (ca. 6.5 min), a significant drop in monoterpene emissions as a result of gas phase ozonolysis can be discounted. While the gas phase ozonolysis of the more reactive sesquiterpenes, such

as  $\alpha$ -farnesene, is likely to account for some of the loss observed, this is insufficient to explain the 82 % decrease observed upon ozone fumigation.

The addition of an excess of an OH scavenger (cyclohexane) to the leaf chamber caused the monoterpene concentrations measured during ozone fumigation to return to the levels observed prior to ozone fumigation. This indicates that the drop in monoterpene emissions following ozone fumigation is a result of a reaction with OH radicals rather than direct reaction with ozone. A burst of cyclohexanone was observed during the period of cyclohexane addition indicating that OH was successfully scavenged. The addition of cyclohexane had no effect on the sesquiterpene emissions from the leaf chamber, thereby demonstrating that the drop in sesquiterpene emissions is driven by ozonolysis. As has been shown by Fruekilde et al. (1998) and Jud et al. (2016), large, semi-volatile terpenoids may undergo ozonolysis on the leaf surface. The loss of sesquiterpenes, either prior to emission from the plant, or after partition back into the condensed phase, could therefore account for the large drop in sesquiterpene emissions observed.

The reaction of ozone with molecules containing the alkene functional group to form a primary ozonide and the subsequent decomposition of this intermediate to a carbonyl and an energy rich carbonyl oxide intermediate was described by Criegee (1975). The so-called Criegee Intermediate (CI) may undergo a number of reactions including collisional stabilisation to form a stabilised CI. In the case of dialkyl-substituted or monosubstituted *syn*- CIs isomerisation leads to a “hot” hydroperoxide followed by decomposition to alkyl and OH radicals and in the case of unsubstituted or monosubstituted *anti*- CIs rearrangement leads to a “hot” ester followed by

decomposition to CO<sub>2</sub> and RH (Atkinson and Arey, 2003b; Kroll et al., 2001). The CIs and radical decomposition products are however expected to be short lived, so in order to observe sesquiterpene ozonolysis products we focused on the stable carbonyl products. The reactions of the cyclic sesquiterpenes  $\beta$ -caryophyllene (Winterhalter et al., 2009),  $\beta$ -elemene and isolongifolene with ozone, yield formaldehyde and a range of large (> 204 amu) oxygenated compounds. Emissions of formaldehyde and these high molecular weight species were not observed during this study. The proton affinity of formaldehyde is only slightly higher than that of water, therefore, at high humidity the instrumental sensitivity to formaldehyde is very low (de Gouw and Warneke, 2007). As the humidity in the leaf chamber was high it is therefore likely that if formaldehyde was produced it would not have been detected. It is likely that the large oxygenated products formed remain on the plant surface, are lost by deposition to the chamber walls, or partition into the aerosol phase (Hoffmann et al., 1997; Winterhalter et al., 2009) and hence are not detected by SRI-ToF-MS in our experimental set-up. However, ozonolysis of the acyclic sesquiterpene  $\alpha$ -farnesene leads to the formation of a number of short chain carbonyl compounds including acetone, methyl vinyl ketone, oxopentanal and 6-methyl-5-hepten-2-one, all of which were observed following ozone fumigation, supporting the suggestion that sesquiterpenes are lost by reaction with ozone (Fig. 4.3). Emissions of oxygenated bVOCs from plant surfaces during ozone exposure have also been observed by Karl et al. (2005) who demonstrated that a number of compounds thought to be formed by gas phase chemistry within the canopy may also originate by reaction with ozone on leaf surfaces, and/or inside the leaf (Salter and Hewitt, 1992).

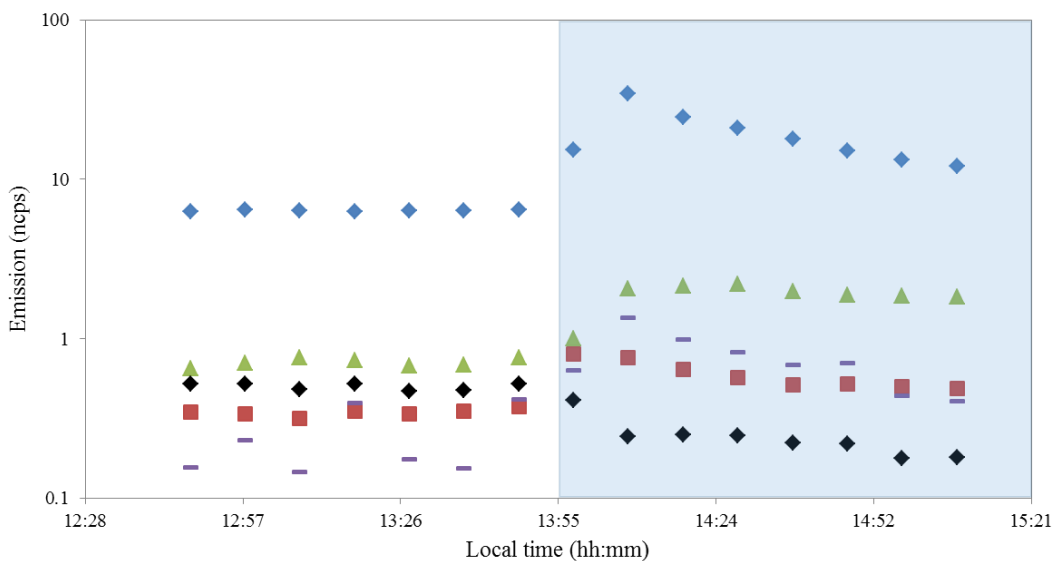


Figure 4.3, the drop in sesquiterpenes ( $m/z$  205.198, black diamonds) following ozone exposure and the increase in the emission of the ozonolysis products acetone ( $m/z$  59.050, blue diamonds), methyl vinyl ketone ( $m/z$ , 71.050 red squares), oxopentanal ( $m/z$  101.061, green triangles) and 6-methyl-5-hepten-2-one ( $m/z$  127.111, purple dashes), from a representative plant. Values are displayed as ten min averages in normalised counts per second (ncps). Shaded area represents fumigation with ca 100 ppbv ozone.

During ozone fumigation, total measured carbon emissions (calculated by summing the moles of carbon emitted) from the leaf chamber increased from 159 nmol C m<sup>-2</sup> min<sup>-1</sup> to 310 nmol C m<sup>-2</sup> min<sup>-1</sup>. This almost doubling in measured volatile carbon emissions clearly demonstrates that many of the compounds observed must be a result of liberation of carbon through ozonolysis of leaf surface compounds and/or the induced emission of oxygenated species from the plant rather than simply ozonolysis of the bVOCs emitted by the plant prior to ozone exposure. The leaf surface waxes of *B. napus* are predominantly made up of alkanes, saturated ketones, esters and alcohols

(Holloway et al., 1977) which are all relatively unreactive with ozone, therefore loss of ozone to the plant surface must be via reaction with emitted sesquiterpenes and triterpenols.

Table 4.3. Gas phase rate coefficients (k) for the reaction of selected terpenes with ozone ( $2.46 \text{ molecules cm}^{-3} \text{ s}^{-1}$ , 100 ppbv) at 298 K and their expected half-lives ( $\tau$ ).

Terpene	$k_{\text{O}_3}$	$\tau_{\text{O}_3}$ (h)	reference
$\alpha$ -pinene	$8.4 \times 10^{-17}$	1.3	Lee et al., 2006
$\beta$ -pinene	$1.5 \times 10^{-17}$	7.5	Lee et al., 2006
$\gamma$ -terpinene	$1.4 \times 10^{-16}$	0.8	Atkinson et al., 1990
$\beta$ -caryophyllene	$5.9 \times 10^{-17}$	1.9	Ghalaieny et al., 2012
isolongifolene	$2.5 \times 10^{-17}$	4.5	Ghalaieny et al., 2012
$\alpha$ -farnesene	$5.9 \times 10^{-16}$	0.19	Kim et al., 2011

#### 4.4 Conclusions

In this study we report for the first time whole plant (both above- and below-ground) bVOC emissions recorded using SRI-ToF-MS. This method combines the high time and mass resolution of traditional PTR-ToF-MS with the advantage of being able to separate certain isomeric compounds (Lanza et al., 2013).

The dominant emissions from the roots of *B. napus* were the sulfur compounds methanethiol, dimethyl sulfide, methyl thiocyanate, methanedithiol and dimethyl disulfide. The emission of bVOCs from plant roots was shown to be unaffected by fumigation of the above-ground leaf tissue with ozone.

Emissions from the above-ground leaf tissue in ambient air were dominated by methanol, monoterpenes, 4-oxopentanal and methanethiol. When the leaves were fumigated with ozone at ~100 ppbv, over 20 oxygenated compounds were immediately observed, together with a drop in monoterpene and sesquiterpene emission rates. The drop in observed monoterpene emission rate was shown to be caused by the gas phase oxidation of the C<sub>10</sub> compounds by the OH radical rather than by ozonolysis. The observed reduction in sesquiterpene emission rate from the leaf chamber was greater than could be explained by the gas phase ozonolysis of sesquiterpenes, suggesting that some of the emitted sesquiterpenes were lost by ozonolysis at the plant surface. As sesquiterpenes have been shown to play a significant role in plant signalling, where plant-plant and plant-insect signalling is reliant upon sesquiterpene emissions (Kessler and Baldwin 2001), such signalling may be significantly altered by increases in tropospheric ozone concentrations. It is not clear how our laboratory observations apply at the community or ecosystem scale, but our observations suggest that multi-trophic communication systems may be disturbed by elevated ozone concentrations in ambient air (Blande et al., 2010).

### **Acknowledgements**

W.J.F. Acton is in receipt of a BBSRC/Ionicon Analytik GmbH Industrial CASE studentship.

## Chapter V

# **Ambient ozone degrades plant volatiles and disrupts tritrophic signalling**

In chapter IV the effect of ozone fumigation on volatile emissions from *B. napus* was investigated. It was shown that following ozone fumigation a wide array of oxygenated compounds were released and that the emission of sesquiterpenes from the leaf chamber reduced dramatically. The drop in sesquiterpene emissions being attributed to ozonolysis of sesquiterpenes both in the gas phase and on surfaces. As sesquiterpenes have been shown to play an important role in tritrophic signalling it was therefore hypothesised that ozone fumigation could disrupt tritrophic signalling. This chapter reports the results of a series of experiments performed using a Y-tube olfactometer designed to investigate the effect of ozone on herbivore host location and predator prey location using the model system *Brassica napus* – *Myzus persicae* - *Adalia bipunctata*.

This work is presented in a traditional thesis format but is intended to be re-written in a style appropriate for submission to a generalist journal. The authors and their contributions are listed below:

**Acton W. J. F. (Lancaster University):** Designed and carried out experiments, analysed data and prepared manuscript.

**Hewitt C. N. (Lancaster University):** Helped with experimental design, interpretation of data and manuscript preparation.

**Taylor J. E. (Lancaster University):** Helped with experimental design, interpretation of data and manuscript preparation.

# Ambient ozone degrades plant volatiles and disrupts tritrophic signalling

Acton W. J. F.<sup>1</sup>, Hewitt C.N.<sup>1</sup> and Taylor J. E.<sup>1</sup>

[1]{Lancaster Environment Centre, Lancaster University, Lancaster, LA1 4YQ, United Kingdom}

## Abstract

In response to herbivory, plants have been shown to emit a wide range of volatile organic compounds. It is known that predatory insects make use of the stress induced volatile emission to locate their prey, with this tritrophic signalling providing an important plant defence mechanism. In this study the effect of ozone on tritrophic signalling and herbivore host location is investigated using a *Brassica napus* – *Myzuz persicae* – *Adalia bipunctata* larvae model system. Using a Y-tube olfactometer *M. persicae* are shown to successfully identify a host plant and *A. bipunctata* larvae successfully identify a *M. persicae* infested plant in clean air. Following ozone fumigation (100 ppbv) both herbivore host location and tritrophic signalling were inhibited. In order to elucidate whether this effect was caused by a change in plant volatile emission as a response to abiotic stress or degradation of the volatile compounds emitted, the experiment was repeated introducing ozone after the plant, and again herbivore host location and tritrophic signalling were inhibited. This suggests that ozone disrupts tritrophic signalling through degradation of plant emitted volatiles. Infestation of *B. napus* with *M. persicae* is shown to induce the emission of the sesquiterpene  $\beta$ -farnesene. Following ozone fumigation, emission of the  $\beta$ -farnesene ozonolysis products: acetone, methylglyoxal, 4-oxopentanal, 4-

methylenehex-5-enal and 6-methylhept-5-en-2-one is observed supporting the hypothesis that tritrophic signalling is disrupted by volatile degradation.

## **5.1 Introduction**

Plants emit a plethora of volatile organic compounds (biogenic VOCs or bVOCs) into the atmosphere. The single most important bVOC is probably isoprene, but the wide array of compounds emitted include terpenoids, alkanes, alkenes, alcohols, aldehydes, aromatic compounds, esters, ketones and organosulfur compounds. These compounds fulfil numerous biological roles including mitigation of abiotic stress, acting in both direct and induced plant defences, the attraction of pollinators and seed dispersers and as signalling compounds in plant-plant communication (Holopainen and Gershenzon, 2010; Maffei, 2010). The emission of bVOCs is influenced by both biotic and abiotic stress and the blend of bVOCs emitted by plants has been shown to change qualitatively and quantitatively following stress (Holopainen and Gershenzon, 2010; Loreto and Schnitzler, 2010; Maffei, 2010).

Following the exposure of plants to biotic stress, the emission of constitutive and induced bVOCs may be stimulated (Maffei, 2010). Constitutive defences are bVOCs stored in structures such as resin ducts or glandular trichomes within the plant which are released following damage to the plant. Induced bVOCs are synthesised following exposure to a herbivore or pathogen and may act as direct or indirect defence. The release of both constitutive and induced bVOCs following biotic stress may enable the priming of plant defences in neighbouring plants (Baldwin et al., 2006) or in distal plant parts (Heil and Ton, 2008). These bVOCs also enable tritrophic signalling, the

so-called “cry for help”, attracting the predators of herbivorous insects attacking the plant (Dicke, 2009; Pichersky and Gershenzon, 2002).

Ground-level ozone is a major secondary air pollutant of global significance. At high concentrations it has detrimental impacts on both human health and crop yields (Ashmore, 2005; Royal Society 2008). Ozone is formed in the troposphere through the photochemical degradation of NO<sub>x</sub> (NO<sub>2</sub> and NO) in the presence of VOCs of biogenic and/or anthropogenic origin (Fehsenfeld et al., 1992). Exposure to ozone has been shown to impact upon the emission of bVOCs from plants (Laothawornkitkul et al., 2009). Both reductions and amplifications of isoprene emission have been observed from plants in response to ozone exposure with the response depending on ozone concentration and/or plant sensitivity to ozone (Fares et al., 2006; Ryan et al., 2009). Ozone can also damage cellular membranes leading to the emission of green leaf volatiles, aldehydes containing 6 carbon atoms (Beauchamp et al., 2005).

As both terpenoids and green leaf volatiles have been shown to play a role in plant signalling (Kappers et al., 2005; Kessler and Baldwin 2001) the emission of these compounds in response to ozone could feasibly disrupt plant signalling. Vuorinen et al. (2004) tested this hypothesis using a model system consisting of lima beans, spider mites and predatory mites and found that tritrophic signalling was not disturbed by ozone exposure. However, Cui et al. (2014) found that ozone fumigation of whitefly infested tomato plants enhanced the emission of monoterpenes, green leaf volatiles and aldehydes, leading to increased attraction of the whitefly parasitoid *Encarsia formosa*.

Together with its impact on the emission of bVOCs from plants, ozone may also affect plant signalling through its reaction with bVOCs. Volatiles containing the alkene functional group will react with ozone both in the gas phase and in the liquid phase on the leaf surface and inside leaves (Hewitt and Terry 1992). The ozonolysis of sesquiterpenes and other large terpenes can lead to the rapid degradation of these signalling molecules (Acton et al., 2016). Ozone has been shown to disrupt plant-plant communication (Blande et al., 2010), plant-pollinator communication (Farre-Armengol et al., 2015) and herbivore host location (Fuentes et al., 2013). Pinto et al. (2007a), however, found that tritrophic communication (using *Brassica oleracea*–*Plutella xylostella*–*Cotesia plutellae* and *Phaseolus lunatus*–*Tetranychus urticae*–*Phytoseiulus persimilis* model systems) was unaffected by ozone exposure suggesting that more atmospherically stable bVOCs, such as the aromatic compounds methyl-salicylate and benzyl cyanide, prevented signal degradation.

In this study we investigate the effect of ozone on herbivore host location and on tritrophic interaction using a *Brassica napus*–*Myzus persicae*–*Adalia bipunctata* model system. Phloem feeding insects such as aphids cause little tissue damage to plants, therefore bVOC emissions from plants following aphid infestation consist mainly of induced compounds. For example, Staudt et al. (2010) reported the emission of methyl-salicylate and terpenoids following *Myzus persicae* attack on a variety of peach genotypes. As terpenoids are known to react rapidly with ozone (Acton et al., 2016; Atkinson and Arey, 2003a) one might expect the volatile signal to be disrupted, although, as reported by Pinto et al. (2007a) the emission of compounds with a low reactivity towards ozone such as methyl-salicylate may preserve tritrophic signalling. Volatile emissions from healthy and *M. persicae* infested plants are recorded here

using GC-MS and the changes in bVOC composition following ozone exposure are recorded at high time resolution using a proton transfer reaction-mass spectrometer (PTR-MS).

## 5.2 Methodology

### 5.2.1 Plant material and insects

Oilseed rape plants (*Brassica napus* cv. DK Cabernet, Monsanto, UK) were grown in plastic pots (55 mm diameter × 48 mm deep) using Levingtons M3 compost. The plants were housed in a greenhouse with a 16 h photoperiod, an average temperature of 24.5 °C, 44.8 % relative humidity and an average day-time light intensity of 286 W m<sup>-2</sup>. Plants were used in decision experiments at 4-6 weeks of age, equivalent to growth stage 1.3 (recorded using the system described by HGCA, 2012). Aphids (*Myzus persicae*) were reared on *B. napus* at ca. 20 °C with a 16 h photoperiod. Ladybird larvae (*Adalia bipunctata*, Fig. 5.1) were obtained from commercial sources (Fargro, Sussex, UK and Green Gardener, Great Yarmouth, UK). *A. bipunctata* were maintained on *M. persicae* infested *B. napus* and were given at least 24 h to acclimatise prior to use in the behavioural assay. Plants were infested with ca. 200 *M. persicae* 48 h prior to *A. bipunctata* decision experiments.

### 5.2.2 Experimental setup

Experiments were conducted in two formats, described henceforth as investigation 1 and investigation 2 (Fig. 5.2). Investigation 1 aimed to investigate the effect of ozone fumigation on a. *A. bipunctata* choosing between a *M. persicae* infested plant and a healthy plant and b. *M. persicae* choosing between a plant and a blank chamber. For

*A. bipunctata* decision experiments, a *M. persicae* infested plant and a healthy plant were installed in two 1 L glass chambers (screw topped jars (Wilkinsons, Lancaster, UK) modified so that the steel/rubber caps were replaced by a PTFE disk). Both a. and b. were repeated 5 times with different plants.



Figure 5.1. *Myzus persicae* and *Adalia bipunctata* larvae

Purified air was generated by pumping ambient air (Eheim Air Pump 100LPH, Warehouse Aquatics, Preston, UK) through a charcoal filter followed by a bubbler to restore humidity. This air stream was then split providing  $200 \text{ ml min}^{-1}$  to each plant chamber. Ozone was generated by passing compressed air through a UV dissociation ozone generator (Opsis, Furulund, Sweden) and was added to the purified air stream before air entered the plant chamber. The outflow from the two plant chambers was then directed into the two side arms of the glass Y-tube olfactometer (main arm 11 cm, side arms 8 cm, O.D. 24 mm, I.D. 20 mm, angle between side arms  $90^\circ$ , Soham Scientific, Ely, UK). All tubing used was  $\frac{1}{4}$  inch (O.D. 6.35 mm, I.D. 4.76 mm) PTFE and all fittings exposed to ozone or bVOCs were made of PTFE or stainless steel. During ozone fumigation experiments, ozone mixing ratios were

recorded using a photometric ozone analyser (model 400E, Enviro Technology, Stroud, UK) connected to the base of the Y-tube olfactometer and were maintained at  $100 \pm 15$  ppbv. Ozone mixing ratios in during clean air experiments ranged from 0-15 ppbv.

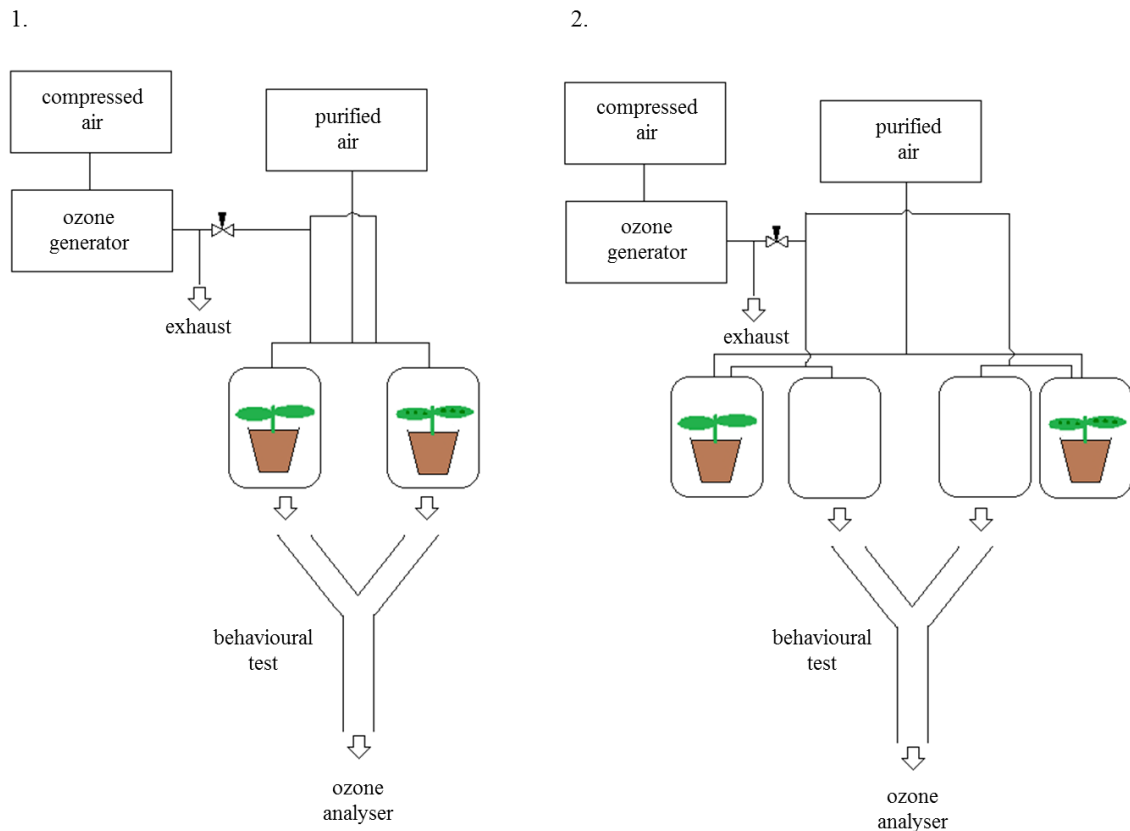


Figure 5.2 experimental setup used for behavioural tests with the setup for investigation 1 displayed on the left and investigation 2 displayed on the right. For aphid decision experiments the Y-tube olfactometer was covered with a cardboard sheet with a circular hole allowing light to shine between the arms of the Y-tube olfactometer.

For *M. persicae* decision experiments, a healthy plant was installed into one chamber and the second chamber remained blank. The experimental setup was then the same as

described above with the addition of a cardboard sheet with a circular hole allowing light to shine between the arms of the Y-tube olfactometer. This was installed so that light only shone on fork of the Y-tube. This encouraged the aphids to move towards the fork of the Y-tube olfactometer and therefore be in position to make a decision.

Decision experiments with both *M. persicae* and *A. bipunctata* were carried out by inserting insects (ca. 10 and ca. 5 at once respectively) 2 cm into the stem of the olfactometer. Insects were then left undisturbed for 10 min and after this period the number of insects which had moved 2 cm or further into each branch of the olfactometer were recorded as having made a decision. This procedure was repeated using different insects until > 50 decisions had been recorded for each pair of plants.

Investigation 2 (Fig. 5.2) was carried out in order to identify whether the behavioural changes observed in investigation 1 were as a result of ozone interaction with the plant or ozone interaction with the bVOCs emitted by the plant and/or ozone interaction with the insects. Investigation 2, therefore, followed a similar procedure to that described for investigation 1 except that ozone was introduced after the plant chamber and air entered a blank chamber (1 L) before the Y-tube olfactometer so that the ozone-bVOC reaction time remained the same as in investigation 1.

### **5.2.3 Preliminary experiments**

In order to confirm that there was no bias towards the left or right hand arm of the Y-tube olfactometer, experiments were performed using *M. persicae* with two healthy plants. In these experiments (data not shown) *M. persicae* showed no significant preference for the left or the right arm of the Y-tube olfactometer demonstrating that

the insects were not bias towards one arm of the Y-tube olfactometer. In order to confirm that *M. persicae* and *A. bipunctata* behaviour was not effected by other insects within the Y-tube olfactometer preliminary experiments were carried out using individual insects and regularly washing the tube to prevent memory effects. These trials (data not shown) generated the same results as when insects were placed into the Y-tube olfactometer in groups indicating that the insects were not influenced by each other.

#### **5.2.4 Statistical analysis**

Statistical analysis was carried out with the aid of the R lme4 package (Bates et al., 2015; R Core Team 2012). The ability of *M. persicae* and *A. bipunctata* to make decisions in clean air was tested against the null hypothesis using the chi-square test ( $\chi^2$ ). The effect of ozone fumigation on insect decisions was assessed using linear mixed models. The data were fitted to a generalised linear mixed effect model (glmer) where the presence/absence of ozone was considered a fixed effect and each plant repetition a random effect. In order to ascertain the effect of ozone, two models, one including ozone and one not, were compared using ANOVA to give a p-value, i.e. the probability of the observed results occurring when the null hypothesis is true.

#### **5.2.5 GC-MS measurements**

The emissions of bVOCs from the fully expanded leaves of healthy and aphid infested plants were recorded with GC-MS using a method based on that described by Vickers et al. (2009). A Li-Cor Li-6400 portable photosynthesis system equipped with a 6400-40 leaf chamber fluorometer (Li-Cor Inc., Lincoln, USA) was used to record stomatal conductance and net photosynthetic rate. The leaf chamber exhaust was modified

using a PTFE t-piece so that 2 L of air (at a flow rate of 200 ml min<sup>-1</sup>) could be subsampled onto sample tubes packed with the adsorbent resins Tenax TA and Carbotrap (Supelco Inc, Bellefonte, USA). Sampling commenced once stable photosynthetic rate and stomatal conductance values were achieved and plants exhibiting very low levels of photosynthesis were excluded from the study. During sampling the leaf in the chamber was held at constant conditions with photosynthetically active radiation (PAR) set to 1000 μmol m<sup>-2</sup> s<sup>-1</sup>, a temperature of 30 °C and a CO<sub>2</sub> mixing ratio of 400 ppbv.

An automated thermal desorption unit (Turbomatrix ATD; Perkin Elmer, Norwalk, USA) was then used to desorb samples. Sample tubes were heated to 280 °C and the released volatiles were trapped onto a Tenax TA cold trap (-30 °C for 6 min) in order to focus the sample before rapid heating to 300 °C in order to release the sample into the GC. The sample was then introduced onto an Ultra-2 capillary column (50 m × 0.22 mm I.D. × 1.05 mm film thickness, 5% phenylmethylsilica, Hewlett Packard; Varian Inc, Palo Alto, USA) with a helium carrier gas. The oven temperature was held initially at 35 °C for 2 min before heating to 160 °C at 4 °C min<sup>-1</sup>, then heating at 45 min<sup>-1</sup> to 300 °C before holding at 300 °C for a final 10 min. Compounds were identified by comparison of their retention time and mass spectral fragmentation pattern with commercially available standards (Sigma-Aldrich Inc., Gillingham, UK), where available, and with the Wiley (John Wiley & Sons, Hoboken, USA) and NIST Mass Spectral Libraries supplied with the TurboMass software (TurboMass version 5.4.2; Perkin Elmer Instruments).

The GC-MS was calibrated using a 6 point calibration. Pure standards ( $\alpha$ -pinene,  $\gamma$ -terpinene, octanol and  $\beta$ -caryophyllene, Sigma-Aldrich Inc., Gillingham, UK) were made up in methanol (ca. 3 ng  $\mu\text{l}^{-1}$ ) and a range of volumes of these standards were then injected onto sample tubes (1-10  $\mu\text{l}$ ). The signal response to increasing mass of standard was found to be linear allowing calibration curves to be constructed. Sesquiterpenes were quantified from  $\beta$ -caryophyllene, monoterpenes from  $\alpha$ -pinene and  $\gamma$ -terpinene and oxygenated compounds from octanol.

### 5.2.6 Emission rate calculation

Emission rates were calculated from the GC-MS results. The mass of the analyte species trapped onto the GC-MS sampling tube was obtained via GC-MS analysis. This value was then divided by the sampling time and the leaf area within the cuvette to obtain the emission rate ( $\mu\text{g m}^{-2} \text{s}^{-1}$ ).

### 5.2.7 PTR-MS measurements

The effects of ozone on bVOC emissions from *B. napus* were recorded using a proton transfer reaction – mass spectrometer (PTR-MS) (Ionicon Analytik GmbH, Innsbruck, Austria). This instrument is described in detail by Blake et al. (2009), Hansel et al. (1995) and Lindinger et al. (1998b) therefore only the instrumental setup and operational parameters are described here. The PTR-MS sampled through a 1/8 inch (3.18 mm O.D., 1.59 mm I.D.) diameter PTFE tube, heated to avoid condensation and memory effects, from the plant chamber outlet. Operation of the PTR-MS was performed in mass scan mode with masses recorded from  $m/z$  21 to 137 with a dwell time ( $\tau$ ) of 0.5 s. Masses above 137 were not analysed due to low quadrupole transmission at high masses. The instrument was operated with a 45 °C drift tube

temperature and 600 V drift voltage giving an  $E/N$  (the ratio of the electric field strength,  $E$ , to the buffer gas number density,  $N$ , in the drift tube) of 130 Td (where  $1 \text{ Td} = 10^{-21} \text{ Vm}^{-2}$ ). Count rates for the primary ion ( $\text{H}_3\text{O}^+$ ), inferred from its isotope at  $m/z$  21 remained in the range  $9.96 \times 10^6 - 2.55 \times 10^7$  cps throughout the measurement period.

A five point PTR-MS calibration was made by dynamic dilution of a  $500 \pm 5\%$  ppb gas standard (3 years old, Apel Riemer Environmental Inc., Broomfield, USA) with zero air generated from ambient air using a home built zero air generator operated at  $300 \text{ }^\circ\text{C}$ . Mixing ratios used in the calibration in ranged from 0-5 ppbv. This generator was made up of 1 g of platinum coated quartz wool packed inside a 3/8 inch stainless steel tube (as described by Shaw et al., 2015). The gas standard contained 14 compounds ranging in molecular mass from 33 to 137 amu. Instrumental sensitivities for compounds present in the gas standard were calculated directly. For compounds not present in the gas standard instrumental sensitivities were calculated using a relative transmission curve generated from the masses present in the analytical standard (Davison et al., 2009; Taipale et al., 2008). The PTR-MS sensitivities for each of the compounds reported are summarised in Table 5.1.

Mixing ratios ( $\chi$ ) were then calculated using the method described in Acton et al. (2015), based on that of Taipale et al. (2008) and Tani et al. (2004).

$$\chi_{\text{VOC}} = \frac{I(\text{RH}^+)_{\text{norm}}}{S_{\text{norm}}} \quad (1)$$

Where  $I(\text{RH}^+)_{\text{norm}}$  is the count rate for each protonated VOC species  $I(\text{RH}^+)$  normalised to a primary ion ( $\text{H}_3\text{O}^+$ ) + primary ion-water cluster ( $\text{H}_3\text{O}^+\text{H}_2\text{O}$ ) count of  $10^6$ , a drift tube pressure ( $p_{\text{drift}}$ ) of 2 mbar and background corrected.  $S_{\text{norm}}$  represents the normalised sensitivity at that mass.

Table 5.1., the mixing ratios of the major bVOCs (> 0.3 ppbv) present in the plant chamber prior to and during ozone fumigation recorded using PTR-MS. Mass spectral fragments are reported at unit mass resolution together with compounds tentatively assigned to each mass and for masses present in gas standard, PTR-MS sensitivity.

unit mass (amu)	compound(s) tentatively assigned to this mass	average VMR prior to ozone fumigation (standard deviation) (ppbv)	average VMR after ozone fumigation (standard deviation) (ppbv)	PTR-MS sensitivity (ncps ppbv <sup>-1</sup> )
33	methanol	3.35 (1.90)	3.19 (2.12)	15.94
41		0.28 (0.09)	0.58 (0.27)	
43	multiple species	1.34 (0.55)	2.68 (1.35)	
45	acetaldehyde	2.66 (0.36)	3.80 (0.58)	16.22
47		0.88 (0.11)	1.12 (0.38)	
49		0.54 (0.31)	0.54 (0.35)	
59	acetone	1.87 (7.18)	12.36 (7.37)	
61	acetic acid	1.07 (1.07)	1.56 (1.45)	
63	dimethyl sulfide	0.54 (0.22)	0.50 (0.20)	7.73
69	isoprene unsaturated alcohol	1.12 (0.36)	3.93 (1.83)	6.14
71	methyl vinyl ketone methacrolein	0.71 (0.02)	1.01 (0.20)	11.52
73	methyl ethyl ketone methylglyoxal	0.27 (0.06)	0.54 (0.18)	15.68
81	monoterpene fragment hexenal fragment hexenol, hexanal and	0.44 (0.06)	0.84 (0.25)	
83	hexenyl acetate fragments	0.94 (0.22)	2.41 (1.00)	
85	ethyl vinyl ketone	0.36 (0.07)	0.46 (0.12)	
87	2-methyl- 3-buten-2-ol	0.48 (0.01)	0.66 (0.07)	
95		0.35 (0.35)	0.66 (0.13)	
97	unsaturated alcohol	0.27 (0.20)	0.95 (0.48)	
99	hexenal	0.24 (0.09)	0.38 (0.15)	
101	4-oxopentanal	0.96 (0.23)	1.72 (0.83)	
109		0.62 (0.10)	1.90 (0.08)	

Table 5.1 (continued)

unit mass (amu)	compound(s) tentatively assigned to this mass	average VMR prior to ozone fumigation (standard deviation) (ppbv)	average VMR after ozone fumigation (standard deviation) (ppbv)	PTR-MS sensitivity (ncps ppbv <sup>-1</sup> )
	4-methylenehex-5-enal,			
111	C <sub>5</sub> -carbonyls and methacrylic acid	0.39 (0.17)	1.08 (0.45)	
113		0.39 (0.26)	0.49 (0.19)	
115	heptanal	0.20 (0.08)	0.40 (0.16)	
120	unknown	0.36 (0.18)	0.32 (0.04)	
121	C <sub>9</sub> -aromatics	0.43 (0.08)	0.42 (0.06)	6.66
122		0.49 (0.04)	0.42 (0.06)	
124		5.31 (1.45)	4.88 (0.72)	
125		0.25 (0.05)	0.46 (0.08)	
126		0.55 (0.13)	0.57 (0.09)	
127	6-methylhept-5-en-2- one	0.27 (0.10)	0.90 (0.17)	
129	octanal	0.24 (0.11)	0.43 (0.15)	
131	p-cymene	0.50 (0.41)	0.51 (0.35)	
137	monoterpenes	0.26 (0.08)	0.35 (0.08)	2.94

## 5.3 Results

### 5.3.1 Insect behavioural tests

In clean air, *M. persicae* were able to discriminate between a *Brassica napus* plant and a blank chamber ( $P < 0.05$ ) in the Y-tube. *A. bipunctata* larvae were also able to distinguish between a *M. persicae* infested plant and a healthy plant in clean air ( $P < 0.05$ ) in the Y-tube. The effect of ozone on *M. persicae* and *A. bipunctata* decision making was assessed in two investigations, with ozone added before the plant chamber in investigation 1 and after the chamber in investigation 2. In investigation 1

ozone was observed to significantly reduce the ability of *M. persicae* to locate a host plant over a blank chamber ( $P < 0.05$ ) and to significantly reduce the ability of *A. bipunctata* to locate a *M. persicae* infested plant over a healthy plant ( $P < 0.01$ ) (Fig. 5.3). In investigation 2 ozone again significantly reduced the ability of *M. persicae* to locate a host plant over a blank chamber ( $P < 0.01$ ) and to significantly reduce the ability of *A. bipunctata* to locate a *M. persicae* infested plant over a healthy plant ( $P < 0.01$ ) (Fig. 5.4).

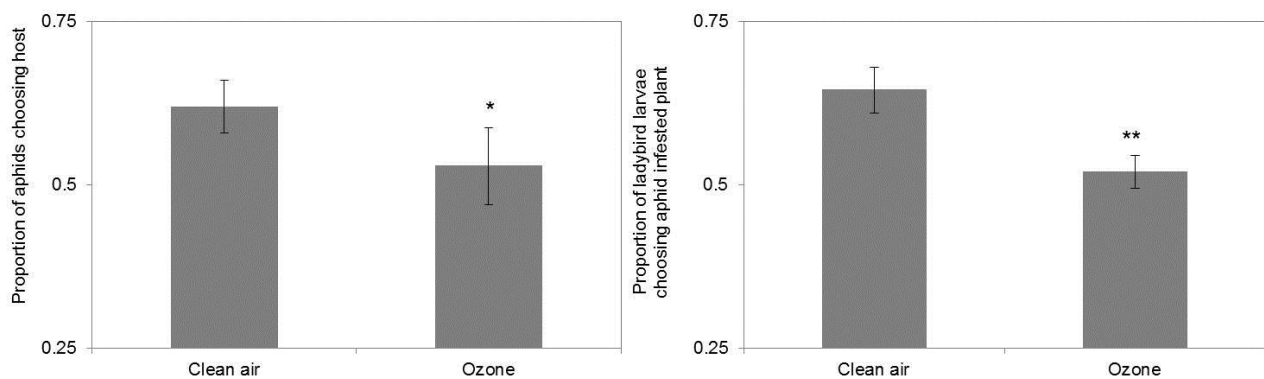


Figure 5.3, proportion of *M. persicae* choosing host plant instead of blank chamber when exposed to clear air and ozone (left) and proportion of *A. bipunctata* larvae choosing *M. persicae* infested plant instead of a healthy plant in investigation 1. The significance of ozone on insect decision making is highlighted with asterisks where \* indicates  $P < 0.05$  and \*\* indicates  $P < 0.01$ . Error bars represent the standard deviation across 5 plants.

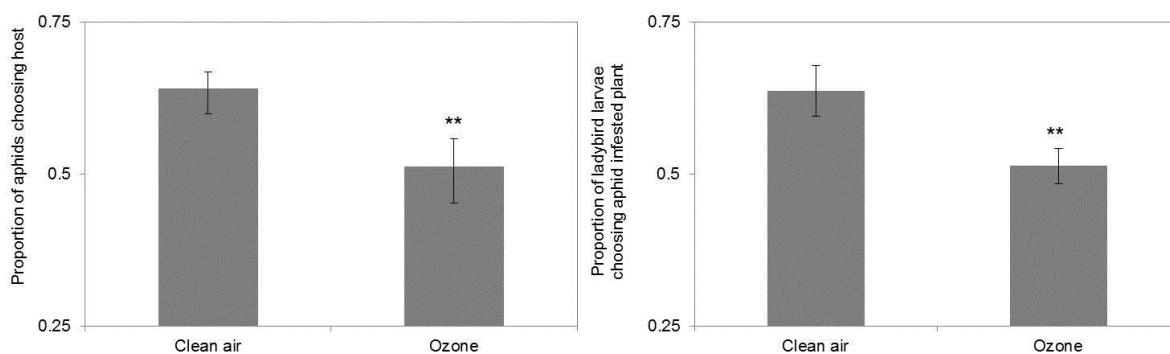


Figure 5.4, proportion of *M. persicae* choosing host plant instead of blank chamber when exposed to clear air and ozone (left) and proportion of *A. bipunctata* larvae choosing *M. persicae* infested plant instead of a healthy plant in investigation 2. The significance of ozone on insect decision making is highlighted with asterisks where \* indicates  $P < 0.05$  and \*\* indicates  $P < 0.01$ . Error bars represent the standard deviation across 5 plants.

### 5.3.2 Effect of *M. persicae* infestation on bVOC emission

The emissions of bVOCs from healthy and *M. persicae* infested plants were recorded using GC-MS and are summarised in Fig. 5.5. Average volatile emissions from nine healthy plants were dominated by the emission of the oxygenated species decanal ( $42 \pm 9 \mu\text{g m}^{-2} \text{h}^{-1}$ ) and an unidentified alcohol ( $58 \pm 17 \mu\text{g m}^{-2} \text{h}^{-1}$ ) together with isothiocyanato-cyclohexane ( $51 \pm 22 \mu\text{g m}^{-2} \text{h}^{-1}$ ), an unidentified compound ( $38 \pm 9 \mu\text{g m}^{-2} \text{h}^{-1}$ ), and the monoterpene  $\alpha$ -thujene ( $54 \pm 50 \mu\text{g m}^{-2} \text{h}^{-1}$ ). Emissions of the monoterpene  $\alpha$ -thujene varied significantly between plants. Emissions of the monoterpenes  $\alpha$ -pinene,  $\alpha$ -terpinolene and  $\alpha$ -phellandrene and the sesquiterpenes  $\beta$ -caryophyllene and  $\beta$ -farnesene were also observed. The emissions of bVOCs from *M. persicae* infested plants showed a very similar pattern to the bVOC emissions from healthy plants with the exception of the sesquiterpene  $\beta$ -farnesene where emission increased from  $3 \pm 1$  to  $7 \pm 4 \mu\text{g m}^{-2} \text{h}^{-1}$  from the infested plants.

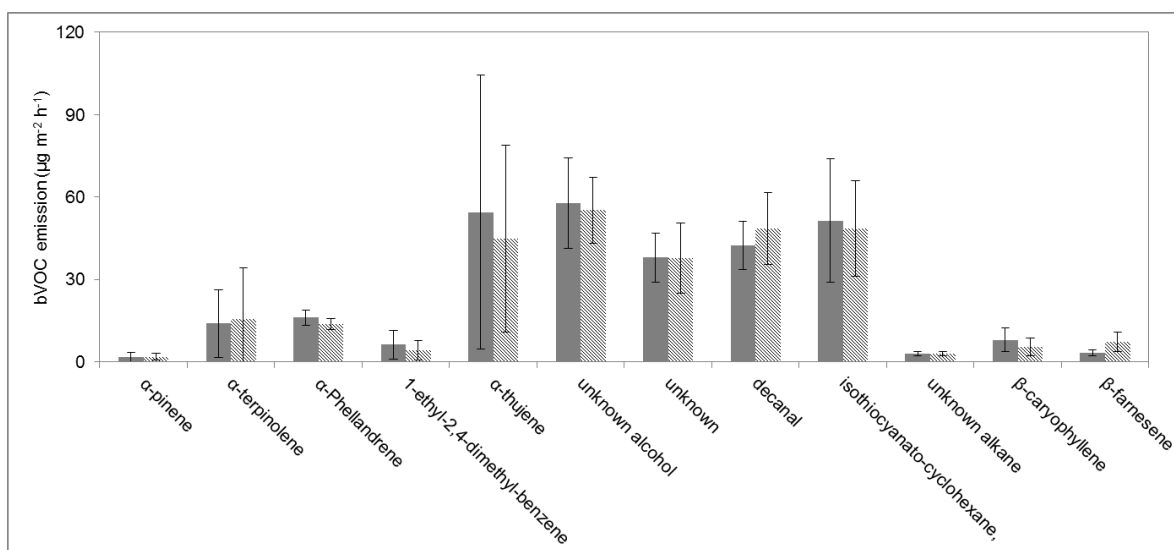


Figure 5.5, bVOC emission ( $\mu\text{g m}^{-2} \text{h}^{-1}$ ) from healthy (solid grey) and *M. persicae* (striped) infested *B. napus* recorded using GC-MS. Error bars represent the standard deviation across 9 plants.

### 5.3.3 Effect of ozone on bVOC emission

The effect of ozone on the bVOC mixing ratios in the plant chamber was monitored using a PTR-MS. The PTR-MS operates at unit mass resolution, therefore the mixing ratios presented at each protonated mass represent the sum of all compounds at this mass. The mixing ratios present in the plant chamber before and during ozone fumigation are reported in table 5.1 for all significant mass spectral peaks ( $> 0.3$  ppbv). Compounds are tentatively assigned to mass spectral peaks on the basis of those observed following ozone fumigation of *B. napus* using a selective reagent ionisation-time of flight-mass spectrometer (SRI-ToF-MS, Acton et al., 2016), compounds commonly observed in the atmosphere (Gouw and Warneke, 2007) and expected sesquiterpene ozonolysis products (Kourtchev et al., 2009). The change in bVOC mixing ratios within the mass range 31-137 amu in the plant chamber

following ozone fumigation is displayed in Fig. 5.6. Acetone was the dominant compound emitted following ozone fumigation with an increase of 10.5 ppbv in the outflowing air, with large increases also observed at  $m/z$  43, 45, 69, 83 and 109.

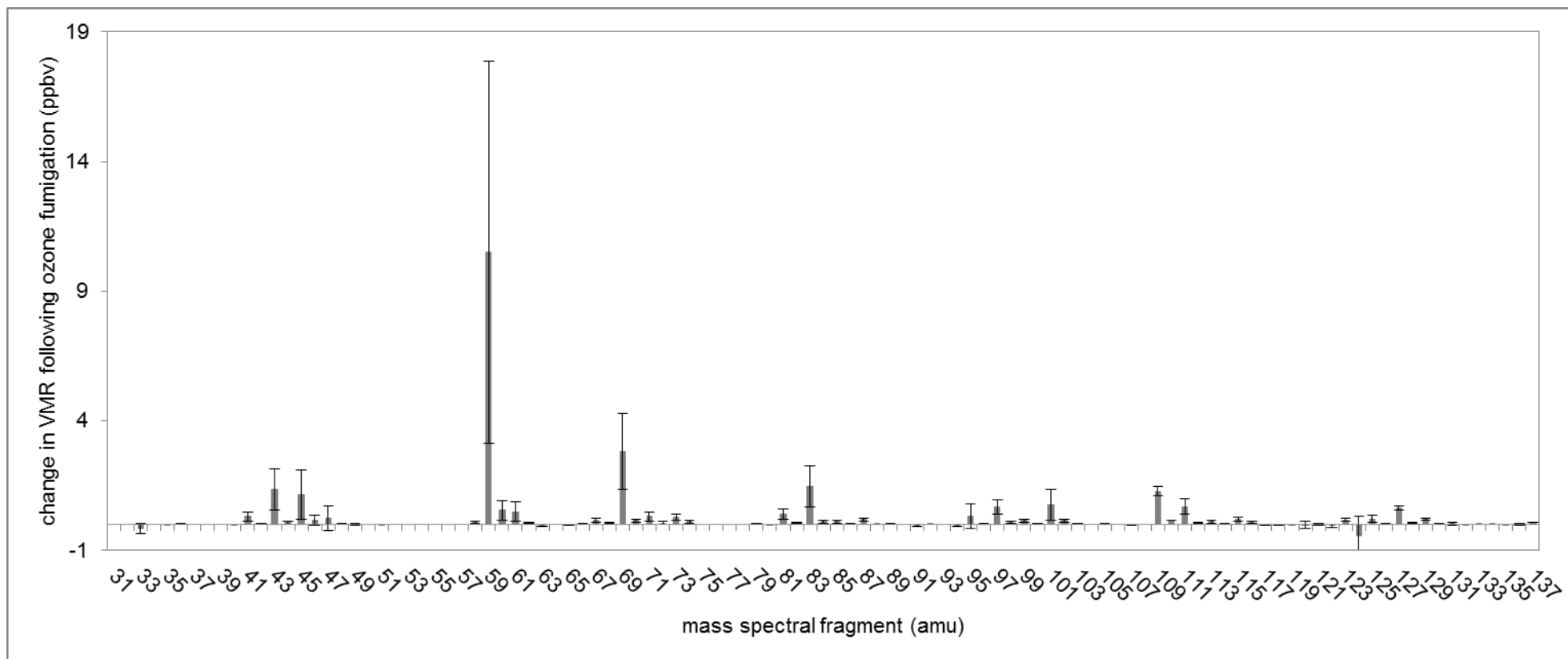


Figure 5.6, the change in the volume mixing ratios (VMR, ppbv) of the mass spectral fragments (amu) recorded using PTR-MS following ozone fumigation of *B. napus*. Error bars represent the standard deviation across the 4 plants measured.

## 5.4 Discussion

*M. persicae* is an important pest of oilseed rape crops, causing both direct damage and transmitting viral infections (Ahuja et al., 2010). Attack by *M. persicae* has been shown to cause the emission of a range of chemical species including isothiocyanates (Blande et al., 2007) and  $\beta$ -farnesene (Francis et al., 2001) from *Brassicaceae* with Blande et al. (2007) showing that herbivore-induced volatiles enable the parasitoid *Diaeretiella rapae* to locate *M. persicae* infested plants. Here we focused on the ability of *M. persicae* to identify host plants (*B. napus*) and, following *M. persicae* infestation, the ability of the aphid predator *A. bipunctata* to locate its prey under an ozone polluted atmosphere.

In clean air, *A. bipunctata* larvae were able to successfully locate *M. persicae* infested plants. Most research on the role of volatiles in aphid host location has focused on alates (the winged form) as they are primarily responsible for the location of suitable host plants (Webster 2012). Wingless aphids have been shown to be more reliant upon visual stimuli in host location (Gish and Inbar, 2006). While *M. persicae* were highly sensitive to light, when light levels were the same on both branches of the olfactometer *M. persicae* were also shown to be able to choose a host plant over a blank chamber in clean air. This is in contrast to previous work which demonstrated using a Y-tube olfactometer that, for an *Artemisia arborescens* - *Macrosiphoniella artemisiae* model system, plant volatiles did not play a significant role in host location (Gish and Inbar, 2006).

Our results show that fumigation with ozone at ca. 100 ppbv significantly reduced the ability of *M. persicae* to identify a host plant instead of a blank chamber and significantly reduced the ability of *A. bipunctata* larvae to distinguish between a *M. persicae* infested plant and a healthy plant (Fig. 5.3). The mixing ratios of ozone used in the investigations (ca. 100 ppbv) are typical of summertime air during photochemical smog episodes in, for example, the Mediterranean basin (Royal Society, 2008). The disruption of plant-insect communication by ozone could occur via one or a combination of three potential mechanisms: 1. oxidative stress causes quantitative and qualitative changes in the bVOC emissions from plants, masking the signals associated with biotic stress; 2. ozone could cause the chemical degradation of the bVOCs responsible for transmitting signals between plants and insects; and 3. ozone could disrupt the ability of insects to detect the bVOCs responsible for host/prey location.

In order to ascertain whether changes in bVOC emissions from plants following oxidative stress were responsible for the disruption in plant-insect communication a second investigation was carried out (Fig. 5.2, right hand side). In this investigation a second chamber was added between the plant chamber and the Y-tube olfactometer and ozone was introduced between the plant chamber and the second chamber. This ensured that while the plant was not exposed to ozone the bVOCs and ozone had comparable reaction time to investigation 1. During this investigation ozone was again observed to significantly reduce the ability of *M. persicae* to identify a host plant instead of the blank chamber and to significantly reduce the ability of *A. bipunctata* larvae to distinguish between a *M. persicae* infested plant and a healthy plant (Fig. 5.4). This, for the first time, suggests that the disruption in *M. persicae* host location

and *A. bipunctata* larvae prey location is driven either by the oxidative degradation of signalling molecules or by disruption of the insects ability to detect bVOCs following ozone exposure and not a change in direct bVOC emission from the plant. Pinto et al. (2007a) investigated the effect of elevated ozone levels (60-120 ppb) on prey location by *Cotesia plutellae* and *Phytoseiulus persimilis*, demonstrating using a Y-tube olfactometer that tritrophic signalling was not disrupted by ozone due to the presence of atmospherically stable aromatic bVOCs such as methyl-salicylate in the suite of emitted compounds. This finding indicates that the insects' ability to detect bVOC species was unaffected by ozone at mixing ratios comparable to those used in this present study. Although it may be that *M. persicae* and *A. bipunctata* larvae are more sensitive to ozone than *C. plutellae* and *P. persimilis*, we believe that the most likely cause of the disruption in plant-insect communication that we observe is the oxidative degradation of plant emitted volatiles.

The emissions of bVOCs from a healthy *Brassica napus* plant were dominated by methanol (table 5.1). Terpene emissions were dominated by the monoterpenes  $\alpha$ -thujene,  $\alpha$ -terpinolene and  $\alpha$ -phellandrene together with the sesquiterpene  $\beta$ -caryophyllene. This shows reasonable agreement with that reported by Acton et al. (2016) where a SRI-ToF-MS instrument was used to record bVOC emission from *B. napus* cv. DK Cabernet. In contrast to this study we did not detect the emission of the aromatic species methyl-salicylate. The differences between this study and that reported by Acton et al. (2016) are likely a result of differences in growth stage and growing conditions. Following infestation with *M. persicae*, the terpene emissions from *B. napus* were unchanged with the exception of  $\beta$ -farnesene, the emission of which increased by a factor of 2.3. Enhanced emission of  $\beta$ -farnesene from *M.*

*persicae* infested plants has been reported by Francis et al. (2001) and this compound is also known to act as an aphid alarm pheromone (Maffei, 2010).

The effects of ozone fumigation on bVOC mixing ratios in the plant chamber were monitored using PTR-MS. Owing to poor instrumental sensitivity at high masses the PTR-MS could not be used to directly monitor the impact of ozone fumigation on the sesquiterpene mixing ratios in the leaf chamber. However, the PTR-MS could be used to indirectly monitor sesquiterpene ozonolysis through the formation of ozonolysis products. Kourtchev et al. (2009) studied the reaction of  $\beta$ -farnesene with ozone, identifying the reaction products acetone, methylglyoxal, 4-oxopentanal, 4-methylenehex-5-enal, 6-methylhept-5-en-2-one and (E)-4-methyl-8-methylenedeca-4,9-dienal. In the PTR-MS these compounds would be expected at  $m/z$  59, 73, 101, 111, 127 and 179 respectively. The change in volume mixing ratio at each unit mass in the range  $m/z$  31-137 during ozone fumigation is displayed in Fig. 5.6. An increased mixing ratio is observed during fumigation at  $m/z$  59, 73, 101, 111, 127, assigned to acetone, methylglyoxal/methyl ethyl ketone, 4-oxopentanal, 4-methylenehex-5-enal and 6-methylhept-5-en-2-one respectively. This suggests that under ozone fumigation  $\beta$ -farnesene was lost through ozonolysis, thereby supporting the hypothesis that plant-insect communication is disrupted by the oxidative degradation of bVOCs in air during transport from the leaf surface to the insect receptor.

Previous investigations into the effect of ozone on tritrophic communication have shown that under elevated ozone tritrophic signalling can be enhanced (Cui et al., 2014), unaffected (Pinto et al., 2007a; Vuorinen et al., 2001) or impeded (Gate et al., 1995; Himanen et al., 2009). The resilience of a tritrophic system is likely to depend

on the nature of the key signalling molecules. Systems reliant upon terpenes will be more sensitive to ozone than those reliant upon aromatic species or green leaf volatiles. While for some plant species phloem feeding insects such as *M. persicae* have been shown to induce the emission of aromatic species such as methyl-salicylate (Staudt et al., 2010), the reliance of tritrophic systems involving phloem feeding insects on induced volatiles rather than constitutive volatiles is likely to make these systems more sensitive to rising ozone concentrations than those involving chewing insects.

As aphids in their wingless form are primarily reliant on visual stimuli to locate suitable host plants (Gish and Inbar, 2006) the impact of ozone on their ability to find a host is unlikely to have a large effect at field scale. The influence of ozone on the ability of aphid predators such as *A. bipunctata* larvae to locate prey could, however, have a significant impact for crop protection. Although there has yet to be a field-scale study on the influence of increased ozone concentrations on tritrophic signalling, an investigation into the effect of elevated ozone on insect community composition in an aspen-birch forest (Hillstrom and Lindroth, 2008) found that elevated ozone resulted in an increased abundance of sucking insects (*Aphididae*, *Cicadellidae* and *Miridae*). While this represents a far more complex system than that observed in the laboratory, the finding is consistent with a reduction in the ability of the predators of phloem feeding insects to locate their prey in an elevated ozone environment.

## 5.5 Conclusions

The results of the Y-tube olfactometry experiments presented here show that in the absence of ozone *M. persicae* can make use of plant emitted volatiles to locate a host plant and that *A. bipunctata* larvae can identify *M. persicae* infested plants. Fumigation of the plants with ca. 100 ppbv ozone caused a significant reduction in the proportion of *M. persicae* successfully locating a host plant ( $P < 0.05$ ) and the proportion of *A. bipunctata* larvae locating a *M. persicae* infested plant ( $P < 0.01$ ). This effect was still observed when ozone was introduced to the system after the plant, indicating for the first time that the disruption to plant-insect communication was caused by the ozonolysis of bVOCs rather than changes in the emission of bVOC species from plants following abiotic stress.

The influence of rising ozone on tritrophic signalling has yet to be tested at a field-scale but these results suggest that the *B. napus*-*M. persicae*-*A. bipunctata* larvae tritrophic system is likely to be sensitive to rising ozone concentrations. As *M. persicae* is an important crop pest globally a reduction in the ability of the natural predators of *M. persicae* (such as *A. bipunctata* larvae) to locate their prey could have a significant impact on crop production

## Acknowledgements

W.J.F. Acton is in receipt of a BBSRC/Ionicon Analytik GmbH Industrial CASE studentship. The authors would like to thank Joseph Fennel and Dr Andy Wilby for kindly providing *Myzus persicae* and for their helpful advice.

## Chapter VI

# **Canopy-scale flux measurements and bottom-up emission estimates of volatile organic compounds from a mixed oak and hornbeam forest in northern Italy**

This chapter details the findings from flux measurements of a range of bVOC species recorded using PTR-MS during a field campaign carried out June and July 2012 at a semi-natural forest situated in the Po Valley. This campaign was carried out as a part of the ÉCLAIRE (Effects of Climate Change on Air Pollution and Response Strategies for European Ecosystems) EC FP7 project. The initial aim of these measurements was to observe the effect of ozone on bVOC emission at a canopy scale, unfortunately no clear ozone effect could be observed. In this chapter, therefore, fluxes and mixing ratios of bVOCs recorded at 4 m above the forest canopy are reported and for the first time the calculation of fluxes of isoprene and monoterpenes using PTR-MS, PTR-ToF-MS and leaf level GC-MS measurements up-scaled to canopy level are compared.

This work was accepted for publication the journal Atmospheric Chemistry and Physics Discussions on the 16th May 2016 and published on the 10th June 2016.

Acton W. J. F., Schallhart S., Langford B., Valach A., Rantala P., Fares S., Carriero G., Tillmann R., Tomlinson S. J., Dragosits U., Gianelle D., Hewitt C. N., and Nemitz E.: Canopy-scale flux measurements and bottom-up emission estimates of volatile organic compounds from a mixed oak and hornbeam forest in northern Italy, *Atmospheric Chemistry and Physics*, 16, 7149-7170, 2016.

The authors and their contributions are listed below:

**Acton W. J. F. (Lancaster University):** Set up and operated PTR-MS during field campaign, carried out data processing and analysis and wrote manuscript.

**Schallhart S. (University of Helsinki):** Set up and operated PTR-ToF-MS during field campaign, processed PTR-ToF-MS data and helped with manuscript preparation.

**Langford B. (Centre for Ecology & Hydrology):** Helped with instrument setup, data analysis, interpretation of results and manuscript preparation.

**Valach A. (Lancaster University):** Set up and operated PTR-MS during field campaign and helped with manuscript preparation.

**Rantala P. (University of Helsinki):** Set up and operated PTR-ToF-MS during field campaign, processed PTR-ToF-MS data and helped with manuscript preparation.

**Fares S. (CRA, Rome):** Carried out GC-MS sampling and analysis and helped with manuscript preparation.

**Carriero G. (Institute for Plant Protection, Sesto Fiorentino):** Carried out GC-MS sampling and analysis.

**Tillmann R. (Institute of Energy and Climate Research, Jülich):** Prepared PTR-ToF-MS for campaign and helped with manuscript preparation.

**Tomlinson S. J. (Centre for Ecology & Hydrology):** Processed land cover data and helped with manuscript preparation.

**Dragosits U. (Centre for Ecology & Hydrology):** Processed land cover data and helped with manuscript preparation.

**Gianelle D. (Research and Innovation Centre, S. Michele all'Adige):** Provided land cover data and helped with manuscript preparation.

**Hewitt C. N. (Lancaster University):** Helped with interpretation of results and manuscript preparation.

**Nemitz E. (Centre for Ecology & Hydrology):** Devised the research and helped with instrument setup, data analysis, interpretation of results and manuscript preparation.

# **Canopy-scale flux measurements and bottom-up emission estimates of volatile organic compounds from a mixed oak and hornbeam forest in northern Italy**

**Acton W. Joe F.** <sup>1</sup>, **Schallhart Simon** <sup>2</sup>, **Langford Ben** <sup>3</sup>, **Valach Amy** <sup>1,3</sup>,  
**Rantala Pekka** <sup>2</sup>, **Fares Silvano** <sup>4</sup>, **Carriero Giulia** <sup>5</sup>, **Tillmann Ralf** <sup>6</sup>,  
**Tomlinson Sam J.** <sup>3</sup>, **Dragosits Ulrike** <sup>3</sup>, **Gianelle Damiano** <sup>7,8</sup>, **Hewitt C. Nicholas** <sup>1</sup> and **Nemitz Eiko** <sup>3</sup>

[1] {Lancaster Environment Centre, Lancaster University, Lancaster, LA1 4YQ, United Kingdom}

[2] {Division of Atmospheric Sciences, Department of Physics, University of Helsinki, Gustaf Hällströmin katu 2, 00560 Helsinki, Finland}

[3] {Centre for Ecology & Hydrology, Bush Estate, Penicuik, Midlothian, EH26 0QB, United Kingdom}

[4] {Research Centre for Soil-Plant System, Council for Agricultural Research and Economics, Rome, Italy}

[5] {Institute for Plant Protection CNR Research Area - Building E, Via Madonna del Piano 10, 50019 Sesto Fiorentino, Italy}

[6] {Institute of Energy and Climate Research, IEK-8: Troposphere, Research Centre Jülich, 52425 Jülich, Germany}

[7] {Sustainable Agro-ecosystems and Bioresources Department, Research and Innovation Centre, Fondazione Edmund Mach, 38010 S. Michele all'Adige, Italy}

[8] {Foxlab Joint CNR-FEM Initiative, Via E. Mach 1, 38010 San Michele all'Adige, Italy}

Correspondence to: E. Nemitz (en@ceh.ac.uk)

## **Abstract**

This paper reports the fluxes and mixing ratios of biogenically emitted volatile organic compounds (BVOCs) 4 m above a mixed oak and hornbeam forest in northern Italy. Fluxes of methanol, acetaldehyde, isoprene, methyl vinyl ketone + methacrolein, methyl ethyl ketone and monoterpenes were obtained using both a proton transfer reaction-mass spectrometer (PTR-MS) and a proton transfer reaction-time of flight-mass spectrometer (PTR-ToF-MS) together with the methods of virtual disjunct eddy covariance (using PTR-MS) and eddy covariance ( using PTR-ToF-MS). Isoprene was the dominant emitted compound with a mean day-time flux of  $1.9 \text{ mg m}^{-2} \text{ h}^{-1}$ . Mixing ratios, recorded 4 m above the canopy, were dominated by methanol with a mean value of 6.2 ppbv over the 28 day measurement period. Comparison of isoprene fluxes calculated using the PTR-MS and PTR-ToF-MS showed very good agreement while comparison of the monoterpene fluxes suggested a slight over estimation of the flux by the PTR-MS. A basal isoprene emission rate for the forest of  $1.7 \text{ mg m}^{-2} \text{ h}^{-1}$  was calculated using the Model of Emissions of Gases and Aerosols from Nature (MEGAN) isoprene emissions algorithms (Guenther et al., 2006). A detailed tree species distribution map for the site enabled the leaf-level emissions of isoprene and monoterpenes recorded using Gas Chromatography-Mass Spectrometry (GC-MS) to be scaled up to produce a “bottom-up” canopy-scale flux. This was compared with the

“top-down” canopy-scale flux obtained by measurements. For monoterpenes, the two estimates were closely correlated and this correlation improved when the plant species composition in the individual flux footprint was taken into account. However, the bottom-up approach significantly underestimated the isoprene flux, compared with the top-down measurements, suggesting that the leaf-level measurements were not representative of actual emission rates.

## 6.1 Introduction

The term volatile organic compound (VOC) describes a broad range of chemical species emitted from natural and anthropogenic sources into the atmosphere. VOCs emitted from the biosphere are commonly termed biogenic VOCs (BVOCs). Of the BVOCs, isoprene is almost certainly the dominant species globally with an estimated annual emission of  $535\text{--}578 \times 10^{12}$  g C (Arneth et al., 2008; Guenther et al., 2012). Isoprene, along with larger terpenoids, are the BVOCs that have received the most attention in the literature to date. Although isoprene is the most commonly measured BVOC, global emission estimates of isoprene continue to differ and there are still large uncertainties associated with the emission estimates of many other compounds. For example, annual monoterpene emission estimates vary between  $32 \times 10^{12}$  and  $127 \times 10^{12}$  g C (Arneth et al., 2008). A better understanding of how emissions change with land cover, temperature, soil moisture and solar radiation is required to constrain model descriptions of the effects of BVOCs on atmospheric chemistry in the past, present and future (Monks et al., 2009).

BVOCs are a major source of reactive carbon into the atmosphere and as such exert an influence on both climate and local air quality. BVOCs are oxidised primarily by the

hydroxyl radical (OH), itself formed by the photolysis of ozone, to form peroxide radicals (RO<sub>2</sub>). In the presence of NO<sub>x</sub> (NO and NO<sub>2</sub>) these RO<sub>2</sub> radicals can oxidise NO to NO<sub>2</sub>, which may undergo photodissociation leading to the net formation of tropospheric ozone (Fehsenfeld et al., 1992). Tropospheric ozone can then impact human health, forest productivity and crop yields (Royal Society 2008; Ashmore 2005). In addition, BVOC species contribute significantly to the formation of secondary organic aerosol (SOA) in the atmosphere. This affects climate both directly and indirectly by the scattering of solar radiation and by acting as cloud condensation nuclei. The formation of cloud condensation nuclei leads to increased cloud cover and therefore an altering of the Earth's albedo (Hallquist et al., 2009).

The Bosco Fontana campaign was carried out as a part of the ÉCLAIRE (Effects of Climate Change on Air Pollution and Response Strategies for European Ecosystems) EC FP7 project to study the surface/atmosphere exchange within a semi-natural forest situated within one of the most polluted regions in Europe, and its interaction with air chemistry. During the Bosco Fontana campaign, VOC fluxes and mixing ratios were measured 4 m above the canopy of a semi-natural forest situated in the Po Valley, northern Italy (45° 11' 51" N, 10° 44' 31" E), during June and July 2012. The Po Valley experiences high levels of anthropogenic pollution caused by its proximity to the city of Milan's high levels of industrial and traffic-related emissions of pollutants, intensive agriculture and periods of stagnant air flow caused by the Alps to the north and west and the Apennines to the south (Bigi et al., 2011; Decesari et al., 2014).

In order to make accurate air quality predictions, precise regional and global models of BVOC emission are necessary. The modelling of BVOC emissions at regional and

global scales is generally dependent upon species specific emission factors for the BVOCs of interest (Guenther et al., 2006; Steinbrecher et al., 2009). These emission factors are usually determined by the measurement of BVOC emission at a leaf level and at standard conditions (generally a leaf temperature of 30 °C and 1000  $\mu\text{mol m}^{-2} \text{s}^{-1}$  PAR). It is, however, important that leaf level BVOC emission factors accurately represent canopy scale emissions. Here we report the fluxes and mixing ratios of a range of BVOCs recorded from mixed mesophile forest at the Bosco Fontana field site. We compare BVOC flux calculation from above canopy eddy covariance measurements using both a proton transfer reaction-mass spectrometer (PTR-MS) and a proton transfer reaction-time of flight-mass spectrometer (PTR-ToF-MS) with isoprene and monoterpene fluxes obtained by scaling up leaf-level emission factors using the Model of Emissions of Gases and Aerosols from Nature (MEGAN) to produce a canopy-scale “bottom-up” modelled flux estimate. We further explore the potential of accounting for the spatial tree species distribution for improving the comparison between top-down and bottom-up approaches, in what we believe is the first approach of its type.

## **6.2 Methods**

### **6.2.1 Site description**

Measurements were taken at a site within the Bosco Fontana natural reserve (45° 11' 51" N, 10° 44' 31" E), a 233 ha area of semi-natural woodland situated in the municipality of Marmirolo in the Po Valley. The forest canopy had an average height of approximately 28 m and was principally comprised of *Carpinus betulus* (hornbeam) and three oak species *Quercus robur* (pedunculate oak), *Quercus cerris*

(turkey oak) and the introduced *Quercus rubra* (northern red oak) (Dalponte et al., 2007). In the centre of the forest there was a cleared area containing a seventeenth century hunting lodge surrounded by hay meadows. The surrounding area was predominantly arable farm land with some pastures to the north and west and a reservoir to the north-west. The city of Mantova lies approximately 5 km to the south east, with the small towns of Marmirolo, Soave and Sant'Antonio approximately 2 km north, 1 km west and 3 km east, respectively. A 42 m measurement tower was situated near the centre of the forest to the south west of the central hay meadows. The measurement tower was ca.760 m from the edge of the forest in the direction of the easterly wind direction that dominated during this measurement period.

### **6.2.2 PTR-MS and PTR-ToF-MS setup and measurement procedure**

In order to record BVOC fluxes and concentrations, both a high sensitivity PTR-MS (Ionicon Analytik GmbH, Innsbruck, described in detail by Blake et al., 2009; de Gouw and Warneke 2007; Hansel et al., 1995; Lindinger et al., 1998b) and a high resolution PTR-ToF-MS (Ionicon Analytik GmbH, Innsbruck, as described by Graus et al., 2010; Jordan et al., 2009) were used, together with a sonic anemometer (Gill HS, Gill Instruments Ltd, UK). The PTR-MS was equipped with a quadrupole mass analyser and three turbo molecular pumps (Varian). The Silcosteel inlet and internal tubing were heated to avoid condensation of BVOCs onto internal surfaces. The application of PTR-MS to atmospheric measurements has previously been described by Hewitt et al. (2003) and Hayward et al. (2002).

The sonic anemometer was situated 32 m above the ground on the north-west corner of the tower. This measurement height was chosen due to the fetch restrictions. Fluxes

of sensible heat and momentum were compared with a flux measurement at the top of the tower (42 m) and were on average 15% larger for sensible heat and 5% for momentum (Finco et al., in preparation). It is unclear whether this reflects differences in fetch, instrumentation or the effect of measuring within the surface roughness layer, but it is possible that fluxes reported here are slightly overestimated for this reason. The angle-of-attack was uncorrelated with wind direction suggesting that there was no local influence on the wind flow. Both the PTR-MS and the PTR-ToF-MS were housed in an air-conditioned cabin at the base of the tower. The PTR-MS sub-sampled via a ca. 10 cm, 1/8 inch (O.D.) PTFE tube (I.D.: 1 mm, flow rate: 300 ml min<sup>-1</sup>, residence time: 0.04 s and with a Reynolds number inside the tube of ca. 258, indicating laminar flow but the very short residence time means that this does not provide the limiting factor for the overall response time of the measurement system) from a 1/2 inch O.D. PTFE common inlet line (I.D. 3/8 inch), heated to avoid condensation, which led from ca. 10 cm below the sonic anemometer to the cabin. Solenoid valves were used to switch between the sample line and zero air which was generated by passing ambient air through a glass tube packed with platinum catalyst powder heated to 200°C. The PTR-ToF-MS subsampled via a 3-way valve from the common inlet line; 0.5 L min<sup>-1</sup> was pumped through a 1/8 inch (O.D.) and 1/16 inch (O.D.) capillary (together ca. 20 cm long), with 30 ml min<sup>-1</sup> entering the instrument and the remaining flow being sent to an exhaust. The common inlet line had a flow rate of ca. 63 L min<sup>-1</sup>, giving a Reynolds number of ca. 9700 which indicates a turbulent flow. There was no observable influence of the high flow rate on readings from the sonic anemometer, even during periods of relatively low turbulence. Data from both the PTR-MS and the sonic anemometer were logged onto a laptop using a program written in LabVIEW (National Instruments, Austin, Texas, USA).

The PTR-MS was operated continuously throughout the measurement campaign with interruptions for the tuning of the instrument and refilling of the water reservoir. PTR-MS settings were controlled so that the reduced electric field strength ( $E/N$ , where  $E$  is the electric field strength and  $N$  the buffer gas density) was held at 122 Td ( $1.22 \times 10^{19} \text{ V m}^{-2}$ ), with drift tube pressure, temperature and voltage maintained at 2.1 mbar, 45 °C and 550 V respectively. The primary ions and the first water cluster were quantified indirectly from the isotope peaks at  $m/z$  21 ( $\text{H}_2^{18}\text{O}^+$ ) and  $m/z$  39 ( $\text{H}_2^{18}\text{O}.\text{H}_2\text{O}^+$ ), respectively. The inferred count rate of  $\text{H}_3\text{O}^+$  ions over the course of the campaign varied between  $1.33 \times 10^6$  and  $9.00 \times 10^6 \text{ counts s}^{-1}$ .  $\text{O}_2^+$  ( $m/z$  32) was kept below 1 % of the primary ion count throughout the campaign in order to limit ionisation of VOCs through charge transfer reactions with  $\text{O}_2^+$  and minimise the contribution of the  $\text{O}_2^+$  isotope ( $^{16}\text{O}^{17}\text{O}^+$ ) to  $m/z$  33.

During PTR-ToF-MS operation the drift tube temperature was held at 60°C with 600 V applied across it. The drift tube pressure was 2.3 mbar resulting in an  $E/N$  of 130 Td. A more detailed description of the PTR-ToF-MS operation is provided by Schallhart et al. (2015).

The PTR-MS was operated in three modes: the instrument measured zero air for 5 min, followed by 25 min in flux mode, 5 min in scan mode and then a final 25 min in flux mode. While in flux mode, 11 protonated masses were monitored sequentially:  $m/z$  21 the hydronium ion isotope,  $m/z$  39 a water cluster isotope and 9 masses relating to VOCs:  $m/z$  33, 45, 59, 61, 69, 71, 73, 81 and 137. The mass spectral peaks at  $m/z$  21 and 39 were analysed with a 0.2 s dwell time ( $\tau$ ). For the nine VOC species  $\tau = 0.5 \text{ s}$

was used in order to increase the instrumental sensitivity to these masses. This gave a total scan time of 4.9 s and the acquisition of ca. 306 data points in each 25 min averaging period. The response time for this instrument, assessed during previous studies and laboratory tests, is ca. 0.5 s, and dwell times were chosen to match this time in order to minimise overall duty cycle loss due to  $m/z$  switching. The uncertainty caused by disjunct sampling was calculated and found to cause a 0.17 % error in the flux estimation (see Supplementary Information for details).

Identification of the compounds observed at each of these masses is complicated by the fact that PTR-MS only allows the identification of nominal masses, therefore it is impossible to distinguish between isobaric compounds. As such there may be more than one compound contributing to each of the measured masses; Table 6.1 displays the masses monitored and the compounds likely to be contributing to each mass together with the exact masses observed at each unit mass using the PTR-ToF-MS which has much greater mass resolution than does the quadrupole PTR-MS instrument. It was assumed that the dominant contributions at  $m/z$  33, 45, 59, 61, 69, 71, 73, 81 and 137 were from protonated methanol, acetaldehyde (ethanal), acetone (propanone), acetic acid (ethanoic acid), isoprene (2-methyl-1,3-butadiene), methyl vinyl ketone (MVK, butenone) and methacrolein (MACR, 2-methylprop-2-enal), methyl ethyl ketone (MEK, butanone), a monoterpene mass spectral fragment and monoterpenes respectively. A further contribution to  $m/z$  71, recently identified, are isoprene hydroxy hydroperoxides (ISOPOOH, Rivera-Rios et al., 2014). However, the concentrations of this intermediate are small if  $\text{NO}_x$  concentrations are high and therefore are likely to be negligible at this site, where  $\text{NO}_x$  concentrations were large (Finco et al., in preparation).

### 6.2.2.1 PTR-MS calibration

The PTR-MS was calibrated using a gas standard (Ionicon Analytic GmbH, Innsbruck) containing 17 VOCs at a mixing ratio by volume of approximately  $1 \times 10^{-6}$  (ca. 1 ppmv). The protonated mass of the VOCs ranged from  $m/z$  31 (formaldehyde,  $\text{CH}_3\text{O}^+$ ) to  $m/z$  181 (1,2,4-trichlorobenzene,  $\text{C}_6\text{H}_4\text{Cl}_3^+$ ). Methanol ( $m/z$  33), acetaldehyde ( $m/z$  45), acetone ( $m/z$  59), isoprene ( $m/z$  69), MEK ( $m/z$  73) and the monoterpene  $\alpha$ -pinene ( $m/z$  81 and  $m/z$  137) were present in the calibration gas standard, allowing sensitivities to be calculated directly. Due to reduced quadrupole transmission for high masses, monoterpenes were quantified using the fragment ion at  $m/z$  81. For compounds not contained in the gas standard (acetic acid ( $m/z$  61) and MVK and MACR ( $m/z$  71)) empirical sensitivities were calculated. A relative transmission curve was created using the instrumental sensitivities calculated from the masses present in the standard, and from this curve sensitivities for the unknown masses were calculated (Davison et al., 2009; Taipale et al., 2008). Error in calibration using the gas standard was assumed to be below 15 %, whereas relative errors in calibrations using the relative transmission approach are  $< 30$  % (Taipale et al., 2008). The change in instrumental sensitivity from before the campaign to the end of the campaign was +1.9, -2, -2.1, -0.3 and -0.7 ncps ppbv<sup>-1</sup> for methanol, acetaldehyde, acetone, isoprene and methyl ethyl ketone respectively.

Table 6.1, Unit masses measured using the PTR-MS during the ÉCLAIRE campaign at Bosco Fontana and the exact masses observed using the PTR-ToF-MS. Where the PTR-MS sensitivity was calculated directly from a compound in the calibration standard this compound is indicated in brackets. At  $m/z$  61 and 71 the sensitivity was calculated from a transmission curve.

Unit mass (PTR-MS)	Exact mass (PTR-ToF-MS)	Contributing compound(s)	Formula	PTR-MS sensitivity (ncps ppbv <sup>-1</sup> )
21	21.023	Water isotope	H <sub>3</sub> <sup>18</sup> O <sup>+</sup>	-
33	32.997	Oxygen isotope	O <sup>17</sup> O <sup>+</sup>	11.60 (methanol)
	33.033	Methanol	CH <sub>5</sub> O <sup>+</sup>	
39	39.033	Water cluster	H <sub>5</sub> O <sup>18</sup> O <sup>+</sup>	-
	44.997	Protonated carbon		
45	45.033	dioxide	C <sub>1</sub> H <sub>1</sub> O <sub>2</sub> <sup>+</sup>	9.90 (acetaldehyde)
		Acetaldehyde	C <sub>2</sub> H <sub>5</sub> O <sup>+</sup>	
59	59.049	Acetone	C <sub>3</sub> H <sub>7</sub> O <sup>+</sup>	8.82 (acetone)
	59.049	Propanal	C <sub>3</sub> H <sub>7</sub> O <sup>+</sup>	
61	61.028	Acetic acid	C <sub>2</sub> H <sub>5</sub> O <sub>2</sub>	8.40 (transmission curve)
	69.0699	Isoprene	C <sub>5</sub> H <sub>9</sub> <sup>+</sup>	
	69.0699	2-Methyl-3-buten-2-ol	C <sub>5</sub> H <sub>9</sub> <sup>+</sup>	
	69.0699	fragment	C <sub>5</sub> H <sub>9</sub> <sup>+</sup>	
69	69.0699	Methyl butanal	C <sub>5</sub> H <sub>9</sub> <sup>+</sup>	3.80 (isoprene)
		fragment		
71	71.049	Methyl vinyl ketone	C <sub>4</sub> H <sub>7</sub> O <sup>+</sup>	5.29 (transmission curve)
	71.049	Methacrolein	C <sub>4</sub> H <sub>7</sub> O <sup>+</sup>	
	71.085	Unknown	C <sub>5</sub> H <sub>11</sub> <sup>+</sup>	
	73.026	Unknown	C <sub>3</sub> H <sub>5</sub> O <sub>2</sub> <sup>+</sup>	
73	73.047	Unknown	Unknown	5.87 (Methyl ethyl ketone)
	73.065	Methyl ethyl ketone	C <sub>4</sub> H <sub>9</sub> O <sup>+</sup>	
	73.065	Butanal	C <sub>4</sub> H <sub>9</sub> O <sup>+</sup>	
	80.997	Unknown	C <sub>4</sub> H <sub>1</sub> O <sub>2</sub> <sup>+</sup>	
81	81.033	Unknown	C <sub>5</sub> H <sub>5</sub> O <sup>+</sup>	1.59 ( $\alpha$ -pinene fragment)
	81.070	Monoterpene fragment	C <sub>6</sub> H <sub>9</sub> <sup>+</sup>	
	81.070	Hexenal fragment	C <sub>6</sub> H <sub>9</sub> <sup>+</sup>	
137	137.056	Unknown	Unknown	0.16 ( $\alpha$ -pinene)
	137.133	Monoterpenes	C <sub>10</sub> H <sub>17</sub> <sup>+</sup>	

### 6.2.2.2 PTR-ToF-MS calibration

Background measurements of the PTR-ToF-MS were made up to three times a day using zero air generated by a custom made catalytic converter. Calibrations were made using a calibration gas (Appel Riemer Environmental Inc., USA) which contained 16 compounds, with masses ranging from 33 to 180 amu. For VOCs not included in the calibration standard, the average instrument sensitivities towards the known  $C_xH_y$ ,  $C_xH_yO_z$  or  $C_xH_yN_z$  compound families were used.

### 6.2.3 Calculation of volume mixing ratios

Mixing ratios by volume were calculated from data generated using the PTR-MS using a program written in LabVIEW (National Instruments, Austin, Texas, USA). Mixing ratios by volume ( $\chi_{VOC}$ ) were calculated from the raw PTR-MS data (in counts per second (cps)) using a method based on those of Taipale et al. (2008) and Tani et al. (2004).

$$\chi_{VOC} = \frac{I(RH^+)_{norm}}{S_{norm}} \quad (1)$$

where  $S_{norm}$  is the normalised sensitivity and  $I(RH^+)_{norm}$  represents the background corrected normalised count rate (ncps) for the protonated compound  $R$  which was calculated as shown below.

$$I(RH^+)_{norm} = I(RH^+) \left( \frac{I_{norm}}{I(H_3O^+) + I(H_3O^+H_2O)} \right) \left( \frac{p_{norm}}{p_{drift}} \right)$$

$$- \frac{1}{n} \sum_{i=1}^n I(RH^+)_{zero,i} \left( \frac{I_{norm}}{I(H_3O^+)_{zero,i} + I(H_3O^+H_2O)_{zero,i}} \right) \left( \frac{p_{norm}}{p_{drift,zero,i}} \right) \quad (2)$$

where  $I(RH^+)$ ,  $I(H_3O^+)$  and  $I(H_3O^+H_2O)$  represent the observed count rate for the protonated compound  $R$ ,  $H_3O^+$  and the  $H_3O^+H_2O$  cluster, respectively. Subscript zero refers to zero air measurements,  $n$  is the number of zero air measurement cycles and  $p_{drift}$  is the drift tube pressure. The drift tube pressure was normalised to 2 mbar ( $p_{norm}$ ) and the sum of the primary ion and first water cluster was normalised to a count rate of  $10^6$  cps ( $I_{norm}$ ). The compound specific limit of detection (LoD) was calculated using the method described by Karl et al. (2003):

$$LoD = 2 \times \frac{\sigma_{Background}}{S_{VOC}} \quad (3)$$

where  $S_{VOC}$  is the instrumental sensitivity to the VOC and  $\sigma_{Background}$  is the mean background normalised count rate.

#### 6.2.4 Flux calculations from PTR-MS

The 25 min PTR-MS flux files were inspected and incomplete or disrupted files were removed. BVOC fluxes were then calculated using a program also written in LabVIEW, based upon the virtual disjunct eddy covariance technique (vDEC) developed by Karl et al. (2002), also termed continuous flow disjunct eddy covariance (Rinne et al., 2008). This method has been successfully applied in a number of studies (e.g. Davison et al., 2009; Langford et al., 2009; 2010a; 2010b; Misztal et al., 2011;

Rinne et al. 2007). This approach allows direct calculation of fluxes of atmospheric constituents, as with standard eddy covariance, yet in this case sampling of scalar concentrations is not continuous. The flux,  $F_x$ , for each compound was calculated using a covariance function between the vertical wind velocity,  $w$ , and the VOC mixing ratios,  $\chi$ :

$$F_x(\Delta t) = \frac{1}{N} \sum_{i=1}^N w'(i - \Delta t / \Delta t_w) \chi'(i) \quad (4)$$

where  $\Delta t$  is the lag time between the PTR-MS concentration measurements and the vertical wind velocity measurements from a sonic anemometer,  $\Delta t_w$  is the sampling interval between wind measurements (0.1 s),  $N$  is the number of PTR-MS measurement cycles in each 25 min averaging period (typically 306 in our study) and primes represent the momentary deviations from the mean concentration or vertical wind speed (e.g.  $w = w' - \bar{w}$ ).

Variations in temperature, pressure and the performance of the sample line pump can cause small deviations in  $\Delta t$ . Therefore these values were calculated using a cross correlation function between  $w'$  and  $\chi'$ . Lag times were calculated individually for each  $m/z$  monitored by the PTR-MS by selecting the absolute maximum value of the covariance function within a 30 s time window (MAX method, Taipale et al., 2010). This analysis resulted in a clear isoprene flux but for most masses a high proportion of the data fell below the limit of detection. These data, especially in the case of acetone, showed a significant amount of flux values with the opposite sign, “mirroring” the true flux. These “mirrored” points occur when the measured flux is of comparable magnitude to the total random error of the system (Langford et al., 2015). As the

cross-correlation maximum is likely to be an over-estimate when the noise to signal ratio is greater than one, these points were substituted with fluxes calculated using a fixed lag time.

A histogram of isoprene lag times calculated using the MAX method is displayed in the Supplementary Information showing a clear maximum at 7.5 s. Therefore 7.5 s was chosen as the isoprene fixed lag time and fixed lag times for the other masses were calculated from the isoprene fixed lag time, accounting for the dwell times of the different compounds in the measurement cycle.

#### **6.2.4.1 Flux quality assessment and potential losses**

In order to assess the quality of each 25 min flux file, the resultant fluxes were subjected to three quality checks following a two-dimensional coordinate rotation which was applied to correct for tilting of the sonic anemometer (see Table 6.7 in the Supplementary Information document for summary). Following the criteria of Langford et al. (2010a), data points were labelled if the mean friction velocity ( $u_*$ ) over the 25 min averaging period was found to be below  $0.15 \text{ m s}^{-1}$ . Data falling below this threshold predominantly occurred at night when wind velocity reached a minimum. Detection limits for each 25 min flux file were calculated using a method based on that of Wienhold et al. (1994) as applied by Spirig et al. (2005) where the signal of the flux at the true lag is compared to the background noise of the covariance function. The 95<sup>th</sup> percentile of the covariance function in the lag range 150-180 s was calculated and flux files falling below this value were labelled as having fallen below the LoD. Finally data points underwent a stationarity test as described by Foken and Wichura (1996), which assessed that stability of the flux across the 25 min averaging

period, data points found to be generated from periods of non-stationarity were also labelled. Flux files in which all three tests were passed and where only the LoD test was failed were included in all further analysis. Files which failed the LoD test were included to prevent a positive bias being introduced to results. Flux files failing the stationarity check or falling below the  $u_*$  threshold were excluded from further analysis.

The integral turbulence characteristics were assessed using the FLUXNET criteria described by Foken et al. (2004). The turbulence at the Bosco Fontana field site was well developed with 87% of the data in the first three categories, defined by Foken et al. (2004) as suitable for fundamental research. Less than 1% of the data fell into category 9, characterised as data to be excluded under all circumstances.

The flux losses in the virtual disjunct eddy covariance system were assessed. Loss of flux at frequencies higher than the PTR-MS response time and/or dwell time was corrected for using the method described by Horst (1997). Correction factors in the range 1.01 - 1.23 were calculated and applied to each 25 min flux file with a mean correction of 8.8 %. Rotating the coordinates in order to set the vertical mean vertical wind velocity to 0 for each twenty five minute flux averaging period and block averaging itself act as a high pass flux filter (Moncrieff et al., 2004), leading to the loss of low frequency fluxes. The loss of these low frequency fluxes due to an insufficient averaging period is assessed in the Supplementary Information. Sensible heat flux data were averaged over 50, 75, 100 and 125 minutes before a coordinate rotation was applied and plotted against the sum of two, three, four and five 25 minute coordinate rotated flux files, respectively. The gradient of the fitted line between the

two fluxes gives an estimate of the flux lost by the use of twenty five minute averaging periods. As is shown in Fig. 6.13 of the Supplementary Information, eddies with a time period between 25 and 125 minutes carry only an additional 2.8 % of the sensible heat flux. Therefore if we assume that the frequency of VOC and sensible heat fluxes are comparable, 1.0-3.6 % of the VOC flux is lost by limiting the averaging period to 25 minutes. This correction has not been applied to the displayed data as it is so small.

The effect of the measurement tower (situated to the south-east of the sonic anemometer) on flux measurements was assessed in two ways. Firstly, the vertical rotation angle ( $\theta$ ) used to realign the anemometer to achieve zero average  $w$  was plotted against wind direction (Fig 6.15 in Supplementary Information). No change in  $\theta$  was observed when the wind came from the south east, demonstrating that the tower did not affect  $\theta$ . Secondly, the potential of wake turbulence created by the tower was assessed using the method developed by Foken (2004). The quality of the turbulence within each flux averaging period was assessed by calculating the percentage difference between the measured integral turbulence statistics of the vertical wind velocity and values modelled for an ideal set of conditions. Plotting the percentage difference between the measured and modelled values against wind direction (Fig 6.15 in Supplementary Information) showed that the tower had little effect on this percentage difference and thus on flux measurements (for a more detailed discussion, see Supplementary Information). Therefore, flux averaging periods during which the wind was coming from the south-east were not systematically excluded from further analysis.

The percentage of flux averaging periods during which > 25 % of the flux originated from outside the forest area was also assessed by footprint analysis and found to account for 26 % of the data set. As the flux footprint moves with atmospheric stability, fluxes from outside the forest predominantly occurred during night-time conditions when emission rates were very small. Therefore it was not deemed necessary to specifically remove these data prior to further bulk analysis of the dataset, although it is recognised that the  $u_*$  filter criterion removed many of these measurements. A more detailed analysis of the effect of the tree species composition within the footprint on measured and modelled fluxes is presented below.

### **6.2.5 Flux calculations from PTR-ToF-MS**

BVOC fluxes were calculated from PTR-ToF-MS data using the eddy covariance (EC) method similar to that described above for the PTR-MS. The PTR-ToF-MS flux analysis differed in that the cross correlation between  $w'$  and  $\chi'$  was calculated using the method described by Park et al. (2013). Whilst in the PTR-MS measurement, the target compounds are predetermined through the measurement cycle, in the PTR-ToF-MS the entire high resolution mass spectrum can be used to search for compounds that carry a flux. PTR-ToF-MS data were analysed using the TOF Analyzer V2.45 as described by Müller et al. (2013) and TofTools (Junninen et al., 2010). An automated flux identification routine was then used to calculate the average of the absolute cross covariance functions during a mid-day period. The maximum value was then automatically selected from the averaged spectrum and checked against the manually selected noise level ( $10 \sigma_{noise}$ ) to determine whether a flux was present.

The fluxes were filtered using the 70% stationary criteria as presented by Foken and Wichura (1996), as was applied to the PTR-MS data and corrected for loss of high

frequency flux Horst (1997). For a more detailed description of the flux calculation from the PTR-ToF-MS see Schallhart et al. (2015).

### **6.2.6 Leaf level GC-MS measurements**

A portable gas exchange system equipped with a controlled-environment 6-cm<sup>2</sup> broadleaf cuvette (LI6400, Li-COR, Lincoln, USA) was used to measure net photosynthetic rate ( $A$ ) and stomatal conductance ( $g_s$ ) at basal conditions of PAR (1000  $\mu\text{mol m}^{-2} \text{s}^{-1}$ ), leaf temperature (30 °C) and a CO<sub>2</sub> concentration (400 ppm) from fully expanded leaves. These conditions were comparable to those observed during the campaign where the average day time temperature was 29 °C. While the cuvette is capable of reproducing ambient light and temperature conditions, unstable environmental conditions below the canopy make it difficult to achieve steady state fluxes. BVOC emission was therefore recorded at basal conditions, to ensure that steady state fluxes could be obtained and to enable comparison between different individual measurements. When  $A$  reached a steady-state, the outlet tube from the leaf cuvette was replaced with a Teflon tube, and the air stream exiting from the cuvette was used to sample BVOCs (according to the methodology in Loreto et al., 2001) by adsorbing them onto a silco-steel cartridge packed with 200 mg of tenax (Supelco, PA, USA). Tenax is a very hydrophobic and adsorbent material with high thermal stability generally used for trapping BVOC (Dettmer and Engewald, 2002). The flow rate through the leaf cuvette was maintained at 500  $\mu\text{mol s}^{-1}$ , and a subsample of 200 mL min<sup>-1</sup> (130  $\mu\text{mol s}^{-1}$ ) was pumped through the cartridge with an external pump (AP Buck pump VSS-1) for a total volume of 6 L of air. Blank samples of air without a leaf in the cuvette were collected every day before and after the BVOC samplings. Finally the cartridges were sealed and stored at 4 °C until analysis.

The cartridges were analyzed using a Perkin Elmer Clarus 580 gas-chromatograph coupled with a Clarus 560 Mass-Detector and a thermal-desorber Turbo Matrix (Perkin Elmer Inc., Waltham, MA, USA). The gas-chromatograph was equipped with an Elite-5-MS capillary column (30 m length, 250  $\mu\text{m}$  diameter and 0.25  $\mu\text{m}$  film thicknesses). The carrier gas was helium. The column oven temperature was kept at 40  $^{\circ}\text{C}$  for 5 min, then increased with a 5  $^{\circ}\text{C min}^{-1}$  ramp to 250  $^{\circ}\text{C}$  and maintained at 250  $^{\circ}\text{C}$  for 5 min. BVOC were identified using the National Institute of Standards and Technology (NIST) library provided with the GC-MS Turbomass software. GC peak retention time was substantiated by analysis of parent ions and main fragments of the spectra. Commercially available reference standards (gaseous standards, Rivoira, Milan, Italy and liquid standards, Sigma Aldrich, Milan, Italy) were used to create the calibration curves and to quantify the emissions. To normalize the BVOC results, the quantities of terpenes collected from the empty cuvette (blanks) were subtracted from the plant emission results.

### **6.2.7 Mapping tree species distribution**

Tree species distribution data were obtained from Dalponte et al. (2007) who used a combination of Light Detection and Ranging (LIDAR) and hyperspectral data to develop a high resolution tree species distribution map of the Bosco Fontana natural reserve.

The overall accuracy (kappa coefficient) of this species map is particularly high (0.89), considering the number of classes (23) and the number of training samples (20% of the data are used in the training set and 80% in the test set) per class. The

LIDAR channels provide relatively sparse information for discriminating between tree species, increasing the overall accuracy of the tree species assignment using the hyperspectral data by only 1 % but the LIDAR data significantly increase the accuracy of understory and underrepresented classes. The kappa coefficient of the main species is also very high (0.88-0.93) showing the effectiveness of this approach for species classification in a very complex forest with 20 different broad-leaves species, some of which, such as *Q. cerris*, *Q. robur* and *Q. rubra*, belong to same genus. For a more detailed discussion of the mapping results and methodology see Dalponte et al. (2007) and Dalponte et al. (2008).

### **6.3 Results and discussion**

#### **6.3.1 Meteorological conditions**

The measurement campaign at Bosco Fontana ran from 01/06/2012 to 11/07/2012 (41 days) with data recorded using the PTR-MS from the 13/06/2012 to the 11/07/2012. The meteorological conditions recorded at the measurement site during this period are summarised in Fig. 6.1, times are reported in central European time (UTC + 1) as used throughout this paper. The campaign average flux footprint is displayed in Fig. 6.2. With the exception of two heavy thunderstorms, the first in the first week of June before measurements began and the second overnight on 6<sup>th</sup> July, there was no precipitation during the measurement period. During the measurement period ambient temperature varied from a low of 14 °C to a high of 35 °C, with temperatures lowest early in the campaign. Daily photosynthetically active radiation (PAR) peaked within the range 1890-2105  $\mu\text{mol m}^{-2} \text{s}^{-1}$  and the relative humidity during the campaign varied between 29 and 90 %. Winds were generally easterly or north westerly. For

most of the campaign wind speeds were below  $3.5 \text{ m s}^{-1}$  but peaked at  $5.6 \text{ m s}^{-1}$  on 23<sup>rd</sup> June, with the mean wind speed for the campaign period of  $1.6 \text{ m s}^{-1}$ .

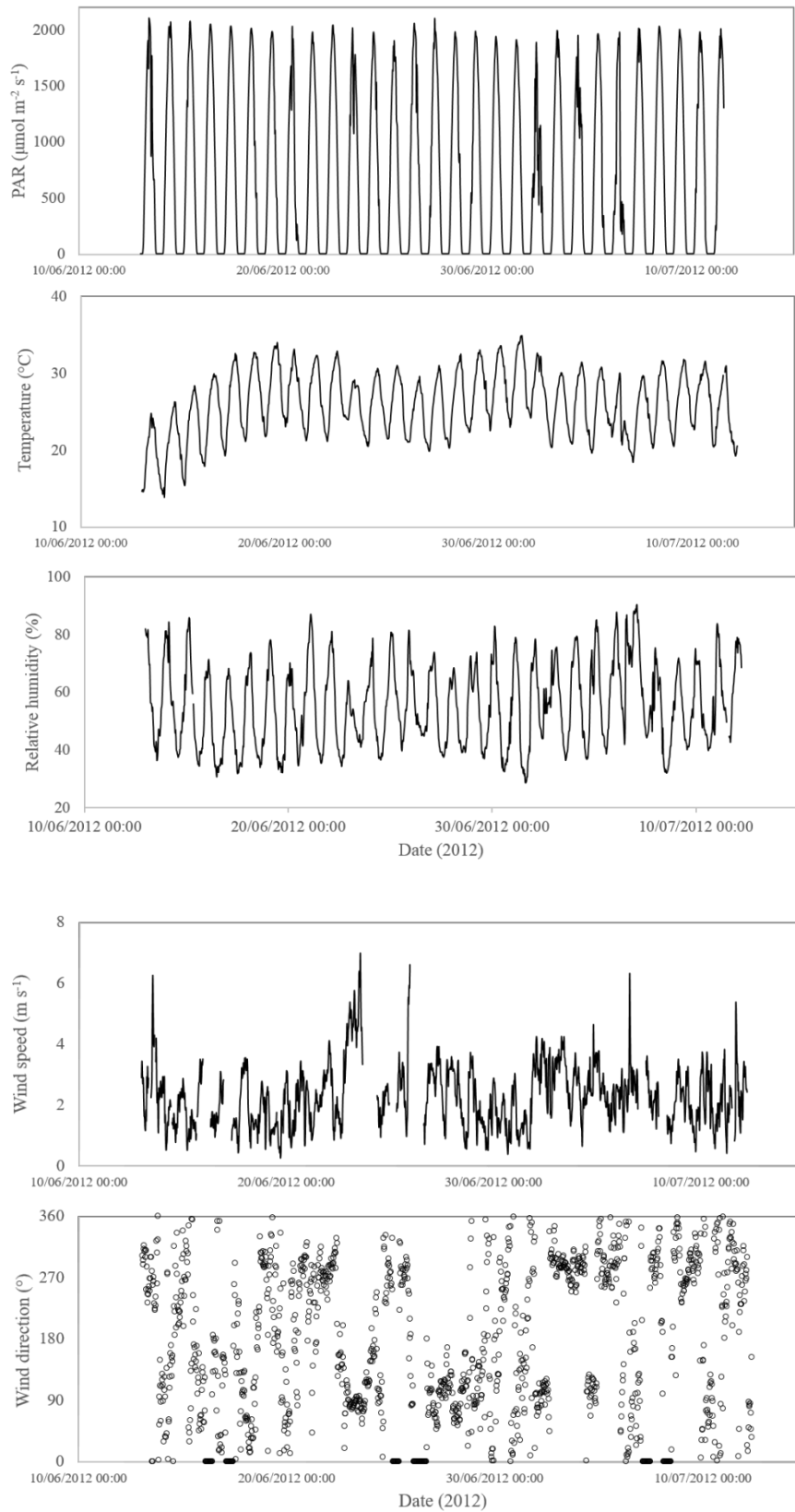


Figure 6.1, Time series of meteorological conditions recorded over the campaign period. From top to bottom: PAR ( $\mu\text{mol m}^{-2} \text{s}^{-1}$ ), air temperature ( $^{\circ}\text{C}$ ), relative humidity (%), wind speed ( $\text{m s}^{-1}$ ) and wind direction ( $^{\circ}$ ).



Figure 6.2, Satellite image (map data © Google 2016) of the field site showing the flux tower and footprint containing 80 % of the flux measured during the campaign (13/06/2012 – 11/07/2012).

### 6.3.2 BVOC mixing ratios and fluxes

BVOC fluxes were recorded at the Bosco Fontana site using both the PTR-MS and the PTR-ToF-MS. Unless stated, the results displayed here were calculated from measurements made using the PTR-MS. Data analysis was carried out with the aid of the R openair package (Carslaw and Ropkins, 2012; R Core Team 2012). For a full discussion of all fluxes and concentrations recorded using the PTR-ToF-MS see Schallhart et al. (2015).

The mixing ratios of the eight BVOC species measured in flux mode using the PTR-MS are displayed in Fig. 6.3 and are summarised in Table 6.2 (for further details, see Fig. 6.17 of the Supplementary Information). These mixing ratios were calculated using the high frequency flux measurements so the presented mixing ratios are an average over 25 minutes. The mixing ratio LoDs, calculated as described above (Karl et al., 2003; Langford et al., 2009; Misztal et al., 2011) were in the same range as those calculated on previous campaigns (Langford et al., 2009; Misztal et al., 2011) and, with the exception of isoprene where the mixing ratio dropped towards zero at night, the recorded mixing ratios generally remained above their respective LoD.

Table 6.2. Summary of the bVOC mixing ratios (ppbv) recorded at 4 m above the forest canopy during the Bosco Fontana measurement campaign and limits of detection (LoD, ppbv), based on 25-minute averages.

<i>m/z</i>	33	45	59	61	69	71	73	81
Compound	Methanol	Acetaldehyde	Acetone	Acetic acid	Isoprene	MVK+MACR	MEK	Monoterpenes
Max	14.6	3.44	7.31	14.9	4.79	1.95	1.05	0.419
Min	2.13	< LOD	1.18	0.396	< LOD	0.083	0.097	< LOD
Mean	6.16	1.46	3.24	1.92	1.07	0.506	0.454	0.198
Standard deviation	2.52	0.67	0.91	1.09	0.80	0.28	0.21	0.07
Median	5.69	1.30	3.14	1.73	0.934	0.506	0.428	0.199
1 <sup>st</sup> Quartile	4.19	0.964	2.68	1.22	0.409	0.325	0.311	0.140
3 <sup>rd</sup> Quartile	7.53	1.87	3.82	2.31	1.53	1.95	0.568	0.245
LOD	0.436	0.712	0.239	0.141	0.167	0.081	0.048	0.067

Table 6.3. Summary of the bVOC fluxes ( $\text{mg m}^{-2} \text{h}^{-1}$ ) recorded during the Bosco Fontana field campaign based on 25-minute values. Values in brackets cover the campaign period where data is available from both instruments to enable direct comparison (15/06-06/07/2012 and 15/06-25/06/2012 for isoprene and monoterpenes, respectively).

<i>m/z</i>	33	45	59	61	69	71	73	81		
Compound	Methanol	Acetaldehyde	Acetone	Acetic acid	Isoprene PTR-MS	Isoprene PTR-ToF-MS	MVK + MACR	MEK	Monoterpenes PTR-MS	Monoterpenes PTR-ToF-MS
Max emission flux	0.492	0.436	0.585	0.328	9.867 (9.867)	9.195 (9.195)	0.641	0.181	0.478 (0.478)	0.609 (0.603)
Max deposition flux	-1.589	-0.335	-0.692	-0.876	-0.238 (-0.238)	-0.305 (-0.305)	-0.457	-0.128	-0.167 (-0.167)	-0.065 (-0.057)
1 <sup>st</sup> Quartile	-0.032	-0.011	-0.029	-0.044	0.005 (0.005)	0.019 (0.019)	-0.012	-0.012	-0.009 (-0.008)	0.005 (0.001)
3 <sup>rd</sup> Quartile	0.070	0.053	0.057	0.033	1.624 (1.796)	2.661 (2.661)	0.054	0.024	0.093 (0.101)	0.159 (0.137)
Mean	0.017	0.024	0.016	-0.007	0.961 (1.003)	1.465 (1.465)	0.025	0.009	0.056 (0.060)	0.098 (0.088)
Standard deviation	0.123	0.067	0.098	0.091	1.369 (1.387)	1.911 (1.911)	0.076	0.039	0.108 (0.111)	0.138 (0.134)
Median	0.010	0.013	0.008	0.000	0.168 (0.199)	0.410 (0.410)	0.011	0.005	0.020 (0.021)	0.036 (0.028)
Mean day-time flux (06:00-18:00)	0.033	0.045	0.030	0.001	1.912 (1.978)	2.917 (2.917)	0.049	0.018	0.117 (0.120)	0.206 (0.207)
Standard deviation	0.161	0.082	0.125	0.096	1.401 (1.383)	1.842 (1.842)	0.095	0.050	0.141 (0.129)	0.141 (0.144)
Median day-time flux (06:00-18:00)	0.038	0.044	0.026	0.001	1.635 (1.790)	2.905 (2.905)	0.041	0.014	0.090 (0.099)	0.192 (0.164)

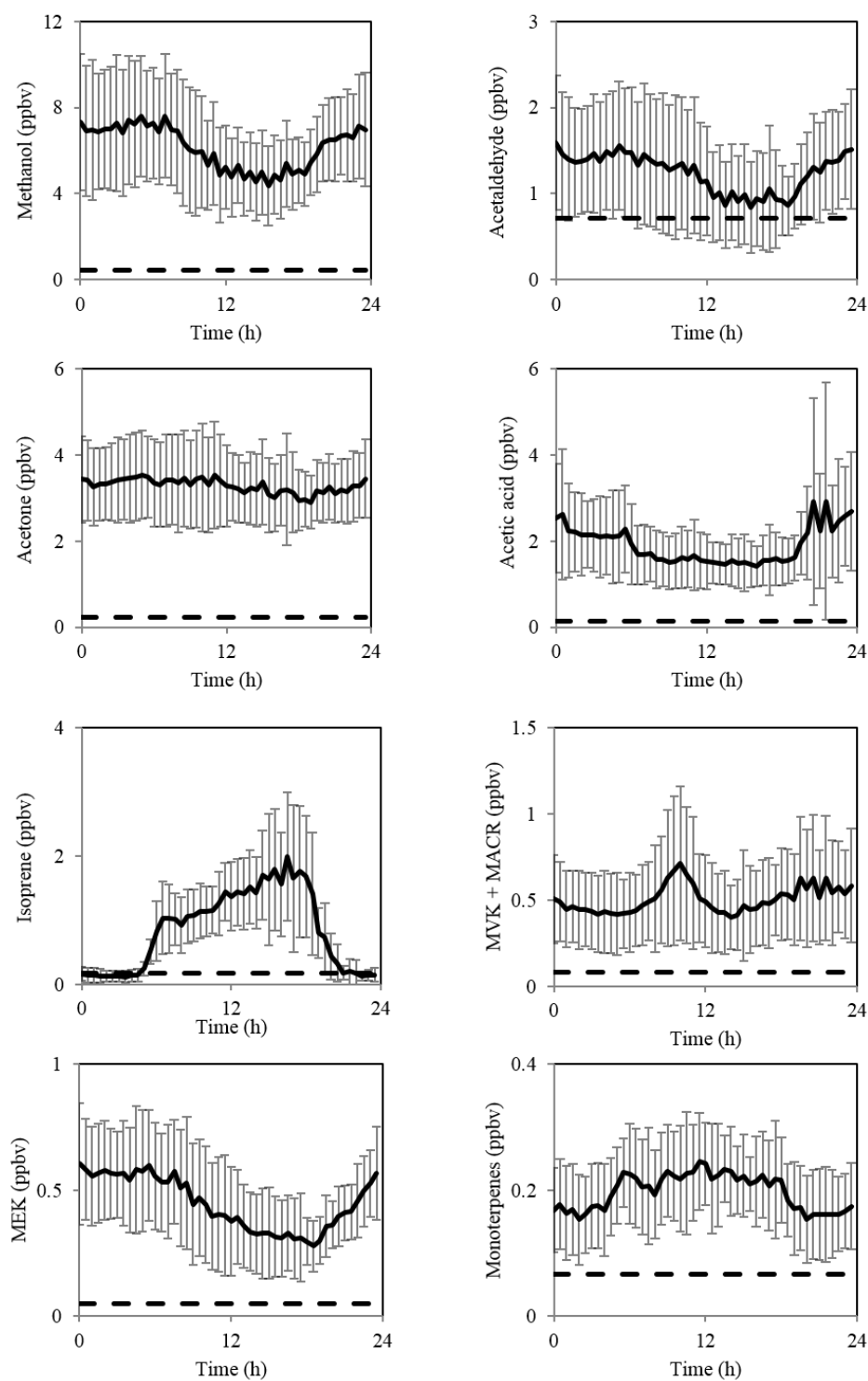


Figure 6.3. Mean 4 m above-canopy diurnal volume mixing ratios of volatile organic compounds measured during the Bosco Fontana field campaign. Error bars represent one standard deviation from the mean and the dashed line denotes limit of detection.

Table 6.3 summarizes the flux data recorded during the Bosco Fontana measurement campaign. Wind speeds decreased at night, leading to a large proportion of the night time data falling below the  $u_*$  threshold of  $0.15 \text{ m s}^{-1}$ . Consequently, average emission fluxes of all eight compounds are reported for the daytime period 10:00-15:00 LT as well as for the whole campaign. Large fluxes of  $m/z$  69 and  $m/z$  81 (assigned to isoprene and monoterpenes respectively) were observed and are shown in Fig. 6.4. Fluxes of  $m/z$  33, 45, 59, 61, 71 and 73 (assigned to methanol, acetaldehyde, acetone, acetic acid, MVK + MACR and MEK, respectively) were also observed, but these fluxes were weaker, leading to a high percentage of fluxes failing the LoD check. However, as is described by Langford et al. (2015), when these flux data are averaged to show the average diurnal cycle, it is appropriate to use a combined LoD value appropriate for the same period rather than the LoD attached specifically to each 25 min flux file. It is, though, essential that each individual flux period be processed carefully to avoid the introduction of a bias due to the use of the MAX method of time-lag identification. The LoD for the mean ( $\overline{LoD}$ ) decreases with the square root of the number of samples averaged (N).

$$\overline{LoD} = \frac{1}{N} \sqrt{\sum_{i=1}^N LoD^2} \quad (5)$$

Therefore, while the flux time series of methanol, acetaldehyde, acetone, acetic acid, MVK + MACR and MEK are not presented here, the campaign average diurnal fluxes are shown (Fig. 6.5). As discussed above, 25 min averaged flux files flagged as below the LoD were included in these diurnal averages. Flux files falling below the  $0.15 \text{ m s}^{-1}$  wind speed threshold were also included to prevent the night time flux being biased high for depositing compounds. For compounds showing emission, night-time fluxes

are close to zero anyway and the application has little influence on the results. Data flagged for non-stationarity were excluded. For a more detailed discussion of the fluxes and mixing ratios of each BVOC and comparison made with other temperate and Mediterranean ecosystems, see the Supplementary Information.

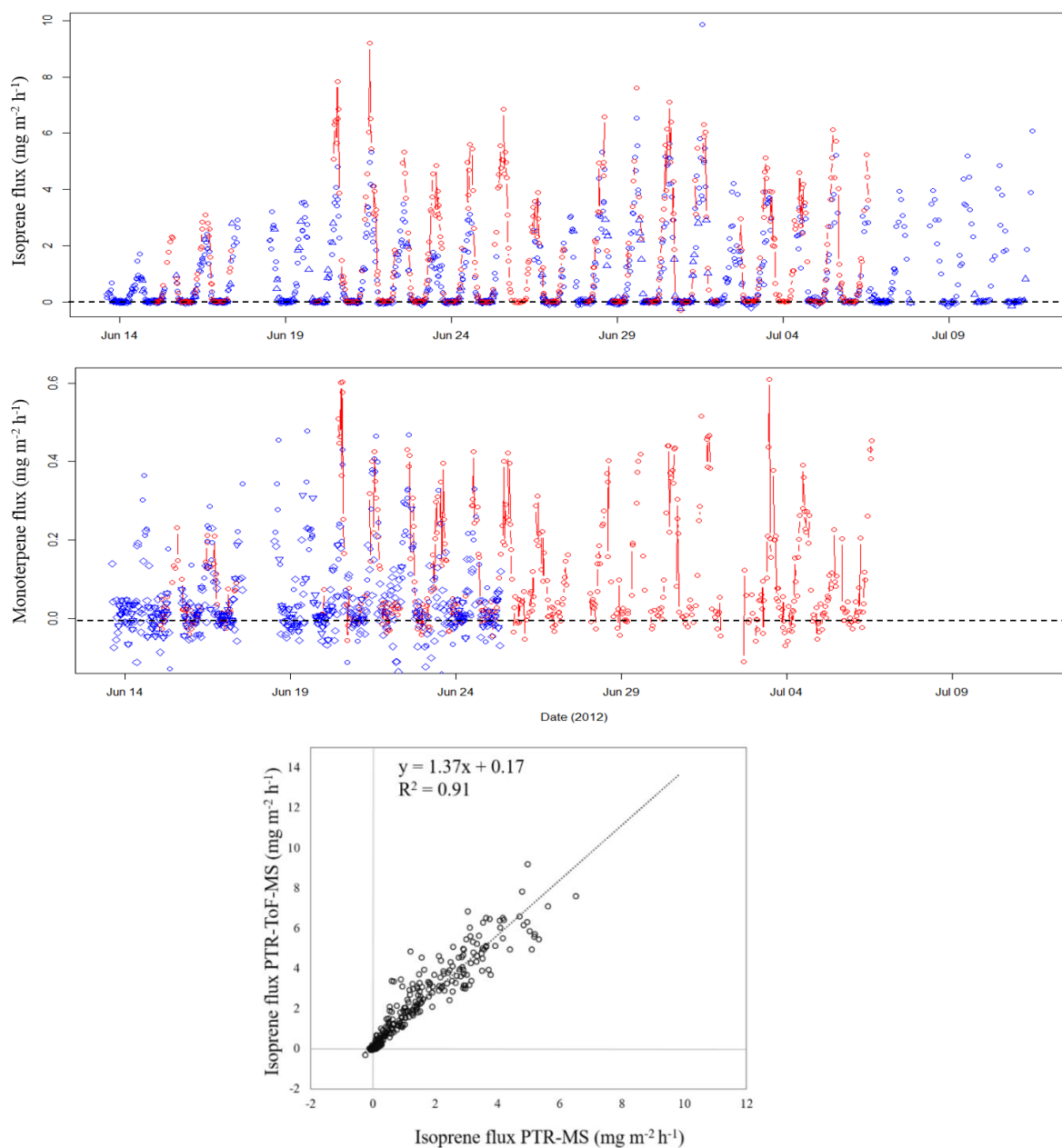


Figure 6.4. Time series of isoprene (top) and monoterpene (middle) fluxes ( $\text{mg m}^{-2} \text{h}^{-1}$ ) measured using vDEC. 25 min averaged flux data from the PTR-MS which passed all tests, fell below the  $u_*$  threshold and fell below the LoD are represented by blue circles, triangles and diamonds respectively. Red circles and lines represent PTR-ToF-MS isoprene and monoterpene fluxes with 30 min averaged flux files failing the stationarity test removed. Bottom, scatter plot showing the relationship between isoprene fluxes calculated using PTR-MS and PTR-ToF-MS.

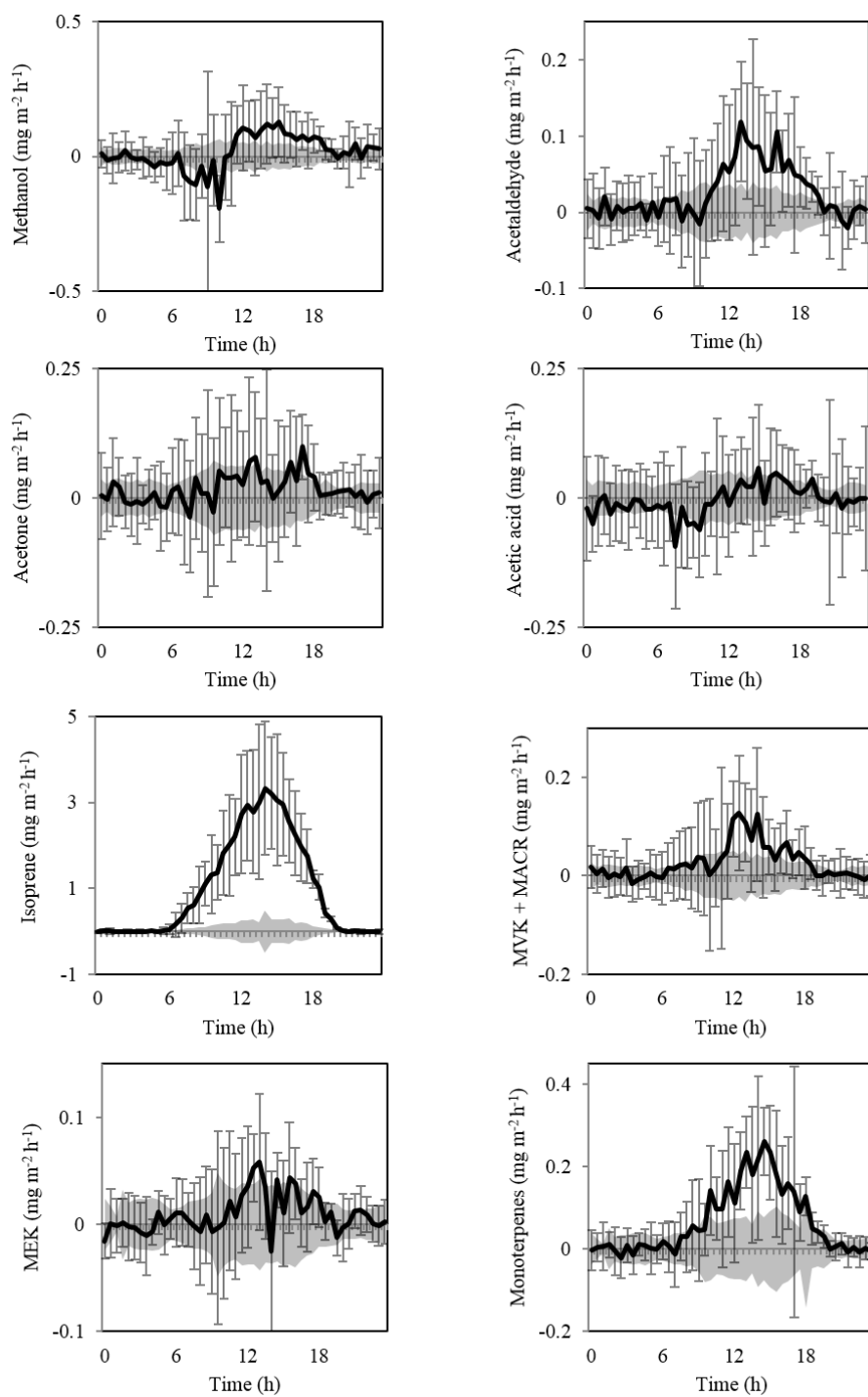


Figure 6.5. Mean diurnal fluxes of volatile organic compounds measured using vDEC. Shaded area represents the limit of detection of the averaged data, and error bars represent one standard deviation between days from the mean.

The fluxes of isoprene and monoterpenes calculated using both the PTR-MS and the PTR-ToF-MS instruments are displayed in Fig. 6.4 and summarised in Table 6.3. The isoprene fluxes calculated using both instruments show very good correlation ( $R^2 = 0.91$ , slope 1.3 and intercept  $0.17 \text{ mg m}^{-2} \text{ h}^{-1}$ ). The monoterpene fluxes, calculated using  $m/z$  81 with the PTR-MS and  $m/z$  81.070 with the PTR-ToF-MS show an  $R^2 = 0.50$ . Three additional mass spectral peaks are observed at  $m/z$  81 in the PTR-ToF-MS:  $m/z$  80.92, 80.99 and 81.03, however statistically significant fluxes from these peaks could not be calculated using the PTR-ToF-MS. Owing to the lower sensitivity of the PTR-MS at  $m/z$  81 and the lower sampling frequency of the disjunct sampling protocol (Rinne and Ammann 2012), the monoterpene flux calculated using this instrument is significantly noisier than the flux calculated using the PTR-ToF-MS.

PTR-MS and PTR-ToF-MS mass scans were averaged over a ten day period (14<sup>th</sup> – 24<sup>th</sup> June). A comparison of these mass scans over the range  $m/z$  33 to 100 at unit mass resolution is displayed in Fig. 6.6, with masses reported relative to  $m/z$  59 (acetone). A good agreement between the PTR-MS and PTR-ToF-MS is seen for all masses, except for  $m/z$  33 where the PTR-MS gives a significantly higher signal. As both instruments have comparable sensitivities at this mass (11.6 and ca. 10-12 ncps ppbv<sup>-1</sup> for the PTR-MS and PTR-ToF-MS respectively) this discrepancy must be the result of interference from another ion at this mass.  $\text{O}^{17}\text{O}^+$  could interfere with the methanol signal at  $m/z$  33 but as a significant peak is not observed at  $m/z$  34 ( $\text{O}^{18}\text{O}^+$ ) a large contribution from  $\text{O}^{17}\text{O}^+$  to  $m/z$  33 is unlikely. This suggests that there is a greater formation of  $\text{O}_2\text{H}^+$  in the PTR-MS than in the PTR-ToF-MS under these particular operation parameters. No major mass spectral peaks are observed in one

instrument alone, indicating that there is no artefact formation or unexpected loss of chemical species with either instrument. The mass scans show a much cleaner spectrum than was reported by Misztal et al. (2011) above an oil palm plantation in South-East Asia, suggesting an atmosphere dominated by fewer chemical species at higher concentrations.

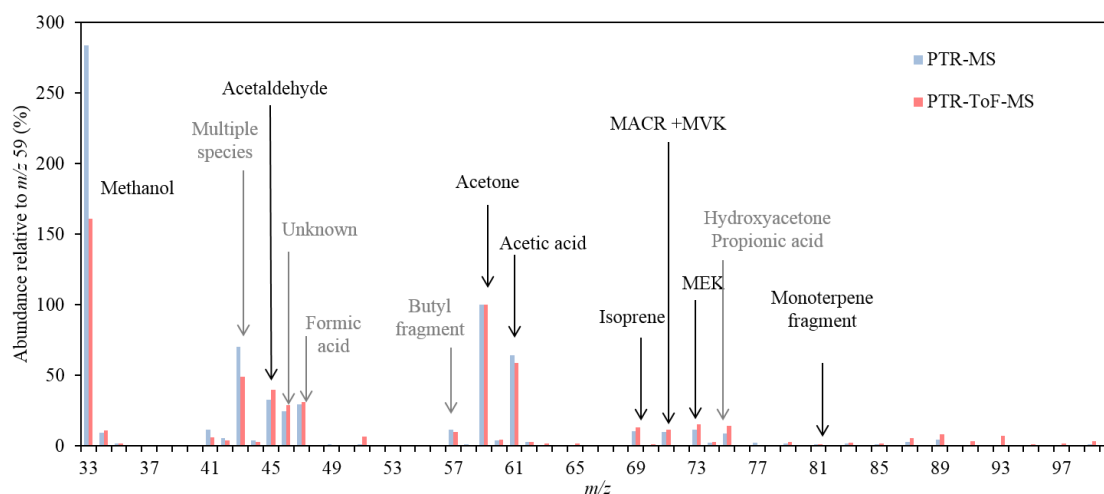


Figure 6.6, Comparison of PTR-MS (blue) and PTR-ToF-MS (red) mass scans relative to  $m/z$  59 at unit mass resolution averaged between 14<sup>th</sup> and 24<sup>th</sup> June. Compounds recorded in flux mode using the PTR-MS are presented in black with compounds tentatively identified in grey.

### 6.3.2.1 BVOC correlations

Scatter plots were used to investigate the relationship between the measured species. Methanol, acetone and MEK (Fig. 6.7) all showed a shift in the regression of the BVOCs with increasing temperature with two linear groupings observed, one at lower temperature (ca.  $< 20^{\circ}\text{C}$ ) and another at higher temperatures (ca.  $> 20^{\circ}\text{C}$ ). The change in regression could be a result of either different proportions of BVOCs present in high and low temperature air masses or by two different sources contributing to the mixing ratios (most likely an atmospheric background and a photochemical source at higher temperatures). It is possible that a second compound could contribute to the nominal mass at higher temperatures but as few compounds have been reported to contribute to  $m/z$  33 or 59, this seems unlikely.

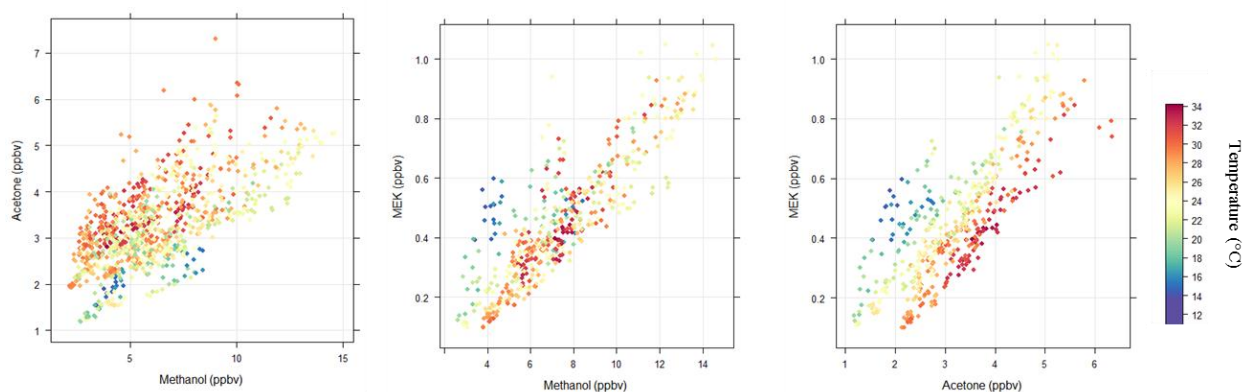


Figure 6.7, Scatter plots displaying the relationship between the volume mixing ratios of methanol, acetone and MEK measured 4 m above the canopy, coloured by temperature.

### 6.3.2.2 Short-chain oxygenated BVOCs

A mean methanol mixing ratio of 6.2 ppbv at 4 m above the canopy was recorded over the duration of the campaign, making it the dominant BVOC observed at Bosco Fontana. Large mixing ratios of methanol compared with other VOC species (caused by its low photochemical reactivity) have been reported in urban landscapes (Langford et al., 2009). This suggests that the large methanol mixing ratios relative to other VOCs observed 4 m above the forest at Bosco Fontana may be due to the surrounding agricultural and urban landscape. Mean acetaldehyde, acetone and acetic acid mixing ratios were 3.4, 3.2 and 1.9 ppbv at 4 m above the canopy, respectively. Methanol, acetaldehyde and acetic acid mixing ratios all followed similar diurnal cycles (Fig. 6.3), with mixing ratios remaining stable through the night before a drop in the morning, probably caused by expansion of the planetary boundary layer after sunrise. Then mixing ratios increased again in the late afternoon as emissions accumulated in a shrinking boundary layer. Acetone mixing ratios remained on average stable throughout the day (Fig. 6.3). This would suggest a day-time source of acetone offsetting the dilution caused by expansion of the planetary boundary layer. As the flux of acetone, where observed, was very small this source must either be photochemical or situated outside the forest.

The flux of methanol peaked at  $0.49 \text{ mg m}^{-2} \text{ h}^{-1}$  with a mean day-time flux of  $0.03 \text{ mg m}^{-2} \text{ h}^{-1}$  (Fig. 6.5). Methanol deposition was observed during the night and mornings followed by a rapid increase in methanol emission in the late morning and peaking in the early afternoon. Bidirectional exchanges of methanol have been reported previously (for example Fares et al., 2012; Karl et al., 2004) with methanol absorption/desorption thought to occur in thin water films within the canopy

(Wohlfahrt et al., 2015). The mean morning (06:30-10:30 LT) methanol deposition velocity ( $V_d$ ) at the measurement height ( $z_m$ ) was calculated using the relationship (Misztal et al., 2011):

$$V_d(z_m) = -\frac{F}{\chi(z_m)} \quad (6)$$

and was found to be  $0.31 \text{ cm s}^{-1}$ . The night-time deposition velocity was lower,  $0.02 \text{ cm s}^{-1}$ , falling at the bottom end of the  $0.02 - 1.0 \text{ cm s}^{-1}$  range reported by Wohlfahrt et al. (2015) from a review of eight different north hemisphere sites.

Acetic acid deposition was also observed in the morning, but any emission flux in the afternoon remained below the limit of detection, even if aggregated into mean diurnal cycles. The mean diurnal acetaldehyde flux is shown in Fig. 6.5. The flux increased from below the detection limit in late morning to a peak in the early afternoon before dropping again towards zero at night. The flux peaked at  $0.44 \text{ mg m}^{-2} \text{ h}^{-1}$  on 29<sup>th</sup> June and the campaign mean day-time flux was  $0.06 \text{ mg m}^{-2} \text{ h}^{-1}$ . As can be seen in Fig. 6.5, the acetone flux remained below the limit of detection for most of the day with a small positive flux observed in the late afternoon.

### **6.3.2.3 MVK + MACR and MEK**

MVK and MACR are the main products formed following the first stage of isoprene oxidation in the atmosphere (Atkinson and Arey 2003a), accounting for ca. 80% of the carbon. MACR can also be directly produced within plants as a by-product in the production of cyanogenic glycosides (Fall 2003) and experimental observation demonstrated that emissions of MVK and MACR increase with temperature stress

(Jardine et al., 2012). The mid-day (10:00-15:00 LT) mixing ratios of MVK + MACR at 4 m above the canopy showed a positive correlation with those of isoprene ( $R^2 = 0.49$ ), suggesting that the oxidation of isoprene was responsible for the formation of MVK and MACR.

The production of MVK and MACR from isoprene at the Bosco Fontana site has been modelled by Schallhart et al. (2015), who estimated that 4 - 27 % of the MVK + MACR flux was formed from isoprene oxidation products. MVK and MACR mixing ratios recorded at 4 m above the canopy (Fig. 6.3) increase in the morning as isoprene concentrations rise, before boundary layer expansion causes them to drop in the middle of the day. The mixing ratios then increase again in the evening as the boundary layer contracts. The flux of MVK + MACR (Fig. 6.5) peaked in the early afternoon with a mean day-time flux of  $0.05 \text{ mg m}^{-2} \text{ h}^{-1}$ . This flux is comparable to the  $0.03$  and  $0.08 \text{ mg m}^{-2} \text{ h}^{-1}$  observed, respectively, by Kalogridis et al. (2014) and Spirig et al. (2005) over European oak and mixed forests.

MEK may be directly emitted by plants (Fall, 2003) or formed photochemically (Luecken et al., 2012). MEK mixing ratios 4 m above the forest canopy remained stable through the night at ca. 0.6 ppbv before dropping in the morning, probably caused by expansion of the planetary boundary layer, to ca. 0.3 ppbv and rising again in the evening (Fig. 6.3). A plot of the mixing ratios of MEK against those of acetone reveals a bimodal distribution suggesting two distinct sinks or sources (Fig. 6.7), the first occurring at lower temperatures (ca. 12-20 °C) with a MEK to acetone ratio of ca. 0.17 and the second at higher temperatures (ca. 20-34 °C) with a MEK to acetone ratio of ca. 0.06. A relationship between acetone and MEK has been reported by Riemer et

al. (1998) who observed an MEK to acetone ratio of 0.07 at temperatures between 20 and 37 °C. This compares well with the observations at Bosco Fontana. This trend was not observed when data were coloured by PAR indicating that the bimodal distribution is not driven by the faster rate of reaction of MEK than of acetone with OH. A low MEK emission flux was observed in the afternoon with a mean day-time flux of  $0.02 \text{ mg m}^{-2} \text{ h}^{-1}$ .

#### **6.3.2.4 Isoprene and monoterpenes**

Isoprene mixing ratios 4 m above the canopy began to rise in the mid-morning from a night-time zero, peaking in the late afternoon at ca. 2 ppbv before falling again to zero in the late evening (Fig. 6.3). Isoprene fluxes were not observed at night, but increased in the morning to a peak in the mid afternoon before dropping to zero again in the evening (Fig. 6.5) with a mean day-time flux of  $1.9 \text{ mg m}^{-2} \text{ h}^{-1}$ .

Isoprene fluxes correlated with leaf temperature (estimated using a method based on that described by Nemitz et al. (2009) and explained in more detail in the Supplementary Information,  $R^2 = 0.73$  for an exponential fit), PAR ( $R^2 = 0.75$  for an exponential fit) and with sensible heat flux (H) ( $R^2 = 0.67$ ). The relationship between isoprene fluxes and mixing ratios, temperature and PAR is displayed in Fig. 6.8. Table 6.4 compares isoprene flux measurements with the fluxes recorded during other field campaigns in the Mediterranean region and the isoprene emission factor under basal conditions. As would be expected, the flux of isoprene is shown to be highly dependent on ecosystem type. The fluxes observed during this measurement period, when normalised to standard conditions, were lower than those observed over woodland dominated by isoprene emitting oak species (Baghi et al., 2012; Kalogridis

et al., 2014) due to the lower proportion of isoprene emitting species in the canopy but closer in magnitude to that observed over a mixed pine and oak forest (Fares et al., 2013).

The campaign mean monoterpene mixing ratio 4 m above the canopy was 0.2 ppbv. The diurnal profile (Fig. 6.3) shows a night-time mixing ratio of ca. 0.18 ppbv which increases to ca. 0.21 ppbv in the morning remaining stable through the day and dropping again to ca. 0.18 ppbv at night. The monoterpene flux (Fig. 6.5) peaked in the early afternoon with a campaign mean mid-day flux of  $0.12 \text{ mg m}^{-2} \text{ h}^{-1}$ . Monoterpene mixing ratios were not significantly correlated with leaf surface temperature or with PAR ( $R^2 = 0.11$  and  $0.12$  respectively). However, the flux displayed a correlation with both leaf surface temperature and PAR ( $R^2 = 0.44$  and  $0.39$  respectively).

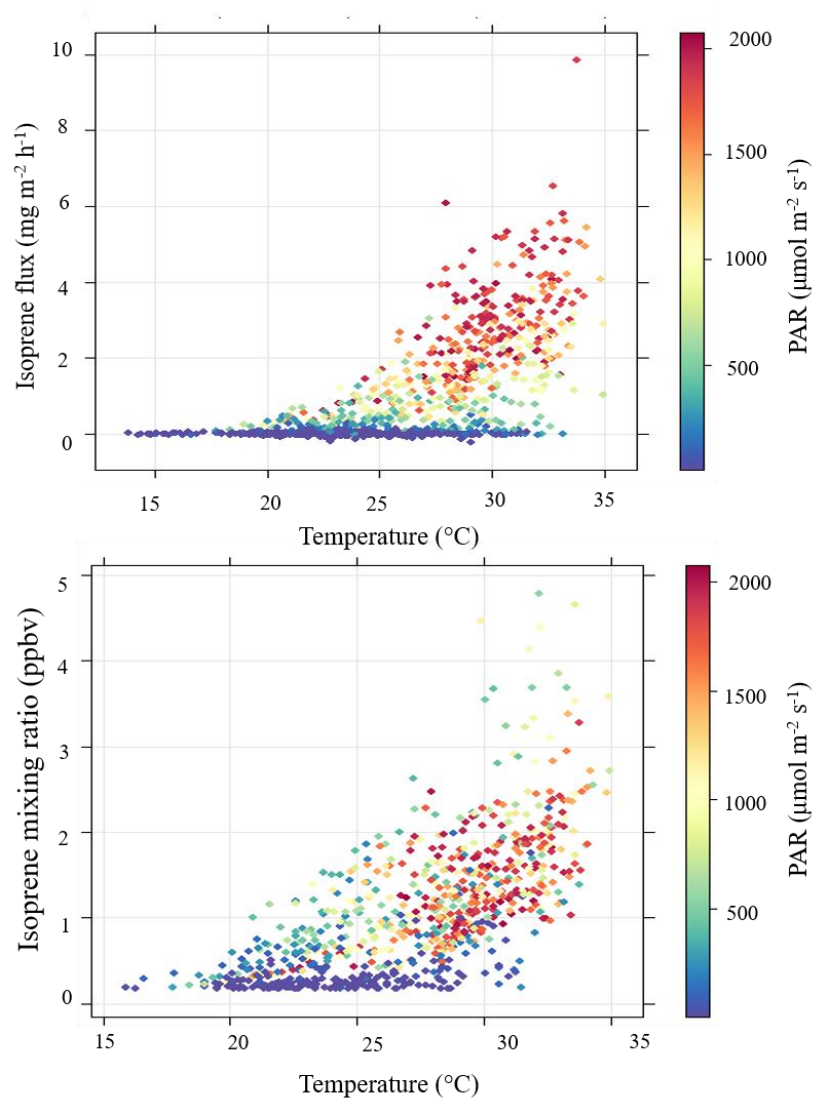


Figure 6.8, the relationship between temperature (°C) and isoprene fluxes (mg m<sup>-2</sup> h<sup>-1</sup>) and volume mixing ratios (ppbv), coloured according to the magnitude of photosynthetically active radiation (μmol m<sup>-2</sup> s<sup>-1</sup>).

Table 6.4, non-exhaustive summary of isoprene fluxes recorded in the Mediterranean region and the isoprene emission factor under basal conditions (temperature: 30 °C and PAR: 1000  $\mu\text{mol m}^{-2} \text{s}^{-1}$ ).

Ecosystem	Dominant species	Season	Mean day time isoprene flux ( $\text{mg m}^{-2} \text{h}^{-1}$ )	Isoprene emission factor under basal conditions ( $\text{mg m}^{-2} \text{h}^{-1}$ )	Reference
Mixed oak and hornbeam forest	<i>Carpinus betulus</i> <i>Quercus robur</i>	Summer	2.6	1.7	This study
Oak forest	<i>Quercus pubescens</i>	Spring	2.8	7.4	Kalogridis et al. 2014
Oak forest	<i>Quercus pubescens</i>	Summer	5.4-10.1	5.4	Baghi et al. 2012
Mixed oak and pine forest	<i>Pinus pinea</i> <i>Quercus ilex</i> <i>Quercus suber</i>	Autumn	ca. 0.13	0.61	Fares et al. 2013

### 6.3.3 Impacts on air quality

The forest at Bosco Fontana provides a large source of BVOCs in a region of predominantly agricultural and urban land use. The oxidation of BVOCs leads to the formation of low volatility organic compounds which in turn contribute to SOA (Ehn et al., 2014). The importance of individual BVOC species to SOA formation is, however, variable, with large and cyclic compounds likely to contribute more to SOA formation (Hallquist et al., 2009). Monoterpenes are known to contribute significantly to SOA formation. The principal monoterpene species observed during this campaign were  $\alpha$ -pinene,  $\beta$ -pinene, sabinene and limonene (Table 6.5). Following ozonolysis of  $\alpha$ -pinene and  $\beta$ -pinene, Lee et al. (2006) observed aerosol yields of 41 and 17 % respectively. Aerosol yields of 41 and 17 % were assigned to limonene and sabinene, respectively, due to the placement of C-C double bonds within/or external to the cyclic structure. The average aerosol yield from monoterpene ozonolysis during the campaign may then be calculated based on the proportion of each compound emitted. This gives a ca. 39 % yield of aerosol, contributing ca.  $0.38 \mu\text{g C m}^{-3}$  to aerosol (based on the campaign average monoterpene mixing ratio (0.198 ppbv)).

Significant aerosol formation from isoprene has been reported in low  $\text{NO}_x$  environments (Claeys et al., 2004), however, the high  $\text{NO}_x$  concentrations at the Bosco Fontana natural reserve (Finco et al., in preparation) make a significant contribution to SOA from isoprene unlikely.

In the presence of  $\text{NO}_x$ , BVOCs can facilitate the formation of tropospheric ozone. As the potential for photochemical ozone formation is five times greater from isoprene than from VOCs emitted following urban anthropogenic activity (Derwent et al.,

2007; Hewitt et al., 2009), the high isoprene emission observed here will have a significant impact on tropospheric ozone formation in the high NO<sub>x</sub> environment at the Bosco Fontana natural reserve and downwind. The emission of isoprene from the Bosco Fontana reserve, together with other forest fragments and poplar plantations with the Po Valley, is likely to have a significant impact upon tropospheric ozone concentrations in the region.

#### **6.3.4 Calculation of isoprene and monoterpene canopy level emission factors**

Although other approaches do exist, isoprene fluxes are widely modelled using the MEGAN (Guenther et al., 2006). MEGAN calculates isoprene fluxes based on the product of an emission activity factor ( $\gamma$ ), a canopy loss and production factor ( $\rho$ ) and a canopy emission factor ( $\epsilon$ ). Therefore, plotting isoprene flux against  $\gamma \times \rho$  enables the calculation of a canopy-specific isoprene emission factor (Fig. 6.9), giving value of 1.68 mg m<sup>-2</sup> h<sup>-1</sup> at standard conditions (1000  $\mu$ mol m<sup>-2</sup> s<sup>-1</sup> PAR and 303 K) for the campaign period. For the purpose of this work,  $\rho$  was assumed to be 0.96. This is supported by Schallhart et al. (2015) who found that between 3 and 5 % of isoprene emissions were lost within the canopy at the Bosco Fontana reserve. The emission activity factor,  $\gamma$ , was calculated using the algorithms described by Guenther et al. (2006). Radiative transfer through the canopy was modelled using the model applied by Müller et al. (2008). This model was based on that of Goudriaan and van Laar (1994) and ambient temperature was recorded 4 m above the canopy. The standard light and temperature conditions for MEGAN canopy scale emissions factors are ~1500  $\mu$ mol m<sup>-2</sup> s<sup>-1</sup> and 303 K (Guenther et al., 2006). In order to enable direct comparison between the GC-MS data and literature emissions factors, the factor

which sets the emission activity to unity at standard conditions ( $C_{CE}$ ) was increased to 1.42. This gave standard light and temperature conditions of  $1000 \mu\text{mol m}^{-2} \text{s}^{-1}$  and 303 K, respectively.

The emission factor is lower than those calculated by Kalogridis et al. (2014) and Baghi et al. (2012) from oak (*Quercus pubescens*) dominated forests in southern France (7.4 and  $5.4 \text{ mg m}^{-2} \text{ h}^{-1}$ , respectively). However, this is to be expected, owing to the high proportion of low or non-isoprene emitting species such as *Carpinus betulus*, *Corylus avellana*, *Sambucus nigra* and *Acer campestre* present in the forest at Bosco Fontana.

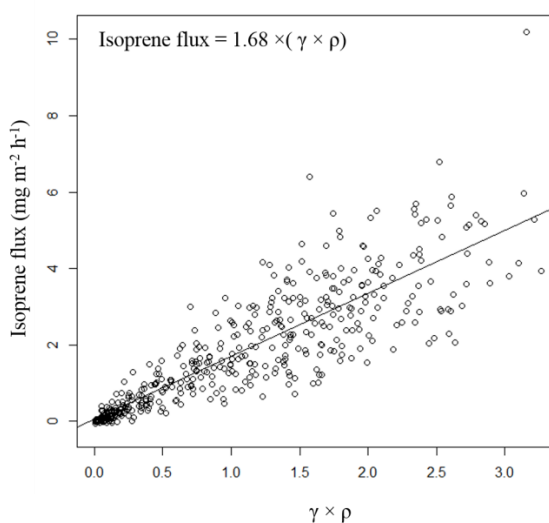


Figure 6.9, measured isoprene fluxes against the product of  $\gamma$  (emission activity factor, itself the product of the temperature, light and leaf area index activity factors) and  $\rho$  (the canopy loss and production factor).

Monoterpene emission from plants may take the form of pool or *de novo* emission. Emission from stored pools is temperature controlled whereas *de novo* is driven by

photosynthesis and is therefore controlled by light as well as temperature (Ghirardo et al., 2010). Emission from stored pools was modelled using the monoterpene-temperature relationship described by Guenther et al. (1995), this model correlated well with the observed monoterpene flux (PTR-ToF-MS) giving  $R^2$  value of 0.55. In order to assess the effect of light on monoterpene emission, the residual values from the temperature only model were plotted against PAR (Fig. 6.10). The residuals displayed a correlation with PAR ( $R^2 = 0.45$ ) indicating that light as well as temperature have a significant impact on monoterpene emissions from the forest canopy and therefore a significant proportion of monoterpene emission represent *de novo* emission. However, in order to accurately assess the contribution of pool and *de novo* emissions to the canopy scale monoterpene flux, a species specific leaf level investigation would be required. A monoterpene canopy emission factor calculated using the MEGAN algorithms, which only simulate *de novo* emission, was found to be  $0.14 \text{ mg m}^{-2} \text{ h}^{-1}$ .

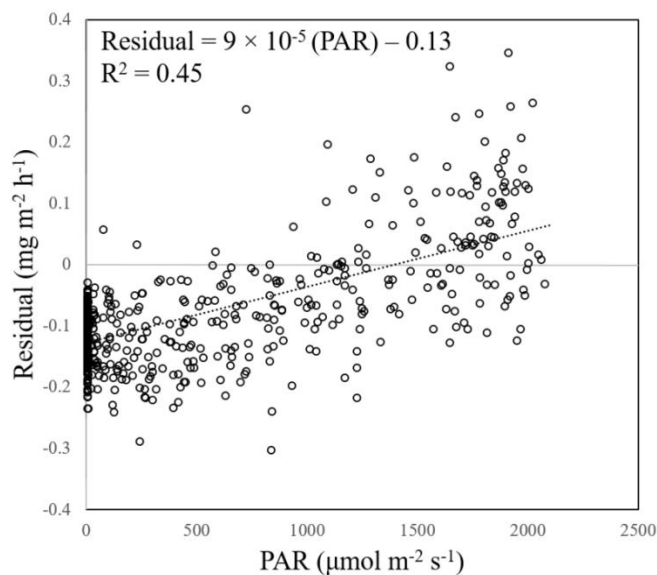


Figure 6.10, plot of the residual values from the temperature only monoterpene emission model against PAR, demonstrating that light as well as temperature has a significant impact on monoterpene emissions.

Table 6.5, leaf level isoprene and monoterpene emission ( $\text{mg m}^{-2} \text{h}^{-1}$ ) from single leaves under basal conditions (temperature: 30 °C and PAR: 1000  $\mu\text{mol m}^{-2} \text{s}^{-1}$ ). ND signifies not detected.

Tree species	isoprene flux (standard error)	$\alpha$ -pinene flux (standard error)	sabinene flux (standard error)	$\beta$ -pinene flux (standard error)	limonene flux (standard error)	sum monoterpene flux
<i>Carpinus betulus</i>	$2.25 \times 10^{-3}$ ( $1.50 \times 10^{-3}$ )	$1.07 \times 10^{-2}$ ( $6.00 \times 10^{-3}$ )	$1.81 \times 10^{-2}$ ( $1.36 \times 10^{-2}$ )	$5.14 \times 10^{-2}$ ( $1.23 \times 10^{-2}$ )	$5.83 \times 10^{-1}$ ( $2.36 \times 10^{-1}$ )	$6.63 \times 10^{-1}$
<i>Quercus robur</i>	$2.39 \times 10^0$ ( $6.12 \times 10^{-1}$ )	$2.81 \times 10^{-2}$ ( $1.45 \times 10^{-2}$ )	ND	$4.70 \times 10^{-3}$ ( $3.08 \times 10^{-3}$ )	$2.16 \times 10^{-1}$ ( $6.49 \times 10^{-2}$ )	$2.49 \times 10^{-1}$
<i>Quercus rubra</i>	$9.14 \times 10^{-1}$ ( $2.02 \times 10^{-1}$ )	ND	ND	$7.95 \times 10^{-3}$ ( $2.22 \times 10^{-3}$ )	$2.34 \times 10^{-2}$ ( $7.11 \times 10^{-3}$ )	$3.13 \times 10^{-2}$
<i>Corylus avellana</i>	$4.97 \times 10^{-4}$ ( $3.93 \times 10^{-4}$ )	$1.30 \times 10^{-2}$ ( $8.00 \times 10^{-3}$ )	ND	$2.08 \times 10^{-2}$ ( $4.80 \times 10^{-3}$ )	$7.57 \times 10^{-1}$ ( $4.15 \times 10^{-1}$ )	$7.90 \times 10^{-1}$
<i>Acer campestre</i>	$4.40 \times 10^{-4}$ ( $3.11 \times 10^{-4}$ )	$5.14 \times 10^{-2}$ ( $2.95 \times 10^{-2}$ )	ND	$2.27 \times 10^{-1}$ ( $3.54 \times 10^{-2}$ )	$1.07 \times 10^{-1}$ ( $1.41 \times 10^{-2}$ )	$3.85 \times 10^{-1}$
<i>Sambucus nigra</i>	$4.09 \times 10^{-3}$ ( $3.66 \times 10^{-3}$ )	ND	ND	$9.67 \times 10^{-3}$ ( $2.69 \times 10^{-3}$ )	$2.49 \times 10^{-1}$ ( $1.41 \times 10^{-1}$ )	$2.59 \times 10^{-1}$
<i>Cornus sanguinea</i>	$4.00 \times 10^{-1}$ ( $4.00 \times 10^{-1}$ )	$1.11 \times 10^{-3}$ ( $1.11 \times 10^{-3}$ )	ND	$1.95 \times 10^{-2}$ ( $4.91 \times 10^{-3}$ )	$2.28 \times 10^{-1}$ ( $1.73 \times 10^{-1}$ )	$2.49 \times 10^{-1}$

### 6.3.5 Speciated bottom-up isoprene and monoterpene flux estimates derived from leaf-level measurements

Tree species distribution data combined with information on leaf-level isoprene and monoterpene emission rates and meteorological data were used to produce a “bottom-up” estimate of the total canopy level flux. Tree species distribution data were obtained from Dalponte et al. (2007), this tree species distribution map reveals an uneven distribution of isoprene emitting species within the forest canopy, with the two main isoprene emitting species (*Q. robur* and *Q. rubra*) concentrated in the south of the forest.

Leaf-level isoprene and monoterpene emissions from the dominant tree species were recorded using GC-MS (Table 6.5). Together these species represent 76.6 % of the total vegetation cover. Isoprene emission was dominated by *Q. robur* and *Q. rubra* with *C. avellana* and *C. betulus* the highest monoterpene emitting species. The isoprene emission recorded for both oak species was lower than that previously reported (Karl et al., 2009; Keenan et al., 2009). For species where GC-MS data were not available, literature values were used. Leaf-level emission factors for minor species for which no GC-MS measurements were made were taken from Karl et al. (2009) with the exception *Rubus* sp. (Owen et al., 2001) and *Acer negundo* and *Morus* sp. (Benjamin et al., 1996). Emission factors taken from the literature were converted from  $\mu\text{g g}_{\text{DW}}^{-1} \text{h}^{-1}$  to  $\text{mg m}^{-2} \text{h}^{-1}$  using the mean leaf mass to area ratio,  $115 \text{ g}_{\text{DW}} \text{m}^{-2}$ , reported by Niinemets (1999) from a study of ca. 600 species. The leaf-level emissions data were then scaled up to a canopy level using the MEGAN algorithms (Guenther et al., 2006) and incorporated measured PAR and temperature values averaged over 30 minutes and a single sided leaf area index (LAI,  $\text{m}^2/\text{m}^2$ ) of 5.5.

The hyperspectral/LIDAR data of Dalponte et al. (2007) was remapped onto a grid centred on the measurement site, with a resolution of 5 m<sup>2</sup>, providing fractional ground cover by each of the 20 tree species within each grid cell. The contribution of each grid cell to each 25-minute flux measurement was then calculated at 5 m<sup>2</sup> resolution using a high resolution 2-D footprint model based on Kormann and Meixner (2001) similar to that described by Neftel et al. (2008). Finally, the MEGAN algorithm was applied to all plant species using the 25-minute meteorology. The information was combined to provide a bottom-up estimate of the flux that the canopy-scale measurements should have detected, based on the leaf-level data. This footprint and species dependent bottom-up flux estimate showed significantly better agreement with the measured isoprene flux ( $R^2 = 0.75$ , slope = 0.56) than was observed when the canopy-scale isoprene emission factor calculated above was used ( $R^2 = 0.65$ , slope = 0.76). This demonstrates the large effect an uneven distribution of isoprene sources can have on the above canopy flux, even within what appears to be a uniform canopy, and the benefit for accounting for spatial species distributions in uniform vegetation canopies.

However, despite capturing the shape of the flux time series, the bottom-up flux underestimated the magnitude of the flux, capturing 56 % of the isoprene flux as measured by vDEC. This could in part be caused by changes in vegetation cover between the tree distribution mapping in 2008 and the flux measurements in 2012. There are anecdotal reports that *Populus* sp. coverage has increased in the understory vegetation but it is unlikely that, despite their high rates of growth, the *Populus* coverage changed significantly in the 4 years between mapping and this campaign.

Since 2008, the non-native *Q. rubra* is gradually being removed from the forest. However, this does not explain the discrepancy between the vDEC isoprene flux measurements and the bottom-up flux estimate as the reduction in the number of *Q. rubra* trees should have decreased the flux. Whilst the hyperspectral/LIDAR tree species data for this site provides a unique opportunity for comparing the canopy-scale measurements with a detailed bottom-up estimate, the hyperspectral/LIDAR data only provides information on projected tree species area as seen from above, whilst the flux is regulated by leaf mass and its exposure to radiation. Thus there are uncertainties in the ability of the hyperspectral/LIDAR to detect understorey vegetation and a single conversion factor was used between projected tree area and leaf mass. However, understorey vegetation is less exposed to sunlight reducing its emission. Indeed, the main reason for the underestimate of isoprene flux is probably that the leaf level isoprene emission rate recorded from the leaves sampled at ground level (albeit taken at the edge of sun exposed clearings) are not representative of those at the canopy top. Substituting the measured *Q. robur* and *Q. rubra* emission factors with those reported by Karl et al. (2009) caused the bottom-up estimate to give 130 % of the measured flux and improved the correlation between bottom-up estimates and canopy-scale measurements further.

The speciated monoterpene flux (calculated using GC-MS data and literature values for species where GC-MS data were not available) also showed good agreement with the above canopy flux ( $R^2 = 0.72$ ) and captured 57 % of the flux. The discrepancy between the magnitude of the speciated monoterpene flux and the above canopy flux could be partially explained by loss of monoterpenes through within canopy oxidation. Schallhart et al. (2015) investigated the flux loss due to chemical degradation using

measured concentrations of ozone and NO<sub>2</sub>, together with calculated OH and NO<sub>3</sub> concentrations. They found that 5-20 % of the monoterpene flux was lost via degradation (in comparison just 3-5 % of the isoprene flux was lost). The bottom-up monoterpene flux estimate may also have been affected by the changes to the tree species distribution in the 4 years between mapping and this campaign, as discussed above, and by deposition of monoterpenes within the forest canopy.

The contribution of different species to the isoprene and monoterpene fluxes over the course of an example day is shown in Fig. 6.11. As is shown, the isoprene flux was dominated by *Q. robur* but was sensitive to the species composition within the flux footprint. The change in wind direction around 14:00 LT reduced the contribution of *Q. robur* to the total flux, with the contribution of *Populus × canescens* increasing significantly. The monoterpene flux was predicted to have been dominated by *C. betulus*, the dominant tree species in the canopy at Bosco Fontana. A greater number of tree species contributed to the monoterpene flux, and emissions were therefore much more uniform across the canopy and less affected by changes in wind direction.

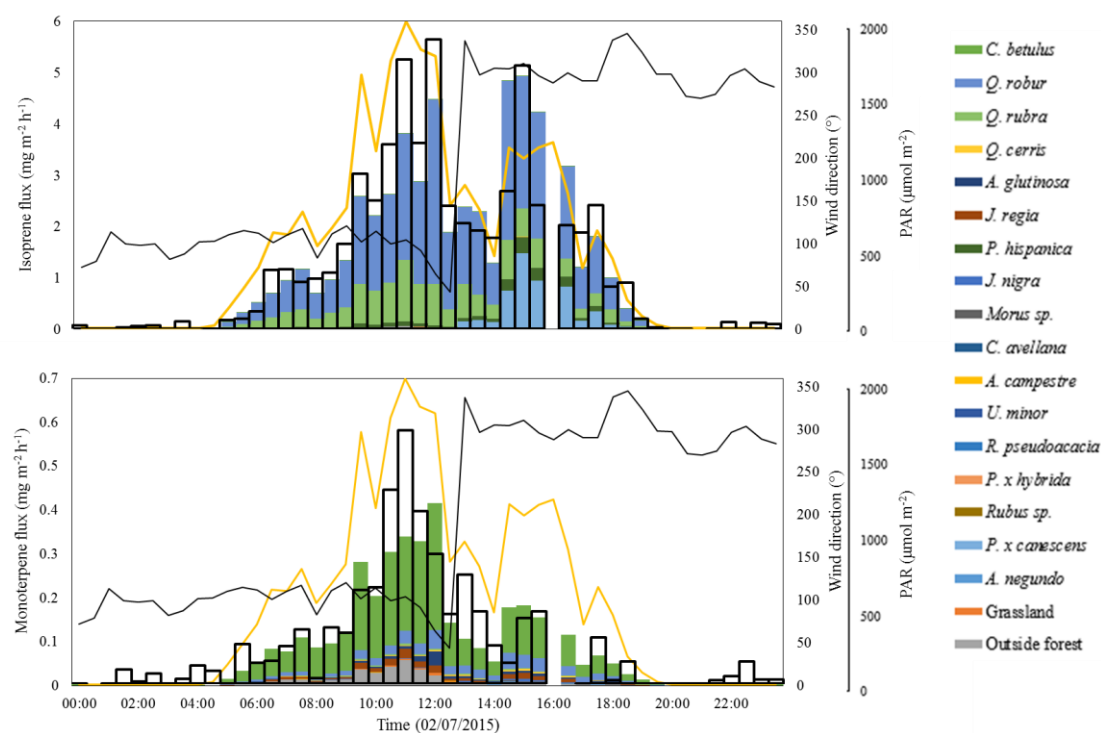


Figure 6.11, the contribution of individual tree species to the speciated isoprene and monoterpene flux on the 2<sup>nd</sup> July 2012 with PAR displayed as a yellow line, wind direction as a black line and the flux recorded using the PTR-MS as bold black bars.

The fit between the above canopy measured isoprene and monoterpene fluxes and the “bottom-up” flux estimate was improved by optimising the leaf-level emission factors, within the constraints displayed in Table 6.6, using  $\text{Chi}^2$  minimisation as implemented by the solver function in Microsoft Excel. Use of the optimised isoprene and monoterpene emission factors gave good correlations with measured fluxes ( $R^2$  values of 0.75 and 0.76, respectively). The optimised isoprene and monoterpene emission factors are presented in Table 6.6 and show a reasonable agreement with literature values (Karl et al., 2009).

Table 6.6, species specific isoprene and monoterpene emission factors (for a standard temperature of 30 °C and a PAR value of 1000  $\mu\text{mol m}^{-2} \text{s}^{-1}$ ) derived from optimising the leaf level emission factors to give the best fit with the measured above canopy isoprene and monoterpene fluxes within the constraints displayed.

Species	Isoprene emission factor ( $\text{mg m}^{-2} \text{h}^{-1}$ )	Isoprene constraint ( $\text{mg m}^{-2} \text{h}^{-1}$ )	Monoterpene emission factor ( $\text{mg m}^{-2} \text{h}^{-1}$ )	Monoterpene constraint ( $\text{mg m}^{-2} \text{h}^{-1}$ )
<i>Acer campestre</i>	0.00	< 1.0	0.15	< 0.50
<i>Acer negundo</i>	0.00	< 1.0	0.33	< 0.64
<i>Alnus glutinosa</i>	0.01	< 1.0	0.22	< 0.50
<i>Carpinus betulus</i>	0.00	< 1.0	0.57	< 0.63
<i>Corylus avellana</i>	0.00	< 1.0	0.23	< 0.50
<i>Fraxinus angustifolia</i>	0.00	< 1.0	0.00	< 0.50
<i>Juglans nigra</i>	0.00	< 1.0	0.12	< 0.50
<i>Juglans regia</i>	0.36	< 1.0	0.15	< 0.50
<i>Morus</i> sp.	0.00	< 1.0	0.19	< 0.50
<i>Platanus hispanica</i>	2.97	< 4.4	0.50	< 0.50
<i>Populus</i> × <i>canescens</i>	10.66	< 16.1	0.29	< 0.50
<i>Populus</i> × <i>hybrida</i>	8.06	< 16.1	0.00	< 0.50
<i>Prunus avium</i>	0.00	< 1.0	0.01	< 0.50
<i>Quercus cerris</i>	0.02	< 1.0	0.07	< 0.50
<i>Quercus robur</i>	7.46	< 16.1	0.19	< 0.50
<i>Quercus rubra</i>	1.38	< 8.1	0.02	< 0.50
<i>Robinia pseudoacacia</i>	1.38	< 2.8	0.01	< 0.50
<i>Rubus</i> sp.	0.00	< 1.0	0.01	< 0.50
<i>Tilia</i> sp.	0.00	< 1.0	0.00	< 0.50
<i>Ulmus minor</i>	0.01	< 1.0	0.01	< 0.50
Grass	0.06	< 1.0	0.06	< 0.15
Not woodland	0.06	< 1.0	0.08	< 0.15
Outside forest	0.06	< 1.0	0.06	< 0.50

## 6.4 Conclusions

Direct above-canopy fluxes of methanol, acetaldehyde, acetic acid, isoprene, MVK + MACR, MEK and monoterpenes were calculated using the method of virtual disjunct eddy covariance from mixing ratio data obtained with a PTR-MS above a semi-natural mixed oak and hornbeam forest in northern Italy from June 13<sup>th</sup> to July 11<sup>th</sup> 2012. Isoprene was the dominant BVOC emitted with a mean day-time flux of 1.91 mg m<sup>-2</sup> h<sup>-1</sup>. When normalised to standard conditions (temperature of 30 °C, PAR of 1000 μmol m<sup>-2</sup> s<sup>-1</sup>) using the MEGAN model (Guenther et al., 2006), a canopy scale emission factor of 1.68 mg m<sup>-2</sup> h<sup>-1</sup> was derived. Mixing ratios of VOCs measured at 4 m above the forest canopy were dominated by those of methanol, with a campaign mean mixing ratio of 6.2 ppbv.

The isoprene fluxes obtained using the PTR-MS/vDEC system showed good agreement with those obtained using a direct eddy covariance (with mixing ratios by volume measured with a fast response PTR-ToF-MS instrument). Monoterpene fluxes recorded using the PTR-MS were noisier and marginally higher than those recorded using the PTR-ToF-MS due to a lower sensitivity and, probably, the inclusion of isobaric compounds. Comparison of mass scan data generated using the PTR-MS and PTR-ToF-MS (*m/z* 33-100) showed very good agreement with no significant masses observed in one instrument but not in the other.

Up-scaling leaf-level isoprene and monoterpene emissions to the canopy scale, using a high spatial resolution tree species database and a 2D footprint model, showed significantly better correlation with the measured above canopy fluxes than was obtained using a canopy scale emission factor. Leaf-level isoprene emissions resulted

in an underestimate of the above-canopy isoprene flux and this was assumed to be the result of differences in isoprene emission rates from leaves sampled at ground-level and those at the canopy top.

Overall, the data obtained give confidence in the measurement of biogenic VOC fluxes by the method of virtual disjunct eddy covariance and highlight the importance of using leaf-level emissions data from sun-lit canopy-top leaves when up-scaling leaf-level emissions to produce a “bottom-up” canopy-scale emissions estimate.

### **Acknowledgements**

W.J.F. Acton would like to thank Alex Guenther for his advice on the use of MEGAN. This work was funded by the EU FP7 grants ÉCLAIRE (grant 282910) and PEGASOS (grant 265148), as well as by a BBSRC/Ionicon Analytik GmbH Industrial CASE studentship awarded to W.J.F.A. We acknowledge access to the measurement site provided by the Italian Corpo forestale dello Stato and provision of the site infrastructure by the Catholic University of Italy at Brescia and in particular by Giacomo Gerosa, Angelo Finco and Riccardo Marzuoli.

## 6.5 Supplementary material for “Canopy-scale flux measurements and bottom-up emission estimates of volatile organic compounds from a mixed oak and hornbeam forest in northern Italy”

### 6.5.1 Virtual disjunct eddy covariance lag time determination

The lag time between the measurement of vertical wind speed and concentration measurements using PTR-MS were calculated by identifying the absolute maximum value of the covariance function within a 30 s time window (MAX method, Taipale et al., 2010). Points for which the noise to signal ratio was greater than one were substituted for a flux calculated using a fixed lag time to prevent an overestimation of the flux from the MAX method. A histogram of isoprene lag times calculated using the MAX method is displayed in Fig. 6.12. This histogram shows a clear maximum at 7.5 s, hence 7.5 s was taken to be the fixed isoprene lag time and lag times of other masses measured were calculated from this value  $\pm$  the instrumental dwell time.

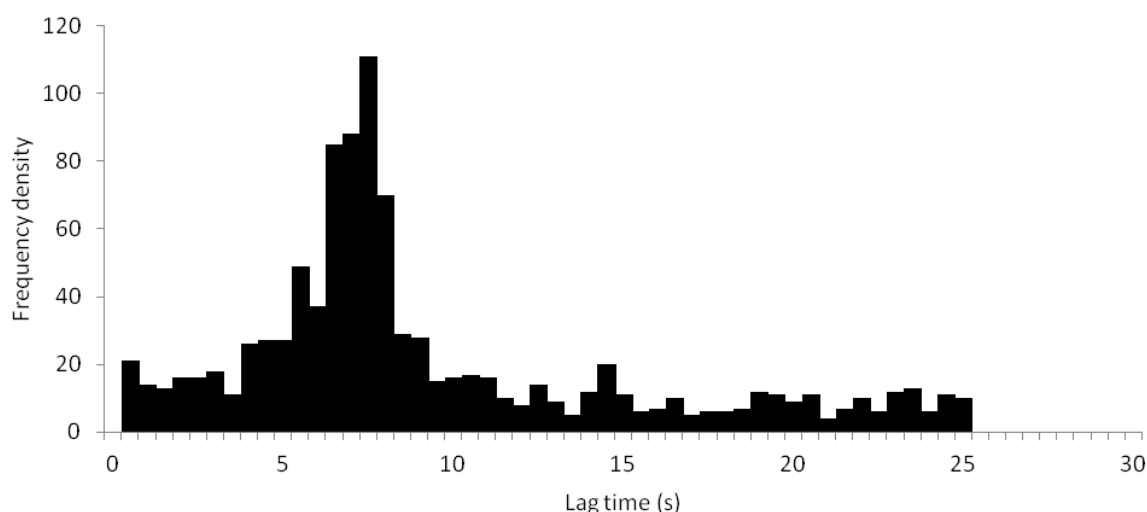


Figure 6.12, histogram of isoprene lag times calculated using the MAX method

## 6.5.2 Assessment of the underestimation of total flux through the loss of low frequency fluxes

The loss of low frequency fluxes caused by the rotation of coordinates in order to set the mean vertical wind velocity to zero for each 25 minute averaging period is assessed in Fig. 6.13. Sensible heat flux data were averaged over 50, 75, 100 and 125 minutes before coordinate rotation and plotted against the sum of two, three, four and five 25 minute coordinate rotated flux files respectively. The flux lost from the use of 25 minute averaging periods can be estimated from the gradient of the fitted line between the two fluxes. Eddies with a time period between 25 and 125 minutes were shown to carry an additional 2.8 % of the sensible heat flux. Therefore assuming that the frequency of VOC and sensible heat fluxes are comparable, 1.0-3.6 % of the VOC flux is lost by limiting the averaging period to 25 minutes.

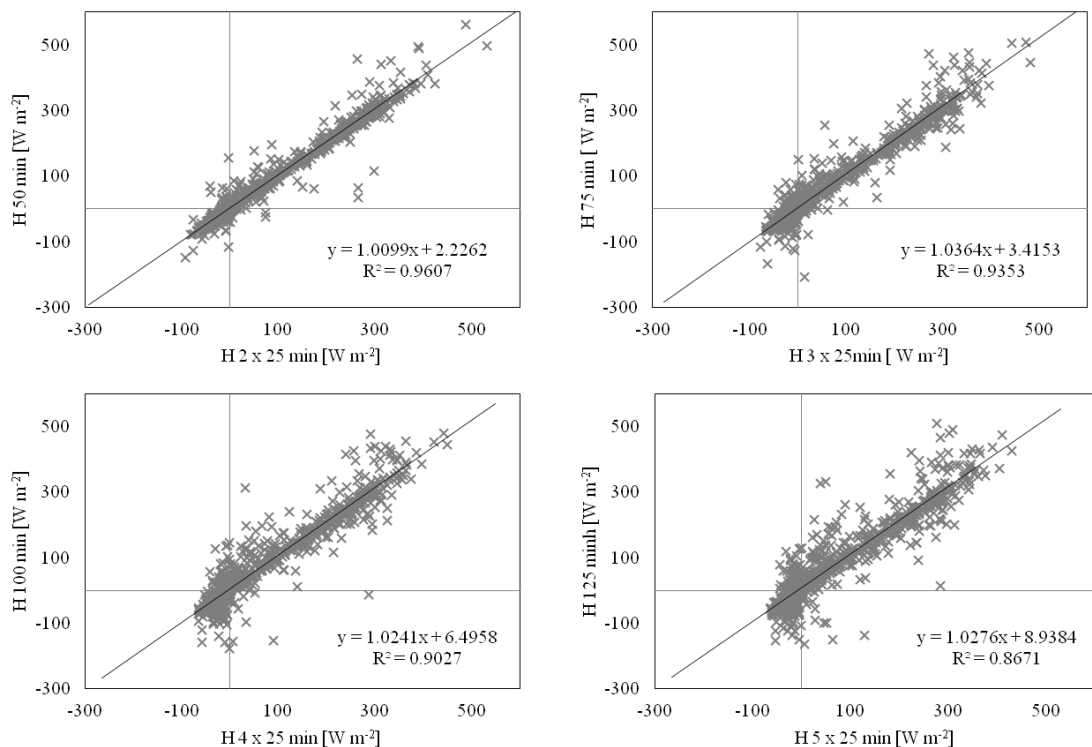


Figure 6.13. Plots of sensible heat flux ( $H$ ) determined over differing averaging times during the intensive field campaign at Bosco Fontana. Solid line represents the best linear fit.

### 6.5.3 The uncertainty caused by disjunct eddy covariance

The uncertainty caused by disjunct eddy covariance was estimated by comparing the sensible heat flux ( $H$ ) calculated using eddy covariance with  $H$  calculated using temperature measurements taken every 4.9 s. Fig. 6.14 shows the correlation between  $H$  measured using eddy covariance and disjunct eddy covariance, as is shown the uncertainty introduced by disjunct sampling is 0.17 %.

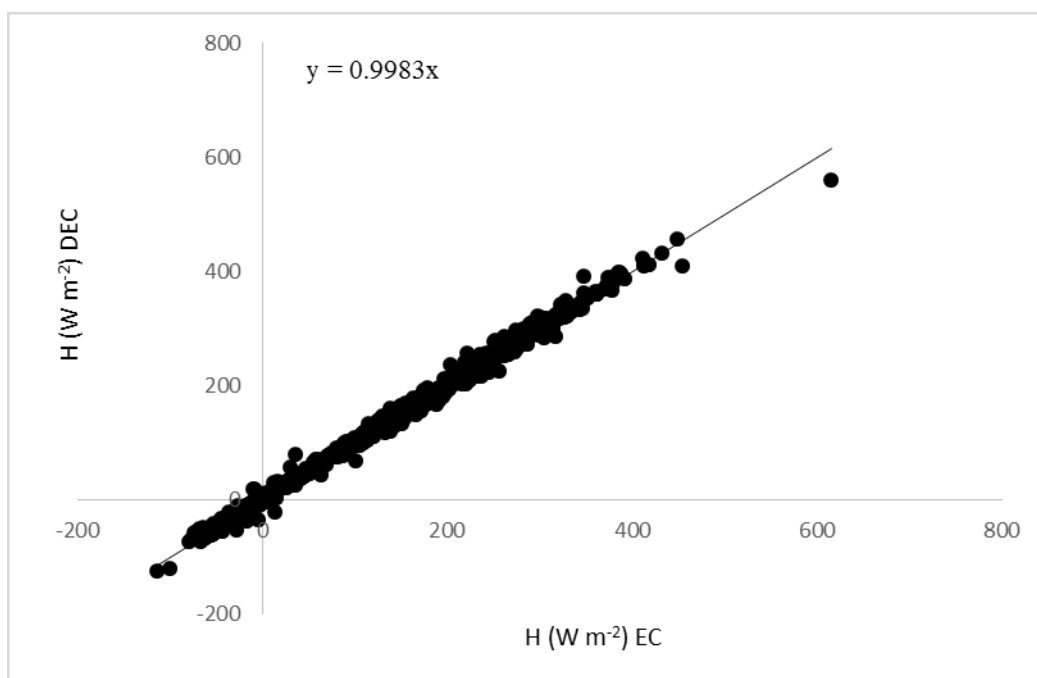


Figure 6.14. Sensible heat flux calculated ( $H$ ) calculated using eddy covariance (EC) and disjunct eddy covariance (DEC).

### 6.5.4 Flux quality assessment

Each 25 min VOC flux file calculated from the PTR-MS data using the virtual disjunct eddy covariance (vDEC) method was subjected to three quality tests, each performed independently (Langford et al., 2010a). Flux files were flagged if they the

mean frictional velocity over the 25 min averaging period dropped below  $0.15 \text{ m s}^{-1}$ , if they dropped below the limit of detection (Wienhold et al., 1994) or if they failed a stationarity test (Foken and Wichura, 1996). The percentage of flux files passing or failing these tests is summarised in Table 6.7 for each compound measured. In addition the percentage of the flux footprint falling outside the forest was assessed for each flux file with 26 % of files having > 25 % of flux from outside the forest area.

Table 6.7. Summary of flux quality assessment test results

Compound	Turbulence test failed ( $u_* < 0.15 \text{ m s}^{-1}$ )	25 minute Limit of detection test failed ( $F < \text{LOD}$ )	Stationarity test fail ( $\Delta s > 60\%$ )	Passed all tests
Methanol ( $m/z$ 33)	29 %	60 %	6 %	25 %
Acetaldehyde ( $m/z$ 45)	29 %	74 %	3 %	18 %
Acetone ( $m/z$ 59)	29 %	82 %	3 %	11 %
Acetic acid ( $m/z$ 61)	29 %	70 %	7 %	14 %
Isoprene ( $m/z$ 69)	29 %	36 %	2 %	50 %
MVK + MACR ( $m/z$ 71)	29 %	78 %	3 %	15 %
MEK ( $m/z$ 73)	34 %	85 %	1 %	7 %
Monoterpenes ( $m/z$ 81)	34 %	74 %	0 %	19 %

### 6.5.5 The effect of the tower on atmospheric flow

The measurement tower was a large structure so could conceivably impact on atmospheric flow and therefore flux measurements. In order to assess the impact of the tower on flux files  $\theta$ , the rotation angle used to realign measurements of  $u$  and  $w$

was plotted against wind direction (Fig. 6.15, top). The measurement tower located to the south east of the sonic anemometer does not appear to significantly affect  $\theta$ .

The effect of wake turbulence from the tower on the flux measurements was assessed using the method developed by Foken (2004). The integral turbulence statistics of the vertical wind velocity ( $\sigma_w/u^*$ , the standard deviation of the vertical wind velocity normalised by the friction velocity) of each flux file were compared with  $\sigma_w/u^*$  calculated for an ideal set conditions. The percentage difference between the measured and modelled data was then used to assess the overall data quality. This percentage difference plotted against wind direction is displayed in Fig. 6.15 (bottom). As can be seen the wind direction has little effect on the percentage difference indicating that the tower does not impact upon the flux measurements.

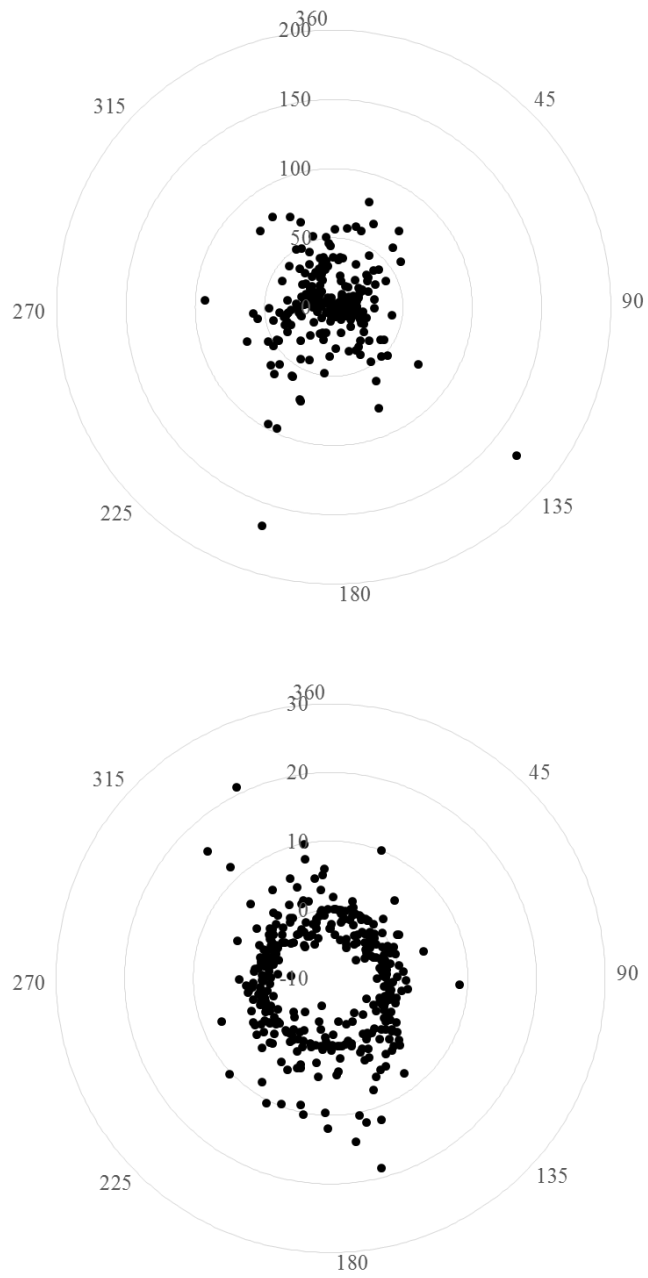


Figure 6.15 Wind rose plots showing the effect of wind direction ( $^{\circ}$ ) on the rotation angle ( $\theta$ ) required to set  $w$  to zero (top) and the % difference between the measured and modelled turbulence statistic (bottom).

### 6.5.6 Leaf surface temperature

The leaf surface temperature was estimated by extrapolation of ambient temperature using the resilience approach described by Nemitz *et al.* (2009). Fig. 6.16 shows the diurnal patterns of average ambient and leaf surface temperature. At night average leaf surface temperature was found to be approximately 2 °C below the average ambient air temperature, during the day average leaf surface temperature peaked approximately 10 °C above the average ambient air temperature.

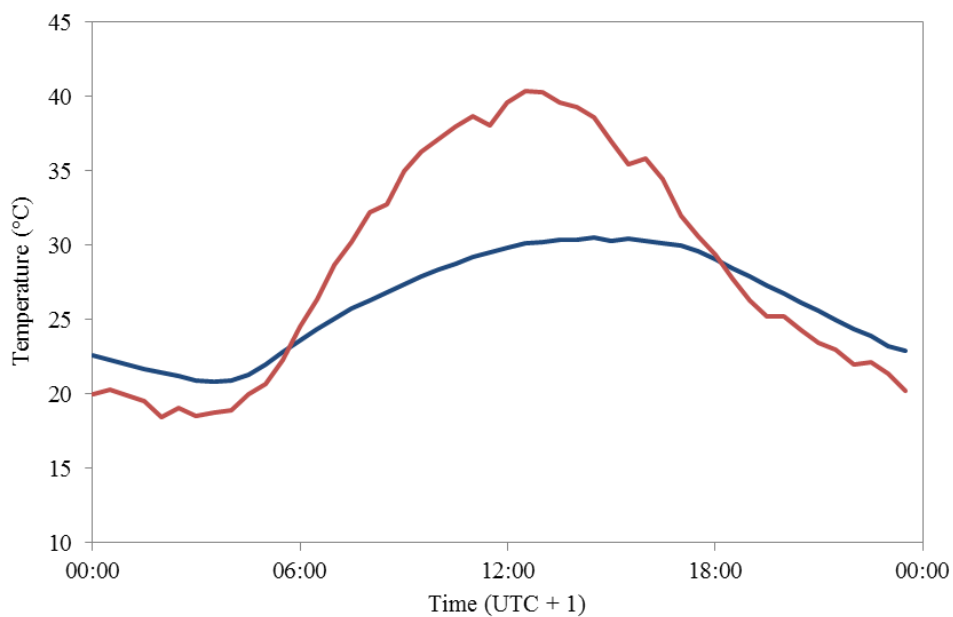


Figure 6.16, the diurnal pattern of average ambient temperature recorded 4 m above the canopy (blue) and leaf surface temperature (red).

### 6.5.6 Discussion of flux measurements

The fluxes and mixing ratios of the 8 masses monitored using the PTR-MS instrument during the field campaign at Bosco Fontana are discussed in more detail below.

### **Methanol ( $m/z$ 33)**

The mass spectral peak at  $m/z$  33 is commonly assigned to methanol (Misztal et al., 2011, Rinne et al., 2005) and published GC-PTR-MS measurements did not reveal any other significant contribution to this mass (de Gouw and Warneke, 2007). Here  $m/z$  33 has been assigned to methanol, there may be some contribution to  $m/z$  33 the  $O_2H^+$  cluster ion but this should be removed in the background subtraction.

Methanol emission is of interest to atmospheric science and has been shown to have a significant effect on tropospheric oxidants (Tie et al., 2003). However, uncertainties in surface emission estimates result in significantly different model predictions of atmospheric oxidants (Jacob et al., 2005; Millet et al., 2008; Tie et al., 2003). Methanol fluxes have been recorded above temperate woodland (Karl et al., 2003; Park et al., 2013; Rinne et al., 2007; Spirig et al. 2005) and agricultural ecosystems (Custer and Schade 2007; Ruuskanen et al., 2011). The methanol mixing ratios recorded over the course of this study are displayed in Fig. 6.17. Methanol was the most abundant compound recorded during the campaign with a mean mixing ratio of 6.2 ppbv over the campaign which is comparable to the results obtained by Sprig et al. (2005) above a mixed European deciduous forest. The diurnal profile of the methanol mixing ratio is shown in Fig. 6.17, it can be seen that mixing ratios are stable through the night at ca. 7 ppbv and drop to a low of ca. 5 ppbv in the mid-afternoon, most probably caused by expansion of the planetary boundary layer. The flux of methanol peaked at  $0.49 \text{ mg m}^{-2} \text{ h}^{-1}$  with a mean day-time flux of  $0.03 \text{ mg m}^{-2} \text{ h}^{-1}$  (Fig. 6.5). Methanol deposition was observed in the mornings followed by a rapid increase in methanol emission in the late morning peaking in the early afternoon, a similar emission pattern of morning deposition followed by afternoon emission was observed

by Langford et al. (2010a) and Misztal et al. (2011) above tropical rain forest and oil palms in South East Asia.

Biogenic methanol emission stems from a number of sources the largest of which is the demethylation of pectin in the primary cell walls (Galbally and Kirstine, 2002; Fall 2003). The strong temperature dependence of emissions reported previously (Hayward et al., 2004; Custer and Schade, 2007) indicates enzymatically driven emission or release from stored pools (inside the leaf or in water on the leaf surface). However, this was not observed in this study (data not shown suggesting that emission directly resulting from the enzymatically controlled demethylation of pectin is unlikely to be the sole source of methanol at this site. Other possible sources of methanol include emissions from decaying biomatter (Warneke et al., 1999; Grey et al., 2010) and as a result of herbivore feeding on the local vegetation and other wounding events (von Dahl et al., 2006; Arneth and Niinemets, 2010).

As a result of its low Henry's law constant methanol can be lost from atmosphere through precipitation, wet deposition and dry deposition (Riemer et al., 1998; Seco et al., 2007). While the rain immediately preceding measurements and on the 6<sup>th</sup> of July corresponded with a period of lower methanol mixing ratios no drop was observed immediately following rainfall. This suggested that lower methanol mixing ratios were not caused by the rain event but by air mass change prior to the rain itself as shown by Schade and Goldstein (2006). There is also evidence (Asensio et al., 2007) that soil may act as a sink of bVOCs, this may therefore also be a contributing factor to the methanol deposition observed in the mornings but from our findings it is

impossible to determine whether the sink driving the downwards flux was the soil, plant surfaces (wet or dry), the stomata or a combination of the above.

### **Acetaldehyde ( $m/z$ 45)**

The signal measured at  $m/z$  45 was attributed to acetaldehyde, while there may be a small contribution at this nominal mass from  $\text{CO}_2$  this was corrected for by background subtraction. It has been reported that acetaldehyde may be formed as an artefact following the reaction of ozone with impurities in the inlet line (de Gouw and Warneke, 2007) but no correlation was observed between ozone and acetaldehyde so this is not thought to be a significant source of acetaldehyde in these measurements.

Together with formaldehyde, methanol and acetone, acetaldehyde is one of the major oxygenated volatile organic compounds in the atmosphere and plays a significant role in atmospheric chemistry (Andrews et al., 2012; Millet et al., 2010). Acetaldehyde emission has previously been reported from woodland (Karl et al., 2002; Karl et al., 2003) and grassland (Custer and Schade, 2007; Ruuskanen et al., 2011), and the close proximity of the forest at Bosco Fontana to urban areas means that a contribution from anthropogenic sources to the observed ambient concentrations is also likely (Langford et al., 2009; Langford et al., 2010b). Acetaldehyde mixing ratios above the Bosco Fontana nature reserve peaked at 3.4 ppbv from a mean value of 1.5 ppbv, a time series of acetaldehyde mixing ratios is displayed in Fig. 6.17. The acetaldehyde daily profile, shown in Fig. 6.3, shows a stable night time mixing ratio of ca. 1.5 ppbv dropping to ca. 1 ppbv in the mid-to-late afternoon. The daily mean acetaldehyde flux is displayed in Fig. 6.5. While the peak acetaldehyde flux was recorded at  $0.44 \text{ mg m}^{-2} \text{ h}^{-1}$  the daily maximum was usually ca  $0.12 \text{ mg m}^{-2} \text{ h}^{-1}$ . The daily flux profile shows

that emission fluxes increased until the early afternoon before stabilizing and then decreasing to zero in the evening. This represents a lower emission flux than reported previously from both a pine canopy (Rinne et al., 2007) and mixed forest (Karl et al., 2003). This may be related to the relatively small area of the forest at Bosco Fontana as the surrounding farmland is unlikely to contribute significantly to the acetaldehyde flux (Custer and Schade, 2007).

Millet et al. (2010) recently used the GEOS-Chem atmospheric chemistry model to identify acetaldehyde sources and sinks, identifying hydrocarbon oxidation as the largest acetaldehyde source. Both isoprene and monoterpenes have been identified as acetaldehyde precursors (Lee et al., 2006; Luecken et al., 2012), no correlation was seen between acetaldehyde and isoprene mixing ratios over the canopy at Bosco Fontana but a weak correlation ( $R^2 = 0.27$ ) was observed between acetaldehyde and monoterpene mixing ratios. As well as formation from hydrocarbon oxidation, acetaldehyde is also directly emitted by plants in response to wounding (Brilli et al., 2011; Loreto et al., 2006) and via ethanolic fermentation in leaves and roots subject to anoxic conditions (Fall, 2003; Seco et al., 2007; Winters et al., 2009). In addition to emission from plants Schade and Goldstein (2001) also determined that soil and litter emission of acetaldehyde contributed significantly to the canopy-scale flux. As well as acting as a source of acetaldehyde into the atmosphere it has been shown that some tree species may act as an acetaldehyde sink at high ambient concentrations (Rottenberger et al., 2005; Seco et al., 2007). However, significant net deposition fluxes were not observed in this campaign.

The correlation between acetaldehyde and monoterpene mixing ratios indicates that there is likely to be a significant contribution from hydrocarbon oxidation to the acetaldehyde mixing ratio. However, the early afternoon peak in acetaldehyde flux coupled with no correlation with ozone suggests that the observed flux is predominantly of biogenic origin and most probably originates from ethanolic fermentation in leaves and soil.

### **Acetone ( $m/z$ 59)**

The mass spectral peak observed at  $m/z$  59 may be attributed to acetone or propanal. However, previous studies have indicated that contribution of propanal to this mass is low, 0-10 %, (de Gouw and Warneke, 2007) therefore  $m/z$  59 is here attributed to acetone.

Acetone is one of the most abundant oxygenated VOCs in the atmosphere and fluxes of acetone have been recorded over both anthropogenic (Langford et al., 2009; Langford et al., 2010b) and woodland environments (Karl et al., 2002; Karl et al., 2003). Acetone may also play a significant role in tropospheric chemistry as it can act as a source of HOx radicals in the upper troposphere leading to increased ozone production (Singh et al., 1995).

At the Bosco Fontana site acetone was the second most abundant volatile recorded after methanol, the mixing ratio remained constant throughout the day (Fig. 6.3) with a mean value of 3.2 ppbv. This value was higher than mixing ratios previously observed over hardwood forest where average mixing ratios have been reported in the range of 1.2-1.9 ppbv (Kalogridis et al., 2014; Karl et al., 2003) but comparable to

mixing ratios recorded over ponderosa pine (Goldstein and Schade, 2000). No significant acetone flux was observed at night, the flux appeared to increase in the afternoon but remained below the LoD throughout the day (Fig. 6.5). The mean day-time emission of  $0.03 \text{ mg m}^{-2} \text{ h}^{-1}$  was significantly lower than that observed by Karl et al. (2003) above a mixed hardwood forest.

Acetone is produced in the atmosphere through the oxidation of VOC precursors (Jacob et al., 2002; Lee et al., 2006). It is also emitted directly by plants into the atmosphere via a number of pathways, for example acetone is produced as a by-product of cyanogenesis and is then released into the atmosphere (Fall, 2003). Acetone may also be produced by acetoacetate decarboxylation in the soil (Fall, 2003). While Jacob et al. (2002) found emission from plant decay inconsistent with the seasonal cycle observed at European sites, Karl et al. (2003) reported emission from decaying biomass based on the emission factors calculated by Warneke et al. (1999). Enhanced acetone emission is also commonly reported following plant wounding events (Davison et al., 2008; Ruuskanen et al., 2011).

### **Acetic acid ( $m/z$ 61)**

The mass spectral peak observed at  $m/z$  61 was assigned to acetic acid, this is supported by de Gouw et al. (2003) who observed a correlation between  $m/z$  61 and acetic acid. This mass spectral peak, assigned to acetic acid, has been detected previously over a Mediterranean oak forest (Kalogridis et al., 2014).

The dominant source of acetic acid in the troposphere is the photochemical oxidation of biogenically emitted hydrocarbons (Glasius et al., 2001; Lee et al., 2006, Paulot et

al., 2011), and the direct emission of acetic acid into the atmosphere is comparatively low. However, acetic acid is emitted into the atmosphere by vegetation (Seco et al., 2007) with emission shown to be predominantly from tree species rather than crop plants (Kesselmeier et al., 1998). Emission is triggered by light (Kesselmeier et al., 1998; Staudt et al., 2000) and has been seen to correlate with transpiration (Kesselmeier et al., 1998; Seco et al., 2007). Acetic acid emission has also been recorded following stress events such as cutting (Ruuskanen et al., 2011) and herbivory (Bartolome et al., 2007; Llusà J. and Peñuelas, 2001; Scutareanu et al., 2002).

Field-scale emission of acetic acid from *Citrus sinensis* L. was observed by Staudt et al. (2000) in the noon and afternoon with deposition occurring in the early morning and night. Sinks of acetic acid include wet deposition and dry deposition with wet deposition the most important sink (Paulot et al., 2011). Photochemical losses are low as acetic acid may be considered as the final product of the photo-oxidation of many BVOCs. Kuhn et al. (2002) hypothesised that the primary control on acetic acid uptake by plants was the ambient mixing ratio and that a mixing ratio compensation point exists. When acetic acid mixing ratios are above this compensation point acetic acid will be absorbed by plants and when ambient mixing ratios drop below this point acetic acid will be emitted. Soil may also act as an acetic acid sink with uptake of acetic acid by a Mediterranean forest soil observed by Asensio et al. (2007). Deposition of acetic acid has been reported both over tropical forests (Karl et al., 2004; Langford et al., 2010a) and pine woodland (Karl et al., 2005), but fluxes of acetic acid over temperate deciduous woodland have yet to be reported.

During the Bosco Fontana campaign the acetic acid mixing ratios dropped in the early morning and remained relatively stable at ca. 1.5 ppbv throughout the day before rising again to ca. 2.5 ppbv, in the evening (Fig. 6.3). This likely corresponded to the changing height of the planetary boundary layer. In the latter half of the campaign a large increase in mixing ratio was observed at ca. 21:00 each day peaking at 14.9 ppbv on the 29<sup>th</sup> June (Fig. 6.17), these spikes correspond to a northerly wind direction but no source could be identified. The acetic acid flux was low but appears to show a pattern similar to that observed by Staudt et al. (2000) with deposition observed in the morning followed by emission in the afternoon (see Fig. 6.5). The change from acetic acid deposition to emission occurs when the ambient mixing ratio drops below ca. 1.9 ppbv which is within the compensation point range calculated by Kuhn et al. (2002) for tropical tree species but no conclusions can be drawn with confidence from such a weak flux.

### **Isoprene ( $m/z$ 69)**

Isoprene measurements using the PTR-MS mass spectral peak at  $m/z$  69 have been shown to agree with GC-MS measurements (Kuster et al., 2004). Isoprene fluxes recorded using PTR-MS have been reported previously from temperate forest canopies (for example Karl et al., 2003) and given the clear diurnal cycle of  $m/z$  69 fluxes and mixing ratios (Figs 6.3 and 6.5) coupled with the presence of two significant isoprene emitting species (*Quercus robur* and *Quercus rubra*). In the Bosco Fontana forest canopy  $m/z$  69 was assigned to isoprene. Interferences from furan, associated with biomass burning, as well as a number of BVOCS, in particular 2-methyl-3-buten-2-ol (MBO) have previously been reported at  $m/z$  69 (de Gouw and Warneke, 2007). While large concentrations of MBO have been observed over

coniferous forests in the USA (Goldan et al., 1993) emission has not been reported from European deciduous species and as biomass burning in the Italian summer is low a significant contribution from these species at  $m/z$  69 was considered to be unlikely.

Four tree species: *Carpinus betulus*, *Quercus robur*, *Quercus rubra* and *Quercus cerris* (Dalponte et al., 2007) make up ca. 75 % of the Bosco Fontana canopy, and of these only *Quercus robur* and *Quercus rubra* are known to emit isoprene (Pérez-Rial et al., 2009; Pier, 1995). Owing to isoprene emission only occurring during the day time coupled with a short atmospheric lifetime both mixing ratios and fluxes peaked in the afternoon, with fluxes peaking ca. 2 h before mixing ratios and dropping to zero at night. At the Bosco Fontana field site large day-to-day variations in the daily maximum isoprene mixing ratios (ppbv) and fluxes were observed due to changing environmental conditions. Isoprene mixing ratios (ppbv) peaked in the late afternoon with maximum values ranging from 0.8 ppbv to 4.8 ppbv (Fig. 6.17). The mean above canopy isoprene mixing ratio (1.1 ppbv) was comparable to that observed by Karl et al. (2003) above a North American hardwood forest but lower than the 1.2 ppbv observed by Kalogridis et al. (2014) above a French oak forest. This is to be expected given that 90 % of this canopy was made up of the isoprene emitting species *Quercus pubescens*. In addition, Bosco Fontana represents a relatively small area of isoprene emitting vegetation in mainly agricultural surroundings, with low isoprene emissions, possibly with the exception of some fields of poplar plantations. This implies that, as local isoprene emissions shut off at night, low-isoprene air is advected into the forest, giving rise to lower night-time concentration that found in extensive isoprene emitting areas.

The mean day-time isoprene flux,  $1.91 \text{ mg m}^{-2} \text{ h}^{-1}$ , was higher than that observed by Laffineur et al. (2011) over a European temperate mixed forest but lower than the flux reported by Spirig et al. (2005) and Kalogridis et al. (2014) over European mixed broadleaf and oak forests, respectively.

### **MVK and MACR ( $m/z$ 71)**

The structural isomers MVK and MACR are both detected at  $m/z$  71 when analysed using PTR-MS. Analysis using PTR-MS only enables compound identification on the basis of nominal mass so it is not possible to separate these species, and for this reason together with their common chemical origin, they will be treated together here. Previous studies have shown good agreement between PTR-MS and GC-MS measurements of MVK+MACR (de Gouw et al., 2003) although a significant contribution from crotonaldehyde at this mass has also been reported (Karl et al., 2007).

MVK and MACR are the main products formed following the first stage of isoprene oxidation in the atmosphere (Atkinson and Arey 2003a), accounting for 80 % of the carbon. Isoprene oxidation predominantly occurs via reaction with OH during the day and with  $\text{NO}_3$  at night with a relatively small contribution from ozone (Monks et al., 2009). It has been proposed that isoprene oxidation to MVK and MACR may occur within the plant (Jardine et al., 2012; Llusà et al., 2011) as well and the atmosphere. MACR can also be directly produced within plants as a byproduct in the production of cyanogenic glycosides (Fall, 2003). Once formed MVK and MACR may undergo further atmospheric oxidation and photochemical reactions (Millet et al., 2010; Atkinson and Arey, 2003b) or be deposited onto the canopy (Karl et al., 2010).

Fluxes and mixing ratios of MVK and MACR have previously been reported over deciduous forests (Apel et al., 2002; Kalogridis et al., 2014; Spirig et al., 2005). Above the canopy of the Bosco Fontana natural reserve a positive flux of MVK + MACR (Fig. 6.5) was observed peaking in the early afternoon with a day-time mean flux of  $0.05 \text{ mg m}^{-2} \text{ h}^{-1}$ , suggesting significant within canopy oxidation of isoprene. This value is comparable to that observed by Spirig et al. (2005) over a European deciduous forest. The flux of MVK + MACR dropped below the limit of detection at night which was expected as isoprene mixing ratios fell to ca. 0 ppb overnight (Fig. 6.3). As with previous campaigns over European deciduous forest no clear evidence for deposition was observed (Kalogridis et al., 2014; Spirig et al., 2005), this is in contrast to measurements over more remote tropical forests where deposition is usually reported (Karl et al., 2004; Langford et al., 2010a; Misztal et al., 2011). This suggests that deposition of these species to the forest canopy is low and that these species are lost through atmospheric transportation or undergo further reaction prior to being deposited. At the Bosco Fontana natural reserve, this is likely to be driven by the high oxidative capacity of the Po valley atmosphere. The mean MVK and MACR mixing ratio observed was 0.51 ppbv.

### **MEK ( $m/z$ 73)**

The mass observed at  $m/z$  73 was assigned here to methyl ethyl ketone (MEK), however the isomeric compound butanal could also contribute to this signal (Table 6.1). Previous studies have shown a quantitative agreement between PTR-MS and GC analysis of MEK at  $m/z$  73 (Davison et al., 2008; de Gouw et al., 2006) but

measurement is complicated by the humidity dependent background contribution from  $\text{H}_3\text{O}^+(\text{H}_2\text{O})_3$ .

MEK can be emitted directly from some plant species as a by-product of hydrogen cyanide production from lotaustralin (Fall, 2003). MEK emission has predominantly been reported following plant wounding events such as grass cutting (Davison et al., 2008; Karl et al., 2001; Llusà et al., 2011) and insect herbivory (Peñuelas et al., 2005; Pinto et al., 2007). As well as direct emission MEK may also be formed photochemically (Luecken et al., 2012). MEK has been recorded over oak (Kalogridis et al., 2014) and coniferous forests (Müller et al., 2006), with mixing ratios peaking at 0.15-0.51 ppbv and 1.8 ppbv respectively. Above the canopy at Bosco Fontana MEK mixing ratios fell between these values peaking at 1.0 ppbv (Fig. 6.3). MEK mixing ratios peaked at night before dropping to a low in the late afternoon, most likely caused by dilution in the expanding planetary boundary layer. Fluxes of MEK have not been reported in the literature and few of the flux files from this campaign passed the quality tests, the daily averaged flux (Fig. 6.5), however, showed a low emission of MEK in the afternoon with a mean day-time flux of  $0.02 \text{ mg m}^{-2} \text{ h}^{-1}$ .

### **Monoterpenes (*m/z* 81)**

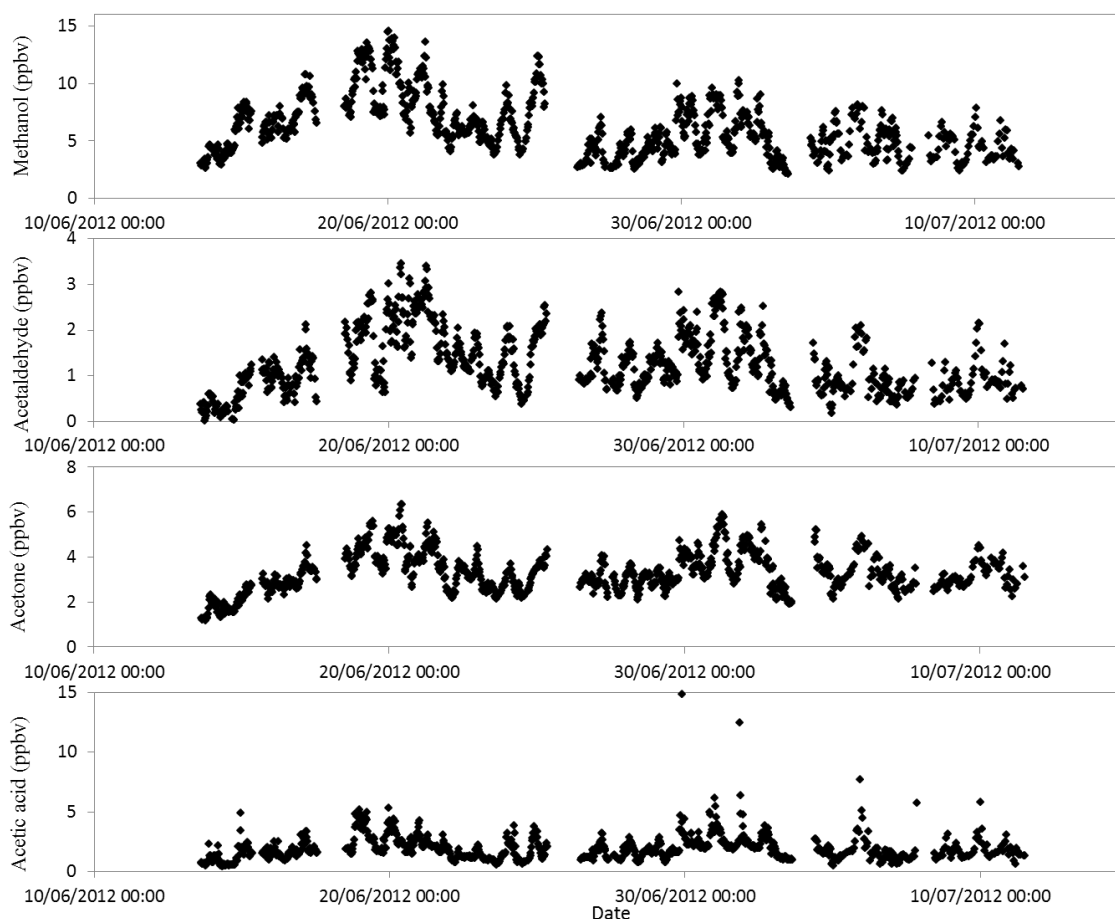
Measurement of monoterpenes using PTR-MS is complicated by the differing fragmentation patterns of the numerous monoterpene species, however monoterpenes are commonly measured using PTR-MS at *m/z* 137 and 81 corresponding to the protonated parent ion and a principle fragment ion respectively (de Gouw and Warneke, 2007). Owing to poor instrumental sensitivity at higher atomic mass units (amus) the monoterpene fluxes and mixing ratios reported here are calculated from

$m/z$  81. While there could be some contribution from sesquiterpene and hexenal fragment ions at this mass, previous studies have demonstrated that this signal can be assigned to monoterpenes (de Gouw et al., 2003; Rinne et al., 2005). Variability in the ratio between parent and fragment ions was limited by ensuring the  $E/N$  ratio was held constant throughout the measurements period.

Many plant species, including the four dominant species in the Bosco Fontana canopy, have been shown to emit monoterpenes (Isebrands et al., 1999; König et al., 1995; Owen et al., 2001; Pérez-Rial et al., 2009). Monoterpenes are emitted from plants both directly and from stored pools such as glandular trichomes and resin ducts (Maffei, 2010). Emission is driven by temperature (Tarvainen *et al.*, 2005) and also occurs as a response to both biotic (Copolovici et al., 2011; Peñuelas et al., 2005) and abiotic (Kaser et al., 2013; Llusà et al., 2002) stress. As well as emission from plants, low levels of monoterpene emission have also been reported from litter and soil (Gray et al., 2010; Hayward et al., 2001; Leff and Fierer, 2008).

Above the Bosco Fontana forest canopy monoterpene fluxes peaked in the early afternoon with a mean day-time flux of  $0.12 \text{ mg m}^{-2} \text{ h}^{-1}$  (Figs 6.4 and 6.5) which is comparable to the flux observed by Spirig et al. (2005) above a European mixed deciduous forest but much lower than those observed by Davison et al. (2009) over a macchia ecosystem in western Italy. As was observed by Spirig et al. (2005) the monoterpene flux dropped to ca.  $0 \text{ mg m}^{-2} \text{ h}^{-1}$  at night. Laffineur et al. (2011) detected a weak temperature dependent monoterpene flux at night over a mixed European forest, this discrepancy may be due to larger emission from monoterpenes stored in pools from the coniferous species present in the mixed forest. While monoterpene

deposition has previously been observed (Bamberger et al.2011) no net deposition was observed above the canopy at Bosco Fontana. The monoterpene mixing ratios followed a diurnal cycle with values peaking at ca. 0.2 ppbv at mid-day, dropping to ca. 0.18 ppbv at night (Figs 6.3 and 6.4). The mean monoterpene mixing ratio observed (0.2 ppbv) was much higher than the 0.06 ppbv observed by Kalogridis et al. (2014) over a Mediterranean oak forest but were within the 0.13-0.30 ppbv range of values recorded by Davison et al. (2009) and comparable to the mixing ratios observed by Spirig et al. (2005).



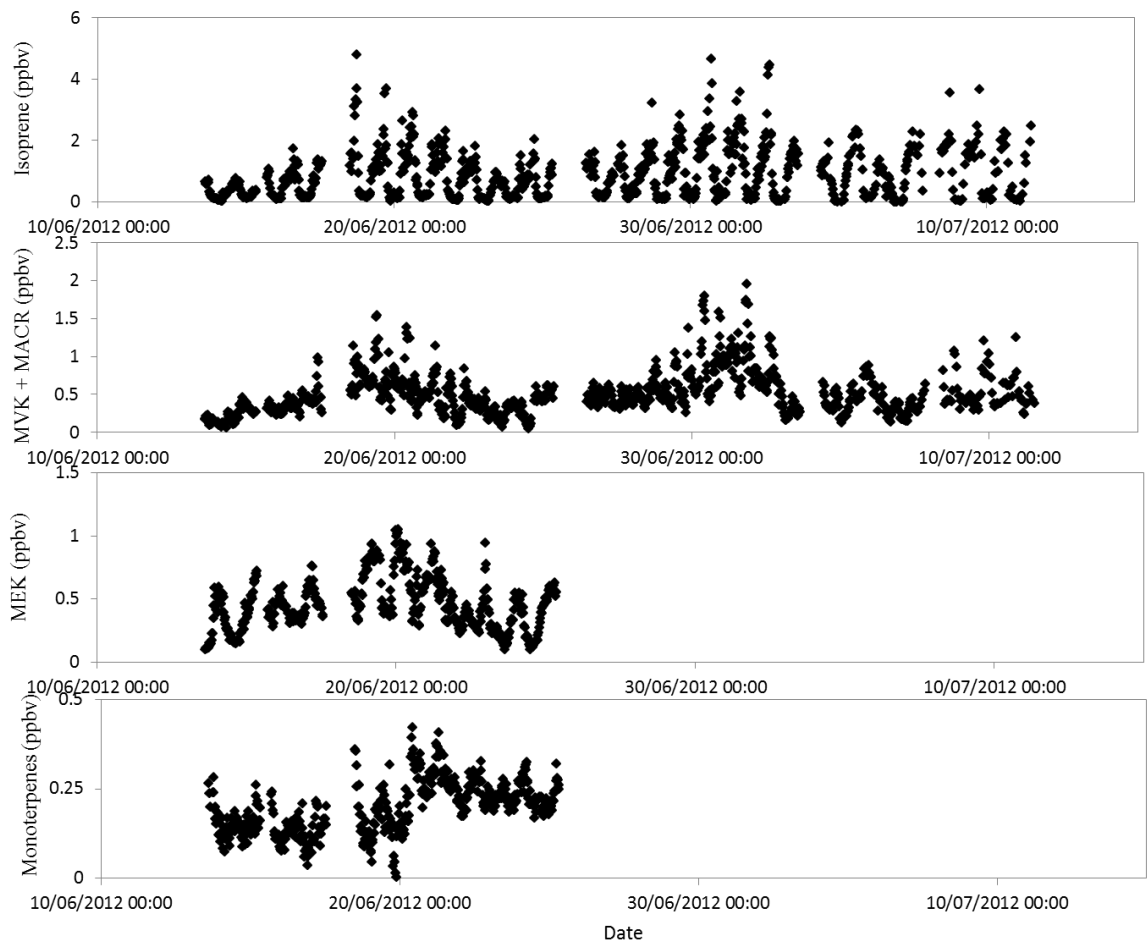


Figure 6.17. Time series of the volume mixing ratios of methanol, acetaldehyde, acetone, acetic acid, isoprene, MVK & MACR, MEK and monoterpene (calculated from fragment at  $m/z$  81) measured at 4 m above the forest canopy

## Chapter VII

### Conclusions

Biogenic volatile organic compounds (bVOCs) play important roles in many ecological systems, including the attraction of pollinators (Dudareva et al., 2006; Pichersky and Gershenzon, 2002), seed dispersal (Dudareva et al., 2006), mitigation of abiotic stresses (Loreto, Schnitzler, 2010; Sharkey et al., 2008), within plant communication (Heil and Ton, 2008), plant–plant communication (Baldwin et al., 2006) and the direct (Vancanneyt et al., 2001) and indirect (Heil, 2008) defence of plants against herbivores. The impact of ground-level ozone, an important and ubiquitous air pollutant, on these systems is now receiving increased attention (Blande et al., 2014; Pinto et al., 2010). However, many aspects of the relationship between ozone and plant signalling remain unknown or unclear, and it was the intention of this study to provide further information on these interactions. The main findings of the work presented in this thesis are, briefly:

#### *Chapter III*

- The new and emerging analytical method of selective reagent ionisation – time of flight – mass spectrometry (SRI-ToF-MS) allows the better detection and identification of a range of bVOCs than does, for example, the more established method of quadrupole PTR-MS. The principal mass spectral fragment ions formed following the ionisation of 10 large organic compounds with  $\text{H}_3\text{O}^+$ ,  $\text{NO}^+$ ,  $\text{O}_2^+$  and  $\text{Kr}^+$  with a at a range of drift tube energies (85-225 Td for  $\text{H}_3\text{O}^+$ ,  $\text{NO}^+$ ,  $\text{O}_2^+$  and 45-115 Td for  $\text{Kr}^+$ ) are reported.

- SRI-ToF-MS enables the separation of two isomeric large organic compounds.

#### *Chapter IV*

- Ozone fumigation of *Brassica napus* leaves at environmentally-realistic mixing ratios (ca. 100 ppbv) does not affect bVOC emission from below ground parts of the plant compared with those observed when the plant is exposed to ozone-free clean air.
- Ozone fumigation of *B. napus* leaves at environmentally-realistic mixing ratios (ca. 100 ppbv) causes the emission of over 20 oxygenated compounds and a drop in monoterpene and sesquiterpene emissions compared with those observed when the plant is exposed to ozone-free clean air.
- The decrease in sesquiterpene emissions observed during ozone fumigation is greater than could be accounted for by gas phase ozonolysis of the sesquiterpenes.
- The emission of reactive carbon from *B. napus* leaves is almost doubled during ozone fumigation compared with that observed when the plant is exposed to ozone-free clean air.

#### *Chapter V*

- Ozone disrupts *Myzus persicae* host location in a *B. napus* - *M. persicae* - *Adalia bipunctata* larvae model system under controlled conditions in a laboratory experiment.
- Ozone disrupts tritrophic signalling in a *B. napus* - *M. persicae* - *A. bipunctata* model system under controlled conditions in a laboratory experiment by inhibiting the location of prey by *A. bipunctata* larvae.

- This disruption of plant–insect signalling is caused by degradation of bVOCs through ozonolysis following their emission from the leaf surface and not by changes in bVOC emission caused by abiotic stress.

## *Chapter VI*

- The fluxes of bVOCs measured above a mixed oak and hornbeam forest in Italy during a field campaign in the summer of 2012 were dominated by isoprene. However the mixing ratios recorded 4 m above the canopy were dominated by methanol.
- Isoprene and monoterpene fluxes recorded using proton transfer reaction – mass spectrometry (PTR-MS) agreed well with those recorded using proton transfer reaction – time of flight – mass spectrometry PTR-ToF-MS).
- Up–scaling leaf level isoprene emission rates to the canopy scale leads to an under-estimation of isoprene flux compared with those observed by the method of eddy covariance but captures variation in the above-canopy flux better than the use of a canopy scale bulk emission factor.

### **7.1 General conclusions**

PTR-MS is widely used for bVOC measurements where a high time resolution is required, for example flux measurements (Davison et al., 2008; Langford et al., 2010a; Müller et al., 2010) and monitoring plant wounding events (Peñuelas et al., 2005; van Dam et al., 2012). However, due to its quadrupole mass analyser the PTR-MS operates only at unit mass resolution therefore providing little structural information. The high mass resolution of the PTR-ToF-MS ( $> 5000 \text{ m}/\Delta\text{m}$ , Jordan et al., 2009a) enables the identification of the molecular formula of mass spectral

fragment ions and therefore the separation of isobaric compounds. In this thesis canopy scale flux measurements of isoprene and monoterpenes made using PTR-MS and PTR-ToF-MS were directly compared. Isoprene fluxes showed very good agreement between the methods and monoterpene fluxes showed good agreement, despite the lower sensitivity of the PTR-MS compared with the time-of-flight method at this mass.

The newly emerging technology of SRI-ToF-MS (Jordan et al., 2009b; Sulzer et al., 2012a) provides more detailed analyte structural information than can be obtained using PTR-ToF-MS. Here we investigated the ionisation of a range of complex organic molecules using  $\text{H}_3\text{O}^+$ ,  $\text{NO}^+$ ,  $\text{O}_2^+$  and  $\text{Kr}^+$  demonstrating that switching between reagent ions enabled rapid separation of isomeric compounds. SRI-ToF-MS also facilitates the identification of analyte functional groups. For example  $\text{NO}^+$  ionises aldehydes through hydride ion abstraction and ketones via clustering reactions (Španěl et al., 1997b) thereby allowing the functional group to be identified. However, the separation of large classes of molecules with the same functionality, for example monoterpenes and sesquiterpenes is still not possible. The identification of these species still requires a chromatographic method such as GC-MS or the recently developed fastGC-PTR-ToF-MS (Materić et al., 2015).

In the work presented here SRI-ToF-MS was used for the first time to record bVOC emission from the economically-important crop *B. napus* (rapeseed) from both above-ground and below-ground parts, before and during ozone fumigation. This enabled the monitoring of volatile emissions at high time resolution and the identification of analyte functionality. As reported by van Dam et al. (2012) volatile emission from the

roots were shown to be dominated by the sulfur compounds methanethiol, dimethyl sulfide, methyl thiocyanate, methanedithiol and dimethyl disulphide. Following ozone fumigation of the leaves (at ca. 100 ppbv) no change in volatile emissions from the roots were observed. This is in contrast to the effects of biotic stress, where it has been previously shown that the addition of a leaf herbivore can effect bVOC emission from below ground biomass (Rasmann and Turlings, 2007). Ozone fumigation of the plant leaves caused the immediate increase in the emission rates of ca. 20 oxygenated compounds as well as a 17 and 82 % decrease in the emissions of monoterpenes and sesquiterpenes respectively from the above-ground biomass. The decrease in monoterpene emissions was shown to be due to gas-phase reactions with the OH radical and the decrease in sesquiterpene emissions to ozonolysis reactions, both in the gas phase and on the plant and/or chamber surfaces. As sesquiterpenes have been shown to play an important role in a number of tritrophic systems (Kappers et al., 2005; Kessler and Baldwin 2001) it was hypothesised that ozone could disrupt tritrophic signalling in a model system.

The impact of ozone on tritrophic signalling was investigated using a *B. napus* – *M. persicae* – *A. bipunctata* larvae (rapeseed – green peach aphid – two-spotted ladybird larvae) model system. In clean air, *M. persicae* was shown to successfully identify a host plant and *A. bipunctata* larvae could locate a *M. persicae* infested plant. Following ozone fumigation at levels typical in polluted summertime ambient air during photochemical smog episodes (ca. 100 ppbv) it was shown that both herbivore host location and tritrophic signalling were disrupted. In order to identify whether this effect was caused by a change in bVOC emissions from the plant due to oxidative stress or degradation of the bVOCs between the plant and insect the experiment was

repeated adding ozone after the plant. In this second experiment herbivore host location and tritrophic signalling were again shown to be disrupted. This effect is summarised in Fig. 7.1, where tritrophic signalling in an unpolluted system (clean air) is shown using green arrows and signalling in the presence of the anthropogenic pollutant  $\text{NO}_x$  ( $\text{NO}$  and  $\text{NO}_2$ ) is shown using blue arrows.  $\text{NO}_x$  acts as an ozone precursor leading to ozone formation and therefore signal disruption and a breakdown in tritrophic signalling.

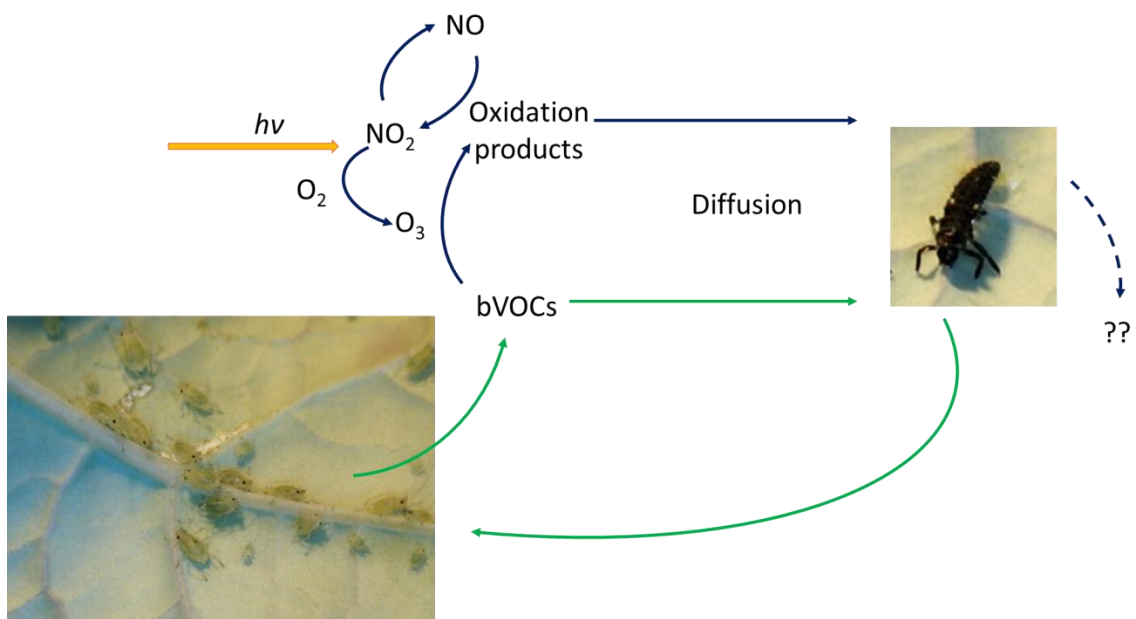


Figure 7.1. The effect of anthropogenic pollution by the oxides of nitrogen on signalling in the *B. napus* – *M. persicae* – *A. bipunctata* larvae tritrophic system. Green arrows represent signalling in unpolluted air and blue lines represent signalling in the presence of the anthropogenic pollutant  $\text{NO}_x$  ( $\text{NO}$  and  $\text{NO}_2$ ) which reacts with volatile organic compounds in the presence of sunlight to form ozone. This ozone, not present at mixing ratios above ~35-40 ppbv in clean air (Royal Society, 2008), can react with the emitted bVOCs, disrupting communications in this tritrophic system.

Previous investigations into the effects of ozone on tritrophic signalling did not show a detrimental effect of ozone. However these studies focussed on the emissions of relatively ozone-resistant compounds such as methyl salicylate and benzyl cyanide and hence any signalling provided by these compounds is not inhibited by elevated ozone concentrations (Pinto et al., 2007a; Pinto et al., 2007b). However, the work presented here, together with earlier studies into the effects of ozone on plant–plant and plant–pollinator communications (Blande et al., 2010; Farre-Armengol et al., 2015) have shown that ozone can disrupt plant signalling, even at mixing ratios commonly observed in polluted summertime air.

In Chapter V, it was shown that the observed disruption to tritrophic signalling is likely to be caused by the chemical reactions of ozone with the signalling compounds ( $\beta$ -farnesene) occurring between the point of emission at the plant leaf surface and the receptor insects. Future work must therefore focus on the identification of the compounds involved in plant signalling, with tritrophic systems reliant upon reactive bVOCs as communication media likely to be susceptible to disruption during high ozone events. Further investigations are also needed to identify whether other oxidative species in the atmosphere such as the hydroxyl and nitrate radicals disrupt plant - insect systems in the same way. Finally it is important that field scale experiments, akin to those reported by Pinto et al. (2008), are carried out to determine whether the breakdown in tritrophic signalling observed in laboratory experiments during the work reported here also occurs at the crop or ecosystem scale in the field.



# Bibliography

Acton W. J. F., Schallhart S., Langford B., Valach A., Rantala P., Fares S., Carriero G., Tillmann R., Tomlinson S. J., Dragosits U., Gianelle D., Hewitt C. N. and Nemitz E.: Canopy-scale flux measurements and bottom-up emission estimates of volatile organic compounds from a mixed oak and hornbeam forest in northern Italy, *Atmospheric Chemistry and Physics*, 16, 7149-7170, 2016.

Acton W. J. F., Jud W., Ghirardo A., Wohlfahrt G., Hewitt C. N., Taylor J., and Hansel A.: The effect of ozone fumigation on the emission of biogenic volatile organic compounds (bVOCs) from *Brassica napus*, article in preparation, 2016.

Agarwal B., Petersson F., Jürschik S., Sulzer P., Jordan A., Märk T. D., Watts P. and Mayhew C. A.: Use of proton transfer reaction time-of-flight mass spectrometry for the analytical detection of illicit and controlled prescription drugs at room temperature via direct headspace sampling, *Analytical and Bioanalytical Chemistry*, 400, 2631-2639, 2011.

Agarwal B., Jürschik S., Sulzer P., Petersson F., Jaksch S., Jordan A. and Märk T. D.: Detection of isocyanates and polychlorinated biphenyls using proton transfer reaction mass spectrometry, *Rapid Communications in Mass Spectrometry*, 26, 983-989, 2012.

Ahuja I., Rohloff J. and Bones A. M.: Defence mechanisms of Brassicaceae: implications for plant-insect interactions and potential for integrated pest management. A review, *Agronomy for Sustainable Development*, 30, 311-348, 2010.

Andrews D. U., Heazlewood B. R., Maccarone A. T., Conroy T., Payne R. J., Jordan M. J. T. and Kable S. H.: Photo-tautomerization of acetaldehyde to vinyl alcohol: a potential route to tropospheric acids, *Science*, 337, 1203-1206, 2012.

Angelov D., O'Brien J. and Kavanagh P.: The syntheses of 1-(2-thienyl)-2-(methylamino) propane (methiopropamine) and its 3-thienyl isomer for use as reference standards, *Drug Testing and Analysis* 5(3), 145-149, 2011.

Anicich V. G.: An index of the literature for bimolecular gas phase cation-molecule reaction kinetics, Jet Propulsion Laboratory: California, USA, 2003.

Apel E.C., Riemer D.D., Hills A., Baugh W., Orlando J., Faloon I., Tan D., Brune W., Lamb B., Westberg H., Carroll M.A., Thornberry T. and Geron C.D.: Measurement and interpretation of isoprene fluxes and isoprene, methacrolein, and methyl vinyl ketone mixing ratios at the PROPHET site during the 1998 Intensive, *Journal of Geophysical Research*, 107, 4034, 2002.

Arneth A., Monson R. K., Schurgers G., Niinemets Ü. and Palmer P. I.: Why are estimates of global terrestrial isoprene emissions so similar (and why is this not so for monoterpenes)?, *Atmospheric Chemistry and Physics*, 8, 4605-4620, 2008.

Arneth A. and Niinemets Ü.: Induced BVOCs: How to bug our models? *Trends in Plant Science*, 15, 118–125, 2010.

Arroyo F. T., Moreno J., Daza P., Boianova L. and Romero F.: Antifungal activity of strawberry fruit volatile compounds against *Colletotrichum acutatum*, *Journal of Agricultural and Food Chemistry*, 55, 5701–5707, 2007.

Arshak K., Moore E., Lyons G. M., Harris J. and Clifford S.: A review of gas sensors employed in electronic nose applications, *Sensor Review*, 24(2), 181–198, 2004.

Asensio D., Peñuelas J., Filella I. and Llusià, J.: On-line screening of soil VOCs exchange responses to moisture, temperature and root presence, *Plant and Soil*, 291, 249-261, 2007.

Ashmore M. R.: Assessing the future global impacts of ozone on vegetation, *Plant, Cell and Environment*, 28, 949–964, 2005.

Atkinson R., Hasegawa D. and Aschmann S. M.: Rate constants for the gas-phase reactions of O<sub>3</sub> with a series of monoterpenes and related compounds at 296 ± 2 K, *International Journal of Chemical Kinetics*, 22, 871-887, 1990.

Atkinson R. and Arey J.: Gas-phase tropospheric chemistry of biogenic volatile organic compounds: a review, *Atmospheric Environment*, 37(2), 197–219, 2003a.

Atkinson R. and Arey J.: Atmospheric degradation of volatile organic compounds, *Chemical Reviews*, 103, 4605-4638, 2003b.

Aubinet M., Vesala T. and Papale D.: *Eddy covariance: A practical guide to measurement and data analysis*, Springer: Springer: Netherlands, 2012.

Baghi R., Durand P., Jambert C., Jarnot C., Delon C., Serça D., Striebig N., Ferlicoq M. and Keravec P.: A new disjunct eddy-covariance system for BVOC flux measurements – validation on CO<sub>2</sub> and H<sub>2</sub>O fluxes, *Atmospheric Measurement Techniques*, 5, 3119-3132, 2012.

Baldwin I. T., Halitschke R., Paschold A., von Dahl C. C. and Preston C. A.: Volatile signaling in plant-plant interactions: “Talking trees” in the Genomics Era, *Science*, 311, 812–815, 2006.

- Bamberger I., Hörtnagl L., Ruuskanen T.M., Schnitzhofer R., Müller M., Graus M., Karl T., Wohlfahrt G. and Hansel A.: Deposition fluxes of terpenes over grassland, *Journal of Geophysical Research*, 116, 1-13, 2011.
- Bari R. and Jones J. D. G.: Role of plant hormones in plant defence responses, *Plant Molecular Biology*, 69, 473-488, 2009.
- Bartolome J., Penuelas J., Filella I., Llusia J., Broncano M. J. and Plaixats J.: Mass scans from a proton transfer mass spectrometry analysis of air over Mediterranean shrubland browsed by horses, *Journal of Environmental Biology*, 28(4), 697–700, 2007.
- Bates D., Mächler M., Bolker B. and Walker S.: Fitting linear mixed-effects models using lme4, *Journal of Statistical Software*, 64(1), 2015, doi: 10.18637/jss.v067.i01.
- Beauchamp J., Wisthaler A., Hansel A., Kleist E., Miebach M., Niinemets Ü., Schurr U. and Wildt J.: Ozone induced emissions of biogenic VOC from tobacco: relationships between ozone uptake and emission of LOX products Volatile organic compound (VOC) emissions from tobacco, *Plant, Cell and Environment*, 28, 1334-1343, 2005.
- Benjamin M.T., Sudol M., Bloch L. and Winer A.M.: Low-emitting urban forests: A taxonomic methodology for assigning isoprene and monoterpene emission rates, *Atmospheric Environment*, 30(9), 1437-1452, 1996.
- Biermann T., Schwarze B., Zedler B. and Betz P.: On-site testing of illicit drugs: the use of the drug-testing device "Toxiquick", *Forensic Science International*, 143, 21-25, 2004.
- Bigi A., Ghermandi G. and Harrison R.M.: Analysis of the air pollution climate at a background site in the Po valley, *Journal of Environmental Monitoring*, 14, 552-563, 2011.
- Blake R. S., Monks P. S. and Ellis A. M.: Proton-transfer reaction mass spectrometry, *Chemical Reviews*, 109, 861–896, 2009.
- Blande J. D., Pickett J. A. and Poppy G. M.: A Comparison of semiochemically mediated interactions involving specialist and generalist *Brassica*-feeding aphids and the braconid parasitoid *Diaeretiella rapae*, *Journal of Chemical Ecology*, 33, 767-779, 2007.
- Blande J. D., Holopainen J. K. and Li, T.: Air pollution impedes plant-to-plant communication by volatiles, *Ecology Letters*, 13, 1172-1181, 2010.

Blande J. D., Holopainen J. K. and Niinemets Ü.: Plant volatiles in polluted atmospheres: stress responses and signal degradation, *Plant, Cell and Environment*, 37, 1892-1904, 2014.

Bleeker A. B. and Kende H.: Ethylene: A gaseous signal molecule in plants, *Annual Review of Cell and Developmental Biology*, 16, 1-18, 2000.

bluelight: <http://www.bluelight.ru/vb/forum.php> (accessed on 06.06.2013)

Brilli F., Ruuskanen T. M., Schnitzhofer R., Müller M., Breitenlechner M., Bittner V., Wohlfahrt G., Loreto F. and Hansel A.: Detection of plant volatiles after leaf wounding and darkening by proton transfer reaction “time-of-flight” mass spectrometry (PTR-TOF), *PIOS ONE*, 6(5), 1-12, 2011.

Brüggemann N. and Schnitzler J.-P.: Comparison of isoprene emission , intercellular isoprene concentration and photosynthetic performance in water-limited oak (*Quercus pubescens* Willd . and *Quercus robur* L.) saplings, *Plant Biology*, 4, 456–463, 2002.

Bruce T. J. A., Wadhams L. J. and Woodcock C. M.: Insect host location: A volatile situation, *Trends in Plant Science*, 10(6), 269–274, 2005.

Bruce T. J. A. and Pickett J. A.: Perception of plant volatile blends by herbivorous insects-finding the right mix, *Phytochemistry*, 72, 1605–1611, 2011.

Burba G.: Eddy covariance method for scientific, industrial, agricultural and regulatory applications. LI-COR Biosciences, Lincoln, USA.

Carslaw D. C. and Ropkins K.: Openair — an R package for air quality data analysis, *Environmental Modelling and Software*, 27-28, 52-61, 2012.

Casale J. F. and Hays P. A.: Ethylphenidate : An analytical profile, *Microgram Journal*, 8(2), 58-61, 2011.

Casale J. F. and Hays P. A.: The characterization of 6-(2-aminopropyl) benzofuran and differentiation from its 4-, 5-, and 7-positional analogues, *Microgram Journal*, 9, 61-74, 2012.

Cha D. H., Nojima S. and Hesler S. P.: Identification and field evaluation of grape shoot volatiles attractive to female grape berry moth (*Paralobesia viteana*), *Journal of Chemical Ecology*, 34, 1180–1189, 2008.

Chaves M. and Davies B.: Drought effects and water use efficiency: improving crop production in dry environments, *Functional Plant Biology*, 37, iii–vi, 2010.

- Claeys M., Graham B., Vas G., Wang W., Vermeylen R., Pashynska V., Cafmeyer J., Guyon P., Andreae M. O., Artaxo P. and Maenhaut W.: Formation of secondary organic aerosols through photooxidation of isoprene, *Science*, 303, 1173-1176, 2004.
- Cook S. M, Khan Z. R. and Pickett J. A.: The use of push-pull strategies in integrated pest management, *Annual Review of Entomology*, 52, 375-400, 2007.
- Copolovici L. and Niinemets Ü.: Flooding induced emissions of volatile signalling compounds in three tree species with differing waterlogging tolerance, *Plant, Cell and Environment*, 33, 1582–1594, 2010.
- Copolovici L., Kännaste A., Rimmel T., Vislap V. and Niinemets Ü.: Volatile emissions from *Alnus glutinosa* induced by herbivory are quantitatively related to the extent of damage, *Journal of Chemical Ecology*, 37, 18-28, 2011.
- Criegee R.: Mechanism of ozonolysis, *Angewandte Chemie International Edition in English*, 14(11), 745-752, 1975.
- Cui H., Su J., Wei J., Hu Y. and Ge F.: Elevated O<sub>3</sub> enhances the attraction of whitefly-infested tomato plants to *Encarsia Formosa*, *Scientific Reports*, 4, 5350, doi: 10.1038/srep05350.
- Custer T. and Schade G.: Methanol and acetaldehyde fluxes over ryegrass, *Tellus*, 59, 673–684, 2007.
- Dal Cason T. A.: Synthesis and identification of N,N-dimethylcathinone hydrochloride, *Microgram Journal*, 5(1-4), 3-12, 2007.
- Dalponte M., Gianelle D. and Bruzzone L.: Use of hyperspectral and LIDAR data for classification of complex forest areas, *Canopy Analysis and Dynamics of a Floodplain Forest* (Gianelle D., Travaglini D., Mason F., Minari E., Chirici G., Chemini C. ed.), 25-37, 2007.
- Dalponte M., Bruzzone L. and Gianelle D.: Fusion of hyperspectral and LIDAR remote sensing data for classification of complex forest areas, *IEEE Transactions on Geoscience and Remote Sensing*, 46(5), 1416-1427, 2008.
- Danner H., Samudrala D., Cristescu S. M. and van Dam N. M.: Tracing hidden herbivores: Time-resolved non-invasive analysis of belowground volatiles by proton-transfer-reaction mass spectrometry (PTR-MS), *Journal of Chemical Ecology*, 38, 785–794, 2012.
- Davison B., Brunner A., Ammann C., Spirig C., Jocher M. and Neftel A.: Cut-induced VOC emissions from agricultural grasslands, *Plant Biology*, 10, 76-85, 2008.

Davison B., Taipale R., Langford B., Misztal P., Fares S., Matteucci G., Loreto F., Cape J.N., Rinne J. and Hewitt C.N.: Concentrations and fluxes of biogenic volatile organic compounds above a Mediterranean macchia ecosystem in western Italy. *Biogeosciences*, 6, 1655-1670, 2009.

de Gouw J.A., Goldan P.D., Warneke C., Kuster W.C., Roberts J.M., Marchewka M., Bertman S.B., Pszenny A.A.P. and Keene W.C.: Validation of proton transfer reaction-mass spectrometry (PTR-MS) measurements of gas-phase organic compounds in the atmosphere during the New England Air Quality Study (NEAQS) in 2002, *Journal of Geophysical Research*, 108, D21 4682, 2003.

de Gouw J.A., Warneke C., Stohl A., Wollny A.G., Brock C.A., Cooper O.R., Holloway J.S., Trainer M., Fehsenfeld F.C., Atlas E.L., Donnelly S.G., Stroud V. and Lueb A.: Volatile organic compounds composition of merged and aged forest fire plumes from Alaska and western Canada, *Journal of Geophysical Research*, 111, D10303, 2006.

de Gouw J. and Warneke C.: Measurements of volatile organic compounds in the earth's atmosphere using proton transfer-reaction mass spectrometry, *Mass Spectrometry Reviews*, 26, 223-257, 2007.

De Moraes C. M., Lewis W. J., Paré P. W., Alborn H. T. and Tumlinson J. H.: Herbivore-infested plants selectively attract parasitoids, *Nature*, 393, 570-573, 1998.

Decesari S., Allan J., Plass-Duelmer C., Williams B.J., Paglione M., Facchini M.C., O'Dowd C., Harrison R.M., Gietl J.K., Coe H., Giulianelli L., Gobbi G.P., Lanconelli C., Carbone C., Worsnop D., Lambe A.T., Ahern A.T., Moretti F., Tagliavini E., Elste T., Gilde S., Zhang Y. and Dall'Osto M.: Measurements of the aerosol chemical composition and mixing state in the Po Valley using multiple spectroscopic techniques, *Atmospheric Chemistry and Physics*, 14, 12109-12132, 2014.

Degenhardt J., Hiltbold I., Köllner T. G., Frey, M., Gierl A., Gershenson J., Hibbard B. E., Ellersieck M. R. and Turlings T. C. J.: Restoring a maize root signal that attracts insect-killing nematodes to control a major pest, *PNAS*, 106(32), 13213-13218, 2009.

Dettmer K., Engewald W.: Adsorbent materials commonly used in air analysis for adsorptive enrichment and thermal desorption of volatile organic compounds, *Analytical Biochemistry* 373, 490-500, 2002.

Dhananjeyan M. R., Bykowski C., Trebdel J. A., Sarver J. G., Ando H. and Erhardt P. W.: Simultaneous determination of procaine and para-aminobenzoic acid by LC-MS/MS method, *Journal of Chromatography B*, 847, 224-230, 2007.

Dicke M., Sabelis M. W., Takabayashi J., Bruin J. and Posthumus M. A.: Plant strategies of manipulating predator-prey interactions through allelochemicals: prospects for application in pest control, *Journal of Chemical Ecology*, 16(11), 3091–3118, 1990.

Dicke M. and van Loon J. J. A.: Multitrophic effects of herbivore-induced plant volatiles in an evolutionary context, *Entomologia Experimentalis et Applicata*, 97, 237–249, 2000.

Dicke M.: Behavioural and community ecology of plants that cry for help, *Plant, Cell and Environment*, 32, 654–65, 2009.

Diskin A. M., Wang T., Smith D. and Španěl P.: A selected ion flow tube (SIFT), study of the reactions of  $\text{H}_3\text{O}^+$ ,  $\text{NO}^+$  and  $\text{O}_2^+$  ions with a series of alkenes; in support of SIFT-MS, *International Journal of Mass Spectrometry*, 218, 87–101, 2002.

Drugsforum: [http:// www.drugsforum.com](http://www.drugsforum.com) (accessed on 01.10.2013)

Drugssyn: <http://www.drugssyn.org> (accessed on 01.10.2013)

Dudareva N., Negre F., Nagegowda D. A. and Orlova I.: Plant volatiles: Recent advances and future perspectives, *Critical Reviews in Plant Sciences*, 25, 417–440, 2006.

Ehn M., Thornton J. A., Kleist E., Sipilä M., Junninen H., Pullinen I., Springer M., Rubach F., Tillmann R., Lee B., Lopez-Hilfiker F., Andres S., Acir I.-H., Rissanen M., Jokinen T., Schobesberger S., Kangasluoma J., Kontkanen J., Nieminen T., Kurtén T., Nielsen L. B., Jørgensen S., Kjaergaard H. G., Canagaratna M., Maso M. D., Berndt T., Petäjä T., Wahner A., Kerminen V.-M., Kulmala M., Worsnop D. R., Wildt J. and Mentel T. F.: A large source of low-volatility secondary organic aerosol, *Nature*, 506, 476-479, 2014.

Erb, M, Foresti N. and Turlings T. C. J.: A tritrophic signal that attracts parasitoids to host-damaged plants withstands disruption by non-host herbivores, *BMC Plant Biology*, 10, 247–258, 2010.

erowid: <http://www.erowid.org> (accessed on 10.05.2013)

European Union: A Strategic Analysis, European Centre for Drugs and Drug Addiction, EMCDDA, Lisbon, 2013.

eve-rave: <http://www.eve-rave.ch/> (08.10.2013)

Fall R., Karl T., Hansel A., Jordan A. and Lindinger W.: Volatile organic compounds emitted after leaf wounding : On-line analysis by proton-transfer-reaction mass spectrometry, *Journal of Geophysical Research*, 104(D13), 15963–15974, 1999.

Fall R.: Abundant Oxygenates in the Atmosphere: A Biochemical Perspective, *Chemical reviews*, 103, 4941-4951, 2003.

Fang C., Monson R. K. and Cowling E. B.: Isoprene emission, photosynthesis, and growth in sweetgum (*Liquidambar styraciflua*) seedlings exposed to short- and long-term drying cycles, *Tree Physiology*, 16, 441–446, 1996.

Fares S., Barta C., Brilli F., Centritto M., Ederli L., Ferranti F., Pasqualini S., Reale L., Tricoli D. and Loreto F.: Impact of high ozone on isoprene emission, photosynthesis and histology of developing *Populus alba* leaves directly or indirectly exposed to the pollutant, *Physiologia Plantarum*, 128, 456-465, 2006.

Fares S., Oksanen E., Lännenpää M., Julkunen-Tiitto R. and Loreto F.: Volatile emissions and phenolic compound concentrations along a vertical profile of *Populus nigra* leaves exposed to realistic ozone concentrations, *Photosynthesis Research*, 104, 61–74, 2010.

Fares S., Park J.-H., Gentner D.R., Weber R., Ormeño E., Karlik J. and Goldstein A.H.: Seasonal cycles of biogenic volatile organic compound fluxes and concentrations in a California citrus orchard, *Atmospheric Chemistry and Physics*, 12, 9865–9880, 2012.

Fares S., Schnitzhofer R., Jiang X., Guenther A., Hansel A. and Loreto F.: Observations of diurnal to weekly variations of monoterpene-dominated fluxes of volatile organic compounds from Mediterranean forests: implications for regional modelling, *Environmental Science and Technology*, 47, 11073-11082, 2013.

Farré-Armengol G., Peñuelas J., Li T., Yli-Pirilä P., Filella I., Llusia J. and Blande J. D.: Ozone degrades floral scent and reduces pollinator attraction to flowers, *New Phytologist*, 2015, doi: 10.1111/nph.13620.

Fehsenfeld F., Calvert J., Fall R., Goldan P., Guenther A.B., Hewitt C.N., Lamb B., Liu S., Trainer M., Westberg H. and Zimmerman P.: Emissions of volatile organic compounds from vegetation and the implications for atmospheric chemistry, *Global Biogeochemical Cycles*, 6, 389–430, 1992.

Finco, A., Coyle, M.; Marzuoli, R.; Chiesa, M.; Loubet, B.; Diaz-Pines, E.; Gasche, R.; Ammann, C.; Sutton, M.A.; Nemitz, E., Gerosa, G. Partitioning of the ozone flux with a mixed deciduous forest in northern Italy - importance of canopy storage and interactions with nitric oxide, *Biogeosciences Discussions* [in preparation]

Francis F., Lognay G., Wathelet J.-P. and Haubruge E.: Effects of allelochemicals from first (*brassicaceae*) and second (*Myzus persicae* and *Brevicoryne brassicae*) trophic levels on *Adalia bipunctata*, *Journal of Chemical Ecology*, 27(2), 243-256, 2001.

Foken, T. and Wichura, B.: Tools for quality assessment of surface- based flux measurements, *Agricultural and Forest Meteorology*, 78, 83–105, 1996.

Foken T., Göckede M., Mauder M., Mahrt L., Amiro B., and Munger W.: Post-field data quality control, in: *Handbook of Micrometeorology: A guide for surface flux measurement and analysis* (Lee, W. M. X. and Law, B. ed.), Kluwer Academic Publishers: Dordrecht, 29, 181–203, 2004.

Fruekilde P., Hjorth J., Jensen N. R., Kotzias D. and Larsen B.: Ozonolysis at vegetation surfaces: a source of acetone, 4-oxopentanal, 6-methyl-5-hepten-2-one, and geranyl acetone into the atmosphere, *Atmospheric Environment*, 32(11), 1893-1902, 1998.

Fu Y. and Tai A. P. K.: Impact of climate and land cover changes on tropospheric ozone air quality and public health in East Asia between 1980 and 2010, *Atmospheric Chemistry and Physics*, 15, 10093-10106, 2015.

Fuentes J. D., Roulston T. H, and Zenker J.: Ozone impedes the ability of a herbivore to find its host, *Environmental Research Letters*, 8, 014048, doi: 10.1088/1748-9326/8/1/014048.

Fürstenberg-Hägg J., Zagrobelny M. and Bak S.: Plant defense against insect herbivores, *International Journal of Molecular Sciences*, 14, 10242-10297, 2013.

Galbally I.E. and Kirstine W.: The Production of Methanol by Flowering Plants and the Global Cycle of Methanol, *Journal of Atmospheric Chemistry* 43, 195–229, 2002.

Gate I. M., McNeill S. and Ashmore M. R.: Effects of air pollution on the searching behaviour of an insect parasitoid, *Water, Air and Soil Pollution*, 85, 1425-1430, 1995.

Ghaffari R., Zhang F., Iliescu D., Hines E., Leeson M., Napier R. and Clarkson, J.: Early detection of diseases in tomato crops: An electronic nose and intelligent systems approach, *The 2010 International Joint Conference on Neural Networks (IJCNN)*. Barcelona, Spain 18-23 July, 2010.

Ghalaieny M., Bacak A., McGillen M., Martin D., Knights A. V., O'Doherty S., Shallcross D. E. and Percival C. J.: Determination of gas-phase ozonolysis rate

coefficients of a number of sesquiterpenes at elevated temperatures using the relative rate method, *Physical Chemistry Chemical Physics*, 14, 6596-6602, 2012.

Ghirardo A., Koch K., Taipale R., Zimmer I., Schnitzler J.-P. and Rinne J.: Determination of de novo and pool emissions of terpenes from four common boreal/alpine trees by  $^{13}\text{CO}_2$  labelling and PTR-MS analysis, *Plant, Cell and Environment*, 33, 781-792, 2010.

Ghirardo A., Heller W., Fladung M., Schnitzler J.P. and Schroeder H.: Function of defensive volatiles in pedunculate oak (*Quercus robur*) is tricked by the moth *Tortrix viridana*, *Plant, Cell and Environment*, 35(12), 2192-2207, 2012.

Ghirardo A., Xie J., Zheng X., Wang Y., Grote R., Block K., Wildt J., Mentel T., Kiendler-Scharr A., Hallquist M., Butterbach-Bahl K. and Schnitzler J.-P.: Urban stress-induced biogenic VOC emissions and SOA-forming potentials in Beijing, *Atmospheric Chemistry and Physics*, 16, 2901-2920, 2016.

Gish M. and Inbar M.: Host location by apterous aphids after escape dropping from the plant, *Journal of Insect Behavior*, 19(1), 143-153, 2006.

Glasius M., Boel C., Bruun N., Easa L.M., Hornung P., Klausen H.S., Klitgaard K.C., Lindeskov C., Moller C.K., Nissen H., Petersen A.P.F., Kleefeld S., Boaretto E., Hansen T.S., Heinemeier J. and Lohse C.: Relative contribution of biogenic and anthropogenic sources to formic and acetic acids in the atmospheric boundary layer, *Journal of Geophysical Research*, 106, 7415-7426, 2001.

Goldan P.D., Kuster W.C., Fehsenfeld F.C. and Montzka S.A.: The observation of a  $\text{C}_5$  alcohol emission in a North American pine forest, *Geophysical Research Letters*, 20, 1039-1042, 1993.

Goldstein A.H. and Schade G.W.: Quantifying biogenic and anthropogenic contributions to acetone mixing ratios in a rural environment, *Atmospheric Environment*, 34, 4997-5006, 2000.

Gonzalez F. R. and Nardillo A. M.: Retention index in temperature-programmed gas chromatography, *Journal of Chromatography A*, 842, 29-49, 1999.

Gosset V., Harmel N., Göbel C., Francis F., Haubruge E., Wathelet J.-P. Jardin P. Feussner I. and Fauconnier M.-L.: Attacks by a piercing-sucking insect (*Myzus persicae* Sultzer) or a chewing insect (*Leptinotarsa decemlineata* Say) on potato plants (*Solanum tuberosum* L.) induce differential changes in volatile compound release and oxylipin synthesis, *Journal of Experimental Botany*, 60(4), 1231-1240, 2009.

- Goudriaan, J. and van Laar, H.: *Modelling Potential Crop Growth Processes. Textbook with Exercises*, Kluwer Academic Publishers: Dordrecht, 1994.
- Gouinguene S. P. and Turlings T. C. J.: The effects of abiotic factors on induced volatile emissions in corn plants, *Plant Physiology*, 129, 1296–1307, 2002.
- Grabmer W., Graus M., Lindinger C., Wisthaler A., Rappenglück B., Steinbrecher R. and Hansel A.: Disjunct eddy covariance measurements of monoterpene fluxes from a Norway spruce forest using PTR-MS, *International Journal of Mass Spectrometry*, 239, 111-115, 2004.
- Graus M., Müller M. and Hansel A.: High resolution PTR-TOF: quantification and formula confirmation of VOC in real time, *Journal of the American Society for Mass Spectrometry*, 21, 1037–1044, 2010.
- Gray C.M., Monson R.K. and Fierer N.: Emissions of volatile organic compounds during the decomposition of plant litter, *Journal of Geophysical Research*, 115, 2010.
- Guenther A., Hewitt C.N., Erickson D., Fall R., Geron C., Graedel T., Harley P., Klinger L., Lerdau M., McKay W.A., Pierce T., Scholes B., Steinbrecher R., Tallamraju R., Taylor J. and Zimmerman P.: A global model for natural volatile organic compound emissions, *Journal of Geophysical Research*, 100(D5), 8873–8892, 1995.
- Guenther A., Karl T., Harley P., Wiedinmyer C., Palmer P.I. and Geron C.: Estimates of global terrestrial isoprene emissions using MEGAN (Model of Emissions of Gases and Aerosols from Nature), *Atmospheric Chemistry and Physics*, 6, 3180-3210, 2006.
- Guenther, A. B., Jiang, X., Heald, C. L., Sakulyanontvittaya, T., Duhl, T., Emmons, L. K., and Wang, X.: The Model of Emissions of Gases and Aerosols from Nature version 2.1 (MEGAN2.1): an extended and updated framework for modeling biogenic emissions, *Geoscientific Model Development*, 5, 1471-1492, 2012.
- Guevremont R.: High-field asymmetric waveform ion mobility spectrometry: A new tool for mass spectrometry, *Journal of Chromatography A*, 1058, 3–19, 2004.
- Hallquist M., Wenger J. C., Baltensperger U., Rudich Y., Simpson D., Claeys M., Dommen J., Donahue N. M., George C., Goldstein A. H., Hamilton J. F., Herrmann H., Hoffmann T., Iinuma Y., Jang M., Jenkin M. E., Jimenez J. L., Kiendler-Scharr A., Maenhaut W., Mcfiggans G., Mentel Th. F., Monod A., Prévôt A. S. H., Seinfeld J. H., Surratt J. D., Szmigielski R. and Wildt J.: The formation, properties and impact of secondary organic aerosol: current and emerging issues, *Atmospheric Chemistry and Physics*, 9, 5155-5236, 2009.

- Hansel A., Jordan A., Holzinger R., Prazeller P., Vogel W. and Lindinger W.: Proton transfer reaction mass spectrometry : on-line trace gas analysis at the ppb level, *International Journal of Mass Spectrometry and Ion Processes*, 149/150, 609–619, 1995.
- Hayward S., Muncey R.J., James A.E., Halsall C.J. and Hewitt C.N.: Monoterpene emissions from soil in a Sitka spruce forest, *Atmospheric Environment*, 35, 4081-4087, 2001.
- Hayward S., Hewitt C. N., Sartin J. H. and Owen S. M.: Performance characteristics and applications of a proton transfer reaction-mass spectrometer for measuring volatile organic compounds in ambient air, *Environmental Science and Technology*, 36(7), 1554–1560, 2002.
- Hayward S., Tani A., Owen S. M. and Hewitt, C.N.: Online analysis of volatile organic compound emissions from Sitka spruce (*Picea sitchensis*), *Tree Physiology*, 24, 721–728, 2004.
- Heiden A. C., Hoffmann T., Kahl J., Kley D., Klockow D., Langebartels C., Mehlhorn H., Sandermann H. Jr., Schraudner M., Schuh G. and Wildt J.: Emission of volatile organic compounds from ozone-exposed plants, *Ecological Applications*, 9(4), 1160–1167, 1999.
- Heiden A. C., Kobel K., Langebartels C., Schuh-Thomas G. and Wildt J.: Emissions of oxygenated volatile organic compounds from plants part I : Emissions from lipoxygenase activity, *Journal of Atmospheric Chemistry*, 45, 143–172, 2003.
- Heil M.: Indirect defence via tritrophic interactions, *The New Phytologist*, 178, 41-61, 2008.
- Heil M. and Ton J.: Long-distance signalling in plant defence, *Trends in Plant Science*, 13, 264-272, 2008.
- Henderson G.: Designer Drugs: Past History and Future Prospects, *Journal of Forensic Sciences*, 33, 569–575, 1988.
- Hewitt N. and Terry G.: Understanding ozone plant chemistry, *Environmental Science and Technology*, 26(10), 1890-1891, 1992.
- Hewitt C. N., Hayward S. and Tani A.: The application of proton transfer reaction-mass spectrometry (PTR-MS) to the monitoring and analysis of volatile organic compounds in the atmosphere, *Journal of Environmental Monitoring* 5, 1-7, 2003.

Hewitt C. N., Mackenzie A. R., Di Carlo P., Di Marco C. F., Dorsey J. R., Evans M., Fowler D., Gallagher M. W., Hopkins J. R., Jones C. E., Langford B., Lee J. D., Lewis A. C., Lim S., F., Mcquaid J., Misztal P., Moller S. J., Monks P. S., Nemitz E., Oram D. E., Owen S. M., Phillips G. J., Pugh T. A. M., Pyle J. A., Reeves C. E., Ryder J., Siong J., Skiba U. and Stewart D. J.: Nitrogen management is essential to prevent tropical oil palm plantations from causing ground-level ozone pollution., *PNAS*, 106(44), 18447-18451, 2009.

HGCA: HGCA descriptive list spring oilseed rape trials protocol 2012, HGCA, Kenilworth, Warwickshire, 2012. Available at <http://cereals.ahdb.org.uk/> (last accessed 24.11.2015).

Hilker M. and Meiners T.: Early herbivore alert :Insect eggs induce plant defense, *Journal of Chemical Ecology*, 32, 1379-1397, 2006.

Hillstrom M. L. and Lindroth R. L.: Elevated atmospheric carbon dioxide and ozone alter forest insect abundance and community composition, *Insect Conservation and Diversity*, 1, 233-241, 2008.

Himanen S. J., Nerg A.-M., Nissinen A., Pinto D. M., Stewart C. N. Jr., Poppy G. M. and Holopainen J. K.: Effects of elevated carbon dioxide and ozone on volatile terpenoid emissions and multitrophic communication of transgenic insecticidal oilseed rape (*Brassica napus*), *The New Phytologist*, 181, 174–186, 2009.

Hoffmann T., Odum J. R., Bowman F., Collins D., Klockow D., Flagan R. C. and Seinfeld J. H.: Formation of organic aerosols from the oxidation of biogenic hydrocarbons, *Journal of Atmospheric Chemistry*, 26, 189-222, 1997.

Holloway P. J., Brown G. A., Baker E. A. and Macey, M. J. K.: Chemical composition and ultrastructure of the epicuticular wax in three lines of *Brassica napus* (L), *Chemistry and Physics of Lipids*, 19, 114-127, 1977.

Holopainen J. K. and Gershenzon J.: Multiple stress factors and the emission of plant VOCs, *Trends in Plant Science*, 15(3), 176–184, 2010.

Horst T. W.: A simple formula for attenuation of eddy fluxes measured with first-order-response scalar sensors, *Boundary-Layer Meteorology*, 82, 219-233, 1997.

Ibrahim M. A., Stewart-Jones A., Pulkkinen J., Poppy G. M. and Holopainen J. K.: The influence of different nutrient levels on insect-induced plant volatiles in Bt and conventional oilseed rape plants, *Plant Biology*, 10, 97–107, 2008.

Intergovernmental Panel on Climate Change (IPCC): *Climate change 2007: The physical science basis*, Cambridge University Press: Cambridge, UK, 2007.

Isebrands J.G., Guenther A.B., Harley P., Helmig D., Klinger L., Vierling L., Zimmerman P. and Geron C.: Volatile organic compound emission rates from mixed deciduous and coniferous forests in Northern Wisconsin USA, *Atmospheric Environment*, 33, 2527-2536, 1999.

Jacob D.J., Field B.D., Jin E.M., Bey I., Li Q., Logan J.A. and Yantosca R.M.: Atmospheric budget of acetone, *Journal of Geophysical Research*, 107, D10, 2002.

Jacob D.J., Field B.D., Li Q., Blake D.R., de Gouw J., Warneke C., Hansel A., Wisthaler A., Singh H.B. Guenther A.: Global budget of methanol: Constraints from atmospheric observations, *Journal of Geophysical Research*, 110, D08303, 2005.

Jansen R. M. C., Hofstee J. W., Wildt J., Verstappen F. W. A., Bouwmeester H., Posthumus M. A. and van Henten E.: Health monitoring of plants by their emitted volatiles: trichome damage and cell membrane damage are detectable at greenhouse scale, *Annals of Applied Biology*, 154, 441–452, 2009.

Jansen R. M. C., Wildt J., Kappers I. F., Bouwmeester H. J., Hofstee J. W. and van Henten E. J.: Detection of diseased plants by analysis of volatile organic compound emission, *Annual Review of Phytopathology*, 49, 157–174, 2011.

Jardine K.J., Monson R.K., Abrell L., Saleska S.R., Arneth, A., Jardine A., Ishida F.Y., Serrano A.M.Y., Artaxo P., Karl T., Fares S., Goldstein A., Loreto F. and Huxman, T.: Within-plant isoprene oxidation confirmed by direct emissions of oxidation products methyl vinyl ketone and methacrolein, *Global Change Biology*, 18, 973–984, 2012.

Jordan A., Haidacher S., Hanel G., Hartungen E., Märk L., Seehauser H., Schottkowsky R., Sulzer P. and Märk T. D.: A high resolution and high sensitivity proton-transfer-reaction time-of-flight mass spectrometer (PTR-TOF-MS), *International Journal of Mass Spectrometry* 286, 122–128, 2009a.

Jordan A., Haidacher S., Hanel G., Hartungen E., Herbig J., Märk L., Schottkowsky R., Seehauser H., Sulzer P. and Märk T. D.: An online ultra-high sensitivity Proton-transfer-reaction mass-spectrometer combined with switchable reagent ion capability (PTR+SRI-MS), *International Journal of Mass Spectrometry*, 286, 32–38, 2009b.

Jud W., Fischer L., Canaval E., Wohlfahrt G., Tissier A. and Hansel A.: Plant surface reactions: an opportunistic ozone defence mechanism impacting atmospheric chemistry, *Atmospheric Chemistry and Physics*, 16, 277-292, 2016.

Junninen H., Ehn M., Petäjä T., Luosujärvi L., Kotiaho T., Kostianinen R., Rohner U., Gonin M., Fuhrer K., Kulmala M. and Worsnop D.R.: A high-resolution mass

spectrometer to measure atmospheric ion composition, *Atmospheric Measurement Techniques*, 3(4), 1039-1053, 2010.

Junninen H., Ehn M., Petäjä T., Luosujärvi L., Kotiaho T., Kostianen R., Rohner U., Gonin M., Fuhrer K., Kulmala M. and Worsnop D.R.: A high-resolution mass spectrometer to measure atmospheric ion composition, *Atmospheric Measurement Techniques*, 3(4), 1039-1053, 2010.

Jürschik S., Sulzer P., Petersson F., Mayhew C. A., Jordan A., Agarwal B., Haidacher S., Seehauser H., Becker K. and Märk T. D.: Proton transfer reaction mass spectrometry for the sensitive and rapid real-time detection of solid high explosives in air and water, *Analytical and Bioanalytical Chemistry*, 398, 2813-2820, 2010.

Jürschik S., Agarwal B., Kassebacher T., Sulzer P., Mayhew C. A. and Märk T. D.: Rapid and facile detection of four date rape drugs in different beverages utilizing proton transfer reaction mass spectrometry (PTR-MS), *Journal of Mass Spectrometry*, 47, 1092–1097, 2012.

Kajos M. K., Rantala P., Hill M., Hellén H., Aalto J., Patokoski J., Taipale R., Hoerger C. C., Reimann S., Ruuskanen T. M., Rinne J. and Petäjä T.: Ambient measurements of aromatic and oxidized VOCs by PTR-MS and GC-MS: intercomparison between four instruments in a boreal forest in Finland, *Atmospheric Measurement Techniques Discussions*, 8, 3753-3802, 2015.

Kalogridis C., Gros V., Sarda-Estève R., Langford B., Loubet B., Bonsang B., Bonnaire N., Nemitz E., Genard A.-C., Boissard C., Fernandez C., Ormeño E., Baisnée D., Reiter I. and Lathièrre J.: Concentrations and fluxes of isoprene and oxygenated VOCs at a French Mediterranean oak forest, *Atmospheric Chemistry and Physics*, 14, 10085–10102, 2014.

Kappers I. F., Aharoni A., van Herpen T. W. J. M., Luckerhoff L. L. P., Dicke M. and Bouwmeester H. J.: Genetic engineering of terpenoid metabolism attracts bodyguards to *Arabidopsis*, *Science*, 309, 2070-2072, 2005.

Karl M., Guenther A., Köble R., Leip A. and Seufert G.: A new European plant-specific emission inventory of biogenic volatile organic compounds for use in atmospheric transport models, *Biogeosciences*, 6, 1059-1087, 2009.

Karl T., Guenther A., Jordan A., Fall R. and Lindinger W.: Eddy covariance measurement of biogenic oxygenated VOC emissions from hay harvesting, *Atmospheric Environment*, 35, 491-495, 2001.

Karl T.G., Spirig C., Rinne J., Stroud C., Prevost P., Greenberg J., Fall R. and Guenther A.: Virtual disjunct eddy covariance measurements of organic compound

fluxes from a subalpine forest using proton transfer reaction mass spectrometry, *Atmospheric Chemistry and Physics*, 2, 279-291, 2002.

Karl T., Guenther A., Spirig C., Hansel A. and Fall R.: Seasonal variation of biogenic VOC emissions above a mixed hardwood forest in northern Michigan, *Geophysical Research Letters*, 30, 2186, 2003.

Karl T., Potosnak M., Guenther A., Clark D., Walker J., Herrick J.D. and Geron C.: Exchange processes of volatile organic compounds above a tropical rain forest: Implications for modeling tropospheric chemistry above dense vegetation, *Journal of Geophysical Research*, 109, D18306, 2004.

Karl T., Harley P., Guenther A., Rasmussen R., Baker B., Jardine K. and Nemitz E.: The bi-directional exchange of oxygenated VOCs between a loblolly pine (*Pinus taeda*) plantation and the atmosphere, *Atmospheric Chemistry and Physics*, 5, 3015-3031, 2005.

Karl T.G., Christian T.J., Yokelson R.J., Artaxo P., Hao W.M. and Guenther A.: The tropical forest and fire emissions experiment: method evaluation of volatile organic compound emissions measured by PTR-MS, FTIR, and GC from tropical biomass burning, *Atmospheric Chemistry and Physics*, 7, 8755-8793, 2007.

Karl T., Harley P., Emmons L., Thornton B., Guenther A., Basu C., Turnipseed A. and Jardine K.: Efficient atmospheric cleansing of oxidized organic trace gases by vegetation, *Science*, 330, 816-819, 2010.

Karl T., Hansel A., Cappellin L., Kaser L., Herdinger-Blatt I. and Jud W.: Selective measurements of isoprene and 2-methyl-3-buten-2-ol based on  $\text{NO}^+$  ionization mass spectrometry, *Atmospheric Chemistry and Physics*, 12, 11877–11884, 2012.

Kaser L., Karl T., Guenther A., Graus M., Schnitzhofer R., Turnipseed A., Fischer L., Harley P., Madronich M., Gochis D., Keutsch F.N. and Hansel A.: Undisturbed and disturbed above canopy ponderosa pine emissions: PTR-TOF-MS measurements and MEGAN 2.1 model results, *Atmospheric Chemistry and Physics*, 13, 11935-11947, 2013.

Kassebacher T., Sulzer P., Jürschik S., Hartungen E., Jordan A., Edtbauer A., Feil S., Hanel G., Jaksch S., Märk L., Mayhew C. A. and Märk T. D.: Investigations of chemical warfare agents and toxic industrial compounds with proton-transfer-reaction mass spectrometry for a real-time threat monitoring scenario, *Rapid Communications in Mass Spectrometry*, 27, 325–332, 2013.

Kanu A. B., Dwivedi P., Tam M., Matz L. and Hill H. H. Jr.: Ion mobility – mass spectrometry, *Journal of Mass Spectrometry*, 43, 1–22, 2008.

Kelleher C., Christie R., Lalor K., Fox J., Bowden M. and O'Donnell C.: An overview of new psychoactive substances and the outlets supplying them, National Advisory Committee on Drugs: Dublin, 2011.

Keller T., Schneider A., Tutsch-Bauer E., Jaspers J., Aderjan R. and Skopp G.: Ion mobility spectrometry for the detection of drugs in cases of forensic and criminalistic relevance, *International Journal for Ion Mobility Spectrometry*, 2/1, 22-34, 1999.

Kelly J. P.: Cathinone derivatives: A review of their chemistry, pharmacology and toxicology, *Drug Testing and Analysis*, 3, 439-453, 2011.

Keenan T., Niinemets Ü., Sabate S., Gracia C. and Peñuelas J.: Process based inventory of isoprenoid emissions from European forests: model comparisons, current knowledge and uncertainties, *Atmospheric Chemistry and Physics*, 9, 4053-4076, 2009.

Kesselmeier J., Bode K., Gerlach C. and Jork, E.-M.: Exchange of atmospheric formic and acetic acids with trees and crop plants under controlled chamber and purified air conditions, *Atmospheric Environment*, 32, 1765-1775, 1998.

Kesselmeier J. and Staudt M.: Biogenic volatile organic compounds (VOC): An overview on emission, physiology and ecology, *Journal of Atmospheric Chemistry*, 33, 23-88, 1999.

Kessler A. and Baldwin I. T.: Defensive function of herbivore-induced plant volatile emissions in nature, *Science*, 291, 2141-2144, 2001.

Khan Z. R., Midega C. A. O., Bruce T. J. A., Hooper A. M. and Pickett J. A.: Exploiting phytochemicals for developing a 'push-pull' crop protection strategy for cereal farmers in Africa, *Journal of Experimental Botany*, 61(15), 4185-4196, 2010.

Kim, S., Karl, T., Helmig, D., Daly, R., Rasmussen, R. and Guenther, A.: Measurement of atmospheric sesquiterpenes by proton transfer reaction-mass spectrometry (PTR-MS), *Atmospheric Measurement Techniques*, 2, 99-112, 2009.

Knudsen J. T., Eriksson R., Gershenzon J. and Ståhl B.: Diversity and distribution of floral scent, *The Botanical Review*, 72(1), 1-120, 2006.

Kolakowski B. M. and Mester Z.: Review of applications of high-field asymmetric waveform ion mobility spectrometry (FAIMS) and differential mobility spectrometry (DMS), *The Analyst*, 132, 842-864, 2007.

König G., Brunda M., Puxbaum H., Hewitt C.N., Duckham S.C. and Rudolph J.: Relative contribution of oxygenated hydrocarbons to the total biogenic VOC

emissions of selected mid-European agricultural and natural plant species, *Atmospheric Environment*, 29, 861-874, 1995.

Kormann R. and Meixner F. X.: An analytical footprint model for non-neutral stratification, *Boundary-Layer Meteorology*, 99, 207-224, 2001.

Kourtchev .I, Bejan I., Sodeau J. R. and Wenger J. C.: Gas-phase reaction of (E)- $\beta$ -farnesene with ozone: Rate coefficient and carbonyl products, *Atmospheric Environment*, 43, 3182-3190, 2009.

Kroll J. H., Sahay S. R., Anderson J. G., Demerjian K. L. and Donahue N. M.: Mechanism of HO<sub>x</sub> formation in the gas-phase ozone-alkene Reaction. 2. Prompt versus thermal dissociation of carbonyl oxides to form OH, *Journal of Physical Chemistry A*, 105, 4446-4457, 2001.

Kreuzwieser J., Scheerer U., Kruse J., Burzlaff T., Honsel A., Alfarraj S., Georgiev P., Schnitzler J.-P., Ghirardo A., Kreuzer I., Hedrich R. and Rennenberg H.: The Venus flytrap attracts insects by the release of volatile organic compounds, *Journal of Experimental Botany*, 65(2), 3753-3802, 2014.

Krieger J. and Breer H.: Olfactory reception in invertebrates, *Science*, 286, 720–723, 1999.

Kuhn U., Rottenberger S., Biesenthal T., Ammann C., Wolf A., Schebeske G., Oliva S.T., Tavares T.M. and Kesselmeier J.: Exchange of short-chain monocarboxylic acids by vegetation at a remote tropical forest site in Amazonia, *Journal of Geophysical Research*, 107, 8069, 2002.

Kulmala M., Kontkanen J., Junninen H., Lehtipalo K., Manninen H. E., Nieminen T., Petäjä T., Sipilä M., Schobesberger S., Rantala P., Franchin A., Jokinen T., Järvinen E., Äijälä M., Kangasluoma J., Hakala J., Aalto P. P., Paasonen P., Mikkilä J., Vanhanen J., Aalto J., Hakola H., Makkonen U., Ruuskanen T., Mauldin R. L. III, Duplissy J., Vehkamäki H., Bäck J., Kortelainen A., Riipinen I., Kurtén T., Johnston M. V., Smith J. N., Ehn M., Mentel T. F., Lehtinen K. E. J., Laaksonen A., Kerminen V.-M. and Worsnop D. R.: Direct Observations of Atmospheric Aerosol Nucleation, *Sciences*, 339, 943-947, 2013.

Kunert M., Biedermann A., Koch T. and Boland W.: Ultrafast sampling and analysis of plant volatiles by a hand-held miniaturised GC with pre-concentration unit : Kinetic and quantitative aspects of plant volatile production, *Journal of Separations Science*, 25, 677–684, 2002.

Kuster W.C., Jobson B.T., Karl T., Riemer D., Apel E., Goldan P.D. and Fehsenfeld F.C.: Intercomparison of volatile organic carbon measurement techniques and data at

La Porte during the TexAQS2000 Air Quality Study, *Environmental Science and Technology*, 38, 221-228, 2004.

Laffineur Q., Aubinet M., Schoon N., Amelynck C., Müller J.-F., Dewulf J., van Langenhove H., Steppe K., Šimpraga M. and Heinesch B.: Isoprene and monoterpene emissions from a mixed temperate forest, *Atmospheric Environment*, 45, 3157-3168, 2011.

Langford B., Davison B., Nemitz B. and Hewitt C.N.: Mixing ratios and eddy covariance flux measurements of volatile organic compounds from an urban canopy (Manchester, UK), *Atmospheric Chemistry and Physics*, 9, 1971-1987, 2009.

Langford B., Misztal P.K., Nemitz E., Davison B., Helfter C., Pugh T.A.M., MacKenzie R.M., Lim S.F. and Hewitt C.N.: Fluxes and concentrations of volatile organic compounds from a South-East Asian tropical rainforest, *Atmospheric Chemistry and Physics*, 10, 8391-8412, 2010a.

Langford B., Nemitz E., House E., Philips G.J., Famulari D., Davison B., Hopkins J.R., Lewis A.C. and Hewitt C.N.: Fluxes and concentrations of volatile organic compounds above central London, UK, *Atmospheric Chemistry and Physics*, 10, 627-645, 2010b.

Langford B., Acton W., Ammann C., Valach A. and Nemitz E.: Eddy-covariance data with low signal-to-noise ratio: time-lag determination, uncertainties and limit of detection, *Atmospheric Measurement Techniques Discussions*, 8, 2913–2955, 2015.

Lanza M., Acton W. J., Sulzer P., Jürschik S., Jordan A., Hartungen E., Hanel G., Märk L., Mayhew C. A. and Märk T. D.: From conventional proton-transfer-reaction mass spectrometry (PTR-MS) to universal trace gas analysis, *Journal of Mass Spectrometry*, 48, 1015–1018, 2013.

Laothawornkitkul J., Moore J. P., Taylor J. E., Possell M., Gibson T. D., Hewitt C. N. and Paul N. D.: Discrimination of plant volatile signatures by an electronic nose: A potential technology for plant pest and disease monitoring, *Environmental Science and Technology*, 42, 8433–8439, 2008.

Laothawornkitkul J., Taylor J., Paul N. D. and Hewitt C. N.: Biogenic volatile organic compounds in the earth system, *The New Phytologist*, 183, 27–51, 2009.

Lee A., Goldstein A. H., Keywood M. D., Gao S., Varutbangkul V., Bahreini R., Ng N. L., Flagan R. C. and Seinfeld J. H.: Gas-phase products and secondary aerosol yields from the ozonolysis of ten different terpenes, *Journal of Geophysical Research*, 111, D07302, 2006, doi:10.1029/2005JD006437.

Leff J.W. and Fierer N.: Volatile organic compound (VOC) emissions from soil and litter samples, *Soil Biology and Biochemistry*, 40, 1629-1636, 2008.

Lin, C., Owen, S. and Penuelas, J.: Volatile organic compounds in the roots and rhizosphere of *Pinus* spp., *Soil Biology and Biochemistry*, 39, 951–960, 2007.

Lindinger W., Hansel A. and Jordan A.: On-line monitoring of volatile organic compounds at pptv levels by means of Proton-Transfer-Reaction Mass Spectrometry (PTR-MS) Medical applications, food control and environmental research, *International Journal of Mass Spectrometry*, 173, 191-241, 1998a.

Lindinger W., Hansel A. and Jordan A.: Proton-transfer-reaction mass spectrometry (PTR-MS): On-line monitoring of volatile organic compounds at pptv levels, *Chemical Society Reviews*, 27, 347–354, 1998b.

Llusià J. and Peñuelas J.: Emission of volatile organic compounds by apple trees under spider mite attack and attraction of predatory mites, *Experimental and Applied Acarology*, 25, 65-77, 2001.

Llusià J., Peñuelas J. and Gimeno B. S.: Seasonal and species-specific response of VOC emissions by Mediterranean woody plant to elevated ozone concentrations, *Atmospheric Environment*, 36, 3931–3938, 2002.

Llusià T.M., Müller M., Schnitzhofer R., Karl T., Graus M. Bamberger I., Hörtnagl L., Brilli F., Wohlfahrt G. and Hansel A.: Eddy covariance VOC emission and deposition fluxes above grassland using PTR-TOF, *Atmospheric Chemistry and Physics*, 11, 611-625, 2011.

Logan, J. A.: Tropospheric ozone: Seasonal behavior, trends, and anthropogenic influence, *Journal of Geophysical Research*, 90(D6), 10463–10482, 1985.

Loreto F., Fischbach R.J., Schnitzler J.P., Ciccioli P., Brancaleoni E., Calfapietra C., Seufert G.: Monoterpene emission and monoterpene synthase activities in the Mediterranean evergreen oak *Quercus ilex* L. grown at elevated CO<sup>2</sup> concentrations, *Global Change Biology*, 7, 709-717, 2001.

Loreto F., Barta C., Brilli F. and Nogues I.: On the induction of volatile organic compound emissions by plants as consequence of wounding or fluctuations of light and temperature, *Plant, Cell, and Environment*, 29, 1820–1828, 2006.

Loreto F. and Schnitzler J.-P.: Abiotic stresses and induced BVOCs, *Trends in Plant Science*, 15(3), 154-166, 2010.

- Luecken D.J., Hutzell W.T., Strum M.L. and Pouliot G.A.: Regional sources of atmospheric formaldehyde and acetaldehyde, and implications for atmospheric modelling, *Atmospheric Environment*, 47, 477-490, 2012.
- Maes K. and Debergh P. C.: Volatiles emitted from in vitro grown tomato shoots during abiotic and biotic stress, *Plant Cell, Tissue and Organ Culture*, 75, 73–78, 2003.
- Maffei M. E.: Sites of synthesis, biochemistry and functional role of plant volatiles, *South African Journal of Botany*, 76, 612–631, 2010.
- Maleknia S. D., Bell T. L. and Adams M. A.: PTR-MS analysis of reference and plant-emitted volatile organic compounds, *International Journal of Mass Spectrometry*, 262, 203–210, 2007.
- Materić D., Lanza M., Sulzer P., Herbig J., Bruhn D., Turner C., Mason N. and Gauci V.: Monoterpene separation by coupling proton transfer reaction time-of-flight mass spectrometry with fastGC, *Analytical and Bioanalytical Chemistry*, 407, 7757-7763, 2015.
- Mayhew C. A., Sulzer P., Petersson F., Haidacher S., Jordan A., Märk L., Watts P. and Märk T.D.: Applications of proton transfer reaction time-of-flight mass spectrometry for the sensitive and rapid real-time detection of solid high explosives, *International Journal of Mass Spectrometry*, 289, 58-63, 2010.
- McCormick A. C., Unsicker S. B. and Gershenson J.: The specificity of herbivore-induced plant volatiles in attracting herbivore enemies, *Trends in Plant Science*, 17(5), 303–310, 2012.
- McEwan M. and Macfarlane Smith W. H.: Identification of volatile organic compounds emitted in the field by oilseed rape (*Brassica napus* ssp. *oleifera*) over the growing season, *Clinical and Experimental Allergy*, 28, 332-338, 1998.
- McMillen R. T.: An eddy correlation technique with extended applicability to non-simple terrain, *Boundary-Layer Meteorology*, 43, 231-245, 1988.
- Millet D.B., Jacob D.J., Custer T.G., de Gouw J.A., Goldstein A.H., Karl T., Singh H.B., Sive B.C., Talbot R.W., Warneke C. and Williams J.: New constraints on terrestrial and oceanic sources of atmospheric methanol, *Atmospheric Chemistry and Physics*, 8, 6887-6905, 2008.
- Millet D.B., Guenther A., Siegel D.A., Nelson N.B., Singh H.B., de Gouw J.A., Warneke C., Williams J., Eerdekens G., Sinha V., Karl T., Flocke F., Apel E., Riemer D.D., Palmer P.I., and Barkley M.: Global atmospheric budget of acetaldehyde: 3-D

model analysis and constraints from in-situ and satellite observations, *Atmospheric Chemistry and Physics*, 10, 3405–3425, 2010.

Mithöfer A. and Boland W.: Plant defense against herbivores: chemical aspects, *Annual Review of Plant Biology*, 63, 431–450, 2012.

Miresmailli S., Gries R., Gries G., Zamar R.H. and Isman M. B.: Herbivore-induced plant volatiles allow detection of *Trichoplusia ni* (Lepidoptera : Noctuidae) infestation on greenhouse tomato plants, *Pest Management Science*, 66, 916–924, 2010.

Misztal P.K., Nemitz E., Langford B., Di Marco C.F., Phillips G.J., Hewitt C.N., MacKenzie A.R., Owen S.M., Fowler D., Heal M.R. and Cape J.N.: Direct ecosystem fluxes of volatile organic compounds from oil palms in South-East Asia, *Atmospheric Chemistry and Physics*, 11, 8995–9017, 2011.

Moayeri H. R. S., Ashouri A., Poll L. and Enkegaard A.: Olfactory response of a predatory mired to herbivore induced plant volatiles: multiple herbivory vs. single herbivory, *Journal of Applied Entomology*, 131, 326–332, 2007.

Moncrieff J., Clement R., Finnigan J. and Meyers T.: Averaging, detrending, and filtering of eddy covariance time series, in: *Handbook of Micrometeorology: A guide for surface flux measurement and analysis* (Lee W.M.X. and Law B. ed.), Kluwer Academic Publishers: Dordrecht, 2004.

Monks P. S., Granier C., Fuzzi S., Stohl A., Williams M. L., Akimoto H., Amann M., Baklanov A., Baltensperger U., Bey I., Blake N., Blake R. S., Carslaw K., Cooper O. R., Dentener F., Fowler D., Fragkou E., Frost G. J., Generoso S., Ginoux P., Grewe V., Guenther A., Hansson H. C., Henne S., Hjorth J., Hofzumahaus A., Huntrieser H., Isaksen I. S. A., Jenkin M. E., Kaiser J., Kanakidou M., Klimont Z., Kulmala M., Laj P., Lawrence M. G., Lee J. D., Liousse C., Maione M., Mcfiggans G., Metzger A., Mieville A., Moussiopoulos N., Orlando J. J., O'Dowd C. D., Palmer P. I., Parrish D. D., Petzold A., Platt U., Pöschl U., Prévôt A. S. H., Reeves C. E., Reimann S., Rudich Y., Sellegri K., Steinbrecher R., Simpson D., ten Brink H., Theloke J., van der Werf G. R., Vautard R., Vestreng V., Vlachokostas Ch. and von Glasow R.: Atmospheric composition change – global and regional air quality, *Atmospheric Environment*, 43, 5268–5350, 2009.

Müller K., Haferkorn S., Grabmer W., Wisthaler A., Hansel A., Kreuzwieser J., Cojocariu C., Rennenberg H. and Herrmann H.: Biogenic carbonyl compounds within and above a coniferous forest in Germany, *Atmospheric Environment*, 40, 81–91, 2006.

Müller J.-F., Stavrou, T., Wallens S., De Smedt I., Van Roozendaal M., Potosnak, J., Rinne, J., Munger B., Goldstein, A. and Guenther A.B.: Global isoprene emissions

estimated using MEGAN, ECMWF analyses and a detailed canopy environment model, *Atmospheric Chemistry and Physics*, 8, 1329-1341, 2008.

Müller M., Graus M., Ruuskanen T. M., Schnitzhofer R., Bamberger I., Kaser L., Titzmann T., Hörtnagl L., Wohlfahrt G., Karl T. and Hansel A.: First eddy covariance flux measurements by PTR-TOF, *Atmospheric Measurement Techniques*, 3, 387-395, 2010.

Müller, M., Mikoviny, T., Jud, W., D'Anna, B. and Wisthaler, A.: A new software tool for the analysis of high resolution PTR-TOF mass spectra, *Chemometrics and Intelligent Laboratory Systems*, 127, 158–165, 2013.

Neftel A., Spirig C. and Ammann C.: Application and test of a simple tool for operational footprint evaluations, *Environmental Pollution*, 152, 644-652, 2008.

Nemitz E., Hargreaves K.J., Neftel A., Loubet B., Cellier P., Dorsey R.J., Flynn M., Hensen A., Weidinger T., Meszaros R., Horvath L., Dämmgen U., Frühauf C., Löpmeier F.J., Gallagher M.W. and Sutton M.A.: Intercomparison and assessment of turbulent and physiological exchange parameters of grassland, *Biogeosciences*, 6, 1445–1466, 2009.

Niinemets, Ü: Research review. Components of leaf dry mass per area – thickness and density – alter leaf photosynthetic capacity in reverse directions in woody plants, *New Phytologist*, 144, 35-47, 1999.

Oltmans S.J., Lefohn A.S., Shadwick D., Harris J.M., Scheel H.E., Galbally I., Tarasick D.W., Johnson B.J., Brunke E., Claude H., Zeng G., Nichol S., Schmidlin F., Davies J., Cuevas E., Redondas A., Naoe H., Nakano T. and Kawasato T.: Recent tropospheric ozone changes – A pattern dominated by slow or no growth, *Atmospheric Environment*, 67, 331-351, 2013.

Ormeño E., Mévy J. P., Vila B., Bousquet-Mélou A., Greff S., Bonin G. and Fernandez C.: Water deficit stress induces different monoterpene and sesquiterpene emission changes in Mediterranean species. Relationship between terpene emissions and plant water potential, *Chemosphere*, 67, 276–284, 2007.

Ortega J. and Helmig D.: Approaches for quantifying reactive and low-volatility biogenic organic compound emissions by vegetation enclosure techniques – Part A, *Chemosphere*, 72, 343–364, 2008.

Owen S.M., Boissard C. and Hewitt C.N.: Volatile organic compounds (VOCs) emitted from 40 Mediterranean plant species: VOC speciation and extrapolation to habitat scale, *Atmospheric Environment*, 35, 5393-5409, 2001.

Paré, P. W. and Tumlinson, J. H.: Induced synthesis of plant volatiles, *Nature*, 385, 30–31, 1997.

Park J.-H., Goldstein A.H., Timkovsky J., Fares S., Weber R., Karlik J., and Holzinger R.: Active atmosphere-ecosystem exchange of the vast majority of detected volatile organic compounds, *Science*, 341, 643-647, 2013.

Parrish D. D., Law K. S., Staehelin J., Derwent R., Cooper O. R., Tanimoto H., Gilge S., Scheel H.-E., Steinbacher M. and Chan E.: Long-term changes in lower tropospheric baseline ozone concentrations at northern mid-latitudes, *Atmospheric Chemistry and Physics*, 12, 11485-11504, 2012.

Paulot F., Wunch D., Crouse J.D., Toon G.C., Millet D.B., DeCarlo P.F., Vigouroux C., Deutscher N.M., González Abad G., Notholt J., Warneke T., Hannigan J.W., Warneke C., de Gouw J.A., Dunlea E.J., De Mazière M., Griffith D.W.T., Bernath P., Jimenez J.L. and Wennberg P.O.: Importance of secondary sources in the atmospheric budgets of formic and acetic acids, *Atmospheric Chemistry and Physics*, 11, 1989-2013, 2011.

Pegoraro E., Rey A., Greenberg J., Harley P., Grace J., Malhi Y. and Guenther A.: Effect of drought on isoprene emission rates from leaves of *Quercus virginiana* Mill, *Atmospheric Environment*, 38, 6149–6156, 2004.

Peñuelas J. and Llusà J.: The complexity of factors driving volatile organic compound emissions by plants, *Biologica Plantarum*, 44(4), 481–487, 2001.

Peñuelas J., Filella I., Stefanescu C. and Llusà J.: Caterpillars of *Euphydryas aurinia* (Lepidoptera: *Nymphalidae*) feeding on *Succisa pratensis* leaves induce large foliar emissions of methanol, *New Phytologist*, 167, 851-857, 2005.

Peñuelas J. and Staudt M.: BVOCs and global change, *Trends in Plant Science*, 15(3), 133–144, 2010.

Pérez-Rial D., Peñuelas J., López-Mahía P. and Llusà J.: Terpenoid emissions from *Quercus robur*. A case study of Galicia (NW Spain), *Journal of Environmental Monitoring*, 11, 1268-1275, 2009.

Petersson F., Sulzer P., Mayhew C. A., Watts P., Jordan A., Märk L. and Märk T. D.: Real-time trace detection and identification of chemical warfare agent simulants using recent advances in proton transfer reaction time-of-flight mass spectrometry, *Rapid Communications in Mass Spectrometry*, 23, 3875-3880, 2009.

Pier P.A.: Isoprene emission rates from Northern Red Oak using a whole-tree chamber, *Atmospheric Environment*, 29, 1347-1353, 1995.

- Pichersky E. and Gershenzon J.: The formation and function of plant volatiles: perfumes for pollinator attraction and defense, *Current Opinion in Plant Biology*, 5, 237–243, 2002.
- Pinto D. M., Bande J. D., Nykänen R., Dong W.-X., Nerg A.-M. and Holopainen J. K.: Ozone degrades common herbivore-induced plant volatiles: does this affect herbivore prey location by predators and parasitoids? *Journal of Chemical Ecology*, 33, 683-694, 2007a.
- Pinto D. M., Nerg A.-M. and Holopainen J. K.: The role of ozone-reactive compounds, terpenes, and green leaf volatiles (glvs), in the orientation of *Cotesia plutellae*, *Journal of Chemical Ecology*, 33, 2218-2228, 2007b.
- Pinto D. M., Himanen S. J., Nissinen A., Nerg A.-M. and Holopainen J. K.: Host location behavior of *Cotesia plutellae* Kurdjumov (Hymenoptera: *Braconidae*) in ambient and moderately elevated ozone in field conditions, *Environmental Pollution*, 156, 227-231, 2008.
- Pinto D. M., Blande J. D., Souza S. R., Nerg A.-M. and Holopainen J. K.: Plant volatile organic compounds (VOCs) in ozone (O<sub>3</sub>) polluted atmospheres: the ecological effects, *Journal of Chemical Ecology*, 36, 22-34, 2010.
- Plaza J., Núñez L., Pujadas M., Pérez-Pastor R., Bermejo V., Garcia-Alonso S. and Elvira S.: Field monoterpene emission of Mediterranean oak (*Quercus ilex*) in the central Iberian Peninsula measured by enclosure and micrometeorological techniques: Observation of drought stress effect, *Journal of Geophysical Research*, 110, 1–12, 2005.
- Pollmann J., Ortega J. and Helmig D.: Analysis of atmospheric sesquiterpenes: Sampling losses and mitigation of ozone interferences, *Environmental Science and Technology*, 39, 9620-9629, 2005.
- Pysanenko A., Španěl P. and Smith D.: A study of sulfur-containing compounds in mouth- and nose-exhaled breath and in the oral cavity using selected ion flow tube mass spectrometry, *Journal of Breath Research*, 046004, 13pp, 2008.
- Quiroz A., Pettersson J., Pickett J. A., Wadhams L. J. and Niemeyer H. M.: Semiochemicals mediating spacing behavior of bird cherry-oat aphid, *Rhopalosiphum padi* feeding on cereals, *Journal of Chemical Ecology*, 23(11), 2599–2607, 1997.
- R Core Team: R: A language and environment for statistical computing. R Foundation for Statistical Computing, Vienna, Austria. ISBN 3-900051-07-0, URL <http://www.R-project.org/>, 2012.

Rasmann S., Köllner T. G., Degenhardt J., Hiltbold I., Toepfer S., Kuhlmann U., Gershenson J. and Turlings T. C. J.: Recruitment of entomopathogenic nematodes by insect-damaged maize roots, *Nature*, 434, 732-737, 2005.

Rasmann S. and Turlings T. C. J.: Simultaneous feeding by aboveground and belowground herbivores attenuates plant-mediated attraction of their respective natural enemies, *Ecology Letters*, 10, 926–936, 2007.

Rennenberg H., Loreto F., Polle A., Brilli F., Fares S., Beniwal R. S. and Gessler A.: Physiological responses of forest trees to heat and drought, *Plant Biology*, 8, 556–571, 2006.

Riemer, D., Pos W., Milne P., Farmer C., Zika R., Apel E., Olszyna K., Kliendienst T. Lonneman W., Bertman S., Shepson P. and Starn T.: Observations of nonmethane hydrocarbons and oxygenated volatile organic compounds at a rural site, *Journal of Geophysical Research*, 103, 28111-28128, 1998.

Rinne J., Ruuskanen T.M., Reissell A., Taipale R., Hakola H. and Kulmala M.: On-line PTR-MS measurements of atmospheric concentrations of volatile organic compounds in a European boreal forest ecosystem, *Boreal Environment Research*, 10, 425-436, 2005.

Rinne J., Taipale R., Markkanen T., Ruuskanen T.M., Hellén H., Kajos M.K., Vesala T., and Kulmala M.: Hydrocarbon fluxes above a Scots pine forest canopy: measurements and modelling, *Atmospheric Chemistry and Physics*, 7, 3361–3372, 2007.

Rinne J., Douffet T., Prigent Y. and Durand P.: Field comparison of disjunct and conventional eddy covariance techniques for trace gas flux measurements, *Environmental Pollution*, 152, 630-635, 2008.

Rinne J. and Ammann C.: Disjunct Eddy Covariance Method, in: *Eddy covariance: A practical guide to measurement and data* (Aubinet M., Vesala T. and Papale D. ed.), Springer: Netherlands, 2012.

Rivera-Rios J.C., Nguyen T.B., Crounse J.D., Jud W., St. Clair J.M., Mikoviny T., Gilman J.B., Lerner B.M., Kaiser J.B., de Gouw J., Wisthaler A., Hansel A., Wennberg P.O., Seinfeld J.H. and Keutsch F.N.: Conversion of hydroperoxides to carbonyls in field and laboratory instrumentation: Observational bias in diagnosing pristine versus anthropogenically controlled atmospheric chemistry, *Geophysical Research Letters*, 41, 8645-8651, 2014.

- Rodriguez-Saona C., Crafts-Brander S. J. and Canas L. A.: Volatile emissions triggered by multiple herbivore damage: beet armyworm and whitefly feeding on cotton plants, *Journal of Chemical Ecology*, 29, 2539-2550, 2003.
- Rösner P., Quednow B., Girreser U. and Junge T.: Isomeric Fluoro-methoxy-phenylalkylamines: a new series of controlled-substance analogues (designer drugs), *Forensic Science International*, 148, 143–156, 2005.
- Rostás M., Ton J., Mauch-Mani B. and Turlings T. C. J.: Fungal infection reduces herbivore-induced plant volatiles of maize but does not affect naïve parasitoids, *Journal of Chemical Ecology*, 32, 1897–1909, 2006.
- Rottenberger S., Kuhn U., Wolf A., Schebeske G., Oliva S.T., Tavares T.M. and Kesselmeier J.: Formaldehyde and acetaldehyde exchange during leaf development of the Amazonian deciduous tree species *Hymenaea courbaril*, *Atmospheric Environment*, 39, 2275-2279, 2005.
- Royal Society, Ground-level ozone in the 21st century: Future trends, impacts and policy implications: Science policy report 15/08. The Royal Society, London. 2008.
- Ruuskanen T.M., Müller M., Schnitzhofer R., Karl T., Graus M., Bamberger I., Hörtnagl L., Brilli F., Wohlfahrt G. and Hansel A.: Eddy covariance VOC emission and deposition fluxes above grassland using PTR-TOF, *Atmospheric Chemistry and Physics*, 11, 611–625, 2011.
- Ryan A., Cojocariu C., Possell M., Davies W.J. and Hewitt C.N.: Defining hybrid poplar (*Populus deltoides* × *Populus trichocarpa*) tolerance to ozone: identifying key parameters, *Plant, Cell and Environment*, 32, 31–45, 2009.
- Salter L. and Hewitt C. N.: Ozone-hydrocarbon interactions in plants, *Phytochemistry*, 31(12), 4045-4050, 1992.
- Sankaran S., Mishra A., Ehsani R. and Davis C.: A review of advanced techniques for detecting plant diseases, *Computers and Electronics in Agriculture*, 72, 1–13, 2010.
- Schade G.W. and Goldstein A.H.: Fluxes of oxygenated volatile organic compounds from a ponderosa pine plantation, *Journal of Geophysical Research*, 106, 3111-3123, 2001.
- Schade G.W. and Goldstein A.H.: Seasonal measurements of acetone and methanol: Abundances and implications for atmospheric budgets, *Global Biogeochemical Cycles*, 20, GB1011, 2006.

Schallhart S., Rantala P., Nemitz E., Mogensen D., Tillmann R., Mentel T.F., Rinne J. and Ruuskanen T.M.: Characterization of Ecosystem scale VOC exchange at a Mediterranean oak-hornbeam forest, *Atmospheric Chemistry and Physics Discussions*, 15, 27627-27673, 2015.

Schaub A., Blande J. D., Graus M., Oksanen E., Holopainen J. K. and Hansel A.: Real-time monitoring of herbivore induced volatile emissions in the field, *Physiologia Plantarum*, 138, 123–133, 2010.

Schmelz E. A., Alborn H. T., Engelberth J. and Tumlinson J. H.: Nitrogen deficiency increases volicitin-induced volatile emission, jasmonic acid accumulation, and ethylene sensitivity in maize, *Plant Physiology*, 133, 295–306, 2003.

Schuh G., Heiden A. C., Hoffmann Th., Kahl J., Rockel P., Rudolph J. and Wildt J.: Emissions of volatile organic compounds from sunflower and beech: Dependence on temperature and light intensity, *Journal of Atmospheric Chemistry*, 27(3), 291–318, 1997.

Schütz S., Weißbecker B., Koch U. T. and Hummel H. E.: Detection of volatiles released by diseased potato tubers using a biosensor on the basis of intact insect antennae, *Biosensors and Bioelectronics*, 14, 221–228, 1999.

Schumann A., Lenth C., Hasener J. and Steckel V.: Detection of volatile organic compounds from wood-based panels by gas chromatography-field asymmetric ion mobility spectrometry (GC-FAIMS), *International Journal for Ion Mobility Spectrometry*, 15, 157–168, 2012.

Scutareanu P., Bruin J., Posthumus M.A. and Drukker B.: Constitutive and herbivore-induced volatiles in pear, alder and hawthorn trees, *Chemoecology*, 74, 63-74, 2003.

Seco R., Peñuelas J. and Filella I.: Short-chain oxygenated VOCs: Emission and uptake by plants and atmospheric sources, sinks, and concentrations, *Atmospheric Environment*, 41, 2477-2499, 2007.

Sevonkaev I. V. and Katz E.: Biosensors based on immobilized insects fragments, *Journal of Solid State Electrochemistry*, 12, 7–14, 2008.

Sharkey T. D. and Singsaas E. L.: Why plants emit isoprene, *Nature*, 374, 769, 1995.

Sharkey T. D., Wiberley A. E. and Donohue A. R.: Isoprene emission from plants: Why and how, *Annals of Botany*, 101, 5–18, 2008.

sigmaaldrich: <http://www.sigmaaldrich.com/safety-center.html> (accessed on 18.8.2013)

Singh H.B., Kanakidou M. Crutzen P.J. and Jacob D.J.: High concentrations and photochemical fate of oxygenated hydrocarbons in the global troposphere, *Nature*, 378, 50-54, 1995.

Smith P.A., Sng M. T., Eckenrode B. A., Leow S. Y., Koch D., Erickson R. P., Jackson Lepage C. R. and Hook G. L.: Towards smaller and faster gas chromatography – mass spectrometry systems for field chemical detection, *Journal of Chromatography. A*, 1067, 285–294, 2005.

Soukoulis C., Cappellin L., Aprea E., Costa F., Viola R., Märk T. D. Gasperi F. and Biasioli F.: PTR-ToF-MS, a novel, rapid, high sensitivity and non-invasive tool to monitor volatile compound release during fruit post-harvest storage: The case study of apple ripening. *Food Bioprocess Technology*, 2012, doi: 10.1007/s11947-012-0930-6.

Španěl, P. and Smith, D.: SIFT studies of the reactions of  $\text{H}_3\text{O}^+$ ,  $\text{NO}^+$  and  $\text{O}_2^+$  with a series of alcohols, *International Journal of Mass Spectrometry and Ion Processes*, 167/168, 375–388, 1997a.

Španěl P., Ji Y. and Smith D.: SIFT studies of the reactions of  $\text{H}_3\text{O}^+$ ,  $\text{NO}^+$  and  $\text{O}_2^+$  with a series of aldehydes and ketones, *International Journal of Mass Spectrometry and Ion Processes*, 165-166, 25-37, 1997.

Spirig C., Neftel A., Ammann C., Dommen J., Grabmer W., Thielmann A., Schaub A., Beauchamp J., Wistthaler A. and Hansel A.: Eddy covariance flux measurements of biogenic VOCs during ECHO 2003 using proton transfer reaction mass spectrometry, *Atmospheric Chemistry and Physics*, 5, 465-481, 2005.

Staudt M., Wolf A. and Kesselmeier J.: Influence of environmental factors on the emissions of gaseous formic and acetic acids from orange (*Citrus sinensis* L.) foliage, *Biogeochemistry*, 48, 199-216, 2000.

Staudt M., Jackson B., El-aouni H., Buatois B., Lacroze J.-P., Poëssel J.-L. and Sauge M.-H: Volatile organic compound emissions induced by the aphid *Myzus persicae* differ among resistant and susceptible peach cultivars and a wild relative, *Tree Physiology*, 30, 1320-1334, 2010.

Su Y.-C., Chang C.-C. and Wang J.-L.: Construction of an automated gas chromatography / mass spectrometry system for the analysis of ambient volatile organic compounds with on-line internal standard calibration, *Journal of Chromatography A*, 1201, 134–140, 2008.

Sulzer P., Edtbauer A., Hartungen E., Jürschik S., Jordan A., Hanel G., Feil S., Jaksch S., Märk L. and Märk T. D.: From conventional proton-transfer-reaction mass spectrometry (PTR-MS) to universal trace gas analysis, *International Journal of Mass Spectrometry* 321-322, 66–70, 2012a.

Sulzer P., Petersson F., Agarwal B., Becker K. H., Jürschik S., Märk T. D., Perry D., Watts P. and Mayhew C. A.: Proton transfer reaction mass spectrometry and the unambiguous real-time detection of 2,4,6 trinitrotoluene, *Analytical Chemistry*, 84, 4161-4166, 2012b.

Szpeiner A., Martínez-Ghersa M. A. and Ghersa C. M.: Wheat volatile emissions modified by top-soil chemical characteristics and herbivory alter the performance of neighbouring wheat plants, *Agriculture, Ecosystems and Environment*, 134, 99–107, 2009.

Taipale R., Ruuskanen T.M., Rinne J., Kajos M.K., Hakola H., Pohja T. and Kulmala M.: Technical Note: Quantitative long-term measurements of VOC concentrations by PTR-MS – measurement, calibration, and volume mixing ratio calculation methods, *Atmospheric Chemistry and Physics*, 8, 6681-6698, 2008.

Taipale R., Ruuskanen T.M. and Rinne J.: Lag time determination in DEC measurements with PTR-MS, *Atmospheric Measurement Techniques*, 3, 853-862, 2010.

Tani A., Hayward S., Hansel A. and Hewitt C.N.: Effect of water vapour pressure on monoterpene measurements using proton transfer reaction-mass spectrometry (PTR-MS), *International Journal of Mass Spectrometry*, 239, 161-169, 2004.

Tarvainen, V., Hakola, H., Hellén, H., Bäck, J., Hari, P. and Kulmala, M.: Temperature and light dependence of the VOC emissions of Scots pine, *Atmospheric Chemistry and Physics*, 5, 989-998, 2005.

Terry G. M., Stokes N. J., Hewitt C. N. and Mansfield T. A.: Exposure to isoprene promotes flowering in plants, *Journal of Experimental Botany*, 46(291), 1629-1631, 1995.

theguardian: <http://www.theguardian.com/uk-news/2013/sep/01/festivalgoer-death-drug-warning-brownstock> (08.10.2013)

Tholl D., Boland W., Hansel A., Loreto F., Röse U. S. R. and Schnitzler J.-P.: Practical approaches to plant volatile analysis, *The Plant Journal*, 45, 540–560, 2006.

Tie X., Guenther A. and Holland E.: Biogenic methanol and its impacts on tropospheric oxidants, *Geophysical Research Letters*, 30, 2003.

Tingey D. T., Manning M., Grothaus L. C. and Burns W. F.: Influence of light and temperature on monoterpene emission rates from slash pine, *Plant Physiology*, 65, 797–801, 1980.

Turlings T. C. J., Tumlinson J. H. and Lewis W. J.: Exploitation of herbivore-induced plant odors by host-seeking parasitic wasps, *Science*, 250(4985), 1251–1253, 1990.

United Nations: World drugs report, United Nations Office of Drugs and Crime: Vienna, 2013.

Unsicker S. B., Kunert G. and Gershenzon J.: Protective perfumes: The role of vegetative volatiles in plant defense against herbivores, *Current Opinion in Plant Biology*, 12, 479–85, 2009.

van Dam N. M., Samudrala D., Harren F. J. M. and Cristescu S. M.: Real-time analysis of sulfur-containing volatiles in Brassica plants infested with root-feeding *Delia radicum* larvae using proton-transfer reaction mass spectrometry, *AoB plants*, pls021, 2012, doi: 10.1093/aobpla/pls021.

Vancanneyt G., Sanz C., Farmaki T., Paneque M., Ortego F., Castañera P. and Sánchez-Serrano J. J.: Hydroperoxide lyase depletion in transgenic potato plants leads to an increase in aphid performance, *PNAS*, 98(14), 8139-8144, 2001.

Velasco-Garcia M. N. and Mottram T.: Biosensor technology addressing agricultural problems, *Biosystems Engineering*, 84(1), 1–12, 2003.

Vercammen J., Pham-Tuan H., Arickx I., van der Straeten D., Sandra P.: Monitoring of isothiocyanates emanating from *Arabidopsis thaliana* upon paraquat spraying, *Journal of Chromatography A*, 912, 127-134, 2001.

Vickers C. E., Possell M., Cojocariu C. I., Velikova V. B., Laothawornkitkul J., Ryan A., Mullineaux P. M. and Hewitt C. N.: Isoprene synthesis protects transgenic tobacco plants from oxidative stress, *Plant, Cell and Environment*, 35(5), 520-531, 2009.

Visser J. H. and Avé D. A.: General green leaf volatiles in the olfactory orientation of the Colorado beetle, *Leptinotarsa decemlineata*, *Entomologia Experimentalis et Applicata*, 24, 738–749, 1978.

von Dahl C.C., Hävecker M., Schlögl R. and Baldwin I. T.: Caterpillar-elicited methanol emission: a new signal in plant – herbivore interactions? *The Plant Journal*, 46, 948–960, 2006.

Vuorinen T., Nerg A.-M. and Holopainen J. K.: Ozone exposure triggers the emission of herbivore-induced plant volatiles, but does not disturb tritrophic signalling, *Environmental Pollution*, 131, 305–311, 2004.

Vuorinen T., Nerg A.-M., Vapaavuori E. and Holopainen J. K.: Emission of volatile organic compounds from two silver birch (*Betula pendula* Roth) clones grown under ambient and elevated CO<sub>2</sub> and different O<sub>3</sub> concentrations, *Atmospheric Environment*, 39, 1185–1197, 2005.

Warneke C., Karl T., Judmaier H., Hansel A., Jordan A., Lindinger W. and Crutzen P.J.: Acetone, methanol and other partially oxidized volatile organic emissions from dead plant matter by abiological processes: Significance for atmospheric HOx chemistry, *Global Biogeochemical Cycles*, 13, 9-17, 1999.

Webster B.: The role of olfaction in aphid host location, *Physiological Entomology*, 37, 10-18, 2012.

Weigl F., Ghirardo A., Schnitzler J.-P. and Pritsch K.: Sesquiterpene emissions from *Alternaria alternata* and *Fusarium oxysporum*: Effects of age, nutrient availability, and co-cultivation, *Scientific Reports*, 6, 22152, 2016.

Werse B. and Morgenstern C.: How to handle legal highs? Findings from a German online survey and considerations on drug policy issues, *Drugs and Alcohol Today*, 12(4), 222-231, 2012.

Westphal F., Rösner P. and Junge Th.: Differentiation of regioisomeric ring-substituted fluorophenethylamines with product ion spectrometry, *Forensic Science International*, 194, 53–59, 2010.

Westwell A. D., Hutchings A. and Caldicott D. G. E.: The identification and chemical characterization of a new arylcyclohexylamine, methoxetamine, using a novel Emergency Department toxicosurveillance tool, *Drug Testing and Analysis*, 5(3), 203-207, 2013.

WHO, Health aspects of air pollution with particulate matter, ozone and nitrogen dioxide. WHO, Copenhagen, 2003.

Wienhold F.G., Frahm H. and Harris G.W.: Measurements of N<sub>2</sub>O fluxes from fertilized grassland using a fast response tunable diode laser spectrometer, *Journal of Geophysical Research*, 99, 16557-16567, 1994.

Wildt J., Kobel K., Schuh-Thomas G. and Heiden A. C.: Emissions of oxygenated volatile organic compounds from plants part II : Emissions of saturated aldehydes, *Journal of Atmospheric Chemistry*, 45, pp.173–196, 2003.

- Wilks A., Hart M., Koehl A., Somerville J., Boyle B. and Ruiz-Alonso D.: Characterization of a miniature, ultra-high-field, ion mobility spectrometer, *International Journal for Ion Mobility Spectrometry*, 15, 199–222, 2012.
- Wilson A. D. and Baietto M.: Applications and advances in electronic-nose technologies, *Sensors*, 9, 5099–5148, 2009.
- Winter T. R., Borkowski L., Zeier J. and Rostás M.: Heavy metal stress can prime for herbivore-induced plant volatile emission, *Plant, Cell and Environment*, 35(7), 1287–1298, 2012.
- Winters A.J., Adams M.A., Bleby T.M., Rennenberg H., Steigner D., Steinbrecher R. and Kreuzwieser J.: Emissions of isoprene, monoterpene and short-chained carbonyl compounds from *Eucalyptus* spp. in southern Australia, *Atmospheric Environment*, 43, 3035-3043, 2009.
- Winterhalter R., Herrmann F., Kanawati B., Nguyen T. L., Peeters J., Vereecken L. and Moortgat G. K.: The gas-phase ozonolysis of beta-caryophyllene (C(15)H(24)). Part I: an experimental study, *Physical Chemistry Chemical Physics*, 11, 4152-4172, 2009.
- Wisthaler A. and Weschler C. J.: Reactions of ozone with human skin lipids: sources of carbonyls, dicarbonyls, and hydroxycarbonyls in indoor air, *Proceedings of the National Academy of Sciences*, 107(15), 6568-6575, 2010.
- Wohlfahrt G., Amelynck C., Ammann C., Arneth A., Bamberger I., Goldstein A.H., Gu L., Guenther A., Hansel A., Heinesch B., Holst T., Hörtnagl L., Karl T., Laffineur Q., Neftel A., McKinney K., Munger J.W., Pallardy S.G., Schade G.W., Seco R., Schoon N.: An ecosystem-scale perspective of the net land methanol flux: synthesis of micrometeorological flux measurements, *Atmospheric Chemistry and Physics Discussions*, 15, 2577-2613, 2015.
- Zhang F., Ghaffari R., Iliescu D., Hines E., Leeson M., and Napier R.: Field asymmetric ion mobility spectrometry based plant disease detection: Intelligent systems approach. In *Applied signal and image processing: Multidisciplinary advancements* (Qahwaji R., Green R. J. and Hines E. L. ed.), IGI Global: Hershey, Chapter 6, 102–114, 2011.
- Zhang Z. and Li G.: A review of advances and new developments in the analysis of biological volatile organic compounds, *Microchemical Journal*, 95(2), 127–139, 2010.

Zhou B. and Wang J.: Discrimination of different types damage of rice plants by electronic nose, *Biosystems Engineering*, 109, 250–257, 2011.

# Appendix

Addition papers W. J. F. Acton has contributed to.

## A1 Selective reagent ionisation-time of flight-mass spectrometry: a rapid technology for the novel analysis of blends of new psychoactive substances

This paper build upon the work presented in Chapter I and demonstrated the ability of SRI-ToF-MS to provide rapid identification of compounds in an unknown blend of new psychoactive substances.

**W. Joe Acton (Lancaster University):** Designed experiment, carried out data analysis and wrote the paper together with M. Lanza.

### Application note

Journal of  
MASS  
SPECTROMETRY

Received: 1 August 2014

Revised: 16 September 2014

Accepted: 17 September 2014

Published online in Wiley Online Library

(wileyonlinelibrary.com) DOI 10.1002/jms.3514

## Selective reagent ionisation-time of flight-mass spectrometry: a rapid technology for the novel analysis of blends of new psychoactive substances

Matteo Lanza,<sup>a,b†</sup> W. Joe Acton,<sup>a,c†</sup> Philipp Sulzer,<sup>a,\*</sup> Kostiantyn Breiev,<sup>a,b</sup> Simone Jürschik,<sup>a</sup> Alfons Jordan,<sup>a</sup> Eugen Hartungen,<sup>a</sup> Gernot Hanel,<sup>a</sup> Lukas Märk,<sup>a</sup> Tilmann D. Märk<sup>a,b</sup> and Chris A. Mayhew<sup>d</sup>

In this study we demonstrate the potential of selective reagent ionisation-time of flight-mass spectrometry for the rapid and selective identification of a popular new psychoactive substance blend called 'synthacaine', a mixture that is supposed to imitate the sensory and intoxicating effects of cocaine. Reactions with  $H_3O^+$  result in protonated parent molecules which can be tentatively assigned to benzocaine and methiopropamine. However, by comparing the product ion branching ratios obtained at two reduced electric field values (90 and 170 Td) for two reagent ions ( $H_3O^+$  and  $NO^+$ ) to those of the pure chemicals, we show that identification is possible with a much higher level of confidence than when relying solely on the  $m/z$  of protonated parent molecules. A rapid and highly selective analytical identification of the constituents of a recreational drug is particularly crucial to medical personnel for the prompt medical treatment of overdoses, toxic effects or allergic reactions. Copyright © 2015 John Wiley & Sons, Ltd.

**Keywords:** SRI-ToF-MS; PTR-MS; new psychoactive substances; drug detection; synthacaine

## **A2 Eddy-covariance data with low signal-to-noise ratio: time-lag determination, uncertainties and limit of detection**

The bVOC flux data presented in Chapter V was used to develop and test new methods to determine bVOC fluxes where the flux data has a low signal to noise ratio.

This method was then used to determine fluxes of bVOCs in Chapter V.

**W. Acton (Lancaster University):** Provided data, helped test the method and contributed to the manuscript.

Atmos. Meas. Tech., 8, 4197–4213, 2015  
www.atmos-meas-tech.net/8/4197/2015/  
doi:10.5194/amt-8-4197-2015  
© Author(s) 2015. CC Attribution 3.0 License.



Atmospheric  
Measurement  
Techniques  
Open Access 

## **Eddy-covariance data with low signal-to-noise ratio: time-lag determination, uncertainties and limit of detection**

**B. Langford<sup>1</sup>, W. Acton<sup>2</sup>, C. Ammann<sup>3</sup>, A. Valach<sup>2</sup>, and E. Nemitz<sup>1</sup>**

<sup>1</sup>Centre for Ecology and Hydrology, Bush Estate, Penicuik, EH26 0QB, UK

<sup>2</sup>Lancaster Environment Centre, Lancaster University, Lancaster, LA1 4YQ, UK

<sup>3</sup>Agroscope Research Station, Climate and Air Pollution Group, Zürich, Switzerland

*Correspondence to:* B. Langford (benngf@ceh.ac.uk)

Received: 28 January 2015 – Published in Atmos. Meas. Tech. Discuss.: 18 March 2015

Revised: 11 September 2015 – Accepted: 22 September 2015 – Published: 12 October 2015